AD-A071 910 MASSACHUSETTS INST OF TECH CAMBRIDGE AEROELASTIC AND--ETC F/G 20/11
A MULTILAYER, TRACTION-FREE EDGE, QUADRILATERAL, WARPING ELEMEN--ETC(U)
APR 79 A HARRIS, O ORRINGER, E A WITMER DAAG46-78-C-0015
UNCLASSIFIED ASRL-TR-193-1 AMMRC-TR-79-26 NL

1 OF 3
AD A071910

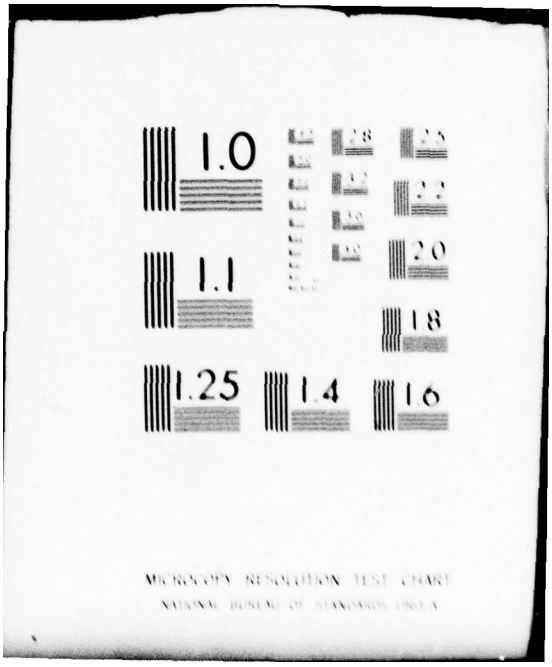
1.0
1.1
1.25
1.4
1.6
2.0
1.8
MICROCOPY RESOLUTION TEST CHART
NATIONAL BUREAU OF STANDARDS 1963-A

LEVEL II

AD

AMMRC TR 79-26

A MULTILAYER, TRACTION-FREE EDGE, QUADRILATERAL, WARPING ELEMENT FOR THE STRESS ANALYSIS OF COMPOSITE PLATES AND SHELLS

April 1979

Aeroelastic and Structures Research Laboratory
Department of Aeronautics and Astronautics
Massachusetts Institute of Technology
Cambridge, Massachusetts 02139

Final Report, Contract Number DAAG46-78-C-0120

Prepared for

ARMY MATERIALS AND MECHANICS RESEARCH CENTER
Watertown, Massachusetts 02172

The findings in this report are not to be construed as an official Department of the Army position, unless so designated by other authorized documents.

Mention of any trade names or manufacturers in this report shall not be construed as advertising nor as an official indorsement or approval of such products or companies by the United States Government.

DISPOSITION INSTRUCTIONS

Destroy this report when it is no longer needed.
Do not return it to the originator.

UNCLASSIFIED

SECURITY CLASSIFICATION OF THIS PAGE (When Data Entered)

REPORT DOCUMENTATION PAGE

READ INSTRUCTIONS BEFORE COMPLETING FORM

1. REPORT NUMBER: AMMRC TR-79-26
2. GOVT ACCESSION NO.
3. RECIPIENT'S CATALOG NUMBER

4. TITLE (and Subtitle): A MULTILAYER, TRACTION-FREE EDGE, QUADRILATERAL, WARPING ELEMENT FOR THE STRESS ANALYSIS OF COMPOSITE PLATES AND SHELLS.

5. TYPE OF REPORT & PERIOD COVERED: Final Report 3-1-78 to 4-30-79

6. PERFORMING ORG. REPORT NUMBER: ASRL-TR-193-1

7. AUTHOR(s): Alexander/Harris, Oscar/orringer and Emmett A./Witmer

8. CONTRACT OR GRANT NUMBER(s): DAAG46-78-C-0015

9. PERFORMING ORGANIZATION NAME AND ADDRESS: Aeroelastic and Structures Research Laboratory, Department of Aeronautics and Astronautics, Massachusetts Institute of Technology, Cambridge, Massachusetts 02139

10. PROGRAM ELEMENT, PROJECT, TASK AREA & WORK UNIT NUMBERS: D/A Project: 8X3633304D215; AMCMS Code: 633304.215D0.03; Agency Accession:

11. CONTROLLING OFFICE NAME AND ADDRESS: Army Materials and Mechanics Research Center, Watertown, Massachusetts 02172

12. REPORT DATE: April 1979

13. NUMBER OF PAGES: 232

14. MONITORING AGENCY NAME & ADDRESS (if different from Controlling Office): 242 p'

15. SECURITY CLASS. (of this report): Unclassified

15a. DECLASSIFICATION/DOWNGRADING SCHEDULE

16. DISTRIBUTION STATEMENT (of this Report): Approved for public release; distribution unlimited.

8X3633304D215

17. DISTRIBUTION STATEMENT (of the abstract entered in Block 20, if different from Report)

18. SUPPLEMENTARY NOTES: Final rept. 1 Mar 78-30 Apr 79,

19. KEY WORDS (Continue on reverse side if necessary and identify by block number)

Finite-Element Method
Elastic Behavior
Composites
Static Response
Transient Response
Stress Analysis
Laminated Plates and Shells
Free-Edge Stress Analysis

20. ABSTRACT (Continue on reverse side if necessary and identify by block number)

Laminated composites develop large interlaminar stresses at traction-free edges; these stresses are significant and often cause ply delaminations. However, these stresses are difficult to analyze and predict accurately because they vary very rapidly over a small region whose extent is of the order of the total laminate thickness at the free edge. Previous solution methods have been able to solve only a very restricted class of free-edge multilayer plate problems.

[BEGIN OVER]

DD FORM 1 JAN 73 1473 EDITION OF 1 NOV 65 IS OBSOLETE

UNCLASSIFIED

SECURITY CLASSIFICATION OF THIS PAGE (When Data Entered)

006 850

Block No. 20

ABSTRACT

In the present research, a hybrid stress multilayer warping quadrilateral element with a traction-free edge (TFQE), based on the Principle of Modified Complementary Energy, has been developed for efficient finite element modeling and analysis at and near free edges. The assumed stress distributions in the element were selected so as to satisfy the basic equations of equilibrium; sufficient detail was implemented throughout each layer of each element to model the steep boundary layer stress gradients, including the important interlaminar stresses. The interlayer stress continuity and traction-free conditions at the free edge are satisfied exactly; the resulting stress distribution was examined for consistency as required by 3-dimensional stress functions. The stress assumption includes no singularity. The traction-free edge is allowed to warp freely.

The interior of the laminate, away from the free edge, is modeled by laminated-plate elements (MLP3K) which are based on lamination theory. These elements include transverse shear deformation and are compatible with the TFQE. Thus, numerical results for general free-edge multilayer plate problems are obtained with efficient lamination-theory element modeling of most of the structure, while TFQE elements provide additional warping degrees of freedom at and near the free edges where the warping effect is important. This method of analysis has been developed for both static (mechanical and thermal loading) and transient response analyses.

Several examples, for which other numerical solutions exist, have been solved by using the TFQE and/or the TFQE in combination with MLP3K elements. The results compare well, but a significant reduction in the number of unknowns of the equations has been achieved in the present TFQE solution.

Finally, some numerical methods for solving static and transient response equations have been reviewed.

FOREWORD

This research has been conducted by the Aeroelastic and Structures Research Laboratory, Department of Aeronautics and Astronautics, Massachusetts Institute of Technology, Cambridge, Massachusetts under Contract No. DAAG46-78-C-0015 from the Army Materials and Mechanics Research Center, Watertown, Massachusetts. Mr. J.F. Dignam of the AMMRC was project manager and Dr. S.C. Chou of the AMMRC served as technical monitor. The advice and guidance of Mr. Dignam and Dr. Chou in this research are much appreciated.

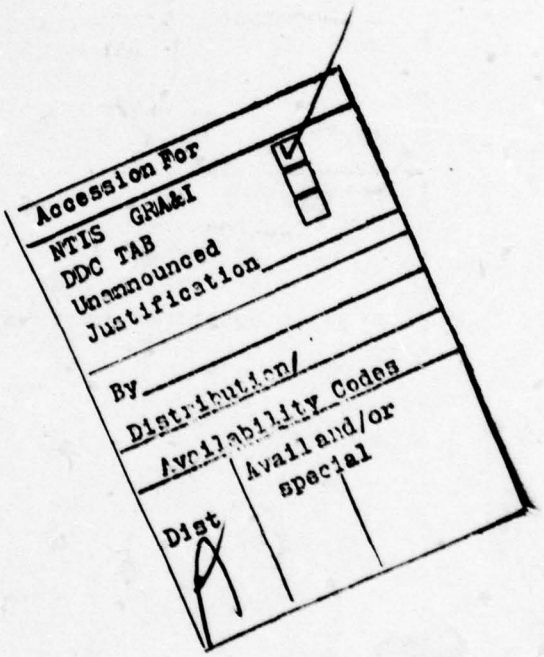

CONTENTS

CONTENTS (Continued)

CONTENTS (Concluded)

LIST OF ILLUSTRATIONS

LIST OF ILLUSTRATIONS (Continued)

LIST OF ILLUSTRATIONS (Continued)

LIST OF ILLUSTRATIONS (Continued)

LIST OF ILLUSTRATIONS (Continued)

LIST OF ILLUSTRATIONS (Concluded)

TABLE

SECTION 1

INTRODUCTION

1.1 Brief State of the Art Review on Traction-Free Edge Effects Studies

Composite materials are often used in missile and aircraft structures. They have high strength-to-weight ratios and, hence, from that viewpoint form good structural materials for plate and shell structures. However, at traction-free edges, laminates tend to develop large interfacial stresses. Further, methods for predicting these stresses accurately and efficiently are not yet available. A basic understanding of and a means of predicting these stresses accurately is sought in the present study. Two classical problems as described in the following can be used to study this interlaminar stress behavior.

The first is a 4-ply $(0/90)_s$ coupon under tension (Fig. 1) with uniform strain ε_x imposed over each end face. The solution [1]*, neglecting loaded-end effects, is independent of x. The stresses are uniform in the interior of the laminate, but rapid changes occur in a "boundary layer" near the free edge as shown in Fig. 2. As indicated schematically in Fig. 3 for individual plies, the interfacial normal stress σ_z balances the moment arising from σ_y on the 0° ply and σ_y on the 90° ply. Thus, a normal stress σ_y induces the interlaminar (a) normal stress σ_z and (b) shear stress τ_{yz} at and near the free edge. The σ_z stress at such locations is usually the more critical.

The second classical problem is an angle-ply coupon $(\pm 45)_s$ in tension as depicted also in Fig. 1. Similarly, neglecting loaded-end effects, the solution is independent of x. The stresses [1,2] are again uniform in the interior of the laminate and rapid changes occur in a "boundary layer" near the free edge as shown in Fig. 4. For equilibrium at the +45/-45 interface (Fig. 5), the interlaminar shear stress τ_{xz} balances τ_{xy}. Here, an inplane shear stress τ_{xy} induces a significant τ_{xz} at and near the free

---

* Numbers in square brackets [ ] denote references which appear in the reference list at the end of the text.

edge. In both coupons even though ε_x is constant, the normal stress σ_x varies rapidly along y near the free edge as shown in Refs. 1 and 2.

In a general laminate problem, importantly large inplane stresses σ_y and τ_{xy} occur near the free edge, and these induce all three interlaminar stresses σ_z, τ_{yz}, and τ_{xz}. When σ_z is tension, these stresses can cause ply delamination [3,4]. These two classical problems have been solved by many researchers using a variety of approximate methods. The methods employed, the results obtained, and the attributes and limitations of those approaches are reviewed in the following paragraphs.

The earliest solution was by Puppo and Evensen [2]. They solved the $(\pm 45)_s$ coupon problem by modeling the bond between the plies of a laminate with a finite isotropic layer to produce equivalent interlaminate shear stiffness and, thus, averaged the shear stresses τ_{yz} and τ_{xz} at ply interfaces. In this method it is assumed that $\sigma_z \equiv 0$ and, hence, this approach cannot be used to solve the $(0/90)_s$ laminate problem.

Finite-difference solutions of both problems were obtained by Pipes and Pagano [1,5]. The solutions for the stresses σ_z and τ_{xz} <u>at the free edge</u> are not shown even for very fine meshes and, hence, these stresses may be singular at this location. The number of unknowns from the resulting equations was about 1200.

Bogy [6] using Airy's stress function analyzed edge-bonded, dissimilar <u>isotropic</u> wedges and found singular stress distributions of type $r^{-\alpha}$ at the interface, where r is the "radial distance" measured from the intersection of the interface with the free edge. The power term α in his solution depends on the ratios of the two shear moduli and of the two Poisson ratios. This analysis has not yet been extended to orthotropic materials. However, in real laminates, the material is two-phase (resin and fiber), and a gradual transition of material properties occurs between plies. Thus, a two-phase modeling of composites may avoid such singularities as found in the problem analyzed in Ref. 6.

Rybicki [7] analyzed both problems with three-dimensional finite elements based on the Principle of Complementary Energy. Rybicki modeled only the upper symmetrical half of the laminate and consequently had to solve for 492 unknowns. The interlaminar stresses at the loaded-ends

are of interest and a detailed discussion of these can be found in Ref. 4.

Wang and Crossman [8] modeled typical cross sections of both coupons with constant-strain triangular finite elements. To achieve an accurate prediction of the rapidly-varying boundary layer stresses, they used 16 elements through the thickness of each ply near the free edge, with a total of 196 elements for each ply. Thus, even simple cases require a large number of elements in this procedure.

Pagano [9] applied a higher order plate theory derived by Whitney and Sun [10] to determine the interlaminar normal stress σ_z in the $(0/90)_s$ laminate depicted in Fig. 1. The solution correlates quite well with the finite-difference results of Pipes and Pagano [5]. However, the theory violates interlaminar stress continuity; hence, the solution for τ_{yz} is poor.

By using Reissner's Principle [11], Pagano [12] developed an approximate theory for laminated composites. By making assumptions of z variations of the stresses, the equations are reduced to two independent variables: x and y. The unknowns are seven generalized displacements and six stresses for each ply or layer; each ply can be modeled by several sublayers for improved accuracy. Using this theory, he solved both of the aforementioned classical examples [13]. However, the resulting equations are coupled partial differential equations, and the boundary conditions involve a combination of various derivatives. Hence, such equations would be difficult to solve for general problems.

Tang [14,15] applied boundary layer theory to solve the classical examples cited in Fig. 1. Based on the proof by Friedrichs and Dressler [16] for isotropic plates, Tang constrains the six stresses and three displacements as either odd or even in each ply. This procedure in each ply is questionable because the solution does not satisfy interply stress continuity. Tang also applied this approach to the analysis of a circular cutout in an infinite plate in tension [17], and a simply-supported uniformly-loaded plate [18].

Wang [19] using 3-D finite elements based on a modified form of Reissner's Principle [11], analyzed both coupon problems. His solutions compare well with the finite-difference solution of Pipes [1]. In this method the traction conditions at the free edge and at layer interfaces are satisfied exactly either analytically or by the use of Lagrange multipliers similar to the method developed by Mau and Witmer [20].

Rybicki and Schmueser [21] analyzed a tension-loaded laminated plate with a circular hole. Taking advantage of symmetry, they modeled an eighth of the plate with 36 three-dimensional finite elements. This mesh is rather crude, but the analysis provides a qualitative picture of the solution.

In classical elasticity, the solution of a tension-loaded isotropic plate with a circular hole is based on the theory of generalized plane stress. However, when the thickness of the plate is of the same order as the diameter of the hole, the deviation from the plane-stress assumption is significant. Alblas [22] analyzed the three-dimensional stresses for this problem by using complex eigenfunctions [23] but the analysis is restricted to special problems. Green [24] also analyzed the same problem by assuming the stresses to be expressible by series in sines and cosines.

The above methods have been applied to solve a very restricted class of problems. The numerical procedures (finite difference and finite element) are limited by computer storage; also, the approximate methods employed are difficult to apply to more general problems which may involve complex edge geometries and loading. Thus, an efficient solution procedure is needed for the stress analysis of laminates to provide accurate predictions of important interlaminar stresses which can occur at and near free edges.

1.2 Outline of the Present Investigation

In the present research, a multilayer warping element with a traction-free edge as depicted in Fig. 6 is developed for finite element modeling at free surfaces; this element is termed the traction-free quadrilateral element (TFQE). The element is based on the Principle of Modified Complementary Energy [25]+, in which the requirements of interelement

+An alternate formulation is also possible by modifying certain surface integrals in the Principle of Modified Complementary Energy; see page 7 of Ref. 48 for details.

traction compatibility and applied boundary traction compatibility are relaxed; that is, these interelement conditions are satisfied in an integral sense by the use of Lagrange multipliers. The free boundary is finely modeled with inplane degrees of freedom, u and v, at each ply face, and a quadratic distribution of w through the thickness. This is necessary because the large interlaminar stresses produce cross-sectional warping. However, these stresses decay rapidly (in a boundary-layer length which is of the order of a laminate thickness, 2H); hence, away from the free edge, the boundary is simply modeled by five degrees of freedom at each of its two nodal stations.

The stresses are assumed in terms of polynomials with unknown coefficients (β) and they satisfy the equations of equilibrium exactly. Since rapid gradients occur normal to the free edge, the stress along y is interpolated with polynomials up to degree four. Tangentially along the free edge (x-axis), the stresses are assumed to vary linearly. The stress assumption includes no singularities.

Previous investigations by Mau and Witmer [20] and Wang [9] included interlayer traction continuity in the formulation by the use of Lagrange multipliers. However, this leads to several additional matrix manipulations and also doubles the storage needed for the element. Hence, the interlayer traction continuity is enforced analytically in the present study.

To analyze a laminate in regions not including the free edge, its interior is modeled by laminated plate elements [26] which are based on lamination theory. These elements (named MLP3K) include transverse shear deformation and are compatible with the free edge element (TFQE). Thus, numerical results for general free-edge problems are obtained with an efficient lamination-theory element modeling of most of the structure, while TFQE elements provide additional warping degrees-of-freedom at and near the free edges where the warping effect is important. The analysis is developed for both static and dynamic problems under mechanical and thermal loading. The traction-free quadrilateral element (TFQE) is tested for accuracy and efficiency by comparing predictions obtained from its use with existing numerical solutions.

SECTION 2

OBSERVATIONS ON ASSUMED-DISPLACEMENT ELEMENTS

2.1 Objectives

Since the assumed-displacement element is widely used for structural analysis, the consequences of its use in terms of efficiency and accuracy are examined in the following for the analysis of "free-edge" problems. A representative eight-node quadrilateral assumed-displacement element (QUAD8), is used to analyze the $(0/90)_s$ coupon in tension as depicted in Fig. 1. The QUAD8 element [27] is based on a biquadratic assumed displacement field (i.e., stresses are fully bilinear with some quadratic terms); a schematic of the QUAD8 element with its node points is given in Fig. 7a. Three uniform meshes are used to analyze this coupon problem: (a) 176 elements with 1178 degrees of freedom, (b) 224 elements with 1490 degrees of freedom (see Fig. 7b), and (c) 320 elements with 2114 degrees of freedom. The midplane interlaminar normal stress solution (σ_z vs. y/b at z=0) were found to be converged for all three meshes. However, serious stress violations occur in all three meshes at the 0/90 interface near the free edge. The inaccuracies in the solution will be illustrated by plots for Mesh (b) to show the limitations of QUAD8 which is representative of assumed-displacement elements.

2.2 Formulation Review

The general stress-strain relation for orthotropic material is [28]

$$\begin{bmatrix} \sigma_x \\ \sigma_y \\ \sigma_z \\ \tau_{yz} \\ \tau_{xz} \\ \tau_{xy} \end{bmatrix} = \begin{bmatrix} C_{11} & C_{12} & C_{13} & 0 & 0 & C_{16} \\ C_{21} & C_{22} & C_{23} & 0 & 0 & C_{26} \\ C_{31} & C_{32} & C_{33} & 0 & 0 & C_{36} \\ 0 & 0 & 0 & C_{44} & C_{45} & 0 \\ 0 & 0 & 0 & C_{54} & C_{55} & 0 \\ C_{61} & C_{62} & C_{63} & 0 & 0 & C_{66} \end{bmatrix} \begin{bmatrix} \varepsilon_x \\ \varepsilon_y \\ \varepsilon_z \\ \gamma_{yz} \\ \gamma_{xz} \\ \gamma_{xy} \end{bmatrix} \qquad (2.1)$$

where the material properties C_{ij} are defined with respect to the element x,y,z axes -- not the material axes of a ply. However, because of the particular orientations of the plies (Fig. 1), the coupling shear stiffness coefficients vanish in every layer; that is,

$$C_{45} = C_{16} = C_{26} = C_{36} = 0 \tag{2.2}$$

In such cases, the displacement field can be assumed to be [9]:

$$u = \varepsilon_x x \tag{2.3a}$$

$$v = v(y,z) \tag{2.3b}$$

$$w = w(y,z) \tag{2.3c}$$

From Eqs. 2.1, 2.2, and 2.3:

$$\gamma_{xz} = \gamma_{xy} = \tau_{xy} = \tau_{xz} = 0 \tag{2.4}$$

The stress-strain relations for the bidirectional laminate then reduce to:

$$\begin{bmatrix} \sigma_x \\ \sigma_y \\ \sigma_z \\ \tau_{yz} \end{bmatrix} = \begin{bmatrix} C_{11} & C_{12} & C_{13} & 0 \\ C_{12} & C_{22} & C_{23} & 0 \\ C_{13} & C_{23} & C_{33} & 0 \\ 0 & 0 & 0 & C_{44} \end{bmatrix} \begin{bmatrix} \varepsilon_x \\ \varepsilon_y \\ \varepsilon_z \\ \gamma_{yz} \end{bmatrix} \tag{2.5}$$

The potential energy functional for a bidirectional laminate with zero body forces and applied tractions is

$$\Pi_p = \iiint_V \bar{U}\,(v, w, \varepsilon_x)\, dV \tag{2.6}$$

where the strain energy $\bar{U}$ per unit volume is [28]:

$$\bar{U} = \frac{1}{2}\left[C_{11}\,\varepsilon_x^2\right] + \left[C_{12}\,\varepsilon_x\,\varepsilon_y + C_{13}\,\varepsilon_x\,\varepsilon_z\right]$$
$$+\frac{1}{2}\left[C_{22}\,\varepsilon_y^2 + C_{33}\,\varepsilon_z^2 + C_{44}\,\gamma_{yz}^2 + 2C_{23}\,\varepsilon_y\,\varepsilon_z\right] \tag{2.7}$$

The first term in Eq. 2.7 is a constant whose contribution vanishes when one evaluates the variation of π_p. The second and third terms generate the element nodal forces and the stiffness matrix, respectively. The displacement field in each element is quadratic and is written as

$$v = p_i(y,z)\,v_i \tag{2.8a}$$

$$w = p_i(y,z)\,w_i \qquad (i = 1,8) \tag{2.8b}$$

where

$p_i(y,z)$ = biquadratic shape functions* [29,30]

v_i, w_i = nodal-displacement degrees of freedom in directions y and z, respectively

The element stiffness and force matrices are obtained by substituting Eqs. 2.8 into Eq. 2.7 and integrating over the element volume, as discussed in Ref. 27.

2.3 Finite Element Mesh and Material Properties

Since the problem is symmetric about both the y and z axes (Fig. 1), only a quadrant of the cross section is analyzed. Three uniform meshes were investigated to assess convergence:

(a) 8 elements along z and 22 elements along y (total of 176 elements with 1178 degrees of freedom).

---

*These very lengthy expressions are not included in this report but may be found in Refs. 29 and 30.

(b) 8 elements along z and 28 elements along y (total of 224 elements with 1490 degrees of freedom).

(c) 8 elements along z and 40 elements along y (total of 320 elements with 2114 degrees of freedom).

The differences in the solutions obtained from the three meshes were negligible. Hence, only the results from Mesh (b) will be presented. This mesh and the nomenclature are shown in Fig. 7.

Of particular interest in the present case are elements 212, 213, 220, and 221 which contain the 0/90 interface near the free edge. Stress plots of this region will be presented subsequently with respect to the auxiliary coordinate $\bar{y}$, which measures inward from the free edge.

The ply properties represent a typical high strength graphite/epoxy material:

$$E_L = 20 \times 10^6 \text{ psi}; \quad E_T = E_z = 2.1 \times 10^6 \text{ psi}$$

$$G_{LT} = G_{Lz} = G_{Tz} = 0.85 \times 10^6 \text{ psi}$$

$$\nu_{LT} = \nu_{Lz} = \nu_{Tz} = 0.21$$

where L, T and z refer, respectively, to the longitudinal, transverse, and thickness directions of the ply.

2.4 Results

A plot of σ_z at the symmetry plane z=0 is shown in Fig. 8. The solution agrees well with the finite element analysis of Wang and Crossman [8], and an analysis based on Reissner's Principle by Pagano [11]. However, such a limited comparison can lead to an erroneous conclusion about the accuracy of the finite element solution at other locations in the laminate.

In formulating displacement elements, traction continuity conditions at interelement boundaries and traction-free conditions at free edges

are not enforced. Hence, when the displacement-field gradients in the structure exceed the gradient capability of the finite-element interpolation polynomials, serious local violations of these conditions can occur. In the present solution, inaccuracies exist at the 0/90 interface (z=h) near the free edge (y=b or $\bar{y}$=0).

At z=h, the normal stress σ_z is plotted along the interface in Fig. 9. Serious errors in stress continuity occur at and near the free edge. Similarly, the shear stress τ_{yz} is plotted at z=h in Fig. 10. Here, not only is stress continuity violated, but also the traction-free condition, τ_{yz}=0 at $\bar{y}$=0, is violated in element 221. In Fig. 11, the in-plane normal stress σ_y is plotted at various locations through the laminate thickness. Serious errors in the traction-free condition σ_y=0 at $\bar{y}$=0, occur at the 0/90 interface (note, however, that σ_y does not have to be continuous across the 0/90 interface). Finally, Fig. 12 shows plots of σ_z through the laminate thickness at the free edge. Each line segment between two dots represents the stress distribution in one element. The curve is discontinuous because of interelement traction continuity violations.

It is apparent that serious traction violations occur in the vicinity of the 0/90 interface. Uncritical acceptance of these results would indicate that a "maximum" in σ_z occurs at z=0.75h. Similar distributions were obtained for Meshes (a) and (c).

2.5 Discussion and Conclusions

A $(0/90)_s$ coupon in tension is analyzed using eight-node quadrilateral assumed-displacement elements. The distribution of σ_z vs. y at the mid-plane agrees well with existing numerical solutions. However, such a limited comparison can lead to an erroneous conclusion about the accuracy of the whole finite element solution because serious violations of traction continuity and traction-free conditions exist. These errors occur when the displacement-field gradients in the structure exceed the ability of the element interpolation polynomials to follow the solution. One possible remedy is to refine the mesh locally, but this increases the unknowns in the model, which is already quite large (1490 degrees-of-freedom). Also, complex mesh generation is required.

In their analysis, Wang and Crossman [8] predicted that $\sigma_{z_{max}}$ occurs at z=h, y=b. In the present assumed-displacement analysis, $\sigma_{z_{max}}$ occurs at z=0.75h, y=b. However, such maxima cannot be taken seriously in view of the many deficiencies present in the assumed-displacement finite-element models and solution.

Thus, it appears that assumed displacement elements are quite inefficient for analyzing the behavior at and near free edges in composites. The critical stress gradients cannot be accommodated in an element without increasing its degrees of freedom rather drastically; however, in hybrid stress elements, this can be done efficiently. Hence, a hybrid stress, multilayer, warping plate element with a traction-free edge has been developed for composite plates and shells in the present study and is described next in Sections 3 and 4.

SECTION 3

REVIEW OF THE HYBRID STRESS FINITE ELEMENT FORMULATION

In order to satisfy explicitly and exactly the zero-stress conditions on the free edge of a multilayer structure[+], it is useful for constructing a finite element analysis to use a variational principle in which conditions on this free-edge bounding surface are accounted for explicitly and separately from the (many) other terms which involve (a) the (interior) volume of the element, (b) element bounding surfaces having non-prescribed tractions, and (c) element boundary surfaces with non-zero prescribed tractions. A variational principle which provides these features and attributes is the Principle of Modified Complementary Energy [25]; this principle is employed as described in Subsection 3.1 for the finite element analysis of mechanically- and thermally-loaded structures under static conditions.

To include inertial forces in a dynamic analysis, it is convenient to employ the modified Hellinger-Reissner Variational Principle [20,31,32] as described in Subsection 3.2.

For clarity, only the general formulation of the finite element equations is outlined in Subsections 3.1 and 3.2. The implementation details in terms of specific finite element descriptions are given in Section 4.

3.1 Static Analysis

3.1.1 Formulation

The Principle of Modified Complementary Energy [25] for a continuum which is to be modeled by a total of N finite elements may be written as

$$\pi_{mc} = \sum_{n=1}^{N} \left[-\int_{V_n} \left(\tfrac{1}{2} \underset{\sim}{\sigma}^T \underset{\sim}{S} \underset{\sim}{\sigma} + \underset{\sim}{\varepsilon}_o^T \underset{\sim}{\sigma} \right) dV + \int_{\partial V_n} \underset{\sim}{T}^T \underset{\sim}{u}^* \, ds - \int_{S\sigma_n} \underset{\sim}{\bar{T}}^T \underset{\sim}{u}^* \, ds \right] \tag{3.1}$$

[+] This is essential if accurate stresses at and near the free edge of a multilayer laminate are to be predicted from a finite-element analysis.

where

$\underset{\sim}{\sigma}$ = stress tensor

$\underset{\sim}{\varepsilon}_o$ = thermal strain (from known temperature change ΔT and given thermal expansion coefficient data)

$\underset{\sim}{S}$ = material elasticity matrix relating strains to stresses

$\underset{\sim}{T}$ = boundary traction

$\underset{\sim}{u}^*$ = displacement vector (note that this quantity appears in Eq. 3.1 only along the boundary (not in the interior of the element); the star superscript means that the displacement is on the boundary[+] Γ

$\underset{\sim}{\bar{T}}$ = prescribed boundary traction

V_n = volume of the nth element

∂V_n = entire boundary surface of the nth element

S_{σ_n} = portion of ∂V_n on which tractions (non-zero or zero) are prescribed

n = the nth element of the N elements which are used to model the structural continuum

The governing finite element equations are obtained from the condition that the variation of π_{mc} shall be zero: $\delta\pi_{mc}=0$.

The stresses $\underset{\sim}{\sigma}$ appearing in Eq. 3.1 pertain to the interior volume V_n of the element n and can be written as

$$\underset{\sim}{\sigma} = \underset{\sim}{P}\underset{\sim}{\beta} + \underset{\sim}{P}_t\underset{\sim}{\beta}_t - \underset{\sim}{S}^{-1}\underset{\sim}{\varepsilon}_o \qquad (3.2)$$

$$= \underset{\sim}{P}\underset{\sim}{\beta} + \underset{\sim}{P}_t\underset{\sim}{\beta}_t + \underset{\sim}{P}_o\underset{\sim}{\beta}_o$$

[+]Later, displacements in the interior are denoted by $\underset{\sim}{u}$.

where the $\underset{\sim}{\beta}$ are unknown parameters and the $\underset{\sim}{P}$ are appropriate spatial interpolation functions such that $\underset{\sim\sim}{P}\underset{\sim}{\beta}$ satisfies equilibrium and traction conditions (see Subsection 4.2 for details); both $\underset{\sim t\sim t}{P}\underset{\sim t}{\beta}$ and $\underset{\sim o\sim o}{P}\underset{\sim o}{\beta}$ are functions of the unknown thermal loading. The term $\underset{\sim o\sim o}{P}\underset{\sim o}{\beta}$ is the equivalent thermal stress obtained from the known $\underset{\sim o}{\varepsilon}(x,y,z,t)$ and the stress-strain relations. The term $\underset{\sim t\sim t}{P}\underset{\sim t}{\beta}$ is chosen such that equilibrium and traction conditions are satisfied for any given $\underset{\sim o\sim o}{P}\underset{\sim o}{\beta}$ (see Subsection 4.3 for details).+

The boundary tractions $\underset{\sim}{T}$ pertain only to the boundary ∂V_n (including S_{σ_n}) -- not to the interior volume V_n -- and may be expressed from Eq. 3.2 and the direction cosines of the boundary as:

$$\underset{\sim}{T} = \underset{\sim}{R}\underset{\sim}{\beta} + \underset{\sim t}{R}\underset{\sim t}{\beta} - \underset{\sim o}{R}\underset{\sim o}{\beta} \tag{3.3}$$

where $\underset{\sim}{R}$, $\underset{\sim t}{R}$, and $\underset{\sim o}{R}$ are the interpolation functions given by Eq. 3.2 but evaluated at the traction-boundary locations. If there are no temperature changes, both $\underset{\sim t\sim t}{R}\underset{\sim t}{\beta}$ and $\underset{\sim o\sim o}{R}\underset{\sim o}{\beta}$ are zero.

The boundary displacements $\underset{\sim}{u}^*$ may be interpolated in terms of the nodal generalized-displacement degrees-of-freedom $\underset{\sim}{q}$ (see Subsection 4.5.2) as:

$$\underset{\sim}{U}^* = \underset{\sim}{L}\,\underset{\sim}{q} \tag{3.4}$$

where, as indicated Fig. 6, the $\underset{\sim}{q}$ have been selected at convenient locations on the boundary of the element.

Substituting Eqs. 3.2, 3.3, and 3.4 into Eq. 3.1, one obtains (constants are omitted since they vanish under variation):

$$\pi_{mc} = \sum_{n=1}^{N}\Big(-\tfrac{1}{2}\underset{\sim}{\beta}^T\underset{\sim}{H}\underset{\sim}{\beta} + \underset{\sim}{\beta}^T\underset{\sim}{G}\underset{\sim}{q} - \underset{\sim}{\beta}^T\underset{\sim t}{H}\underset{\sim t}{\beta} + \underset{\sim t}{\beta}^T\underset{\sim t}{G}\underset{\sim}{q} - \underset{\sim o}{\beta}^T\underset{\sim o}{G}\underset{\sim}{q} - \underset{\sim}{q}^T\underset{\sim M}{Q}\Big) \tag{3.5}$$

+Note that one could assume the stresses (Eq. 3.2) as $\sigma = P\beta$. However, this approach could be restrictive if one has a more general prescribed ε_o distribution than that assumed in $P\beta$ (see p. 43 of Ref. 20).

where

$$\underset{\sim}{H} = \int_{V_n} \underset{\sim}{P}^T \underset{\sim}{S} \underset{\sim}{P} \, dv \tag{3.6}$$

$$\underset{\sim}{G} = \int_{\partial V_n} \underset{\sim}{R}^T \underset{\sim}{L} \, ds \tag{3.7}$$

$$\underset{\sim}{H}_t = \int_{V_n} \underset{\sim}{P}^T \underset{\sim}{S} \underset{\sim}{P}_t \, dv \tag{3.8}$$

$$\underset{\sim}{G}_t = \int_{\partial V_n} \underset{\sim}{R}_t^T \underset{\sim}{L} \, ds \tag{3.9}$$

$$\underset{\sim}{G}_0 = \int_{\partial V_n} \underset{\sim}{R}_0^T \underset{\sim}{L} \, ds \tag{3.10}$$

$$\underset{\sim}{Q}_M = \int_{S\sigma_n} \underset{\sim}{L}^T \underset{\sim}{\bar{T}} \, ds = \text{applied mechanical generalized traction loads} \tag{3.11}$$

Since the $\underset{\sim}{\beta}$ are independent for each element, they can be eliminated in terms of the $\underset{\sim}{q}$ by setting

$$\delta \pi_{mc} = \frac{\partial \pi_{mc}}{\partial \beta} \delta \beta + \frac{\partial \pi_{mc}}{\partial q} \delta q = 0 \tag{3.12a}$$

In particular, $\frac{\partial \pi_{mc}}{\partial \beta} = 0$ for each element separately; this yields:

$$\underset{\sim}{\beta} = \underset{\sim}{H}^{-1} \underset{\sim}{G} \underset{\sim}{q} - \underset{\sim}{H}^{-1} \underset{\sim}{H}_t \underset{\sim}{\beta}_t \tag{3.12b}$$

Substituting Eq. 3.12b into Eq. 3.5, one obtains

$$\pi_{mc} = \sum_{n=1}^{N} \left[\frac{1}{2} \underset{\sim}{q}^T \underset{\sim}{k} \underset{\sim}{q} - \underset{\sim}{q}^T \underset{\sim}{Q}_T - \underset{\sim}{q}^T \underset{\sim}{Q}_M \right] \tag{3.13}$$

where

$$\underset{\sim}{k} = \underset{\sim}{G}^T \underset{\sim}{H}^{-1} \underset{\sim}{G} \quad = \text{element stiffness matrix,} \tag{3.14}$$

$$\underset{\sim}{Q}_T = \underset{\sim}{G}^T \underset{\sim}{H}^{-1} \underset{\sim}{H}_t \underset{\sim}{\beta}_t + \underset{\sim}{G}_o^T \underset{\sim}{\beta}_o - \underset{\sim}{G}_t^T \underset{\sim}{\beta}_t \tag{3.15}$$

= generalized thermal loads vector for the element

and $\underset{\sim}{Q}_M$ is given by Eq. 3.11.

Next, let the element property descriptions which are now expressed in terms of local element coordinates x,y,z and local element generalized displacements $\underset{\sim}{q}$ be described with respect to the same global reference coordinates X,Y,Z and <u>global</u> element generalized displacement $\underset{\sim}{q}^*$ by the usual geometric transformation matrix $\underset{\sim}{T}$ [30]:

$$\underset{\sim}{q}_n = \underset{\sim}{T}_n \, \underset{\sim}{q}_n^* \tag{3.16}$$

Accordingly, Eq. 3.13 becomes

$$\pi_{mc} = \sum_{n=1}^{N} \left[\frac{1}{2} \underset{\sim}{q}_n^{*T} \underset{\sim}{k}_n^* \underset{\sim}{q}_n^* - \underset{\sim}{q}_n^{*T} \underset{\sim}{Q}_{M_n}^* - \underset{\sim}{q}_n^{*T} \underset{\sim}{Q}_{T_n}^* \right] \tag{3.17}$$

where

$$\underset{\sim}{k}_n^* = \underset{\sim}{T}_n^T \underset{\sim}{k}_n \underset{\sim}{T}_n = \text{element global stiffness matrix}$$

$$\underset{\sim}{Q}_{T_n}^* = \underset{\sim}{T}_n^T \underset{\sim}{Q}_{T_n} \quad = \text{global thermal loads vector} \tag{3.17a}$$

$$\underset{\sim}{Q}^{*}_{M_\lambda} = \underset{\sim}{T}^{T}_{\lambda}\,\underset{\sim}{Q}_{M_\lambda} = \text{global mechanical loads vector} \qquad \text{(3.17a concluded)}$$

Finally, let the structure be represented by N finite elements which are joined to each other compatibly along interelement boundaries. In particular, let that compatibility be expressed in terms of compatibility of the generalized global nodal displacements $\underset{\sim}{q}^*$ defined at the interelement boundaries. Then setting $\delta\pi_{mc}=0$ for the complete assembled discretized structure gives

$$\left[\delta \underset{\sim}{q}^{*}\right]^{T}\left(\underset{\sim}{K}\,\underset{\sim}{q}^{*} - \underset{\sim}{F}_{M} - \underset{\sim}{F}_{T}\right) = 0 \qquad (3.18)$$

Since the $\delta\underset{\sim}{q}^*$ are independent and arbitrary, one obtains the following algebraic equations of <u>static</u> equilibrium for the complete assembled discretized structure:

$$\underset{\sim}{K}\,\underset{\sim}{q}^{*} = \underset{\sim}{F}_{M} + \underset{\sim}{F}_{T} \qquad (3.19)$$

where the assembled stiffness $\underset{\sim}{K}$ and force matrices $\underset{\sim}{F}_M$ and $\underset{\sim}{F}_T$ are found from assembling the Eq. 3.17a element global contributions:

$$\underset{\sim}{K} = \begin{bmatrix} \underset{\sim}{k}^{*}_{1} & & \\ & \ddots & \\ & & \underset{\sim}{k}^{*}_{N} \end{bmatrix} \qquad (3.19a)$$

$$\underset{\sim}{F}_{M} = \left[\underset{\sim}{Q}^{*}_{M_1} - - - - - \underset{\sim}{Q}^{*}_{M_N}\right]$$

$$\underset{\sim}{F}_{T} = \left[\underset{\sim}{Q}^{*}_{T_1} - - - - - \underset{\sim}{Q}^{*}_{T_N}\right]$$

3.1.2 Solution Procedure

For static analysis the algebraic equilibrium equations of the structure (Eq. 3.19) can be written as

$$\underset{\sim}{K}\,\underset{\sim}{q}^{*} = \underset{\sim}{F} \tag{3.20}$$

where

$$F = \underset{\sim}{F}_{M} + \underset{\sim}{F}_{T}$$

The stiffness matrix $\underset{\sim}{K}$ is banded, symmetric, and positive-definite. The "direct" method for solving Eq. 3.20 is to compute $\underset{\sim}{K}^{-1}$ and to obtain the displacements $\underset{\sim}{q}^{*}$ as

$$\underset{\sim}{q}^{*} = \underset{\sim}{K}^{-1}\,\underset{\sim}{F} \tag{3.21}$$

However, this procedure is inefficient and hazardous numerically because $\underset{\sim}{K}^{-1}$ is fully populated and, therefore, requires more storage than $\underset{\sim}{K}$.

An alternate scheme is the triple-factorization and sequential solution method (see pp. 162-167 of Ref. 33 or pp. 3-11 through 3-17 of Ref. 34). This method is also called the Gauss-Doolittle decomposition with sequential solution (see pp. 21-22 of Ref. 29) and consists of two major steps:

1. The global stiffness matrix is factored into a triple product (triple factorization or Gauss-Doolittle decomposition).
2. The displacements are solved for sequentially, in three sub-steps.

The global stiffness matrix $\underset{\sim}{K}$ is factored into the form:

$$\underset{\sim}{K} = \underset{\sim}{L}\,\underset{\sim}{D}\,\underset{\sim}{L}^{T} \tag{3.22}$$

where $\underset{\sim}{L}$ is a lower triangular matrix[+] with zeros in it's upper triangular portion and unity on the diagonal, and $\underset{\sim}{D}$ is a pure diagonal matrix.

[+] Note that $\underset{\sim}{L}$ in Eq. 3.22 is totally different from the interpolation function $\underset{\sim}{L}$ defined in Eq. 3.4.

By direct substitution and comparison, one can show readily that

$$D_m = K_{mm} - \sum_{p=1}^{m-1} L_{mp}^2 D_p \tag{3.22a}$$

and

$$L_{im} = \frac{1}{D_m}\left[K_{im} - \sum_{p=1}^{m-1} L_{ip} L_{mp} D_p\right] \tag{3.22b}$$

Note that for m=1, there are no summation terms. By the use of Eq. 3.22, Eq. 3.20 may be rewritten as

$$\underset{\sim}{L}\,\underset{\sim}{D}\,\underset{\sim}{L}^T \underset{\sim}{q}^* = \underset{\sim}{F} \tag{3.23}$$

Next, let

$$\underset{\sim}{L}\,\underset{\sim}{R} = \underset{\sim}{F} \tag{3.24}$$

where

$$\underset{\sim}{R} = \underset{\sim}{D}\,\underset{\sim}{L}^T \underset{\sim}{q}^* \tag{3.24a}$$

Solving Eq. 3.24 for R, one obtains by forward solution

$$R_m = \frac{1}{L_{mm}}\left[F_m - \sum_{p=1}^{m-1} L_{mp} R_p\right] \tag{3.25}$$

Next, rewrite Eq. 3.24a as

$$\underset{\sim}{D}\,\underset{\sim}{P} = \underset{\sim}{R} \tag{3.26}$$

where

$$\underset{\sim}{L}^T \underset{\sim}{q}^* = \underset{\sim}{P} \tag{3.26a}$$

Solving Eq. 3.26, one finds

$$\underset{\sim}{P} = \underset{\sim}{D}^{-1}\underset{\sim}{R} \equiv \begin{bmatrix} R_1/D_1 \\ R_2/D_2 \\ \vdots \\ R_n/D_n \end{bmatrix} \tag{3.27}$$

Finally, Eq. 3.26a is solved by backward substitution to obtain:

$$q_n^* = \frac{P_n}{L_{nn}}$$

$$q_{n-1}^* = \frac{1}{L_{n-1\,n-1}}\left[P_{n-1} - L_{n\,n-1}\, q_n^*\right]$$

$$q_1^* = \frac{1}{L_{11}}\left[P_1 - L_{21}\, q_2^* - L_{31}\, q_3^* - \cdots - L_{n1}\, q_n^*\right] \tag{3.28}$$

Sequentially, this "computing and storing" process involves (a) solving Eq. 3.24 for $\underset{\sim}{R}$ and replacing $\underset{\sim}{F}$ by $\underset{\sim}{R}$, (b) solving Eq. 3.26 for $\underset{\sim}{P}$ and replacing $\underset{\sim}{R}$ by $\underset{\sim}{P}$, and (c) solving Eq. 3.26a for $\underset{\sim}{q}^*$ and replacing P by $\underset{\sim}{q}^*$.

Thus, by this procedure, $\underset{\sim}{q}^*$ is obtained without computing $\underset{\sim}{K}^{-1}$. The method does not require any additional space, but less computing time is required when compared with the "direct" method. For more details on factoring and sequential solving, see Ref. 34.

3.2 Dynamic Analysis

3.2.1 Formulation

For dynamic analysis an appropriate hybrid functional may be obtained from the Modified Hellinger-Reissner Principle [20,31,32]; the associated functional π_{MHR} in tensor notation with (initial) known thermal strain ϵ_{ij}^o included is

$$\Pi_{MHR} = \int_{t_1}^{t_2} \sum_{n} \left\{ \int_{V_n} \left[-\tfrac{1}{2} S_{ijkl} \sigma_{ij} \sigma_{kl} - \varepsilon^{o}_{ij} \sigma_{ij} + \tfrac{1}{2} \sigma_{ij} \left(u_{i,j} + u_{j,i} \right) \right. \right.$$

$$\left. - \tfrac{1}{2} \rho \dot{u}_i \dot{u}_i \right] dV - \int_{\partial V_n} T_i \left(u_i - u_i^* \right) ds \qquad (3.29)$$

$$\left. - \int_{S_{\sigma_n}} \bar{T}_i \, u_i^* \, ds \right\} dt$$

where the structure (continuum) has a known configuration at times t_1 and t_2, and

σ_{ij} = stress tensor

u_i = element <u>interior</u> displacement field

u_i^* = element <u>boundary</u> displacement field

S_{ijkl} = material elastic properties matrix

ρ = material mass per unit volume

T_i = boundary traction

$\bar{T}_i$ = prescribed boundary traction

V_n = volume of the nth element

∂V_n = boundary surface of the nth element

S_{σ_n} = portion of ∂V_n on which tractions are prescribed

ε^{o}_{ij} = known thermal (initial) strain

t = time

Let the boundary tractions, T_i, be expressed in terms of the stresses σ_{ij} as

$$T_i = \sigma_{ij} \nu_j \quad \text{on } \partial V_n \qquad (3.30)$$

where ν_j is the direction cosine on the element's boundary. Then using the Divergence Theorem, one of the integrals in Eq. 3.29 can be written as

$$\int_{V_n} \tfrac{1}{2} \sigma_{ij} \left(u_{i,j} + u_{j,i} \right) dV = \int_{\partial V_n} T_i \, u_i \, ds - \int_{V_n} \sigma_{ij,j} \, u_i \, dV \tag{3.31}$$

Substituting this into Eq. 3.29, one obtains a modified principle π_{MOD}:

$$\pi_{MOD} = \int_{t_1}^{t_2} \sum \left\{ \int_{V_n} \left[-\tfrac{1}{2} S_{ijkl} \sigma_{ij} \sigma_{kl} - \overset{\circ}{\varepsilon}_{ij} \sigma_{ij} - \sigma_{ij,j} \, u_i - \tfrac{1}{2} \rho \dot{u}_i \dot{u}_i \right] dV + \int_{\partial V_n} T_i \, u_i^* \, ds - \int_{S_{\sigma_n}} \bar{T}_i \, u_i^* \, ds \right\} dt \tag{3.32}$$

Also, let the stress field within each element satisfy the homogeneous portion of the equilibrium equations; that is,

$$\sigma_{ij,j} = 0 \tag{3.33}$$

Then Eq. 3.32 can be written in matrix form as

$$\pi_{DMC} = \int_{t_1}^{t_2} \sum \left\{ \int_{V_n} \left[-\tfrac{1}{2} \underset{\sim}{\sigma}^T \underset{\sim}{S} \underset{\sim}{\sigma} - \underset{\sim}{\varepsilon}_0^T \underset{\sim}{\sigma} - \tfrac{1}{2} \rho \underset{\sim}{\dot{u}}^T \underset{\sim}{\dot{u}} \right] dV + \int_{\partial V_n} \underset{\sim}{T}^T \underset{\sim}{u}^* \, ds - \int_{S_{\sigma_n}} \underset{\sim}{\bar{T}}^T \underset{\sim}{u}^* \, ds \right\} dt \tag{3.34}$$

where π_{DMC} denotes the dynamic modified complementary energy principle.

Note that Eq. 3.34 is the dynamic equivalent of Eq. 3.1 for π_{mc}. The kinetic energy term yields the mass matrix. Note that the velocity field is obtained from the interior displacement field which need not be compatible with the boundary displacements as can be seen from an inspection of Eq. 3.29 or Eq. 3.34. The interior displacement and velocity field may be written as (see Subsection 4.5.3 for details):

$$\underset{\sim}{u} = \underset{\sim}{N}\underset{\sim}{q} \qquad \dot{\underset{\sim}{u}} = \underset{\sim}{N}\dot{\underset{\sim}{q}} \tag{3.35}$$

where

$\underset{\sim}{q}$ = nodal degrees-of-freedom

$\underset{\sim}{N}$ = spatial interpolation functions

Substituting the velocity matrix into the kinetic energy expression, the mass matrix is given by

$$\underset{\sim}{m} = \int_{V_n} \rho \underset{\sim}{N}^T \underset{\sim}{N}\, dV \tag{3.36}$$

This procedure is not fully consistent with the hybrid-stress model because the hybrid stress model requires that the stresses satisfy the equilibrium equations; however, for dynamic analysis, the equations contain an inhomogeneous part caused by the inertia terms. Since only the homogeneous part (Eq. 3.33) has been satisfied in the present formulation, the mass matrix has been termed a "hybrid semi-rational" mass matrix; similar mass matrices have been employed in Refs. 20 and 35 with encouraging success.

Utilizing Eq. 3.35 and the geometric transformation matrix $\underset{\sim}{T}_n$ given by Eq. 3.16 to relate local to global element generalized nodal displacements $\underset{\sim}{q}^*$ and velocities $\dot{\underset{\sim}{q}}^*$ as well, one can show that the element mass matrix $\underset{\sim}{m}_n^*$ referred to the element's nodal global generalized velocities $\dot{\underset{\sim}{q}}_n^*$ is

$$\underset{\sim}{m}_n^* = \underset{\sim}{T}_n^T \underset{\sim}{m} \underset{\sim}{T}_n \tag{3.37}$$

Finally, imposing global generalized nodal displacement compatibility, setting $\delta\pi_{DMC}=0$, integrating by parts with respect to time, and imposing the requirements that $\delta\underset{\sim}{q}^*$ at t_1 and t_2 must be zero, one obtains the following ordinary differential equations of dynamic equilibrium:

$$\underset{\sim}{M}\ddot{\underset{\sim}{q}}^* + \underset{\sim}{k}\underset{\sim}{q}^* = \underset{\sim}{F}_M + \underset{\sim}{F}_T \tag{3.38}$$

where analogously the assembled mass matrix is

$$\underset{\sim}{M} = \begin{bmatrix} \underset{\sim}{m}_1^* & & & \\ & \ddots & & \\ & & \ddots & \\ & & & \underset{\sim}{m}_n^* \end{bmatrix} \tag{3.38a}$$

and initial conditions (at t=0 or subscript "o") $\underset{\sim}{q}_o^*$ and $\dot{\underset{\sim}{q}}_o^*$ are given.

3.2.2 Solution Procedure

For present purposes, it is assumed that only (1) prescribed transient externally-applied mechanical loads are applied and/or (2) transient temperature distributions throughout the volume of the structure are prescribed. Further, the temperature levels are assumed to be such that they do not affect the mechanical properties of the material. Also, there is no thermo-mechanical coupling in the sense that structural dynamic response does not influence the temperature distribution whereas the independently-determined transient temperatures can influence the stresses and transient mechanical response of the structure.

If transient externally-applied mechanical loads and/or thermal loads were applied to the system, one could predict the resulting transient response by one of two well-known methods. The first involves the use of normal modes which permits one to replace Eq. 3.38 by a set of single degree-of-freedom (DOF) equations of motion each of which can be solved exactly in closed form for given transient generalized modal loading by the use of the Duhamel superposition integral. However, one must first find the

natural mode shapes and frequencies embedded in the homogeneous version of Eq. 3.38 in order to obtain the normal-mode equations of motion. This was the procedure which was adopted, for example, in Ref. 35; hence, its description is not repeated here.

The second method involves the direct timewise numerical integration of Eq. 3.38 by the use of an appropriate finite-difference time operator. This is a more direct method; however, only approximate solutions at a discrete sequence of time instants can be obtained. In practice, the solution errors (a) always consist of phase distortion and (b) may also arise from false damping (positive or negative) introduced by the finite-difference time operator itself. Further, the time increment size Δt may be limited by roundoff-error instability properties of the operator; operators of the explicit type always exhibit this behavior, and the Δt size must be restricted accordingly. On the other hand timewise finite difference operators of the implicit type do not exhibit roundoff error instability and hence this effect does not limit the size of the allowable Δt. However, all of these implicit (and explicit) operators produce predictions with phase distortion which becomes increasingly severe as one utilizes a larger and larger Δt. Also, many but not all of these implicit operators exhibit false damping.

The properties of many timewise finite-difference operators have been reviewed, for example, in Refs. 36-38 for application to linear transient response problems such as represented by Eq. 3.38. For application to linear mutli-DOF systems, let it suffice to note that the Newmark β-method [39] with $\beta=1/4$ is generally regarded as being the most useful of the available implicit operators since it (a) is unconditionally stable, (b) exhibits no false damping, and (c) displays less phase distortion than the other available implicit methods. Since this method was used to obtain the transient response predictions shown in Subsection 5.2, its essentials are reviewed briefly in the following.

For this purpose consider equations of motion of the following form for linear transient response analysis:

$$\underset{\sim}{M}\ddot{\underset{\sim}{q}} + \underset{\sim}{K}\underset{\sim}{q} = \underset{\sim}{F} \tag{3.39}$$

which is similar to Eq. 3.38. Let this equation be solved in small equal increments $\Delta t(\equiv d)$ of time by the use of the Newmark-β finite-difference time operator expressed by [39]:

$$\dot{\underset{\sim}{q}}_{n+1} = \dot{\underset{\sim}{q}}_n + \left[\tfrac{1}{2}\ddot{\underset{\sim}{q}}_n + \tfrac{1}{2}\ddot{\underset{\sim}{q}}_{n+1}\right] d \qquad \text{where } d = \Delta t \tag{3.40a}$$

and

$$\underset{\sim}{q}_{n+1} = \underset{\sim}{q}_n + \dot{\underset{\sim}{q}}_n d + \left[\left(\tfrac{1}{2} - \beta\right)\ddot{\underset{\sim}{q}}_n + \beta\ddot{\underset{\sim}{q}}_{n+1}\right] d^2 + \tag{3.40b}$$

where subscripts n and n+1 denote quantities at time instants t_n and t_{n+1}; also $(\dot{})$ means differentiation with respect to time. At time t=0, let it be assumed that $\underset{\sim}{q}_o$ and $\dot{\underset{\sim}{q}}_o$ are given. Note that one can also write expressions similar to Eqs. 3.40a and 3.40b to represent $\dot{\underset{\sim}{q}}_n$, $\underset{\sim}{q}_n$, $\dot{\underset{\sim}{q}}_{n-1}$, and $\underset{\sim}{q}_{n-1}$. By so doing, then applying the results to write Eq. 3.39 at time instants t_{n+1}, t_n, and t_{n-1}, and carrying out eliminations, the following "explicit" recurrence equation [40] can be obtained:

$$\begin{aligned}\left(\underset{\sim}{M} + \beta d^2 \underset{\sim}{K}\right)\underset{\sim}{q}_{n+1} = {} & \left(2\underset{\sim}{M} - \left(1 - 2\beta\right) d^2 \underset{\sim}{K}\right)\underset{\sim}{q}_n \\ & - \left(\underset{\sim}{M} + \beta d^2 \underset{\sim}{K}\right)\underset{\sim}{q}_{n-1} \\ & + \beta d^2 \left(\underset{\sim}{F}_{n+1} + \left(\frac{1}{\beta} - 2\right)\underset{\sim}{F}_n + \underset{\sim}{F}_{n-1}\right)\end{aligned} \tag{3.41}$$

A starting procedure may be obtained in a similar fashion [40] and reads

$$\underset{\sim}{B}^*\underset{\sim}{q}_1 = \underset{\sim}{P}^*\underset{\sim}{q}_o + \underset{\sim}{Q}^*\dot{\underset{\sim}{q}}_o + \beta d^2 \underset{\sim}{F}_1 + \underset{\sim}{R}^*\underset{\sim}{F}_o \tag{3.42}$$

+ Note that β in Eq. 3.40b is totally different from the stress parameters $\underset{\sim}{\beta}$ defined in Eq. 3.2.

where

$\underset{\sim}{B}^* = \underset{\sim}{M} + \beta d^2 \underset{\sim}{K}$ $\qquad$ $\underset{\sim}{Q}^* = d\underset{\sim}{M}$

$\underset{\sim}{P}^* = \underset{\sim}{M} - (\frac{1}{2} - \beta) d^2 \underset{\sim}{K}$ $\qquad$ $\underset{\sim}{R}^* = d^2 \underset{\sim}{I} (\frac{1}{2} - \beta)$

$\underset{\sim}{I}$ = unit matrix

$\underset{\sim}{q}_o$ = known generalized displacements at t=0

$\dot{\underset{\sim}{q}}_o$ = known generalized velocities at t=0

With $\underset{\sim}{q}_1$ now known from Eq. 3.42, one can write Eq. 3.41 at n=1 to obtain:

$$\begin{aligned}\left(\underset{\sim}{M} + \beta\alpha^2 \underset{\sim}{K}\right)\underset{\sim}{q}_2 = &\left(2\underset{\sim}{M} - (1-2\beta)\alpha^2 \underset{\sim}{K}\right)\underset{\sim}{q}_1 \\ &- \left(\underset{\sim}{M} + \beta\alpha^2 \underset{\sim}{K}\right)\underset{\sim}{q}_0 \\ &+ \beta\alpha^2\left(\underset{\sim}{F}_2 + \left(\frac{1}{\beta} - 2\right)\underset{\sim}{F}_1 + \underset{\sim}{F}_0\right)\end{aligned} \tag{3.43}$$

One can then solve Eq. 3.43 for $\underset{\sim}{q}_2$ since all else is known. Next, proceed similarly to compute $\underset{\sim}{q}_3$, $\underset{\sim}{q}_4$, ... for as many time steps as desired.

To choose an appropriate time increment size $\Delta t (\equiv d)$ a rough rule-of-thumb is to provide about 20 time increments for the period of the highest significantly responding mode of the system, if known. An alternate selection might be to choose Δt to be α/ω_{max} where ω_{max} is the highest frequency of the mathematical model of the structure (homogeneous form of Eq. 3.39) and α is some number like 200 to 400 perhaps -- presuming that the principal structural response involves roughly the lowest 20 to 50 percent of the normal modes of the structure.

Observe that Eq. 3.43 at any time instant "n" can be written in the form:

$$\underset{\sim}{B}^* \underset{\sim}{q}_n = \underset{\sim}{A}_n \tag{3.44}$$

Also, note that Eq. 3.44 is of the same form as Eq. 3.29 in Subsection 3.1.2. Thus, instead of computing $\underset{\sim}{B}^{*-1}$, the triple-factorization and sequential solution method is used to obtain $\underset{\sim}{q}_n$. If the matrix $\underset{\sim}{B}^*$ does not change with time, the factored form at the first time step can be used at all of the remaining steps.

SECTION 4

FORMULATION FOR THE HYBRID STRESS MULTILAYER QUADRILATERAL FINITE ELEMENT WITH ONE TRACTION-FREE EDGE

4.1 General Considerations

As indicated in the discussion in Sections 1 and 2, it is desirable from the standpoints of stress-prediction accuracy and efficiency to base a finite element analysis of multilayer laminated thin plates upon a Modified Principle of Complementary Energy (MPCE). Finite elements based upon that variational principle are called hybrid-stress elements and have been shown to be superior for predicting displacements in static loading problems to either assumed-displacement or assumed-stress finite elements [41].

For finite-element structural analysis involving static mechanical and/or thermal loading, one can utilize the MPCE function π_{mc} given by Eq. 3.1. An examination of this equation reveals that for a finite-element analysis, one needs to devise: (a) an appropriate assumed-stress distribution throughout the volume of each element and (b) an appropriate assumed displacement field only along the side boundaries A to B, B to D, D to E, and E to A as identified, for example, in Fig. 6. This approach has been employed successfully for the analysis of multilayer laminated plates and has been reported, for example, in Refs. 20, 26, and 35. Those previous studies, however, did not include a detailed examination of the often-very-critical stresses which occur at and near the free edge of a multilayer laminated composite structure. Hence, the present study focusses chiefly upon an accurate finite-element prediction of these "critical stresses" at and near a traction-free edge. Accordingly, a special finite element called the traction-free edge quadrilateral element (TFQE) as depicted in Fig. 6 has been constructed to provide "fine detail information" at and near its traction-free edge AB, and to be compatible at its opposite edge DE with the MLP3K multilayer element of Ref. 26. The hope is that the use of the TFQE element only along the traction-free edge(s) together with another element such as MLP3K (or other similar elements) will provide the analyst with accurate and efficient predictions

of stresses at all critical locations in the multilayer laminated plate structure. Accordingly, for the TFQE depicted in Fig. 6, appropriate assumed-stress distributions have been devised as described next in Subsection 4.2. A description of the prescribed or initial (thermal) stresses is given in Subsection 4.3, while interlayer continuity conditions and the free-surface conditions on the two surfaces at $z=\pm H$ are discussed in Subsection 4.4. The selected assumed-displacement distributions along the edge boundaries of the TFQE are discussed in Subsection 4.5.2.

For dynamic response problems, the presence of inertia forces throughout the volume of the material must be taken into account. An approximate means for achieving this in a variationally-based finite element analysis of the present (hybrid) type has been indicated in Subsection 3.2 where a modification of the Hellinger-Reissner Variational Principle resulted in a π_{DMC} functional, Eq. 3.34, with inertia effects included. As Eq. 3.34 shows, for a finite element analysis one must construct an assumed displacement field throughout the volume of the element (see Subsection 4.5.3) as well as independently along the edges of the element as in the static formulation given by Eq. 3.1; also, an assumed stress distribution throughout the volume of the element is required and remains the same for the dynamic as in the static case.

Finally, Subsection 4.6 is devoted to describing the resulting behavioral features of preliminary and subsequent versions of the TFQE. In particular, in hybrid-stress formulations, one often encounters "kinematic modes" [26,42]; procedures for their identification and elimination are discussed briefly. However, an evaluation of the stress-prediction accuracy and efficiency provided by the TFQE is deferred to Section 5.

4.2 Assumed Stress Distribution

4.2.1 Selection Guidelines

If the TFQE were to provide accurate and efficient predictions of interlaminar normal and shear stresses at and near a traction-free edge,

its assumed-stress distribution should be comprehensive enough to permit representing very closely the rapid variations of each of these stresses at each interface as a function of distance y (see Fig. 6) from the free edge. Some guidance in this regard is available from the coupon-problem whose features were examined and discussed in Subsection 1.1; as a minimum therefore, the stress-distribution assumptions of the TFQE should be capable of representing those observed stress distributions faithfully. Other more complex problems may exhibit more severely changing stresses than revealed by the available pertinent examples discussed in Section 1. Thus, more general and comprehensive guidance in selecting assumed-stress distributions throughout the volume of the TFQE is desired.

Some assistance in this respect may be gained by examining well-known three-dimensional stress function formulations, and their implications for a sequence of special cases. The latter serve to indicate which terms of a general power series representation for the stress functions must be present for consistency in these several special cases. For example, consider for a Cartesian rectangular system the following stress functions for the case of no body forces:

Morera's Stress Functions [43]

$$\sigma_x = \frac{\partial^2 \psi_1}{\partial y \, \partial z} \tag{4.1a}$$

$$\sigma_y = \frac{\partial^2 \psi_2}{\partial z \, \partial x} \tag{4.1b}$$

$$\sigma_z = \frac{\partial^2 \psi_3}{\partial x \, \partial y} \tag{4.1c}$$

$$\tau_{yz} = -\frac{1}{2} \frac{\partial}{\partial x} \left(-\frac{\partial \psi_1}{\partial x} + \frac{\partial \psi_2}{\partial y} + \frac{\partial \psi_3}{\partial z} \right) \tag{4.1d}$$

$$\tau_{xz} = -\frac{1}{2}\frac{\partial}{\partial y}\left(\frac{\partial \psi_1}{\partial x} - \frac{\partial \psi_2}{\partial y} + \frac{\partial \psi_3}{\partial z}\right) \tag{4.1e}$$

$$\tau_{xy} = -\frac{1}{2}\frac{\partial}{\partial z}\left(\frac{\partial \psi_1}{\partial x} + \frac{\partial \psi_2}{\partial y} - \frac{\partial \psi_3}{\partial z}\right) \tag{4.1f}$$

where ψ_1, ψ_2, and ψ_3 are known as Morera's stress functions. For present purposes it is not necessary to examine or review the formulation of the 3-d elasticity problem in terms of these stress functions. Instead, it suffices to take note of the stress expressions which apply in the following three special cases:

Case MO-1: $\psi_2=\psi_3=0$

$$\sigma_x = \frac{\partial^2 \psi_1}{\partial y\, \partial z} \qquad \tau_{xz} = -\frac{1}{2}\frac{\partial^2 \psi_1}{\partial x\, \partial y} \tag{4.2}$$

$$\tau_{yz} = \frac{1}{2}\frac{\partial^2 \psi_1}{\partial x^2} \qquad \tau_{xy} = -\frac{1}{2}\frac{\partial^2 \psi_1}{\partial z\, \partial x}$$

Case MO-2: $\psi_1=\psi_3=0$

$$\sigma_y = \frac{\partial^2 \psi_2}{\partial z\, \partial x} \qquad \tau_{xz} = \frac{1}{2}\frac{\partial^2 \psi_2}{\partial y^2} \tag{4.3}$$

$$\tau_{yz} = -\frac{1}{2}\frac{\partial^2 \psi_2}{\partial x\, \partial y} \qquad \tau_{xy} = -\frac{1}{2}\frac{\partial^2 \psi_2}{\partial y\, \partial z}$$

Case MO-3: $\psi_1=\psi_2=0$

$$\sigma_z = \frac{\partial^2 \psi_3}{\partial x \partial y} \qquad \tau_{xz} = -\frac{1}{2}\frac{\partial^2 \psi_3}{\partial y \partial z} \tag{4.4}$$

$$\tau_{yz} = -\frac{1}{2}\frac{\partial^2 \psi_3}{\partial z \partial x} \qquad \tau_{xy} = \frac{1}{2}\frac{\partial^2 \psi_3}{\partial z^2}$$

Similarly, consider for the case of no body forces:

Maxwell's Stress Functions [43]

$$\sigma_x = \frac{\partial^2 \chi_3}{\partial y^2} + \frac{\partial^2 \chi_2}{\partial z^2} \tag{4.5a}$$

$$\sigma_y = \frac{\partial^2 \chi_1}{\partial z^2} + \frac{\partial^2 \chi_3}{\partial x^2} \tag{4.5b}$$

$$\sigma_z = \frac{\partial^2 \chi_2}{\partial x^2} + \frac{\partial^2 \chi_1}{\partial y^2} \tag{4.5c}$$

$$\tau_{yz} = -\frac{\partial^2 \chi_1}{\partial y \partial z} \tag{4.5d}$$

$$\tau_{zx} = -\frac{\partial^2 \chi_2}{\partial y \partial z} \tag{4.5e}$$

$$\tau_{xy} = -\frac{\partial^2 \chi_3}{\partial x \partial y} \tag{4.5f}$$

where χ_1, χ_2, and χ_3 are known as Maxwell's stress functions. Similarly, consider the stress expressions which apply in the following three special cases for the Maxwell stress functions:

Case MA-1: $\chi_2=\chi_3=0$

$$\sigma_y = \frac{\partial^2 \chi_1}{\partial z^2} \quad , \quad \sigma_z = \frac{\partial^2 \chi_1}{\partial y^2} \quad , \quad \tau_{yz} = -\frac{\partial^2 \chi_1}{\partial y \, \partial z} \tag{4.6}$$

Case MA-2: $\chi_1=\chi_3=0$

$$\sigma_x = \frac{\partial^2 \chi_2}{\partial z^2} \quad , \quad \sigma_z = \frac{\partial^2 \chi_2}{\partial x^2} \quad , \quad \tau_{xz} = -\frac{\partial^2 \chi_2}{\partial z \, \partial x} \tag{4.7}$$

Case MA-3: $\chi_1=\chi_2=0$

$$\sigma_x = \frac{\partial^2 \chi_3}{\partial y^2} \quad , \quad \sigma_y = \frac{\partial^2 \chi_3}{\partial x^2} \quad , \quad \tau_{xy} = -\frac{\partial^2 \chi_3}{\partial x \, \partial y} \tag{4.8}$$

For the present finite element formulation procedure, one may proceed in general to assume that each stress component within each layer of the multilayer element varies in x, y, and z according to some suitably comprehensive polynomial approximation in terms of unknown stress parameters β. Also, one may utilize the above special-case conditions as a check to insure that essential terms in the polynomial expressions have not been overlooked, or redundant terms are identified and deleted. A more comprehensive and systematic use of stress-function formulations could be employed perhaps; however, in the present development, distribution functions for the various stresses were selected so as to

satisfy the basic equilibrium equations, as well as the traction-free conditions on the edge AB of the TFQE, and certain interlaminar continuity conditions on the stresses and strains. Subsequently, the resulting distribution or interpolation functions were examined for consistency as required by the cited stress-function conditions.

Before discussing the selection of the assumed-stress distributions further, it is useful to define the geometry and the multilayer features of the desired finite element: the traction-free edge quadrilateral element (TFQE) which is depicted in Fig. 6. This flat-plate multilayer element shall be described with respect to the local Cartesian rectangular coordinate system x,y,z for the element with corresponding displacement u, v, and w; the single traction-free edge is selected for formulation convenience to be edge AB which is located at y=0. The origin of the coordinate system is located at corner A at the geometric midplane of the element. Without loss of generality and for reasons explained better later, side DE is chosen to be parallel to free-edge AB; also the indicated plane passing through points C and F on the non-parallel sides of the element is parallel to the planes passing through AB and DE. The TFQE is a multilayer element which need not be symmetric and consists of "many" layers; its total thickness is defined to be 2H. Each layer is assumed to consist of one or more plies of unidirectional laminate which is assumed to behave as an orthotropic linear elastic material*; each layer i may have a different thickness (defined to be $2h_i$) and a different in-plane "grain orientation" from all other layers.

Since free-edge effects typically lead to severe interlaminar stresses and stress gradients at and near a free edge but diminish rapidly with distance y normal to the free edge, it is important to represent the stress behavior in considerable detail in each layer of the multilayer laminate for a substantial region (0.95b) of the element's width b (A to E', for example) in the y direction. In particular, fine detail is desired in region ABCF while CDEF will serve as a transition region with lesser detail -- providing nodal stations D and E which can

*A layer may also consist of laid-up plies oriented in sequence such that the resulting "entire layer" acts as a homogeneous orthotropic ply.

connect "compatibly" with appropriate multilayer elements of simpler description. Accordingly, at nodal stations A, B, C, and F:

(a) nodal control displacement u_i and v_i are employed at every layer interface i to accommodate the very important warping behavior and

(b) nodal control w displacements are employed at only three locations through the thickness: top, midsurface, and bottom -- since the stresses are much less sensitively affected by the w-displacement variation through the thickness; this also reduces the number of degrees of freedom and computation compared with using a w_i at each interface.

At each of nodal stations D and E, a total of only five nodal control generalized displacements are used. These are located at the midplane nodal points D and E, and consist of u, v, w, $\theta_x (\equiv -\frac{\partial v}{\partial z})$, and $\theta_y (\equiv \frac{\partial u}{\partial z})$; where θ_x and θ_y are the rotations of the vertical plane along x and y, respectively. This assumption imposes an artificial constraint on ε_z, the alleviation of which is discussed later in Subsection 4.5.2.

4.2.2 Stress Conditions to be Satisfied

In each layer of the multilayer laminate, the following equilibrium equations (in the absence of body forces) must be satisfied:

$$\frac{\partial \sigma_x}{\partial x} + \frac{\partial \tau_{yx}}{\partial y} + \frac{\partial \tau_{zx}}{\partial z} = 0 \qquad (4.9a)$$

$$\frac{\partial \tau_{xy}}{\partial x} + \frac{\partial \sigma_y}{\partial y} + \frac{\partial \tau_{zy}}{\partial z} = 0 \qquad (4.9b)$$

$$\frac{\partial \tau_{xz}}{\partial x} + \frac{\partial \tau_{yz}}{\partial y} + \frac{\partial \sigma_z}{\partial z} = 0 \qquad (4.9c)$$

Also, at each interface i between material layers i and i+1, the following interlayer continuity conditions must be fulfilled:

$$\sigma_z^{i+1} = \sigma_z^i \,,\quad \tau_{zx}^{i+1} = \tau_{zx}^i \,,\quad \tau_{zy}^{i+1} = \tau_{zy}^i \,,\quad \text{and}\quad \varepsilon_x^{i+1} = \varepsilon_x^i \tag{4.10}$$

where superscripts i+1 and i, respectively, represent the material in layers i+1 and i. Finally, at the traction-free edge AB of the TFQE (see Fig. 6), one must satisfy on the face of every layer:

$$\sigma_y = \tau_{yx} = \tau_{yz} = 0 \qquad \text{(face AB at y=0)} \tag{4.11}$$

Since the stresses in the interior of the element are, in general, for a loaded laminated structure much greater than those applied externally to the two surfaces $z=\pm H$, the following conditions are imposed at $z=\pm H$:

$$\sigma_z = \tau_{zx} = \tau_{zy} = 0 \tag{4.12}$$

for the purpose of representing the interior stress field by assumed-stress expressions to evaluate the volume integral term in Eq. 3.1. However, non-zero externally-applied stresses or tractions on these surfaces will be taken into account to evaluate Q_M (Eq. 3.11) from the last term of Eq. 3.1.

4.2.3 Selected Stress Distributions

As depicted qualitatively for the tension-loaded 4-ply $(0/90)_s$ and $(\pm 45)_s$ coupons in Figs. 1, 2, 3, 4, and 5 -- and quantitatively in Figs. 8-12, the significant interlaminar stresses at and near the free edge are σ_z and τ_{zx}. From Fig. 8, for example, it is seen that the interlaminar σ_z varies rapidly with y (or y/b) as one proceeds along the normal from the free edge (along y) to the interior; this general type of behavior of σ_z is anticipated for many other "free edge" examples. Thus, in constructing an assumed stress distribution $\sigma_z(x,y,\bar{z})$ throughout

the interior of <u>any given layer</u>, it is apparent that a polynomial of high degree in y (or y/b) will be required; note that $\bar{z}$ is the through-the-thickness coordinate measured from the midsurface of each layer. Since for many cases σ_z is expected to vary more slowly with x and z, polynomials of lesser powers in these coordinates would be plausible; alternatively, a finer mesh of finite elements along x could be employed readily if needed. Thus, a stress distribution which is quartic in y, cubic in z, and linear in x throughout a given layer of the TFQE has been assumed as follows in terms of unknown stress parameters β:

$$\begin{aligned}
\sigma_z(x,y,\bar{z}) = {} & \left[T_0(y)\beta_1 + T_1(y)\beta_2 + T_2(y)\beta_3 + T_3(y)\beta_4 + T_4(y)\beta_5\right] \\
& + \bar{z}\left[T_0(y)\beta_6 + \cdots + T_4(y)\beta_{10}\right] \\
& + \frac{\bar{z}^2}{2}\left[T_0(y)\beta_{11} + \cdots + T_4(y)\beta_{15}\right] \\
& + \frac{\bar{z}^3}{6}\left[T_0(y)\beta_{16} + \cdots + T_4(y)\beta_{20}\right] \\
& + x\left[T_0(y)\beta_{21} + \cdots + T_4(y)\beta_{25}\right] \\
& + x\bar{z}\left[T_0(y)\beta_{26} + \cdots + T_4(y)\beta_{30}\right] \\
& + \frac{x\bar{z}^2}{2}\left[T_0(y)\beta_{31} + \cdots + T_4(y)\beta_{35}\right] \\
& + \frac{x\bar{z}^3}{6}\left[T_0(y)\beta_{36} + \cdots + T_4(y)\beta_{40}\right]
\end{aligned} \tag{4.13}$$

where the following Chebychev [44] polynomials $T_i(y)$ are used in Eq. 4.13 instead of regular polynomials since numerical tests reveal less roundoff error when the former are used:

$$T_0(y) = 1$$

$$T_1(y) = 2(y/b) - 1$$

$$T_2(y) = 8(y/b)^2 - 8(y/b) + 1$$

$$T_3(y) = 32(y/b)^3 - 48(y/b)^2 + 18(y/b) - 1$$

$$T_4(y) = 128(y/b)^4 - 256(y/b)^3 + 160(y/b)^2 - 32(y/b) + 1 \qquad (4.14)$$

$$0 \le y/b \le 1$$

where b is the y-direction width of the TFQE as indicated in Fig. 6. The $\bar{z}$ origin of each layer is located at the midsurface of that layer.

For the special case of the $(0/90)_s$ coupon (Figs. 1 and 3) with a uniform ε_x imposed on each end, $\frac{\partial \tau_{xz}}{\partial x} \doteq 0$ and $\frac{\partial \tau_{xy}}{\partial x} \doteq 0$; hence integration of Eqs. 4.9b and 4.9c, respectively, with respect to y gives

$$\sigma_y = -\int \frac{\partial \tau_{zy}}{\partial \bar{z}}\, dy + f_1(x, \bar{z}) \qquad (4.15a)$$

$$\tau_{yz} = -\int \frac{\partial \sigma_z}{\partial \bar{z}}\, dy + f_2(x, \bar{z}) \qquad (4.15b)$$

Since at the y=0 free surface, $\tau_{yx}=\tau_{yz}=0$, and after integration all terms contain y or powers of y, it follows that

$$f_1(x, \bar{z}) = f_2(x, \bar{z}) = 0 \qquad (4.16)$$

Thus, this integration does not add new $\underset{\sim}{\beta}$'s.

Similarly, the other stress which is significant at and near a free

edge is τ_{zx} and its distribution throughout a given layer of TFQE is assumed to be

$$\begin{aligned}
\tau_{zx} = & \left[T_0(y)\beta_{41} + \; - \; - \; - \; + T_4(y)\beta_{45}\right] \\
& + \bar{z}\left[T_0(y)\beta_{46} + \; - \; - \; - \; + T_4(y)\beta_{50}\right] \\
& + \frac{\bar{z}^2}{2}\left[T_0(y)\beta_{51} + \; - \; - \; - \; + T_4(y)\beta_{55}\right] \\
& + x\left[T_0(y)\beta_{56} + \; - \; - \; - \; + T_4(y)\beta_{60}\right] \\
& + x\bar{z}\left[T_0(y)\beta_{61} + \; - \; - \; - \; + T_4(y)\beta_{65}\right] \\
& + x\frac{\bar{z}^2}{2}\left[T_0(y)\beta_{66} + \; - \; - \; - \; + T_4(y)\beta_{70}\right]
\end{aligned} \tag{4.17}$$

Note that the distribution function chosen for τ_{zx} is quartic in y, quadratic in $\bar{z}$, and linear in x. The choice of quadratic rather than cubic in $\bar{z}$ (as for σ_z) was made in an effort to minimize the number of unknowns introduced without, hopefully, a serious degrading of the accuracy of this representation; the quadratic $\bar{z}$ dependence for τ_{zx} leads (as will be seen later) to a τ_{xy} expression which is linear in $\bar{z}$. However, the τ_{zx} assumed distribution could have been chosen identical to that shown for σ_z in Eq. 4.13 without apparent difficulty.

For the "tension-loaded" 4-ply $(+45, -45)_s$ coupon with imposed uniform ε_x on each end as depicted in Figs. 1, 4, and 5, one finds that σ_z, σ_y, and τ_{zy} are present but are negligible compared with τ_{xy} and τ_{zx}. Accordingly, integrating (equilibrium) Eqs. 4.9a and 4.9b with respect to y gives, respectively:

$$\tau_{yx} = -\int \frac{\partial \tau_{xz}}{\partial z}\, dy + f_3(x,z) \tag{4.18a}$$

$$\tau_{yz} = \int \frac{\partial \tau_{xz}}{\partial x}\, dy + f_4(x,\bar{z}) \tag{4.18b}$$

Since at the y=0 free surface $\tau_{yx}=\tau_{yz}=0$, and after integration all terms contain y or powers of y, it follows that

$$f_3(x,z) = f_4(x,\bar{z}) = 0 \tag{4.19}$$

Next, note that $\bar{z}$ integration of the $\bar{z}$-direction equilibrium equation (4.9c) with the inclusion of Eq. 4.18b gives

$$\sigma_{\bar{z}} = -2\int \frac{\partial \tau_{xz}}{\partial x}\, dz + f_5(x,y) \tag{4.20}$$

It should be observed that Eq. 4.20 requires the presence in σ_z of a "term" (f_5) depending only upon x and y; the "fifth" bracket term in Eq. 4.13 fulfills this need. Thus, no new β's are added after integration.

To this point in the selection of an assumed stress distribution throughout the interior of any given layer of the TFQE, a plausible polynomial expression for the spatial behavior of the stress σ_z has been chosen; Eq. 4.13 involving 40 stress parameters β is the resulting assumed distribution for $\sigma_z(x,y,\bar{z})$. Next, calling upon features observed in the $(0/90)_s$ "coupon problem", the y- and the $\bar{z}$-direction force equilibrium equations (4.9b and 4.9c) and the free-edge stress boundary conditions on side AB of the TFQE were used to deduce appropriate distribution expressions for $\sigma_y(x,y,\bar{z})$ and $\tau_{yz}(x,y,\bar{z})$: Eqs. 4.15a and 4.15b, respectively. Similarly, a plausible distribution function given by Eq. 4.17 was selected for $\tau_{zx}(x,y,\bar{z})$ for the TFQE in terms of 30 unknown stress parameters β; then physical insight from the $(+45/-45)_s$ "coupon problem", in conjunction with the x- and y-direction force equilibrium equations (4.9a and 4.9b) and the free-edge stress boundary conditions on free edge AB of the TFQE, was

used to deduce an appropropriate distribution function (Eq. 4.18a) for $\tau_{yx}(x,y,\bar{z})$ and to assess the implied relations: (1) between τ_{xz} and τ_{yz}: (Eq. 4.18b) and (2) between σ_z and τ_{xz}: (Eq. 4.20). The assumed stress distributions and the resulting expressions just cited are both plausible and exhibit no apparent inconsistencies. By this convenient but somewhat circuitous procedure, assumed distribution functions involving a total of 70 unknown stress parameters β for any given layer of the TFQE have been constructed for the stresses σ_z, σ_y, τ_{zx}, τ_{zy}, and τ_{xy}. Only $\sigma_x(x,y,\bar{z})$ remains to be constructed.

It is convenient to construct an assumed stress distribution function for $\sigma_x(x,y,\bar{z})$ in the following way. First note that in general for an orthotropic (filamentary composite) material whose "filaments" lie in the x,y plane (not necessarily aligned with either the x or the y axis), the strain ε_x may be expressed in terms of the stresses σ_x, σ_y, σ_z, and τ_{xy} from the stress-strain relations by:

$$\varepsilon_x = S_{11}\sigma_x + S_{12}\sigma_y + S_{13}\sigma_z + S_{16}\tau_{xy} \tag{4.21}$$

where the S_{ij} are the known compliance coefficients[+] of the material. Equation 4.21 can be rearranged to read

$$\sigma_x = -\frac{1}{S_{11}}\left[S_{12}\sigma_y + S_{13}\sigma_z + S_{16}\tau_{xy}\right] + \frac{\varepsilon_x}{S_{11}} \tag{4.22}$$

Note that distribution functions for σ_y, σ_z, and τ_{xy} have already been expressed in terms of many unknown stress parameters β. However, an additional contribution: ε_x/S_{11} is present; let this be termed $\bar{\sigma}_x$ where $\bar{\sigma}_x \equiv \varepsilon_x/S_{11}$. Whereas in the Fig. 1 "coupon problems" a uniform ε_x was imposed over the ends of these specimens, in general ε_x may have a significant $x,y,\bar{z}$ dependence in other more general physical situations. Hence, the contribution $\bar{\sigma}_x$ in any given layer of the TFQE is assumed to have the following spatial character:

[+]These S_{ij} coefficients are defined with respect to the x,y,z element axes -- not the material axes of the ply.

$$\bar{\sigma}_x \equiv \frac{\epsilon_x}{S_{11}} = \left[T_0(y)\beta_{71} + T_1(y)\beta_{72} + T_2(y)\beta_{73} + T_3(y)\beta_{74} + T_4(y)\beta_{75}\right]$$
$$+ \bar{z}\left[T_0(y)\beta_{76} + \quad + T_4(y)\beta_{80}\right]$$
$$+ x\left[T_0(y)\beta_{81} + \quad + T_4(y)\beta_{85}\right]$$
$$+ x\bar{z}\left[T_0(y)\beta_{86} + \quad + T_4(y)\beta_{90}\right]$$
$$+ x^2\left(\beta_{91} + \bar{z}\beta_{92} + y\beta_{93} + y\bar{z}\beta_{94}\right) \qquad (4.23)$$

Note that in this form, the special case in which ϵ_x is uniform is accounted for by a single term in Eq. 4.23; namely, $T_0(y)\beta_{71}$.

It should also be noted that consistent with the earlier assumed distribution functions (Eqs. 4.13 and 4.17), the terms in square brackets [ ] in Eq. 4.23 are quartic in y in terms of Chebychev polynomials, with these bracketed type terms added and multiplied by $\bar{z}$, x, and $x\bar{z}$; hence, these terms are of the same <u>form</u> as certain terms appearing in Eq. 4.13 and Eq. 4.17. However, Eq. 4.23 includes four terms of a type not used previously; these involve x^2: $x^2\beta_{91} + x^2\bar{z}\beta_{92} + x^2y\beta_{93} + x^2y\bar{z}\beta_{94}$. These four terms were not included in initial studies but were found to be needed to eliminate kinematic modes. This matter is discussed further in Subsection 4.6.

Returning attention once more to the special case represented by the $(0/90)_s$ coupon problem, y-direction integration of the x- and the y-direction force equilibrium equations Eq. 4.9a and Eq. 4.9b, respectively gives

$$\tau_{xy} = -\int \frac{\partial \sigma_x}{\partial x}\, dy + f_6(x, \bar{z}) \qquad (4.24a)$$

$$\sigma_y = -\int \frac{\partial \tau_{xy}}{\partial x}\, dy + f_7(x, \bar{z}) \qquad (4.24b)$$

Applying the conditions $\sigma_y = \tau_{xy} = 0$ at the y=0 free edge after integration of these equations yields

$$f_6(x, \bar{z}) = f_7(x, z) = 0 \tag{4.25}$$

Thus, the assumed stresses have been constructed from basic mechanics considerations and the required stress boundary conditions. However, these distributions could also be obtained by using the stress functions discussed in Subsection 4.2.1. For instance, if χ_1 (see Eq. 4.6) were derived as

$$\chi_1 = \int dy \int \sigma_z \, dy$$

and substituting for σ_z from Eq. 4.13, the resulting expressions for σ_y and τ_{yz} would be the same. Other similarities can also be derived for Eqs. 4.4 and 4.8, and the present stress assumptions. However, this procedure alone is awkward because of the traction-free conditions, and significant terms could be omitted inadvertently. Thus, probably the best procedure would be to combine the stress-function approach with physical insight obtained from pertinent examples.

Since the stresses in the TFQE arise not only from mechanical loads but also from thermal effects, it is necessary to consider the latter before imposing the interlayer continuity requirements cited in Eq. 4.10. Hence, an examination of these thermal-effects terms follows.

4.3 Description of Prescribed Initial Strain

First, note that for an orthotropic ply, the stress-strain relations may be expressed as

$$\begin{Bmatrix} \epsilon_\xi \\ \epsilon_\eta \\ \epsilon_\zeta \\ \gamma_{\eta\zeta} \\ \gamma_{\xi\zeta} \\ \gamma_{\xi\eta} \end{Bmatrix} = \begin{bmatrix} S_{11}^* & S_{12}^* & S_{13}^* & 0 & 0 & 0 \\ S_{21}^* & S_{22}^* & S_{23}^* & 0 & 0 & 0 \\ S_{31}^* & S_{32}^* & S_{33}^* & 0 & 0 & 0 \\ 0 & 0 & 0 & S_{44}^* & 0 & 0 \\ 0 & 0 & 0 & 0 & S_{55}^* & 0 \\ 0 & 0 & 0 & 0 & 0 & S_{66}^* \end{bmatrix} \begin{Bmatrix} \sigma_\xi \\ \sigma_\eta \\ \sigma_\zeta \\ \tau_{\eta\zeta} \\ \tau_{\xi\zeta} \\ \tau_{\xi\eta} \end{Bmatrix} + \begin{Bmatrix} \alpha_1 \\ \alpha_2 \\ \alpha_3 \\ 0 \\ 0 \\ 0 \end{Bmatrix} T_I \tag{4.26}$$

The elastic compliance coefficients S^*_{ij} are defined with respect to the material axes ξ,η,ζ of the ply.

Let the distribution of temperature change from a reference unstressed unstrained state at temperature T_r be denoted by $T_I(x,y,\bar{z})$ for any layer I of the layered plate. For the element let that temperature change distribution in any layer I be prescribed and assumed to be approximated adequately by the following simple expression:

$$T_I(x,y,z) = \Delta T_1 + \Delta T_2\, x + \Delta T_3\, y + \bar{z}\left[\Delta T_4 + \Delta T_5\, x + \Delta T_6\, y\right] \tag{4.27}$$

where the $\bar{z}$ origin is located at the midsurface of layer I, and the quantities ΔT_1, ΔT_2, ... ΔT_6 are known "fitting" constants used to describe the $T_I(x,y,\bar{z})$ prescribed data. However, if the $\bar{z}$ distribution of T_I is more severe than accommodated by Eq. 4.27, layer I could be

subdivided into a number of sublayers[+] in the $\bar{z}$ direction, and the Eq. 4.27-description employed for each sublayer. Since the material axes (ξ, η, ζ) of the material in layer I might not coincide with the axes x,y,$\bar{z}$ of the TFQE element, the "element-direction" prescribed thermal strains ε^{o}_{ij} may be expressed as (where directions ζ and $\bar{z}$ are defined to coincide):

$$\underset{\sim}{\varepsilon}^{\circ} = \begin{bmatrix} \varepsilon^{\circ}_{x} \\ \varepsilon^{\circ}_{y} \\ \varepsilon^{\circ}_{z} \\ \gamma^{\circ}_{yz} \\ \gamma^{\circ}_{xz} \\ \gamma^{\circ}_{xy} \end{bmatrix} = \begin{bmatrix} \ell^2 & m^2 & 0 \\ m^2 & \ell^2 & 0 \\ 0 & 0 & 1 \\ 0 & 0 & 0 \\ 0 & 0 & 0 \\ -2\ell m & -2\ell m & 0 \end{bmatrix} \begin{bmatrix} \alpha_1 \\ \alpha_2 \\ \alpha_3 \end{bmatrix} T_I(x,y,\bar{z}) \tag{4.26a}$$

or

$$\underset{\sim}{\varepsilon}^{\circ} \equiv \underset{\sim}{\bar{\varepsilon}}^{\circ} T_I(x,y,z) \tag{4.26b}$$

where α_1, α_2, and α_3 are the coefficients of linear thermal expansion along material axes ξ, η, and ζ, respectively, and ℓ and m are the "direction cosines" between the x,y element and the ξ,η material axes:

$$\ell = \cos(\widehat{x,\xi}) \qquad m = \sin(\widehat{x,\xi}) \tag{4.26c}$$

[+]Alternatively, to reduce the number of DOF's one could represent T_I by a higher-order interpolation function.

It is useful to recall that with respect to the element axes x, y, $\bar{z}$, the stress-strain relations for any given orthotropic layer of the TFQE may be expressed as

$$\begin{bmatrix} \varepsilon_x \\ \varepsilon_y \\ \varepsilon_z \\ \gamma_{yz} \\ \gamma_{xz} \\ \gamma_{xy} \end{bmatrix} = \begin{bmatrix} S_{11} & S_{12} & S_{13} & 0 & 0 & S_{16} \\ S_{21} & S_{22} & S_{23} & 0 & 0 & S_{26} \\ S_{31} & S_{32} & S_{33} & 0 & 0 & S_{36} \\ 0 & 0 & 0 & S_{44} & S_{45} & 0 \\ 0 & 0 & 0 & S_{54} & S_{55} & 0 \\ S_{61} & S_{62} & S_{63} & 0 & 0 & S_{66} \end{bmatrix} \begin{bmatrix} \sigma_x \\ \sigma_y \\ \sigma_z \\ \tau_{yz} \\ \tau_{xz} \\ \tau_{xy} \end{bmatrix} + \begin{bmatrix} \varepsilon_x^\circ \\ \varepsilon_y^\circ \\ \varepsilon_z^\circ \\ \gamma_{yz}^\circ \\ \gamma_{xz}^\circ \\ \gamma_{xy}^\circ \end{bmatrix} \quad (4.28)$$

or

$$\underset{\sim}{\varepsilon} = \underset{\sim}{S}\,\underset{\sim}{\sigma} + \underset{\sim}{\varepsilon}^\circ \quad (4.28a)$$

where $\underset{\sim}{\varepsilon}$ represents the total strain from the compatible displacement field, $\underset{\sim}{S}$ represents the matrix of elastic compliance coefficients with respect to the x,y,z axes of the element*, $\underset{\sim}{\sigma}$ denotes the actual stresses, and $\underset{\sim}{\varepsilon}^\circ$ represents the prescribed (or thermal) strains. Pre-multiplying Eq. 4.28a by $\underset{\sim}{S}^{-1}$ and rearranging, one obtains

$$\begin{aligned} \underset{\sim}{\sigma} &= \underset{\sim}{S}^{-1}\underset{\sim}{\varepsilon} - \underset{\sim}{S}^{-1}\underset{\sim}{\varepsilon}^\circ \\ &= S^{-1}\underset{\sim}{\varepsilon} - \underset{\sim}{\sigma}^\circ \end{aligned} \quad (4.29)$$

where $\underset{\sim}{C}=\underset{\sim}{S}^{-1}$ could also be written if desired as in Section 2.

*These S coefficients are obtained from the ply S^*_{ij} values by employing the proper transformations (see pg. 52 of Ref. 28).

Since from Eq. 4.26b $\underset{\sim}{\varepsilon}^{o}=\bar{\underset{\sim}{\varepsilon}}^{o}T_I$ and from Eq. 4.29 $\underset{\sim}{\sigma}^{o}$ is defined as $\underset{\sim}{S}^{-1}\,\underset{\sim}{\varepsilon}^{o}$, one may write

$$\underset{\sim}{\sigma}^{\circ} \equiv \underset{\sim}{S}^{-1}\,\underset{\sim}{\bar{\varepsilon}}^{\circ} = \underset{\sim}{S}^{-1}\,\bar{\underset{\sim}{\varepsilon}}^{\circ}T_I \equiv \bar{\underset{\sim}{\sigma}}^{\circ}T_I \tag{4.30}$$

where

$$\bar{\underset{\sim}{\sigma}}^{\circ} = \begin{bmatrix} \bar{\sigma}_x^{\circ} \\ \bar{\sigma}_y^{\circ} \\ \bar{\sigma}_z^{\circ} \\ \bar{\tau}_{yz}^{\circ} \\ \bar{\tau}_{xz}^{\circ} \\ \bar{\tau}_{xy}^{\circ} \end{bmatrix} = \begin{bmatrix} C_{11}\bar{\varepsilon}_x^{\circ} + C_{12}\bar{\varepsilon}_y^{\circ} + C_{13}\bar{\varepsilon}_z^{\circ} + C_{16}\bar{\gamma}_{xy}^{\circ} \\ C_{21}\bar{\varepsilon}_x^{\circ} + C_{22}\bar{\varepsilon}_y^{\circ} + C_{23}\bar{\varepsilon}_z^{\circ} + C_{26}\bar{\gamma}_{xy}^{\circ} \\ C_{31}\bar{\varepsilon}_x^{\circ} + C_{32}\bar{\varepsilon}_y^{\circ} + C_{33}\bar{\varepsilon}_z^{\circ} + C_{36}\bar{\gamma}_{xy}^{\circ} \\ 0 \\ 0 \\ C_{61}\bar{\varepsilon}_x^{\circ} + C_{62}\bar{\varepsilon}_y^{\circ} + C_{63}\bar{\varepsilon}_z^{\circ} + C_{66}\bar{\gamma}_{xy}^{\circ} \end{bmatrix} \tag{4.30a}$$

In the present formulation $\bar{\sigma}_x^{o}$ may be rewritten in a useful alternate form without loss of generality as

$$\bar{\sigma}_x^{\circ} = \bar{\varepsilon}_x^{\circ} - \frac{1}{S_{11}}\left(S_{12}\bar{\sigma}_y^{\circ} + S_{13}\bar{\sigma}_z^{\circ} + S_{16}\bar{\tau}_{xy}^{\circ}\right) \tag{4.30b}$$

This form is consistent with the assumed stress σ_x given by Eq. 4.22. Hence, the stress quantity denoted by $\underset{\sim}{\sigma}^{o}$ in Eqs. 4.29 and 4.30 and which is given completely from the known thermal strain $\underset{\sim}{\varepsilon}^{o}$ may be written in the following symbolic form:

$$\underset{\sim}{\sigma}^{\circ} = \bar{\underset{\sim}{\sigma}}^{\circ}T_I \equiv \underset{\sim}{P}_{\circ}\,\underset{\sim}{\beta}_{\circ} \tag{4.31}$$

Note that the correct total stresses are $\underset{\sim}{\sigma}$ as defined in Eqs. 4.28, 4.28a, and 4.29. These total stresses are represented in the present approach by the two terms $\underset{\sim}{S}^{-1}\underset{\sim}{\varepsilon}-\underset{\sim}{\sigma}^{o}$ on the right-hand side of Eq. 4.29. In turn, the first term can be regarded as a stress term represented by two parts: (a) the assumed stress field already selected (i.e., σ_x, σ_y, σ_z, τ_{yz}, τ_{xz}, and τ_{xy} from Eqs. 4.22 and 4.23, 4.15a, 4.13, 4.15b, 4.17, and 4.24a, respectively) and denoted now collectively by $\underset{\sim}{\sigma}_A$ and (b) a second stress field yet to be determined and denoted by $\underset{\sim}{\sigma}_C$ where subscript "C" may be interpreted as compensatory since such terms must be devised to accommodate the following requirements:

(1) equilibrium of each layer of the TFQE,

(2) the traction free conditions in every layer on face AB where y=0,

(3) the interlayer continuity requirements as indicated in Eq. 4.10, and

(4) the stress-free conditions on the two surfaces z=±H of the multilayer element (Fig. 6).

Thus, with this interpretation, one may "rewrite" Eq. 4.29 as

$$\underset{\sim}{\sigma} = \underset{\sim}{\sigma}_A + \underset{\sim}{\sigma}_C - \underset{\sim}{\sigma}^{o} \tag{4.32}$$

where

$\underset{\sim}{\sigma}_A \equiv \underset{\sim\sim}{P}\underset{\sim}{\beta}$ = the already-selected assumed stress field

$\underset{\sim}{\sigma}_C \equiv \underset{\sim C\sim C}{P}\underset{\sim}{\beta}_C$ = compensatory stress field for the known $\underset{\sim}{\sigma}^{o}$; $\underset{\sim}{\sigma}_C$ is to be determined

$\underset{\sim}{\sigma}^{o} \equiv \underset{\sim o\sim o}{P}\underset{\sim}{\beta}_o$ = "stress field" known from the prescribed thermal strains

In the present subsection, only a portion of $\underset{\sim}{\sigma}_C$ is discussed -- that associated with requirements (1) and (2) -- and denoted as $\underset{\sim}{\sigma}_{CA}$; the remainder, $\underset{\sim}{\sigma}_{CB}$, arising from satisfying items (3) and (4) is discussed

in Subsection 4.4. Hence, for reference convenience, one may write

$$\underset{\sim}{\sigma}_C = \underset{\sim}{\sigma}_{CA} + \underset{\sim}{\sigma}_{C^\circ} \tag{4.33}$$

In computing $\underset{\sim}{\sigma}_{CA}$, each term in $\underset{\sim}{\sigma}^\circ$ is considered separately for convenience. Also, in satisfying equilibrium, the stresses are combined exactly as discussed in Subsection 4.2.3. The stress σ_x° can be written from Eqs. 4.26, 4.30b, and 4.31 as

$$\sigma_x^\circ = \overline{\sigma}_x^\circ \left[\Delta T_1 + \Delta T_2 x + \Delta T_3 y + \bar{z}\left(\Delta T_4 + \Delta T_5 x + \Delta T_6 y\right)\right] \tag{4.34}$$

Satisfying the equilibrium Eq. 4.9a, one obtains the shear stress as

$$\begin{aligned}\left(\tau_{xy}\right)_{CA} &= \int \frac{\partial \sigma_\circ}{\partial x}\, dy \\ &= \overline{\sigma}_x^\circ \left(\Delta T_2 y + \Delta T_5\, y\bar{z}\right)\end{aligned} \tag{4.35}$$

which satisfies the traction-free condition at y=0. Note that since σ_x° is expressed in terms of other stresses (Eq. 4.30b),

$$\left(\sigma_x\right)_{CA} = -\frac{S_{16}}{S_{11}}\left[\left(\tau_{xy}\right)_{CA}\right] \tag{4.36}$$

Next, the stress σ_y° can be written from Eqs. 4.27, 4.30a, and 4.31 as

$$\begin{aligned}\sigma_y^\circ = \overline{\sigma}_y^\circ \big[&\Delta T_1 + \Delta T_2 x + \Delta T_3 y + \\ &\bar{z}\left(\Delta T_4 + \Delta T_5 x + \Delta T_6 y\right)\big]\end{aligned} \tag{4.37}$$

Satisfying traction-free conditions at y=0 yields

$$\left(\sigma_y\right)_{CA} = \overline{\sigma}_y^\circ \left[\Delta T_1 + \Delta T_2 x + \bar{z}\left(\Delta T_4 + \Delta T_5 x\right)\right]$$

However, the remaining terms in y also have to be eliminated because in satisfying equilibrium (Eq. 4.9b), the resulting shear term

$$(\tau_{xy})_{CA} = \bar{\sigma}_y^{\circ}[\Delta T_3 x + \Delta T_6 x\bar{z}]$$

violates traction-free conditions. Thus, the compensating terms arising from σ_y° in Eq. 4.33 are

$$(\sigma_y)_{CA} = \bar{\sigma}_y^{\circ}[\Delta T_1 + \Delta T_2 x + \Delta T_3 y + \bar{z}(\Delta T_4 + \Delta T_5 x + \Delta T_6 y)] \tag{4.38a}$$

and

$$(\sigma_x)_{CA} = -\frac{1}{S_{11}}[S_{12}(\sigma_y)_{CA}] \tag{4.38b}$$

Next, the stress σ_z° can be written as

$$\sigma_z^{\circ} = \bar{\sigma}_z^{\circ}[\Delta T_1 + \Delta T_2 x + \Delta T_3 y + \bar{z}(\Delta T_4 + \Delta T_5 x + \Delta T_6 y)] \tag{4.39}$$

Satisfying equilibrium (Eq. 4.9c) yields

$$(\tau_{yz})_{CA} = \int \frac{\partial \sigma_z^{\circ}}{\partial \bar{z}}\, dy = \bar{\sigma}_z^{\circ}[\Delta T_4 y + \Delta T_5 xy + \Delta T_6 y^2/2] \tag{4.40}$$

which satisfies Eq. 4.11 at y=0.

The stresses τ^{o}_{yz} and τ^{o}_{xz} are zero; hence, finally one obtains

$$\tau^{\bullet}_{xy} = \bar{\tau}^{\bullet}_{xy}\left[\Delta T_1 + \Delta T_2 x + \Delta T_3 y + \bar{z}\left(\Delta T_4 + \Delta T_5 x + \Delta T_6 y\right)\right] \tag{4.41}$$

The compensating term required to satisfy traction-free conditions is

$$\left(\tau_{xy}\right)_{CA} = \bar{\tau}^{\bullet}_{xy}\left[\Delta T_1 + \Delta T_2 x + \bar{z}\left(\Delta T_4 + \Delta T_5 x\right)\right] \tag{4.42}$$

Also for equilibrium, one obtains from Eq. 4.9a

$$\left(\tau_{xz}\right)_{CA} = \int \frac{\partial \tau^{\bullet}_{xy}}{\partial y}\, dz - \int \frac{\partial \left(\tau_{xy}\right)_{CA}}{\partial y}\, d\bar{z} \tag{4.43}$$

$$= \bar{\tau}^{\bullet}_{xy}\left[\Delta T_3 \bar{z} + \Delta T_6 \bar{z}^2/2\right]$$

Also from Eq. 4.30b,

$$\left(\sigma_x\right)_{CA} = -\frac{1}{S_{11}}\left[S_{16}\left(\tau_{xy}\right)_{CA}\right] \tag{4.44}$$

Thus, all terms in $\underset{\sim}{\sigma}_{CA}$ have been computed. Combining the terms, one can summarize and write these $\underset{\sim}{\sigma}_{CA}$ terms as

$$\left(\sigma_x\right)_{CA} = -\frac{1}{S_{11}}\left[S_{12}\sigma_y + S_{13}\sigma_z + S_{16}\tau_{xy}\right]_{CA}$$

$$\left(\sigma_y\right)_{CA} = \sigma^{\bullet}_{y}$$

$$\left(\sigma_z\right)_{CA} = 0 \tag{4.45}$$

$$(\tau_{yz})_{CA} = \int \frac{\partial \sigma_z^\circ}{\partial z}\, dy$$

$$(\tau_{xz})_{CA} = \int \frac{\partial \tau_{xy}^\circ}{\partial y}\, dz - \int \frac{\partial (\tau_{xy})_{CA}}{\partial y}\, dz$$

$$(\tau_{xy})_{CA} = \int \frac{\partial \sigma_x^\circ}{\partial x}\, dy + \bar{\tau}_{xy}^\circ \left[\Delta T_1 + \Delta T_2 x + \bar{z}\left(\Delta T_4 + \Delta T_5 x\right)\right] \qquad \text{(4.45 Cont.)}$$

4.4 Interlayer Continuity and the Remaining Free-Surface Conditions

To this point, the total stresses $\underset{\sim}{\sigma}$ in any given layer of the multilayer finite element have been described as consisting of:

$$\underset{\sim}{\sigma} = \underset{\sim}{\sigma}_A + \underset{\sim}{\sigma}_{CA} + \underset{\sim}{\sigma}_{CB} - \underset{\sim}{\sigma}^\circ \qquad (4.46)$$

where all of the contributions on the right-hand side of Eq. 4.46 have been defined except for $\underset{\sim}{\sigma}_{CB}$ (called part B of the compensatory stress contribution). This final contribution can be determined by satisfying the interlayer continuity conditions and the stress-free conditions of the surfaces at $z=\pm H$. It should be recalled that $\underset{\sim}{\sigma}_A$ for any given layer was constructed in terms of unknown coefficients so as to satisfy (i) the force equilibrium equations in that layer and (ii) the stress-free conditions on side AB of the TFQE. Hence, since $\underset{\sim}{\sigma}^\circ$ is prescribed, $\underset{\sim}{\sigma}_{CA}$ was chosen to compensate for the "violations" of (a) equilibrium within a given layer and (b) the stress-free state on edge AB of the TFQE.

Next, therefore, consider the construction of the proper $\underset{\sim}{\sigma}_{CB}$ such that all of the aforementioned conditions remain fulfilled while satisfying: (a) the interlayer continuity condition at interface i given by Eq. 4.10 (and repeated and clarified here for convenience):

$$\left(\sigma_z^{i+1}\right)_{\bar{z}=-h_{i+1}} = \left(\sigma_z^{i}\right)_{\bar{z}=h_i} \; ; \left(\tau_{zx}^{i+1}\right)_{-h_{i+1}} = \left(\tau_{zx}^{i}\right)_{+h_i}$$

$$\left(\tau_{zy}^{i+1}\right)_{-h_{i+1}} = \left(\tau_{zy}\right)_{+h_i} \; ; \left(\varepsilon_x^{i+1}\right)^*_{-h_{i+1}} = \left(\varepsilon_x^{i}\right)^*_{+h_i} \qquad (4.10)$$

which must be satisfied <u>at all x,y locations</u> on the interface, where the ith interface is bounded by material layers i and i+1 (of respective thicknesses $2h_i$ and $2h_{i+1}$) and (b) the stress-free conditions (Eq. 4.12) on the two faces located at $z=\pm H$:

$$\sigma_z = \tau_{zy} = \tau_{zx} = 0 \qquad (4.12)$$

Now these conditions will be satisfied <u>exactly</u> for the TFQE by selecting $\underset{\sim}{\sigma}_{CB}$ such that the actual stress $\underset{\sim}{\sigma}$ given by Eq. 4.46 will be guaranteed to satisfy <u>all</u> of the aforementioned requirements. However, this $\underset{\sim}{\sigma}_{CB}$ construction process may be described most clearly perhaps by examining a few illustrative terms.

Consider, for example, the interface continuity condition on $\sigma_z(x,y,\bar{z})$ as defined by the following description:

$$\left(\sigma_z^{A} + \sigma_z^{CA} + \sigma_z^{CB} - \sigma_z^{o}\right)^{i+1}_{\bar{z}=-h_{i+1}} =$$

$$\left(\sigma_z^{A} - \sigma_z^{CA} + \sigma_z^{CB} - \sigma_z^{o}\right)^{i}_{\bar{z}=+h_i} \qquad (4.47)$$

One need not add explicitly the contributions σ_z^{CB} in layers i and i+1; instead relations of this type supply a set of required conditions which can serve to eliminate a number of the unknown β's already present, thereby reducing the number of unknowns to be handled finally. That is, the eliminated β's will be functions of other β's and the prescribed stresses $\underset{\sim}{\sigma}^{o}$ and $\underset{\sim}{\sigma}_{CA}$; the latter part will constitute $\underset{\sim}{\sigma}_{CB}$. Also, it should

*Strictly speaking, the variational principal employed does not require one to satisfy this physically present strain continuity condition; however, its use in the TFQE formulation reduces the number of unknown β's without, hopefully, unduly degrading the performance of the element.

be recalled that τ_{yz} was constructed from the Eq. 4.13 assumed function for σ_z through the use of Eq. 4.15b; hence τ_{yz} is expressed in terms of many of the same β's that appear in Eq. 4.13. In this β-elimination spirit, the pertinent equations satisfying Eq. 4.10 will be illustrated for one typical term taken from one of the following 10 different sets of terms which can be identified in Eq. 4.13:

Term Set	Associated β's Present				Associated $T_i(y)$
1	β_1	β_6	β_{11}	β_{16}	$T_o(y)$
2	β_{21}	β_{26}	β_{21}	β_{36}	$T_o(y)$
3	β_2	β_7	β_{12}	β_{17}	$T_1(y)$
4	β_{22}	β_{27}	β_{32}	β_{37}	$T_1(y)$
5	β_3	β_8	β_{13}	β_{18}	$T_2(y)$
6	β_{23}	β_{28}	β_{33}	β_{38}	$T_2(y)$
7	β_4	β_9	β_{14}	β_{19}	$T_3(y)$
8	β_{24}	β_{29}	β_{34}	β_{39}	$T_3(y)$
9	β_5	β_{10}	β_{15}	β_{20}	$T_4(y)$
10	β_{25}	β_{30}	β_{35}	β_{40}	$T_4(y)$

The continuity conditions are to be satisfied exactly term by term.

Therefore consider, for example, set 2 which reads for the ith layer:

$$\left(\sigma_z^A\right)_i = \times T_o(y)\left[\beta_{21} + \bar{z}\beta_{26} + \frac{\bar{z}^2}{2}\beta_{31} + \frac{\bar{z}^3}{6}\beta_{36}\right]_i \qquad (4.48)$$

Also, from Eq. 4.39, the corresponding type of term in σ_z^o reads

$$\left(\sigma_z^o\right)_i = \times \overline{\sigma_z}^o\left[\Delta T_2 + \bar{z}\,\Delta T_5\right] \qquad (4.49)$$

Collecting,

$$(\bar{\sigma_z})_i = (\bar{\sigma_z}^A)_i + (\bar{\sigma_z}^{CA})_i - (\bar{\sigma_z}^\circ)_i$$

$$= \times T_o(y)\Big[\beta_{21} + \bar{z}\beta_{26} + \frac{\bar{z}^2}{2}\beta_{31} + \frac{\bar{z}^3}{6}\beta_{36} \tag{4.50}$$

$$- \bar{\sigma_z}^\circ\left(\Delta T_2 + \bar{z}\,\Delta T_5\right)\Big]$$

$$\text{for } -h_i \le \bar{z} \le h_i$$

Hence, from Eq. 4.45, $\sigma_z^{CA}=0$.

For the terms $(\sigma_z^A)_i$ given by Eq. 4.50, Eq. 4.15b may be used to evaluate the associated $(\tau_{yz})_i$:

$$(\tau_{yz})_i = -\int \frac{\partial}{\partial \bar{z}}(\bar{\sigma_z})_i\, dy$$

$$= -\int T_o(y)\, dy\Big[\beta_{26} + \bar{z}\beta_{31} + \frac{\bar{z}^2}{2}\beta_{36} - \bar{\sigma_z}^\circ\,\Delta T_5\Big]\times \tag{4.51}$$

$$\text{for } -h_i \le \bar{z} \le h_i$$

where $2h_i$ is the thickness of the ith layer.

Next, let Eq. 4.50 be used to write for "set 2" the σ_z continuity condition at interface i where $\bar{z} = -h_{i+1}$ in material layer i+1 and $\bar{z} = +h_i$ in material layer i:

$$\text{Set 2}\left(\bar{\sigma_z}^{i+1}\right)_{\bar{z}=-h_{i+1}} = \text{Set 2}\left(\bar{\sigma_z}^{i}\right)_{\bar{z}=+h_i} \tag{4.52}$$

or

$$\left[\beta_{21}^{i+1} - h_{i+1}\beta_{26}^{i+1} + \frac{h_{i+1}^2}{2}\beta_{31}^{i+1} - \frac{h_{i+1}^3}{6}\beta_{36}^{i+1} - \bar{\sigma}_z^{o\,i+1}\left(\Delta T_2^{i+1} - h_{i+1}\Delta T_5^{i+1}\right)\right]$$

$$= \left[\beta_{21}^{i} + h_i\beta_{26}^{i} + \frac{h_i^2}{2}\beta_{31} + \frac{h_i^3}{6}\beta_{36} - \bar{\sigma}_z^{o\,i}\left(\Delta T_2^{i} + h_i\Delta T_5^{i}\right)\right] \qquad (4.52a)$$

Rearranging Eq. 4.52a, one obtains

$$\beta_{21}^{i} + h_i\beta_{26}^{2} + \frac{h_i^2}{2}\beta_{31} + \frac{h_i^3}{6}\beta_{36}^{i}$$

$$= \beta_{21}^{i+1} - h_{i+1}\beta_{26} + \frac{h_{i+1}^2}{2}\beta_{31}^{i+1} - \frac{h_{i+1}^3}{6}\beta_{36}^{i+1}$$

$$+ \bar{\sigma}_z^{o\,i}\left(\Delta T_2^{i} + h_i\Delta T_5^{i}\right) - \bar{\sigma}_z^{o\,i+1}\left(\Delta T_2^{i+1} - h_{i+1}\Delta T_5^{i+1}\right) \qquad (4.52b)$$

Similarly, writing continuity of τ_{yz} at interface i for the present set-2 term gives

$$\text{Set 2}\left(\tau_{yz}^{i+1}\right)_{\bar{z}=-h_{i+1}} = \text{Set 2}\left(\tau_{yz}^{i}\right)_{\bar{z}=+h_{i+1}} \qquad (4.53)$$

or

$$\left[\beta_{26}^{i+1} - h_{i+1}\beta_{31}^{i+1} + \frac{h_{i+1}^2}{2}\beta_{36}^{i+1} - \bar{\sigma}_z^{o\,i+1}\Delta T_5^{i+1}\right]$$

$$= \left[\beta_{26}^{i} + h_i\beta_{31}^{i} + \frac{h_i^2}{2}\beta_{36} - \bar{\sigma}_z^{o\,i}\Delta T_5^{i}\right] \qquad (4.53a)$$

Rearranging Eq. 4.53a, one obtains

$$\beta_{26}^{i} + h_i\beta_{31}^{i} + \frac{h_i^2}{2}\beta_{36}^{i} = \beta_{26}^{i+1} - h_{i+1}\beta_{31}^{i+1} + \frac{h_{i+1}^2}{2}\beta_{36}^{i+1}$$

$$+ \bar{\sigma}_z^{o\,i}\Delta T_5^{2} - \bar{\sigma}_z^{o\,i+1}\Delta T_5^{i+1} \qquad (4.54)$$

One can also write for these "set-2" terms the continuity conditions at interface i-1 to obtain another equation each similar to Eq. 4.52b and to Eq. 4.54. Therefore, one has four equations from which one can solve for β^i_{21}, β^i_{26}, β^i_{31}, and β^i_{36} in terms of the remaining β's and the "known thermal terms"; thereby, one can eliminate β^i_{21}, β^i_{26}, β^i_{31}, and β^i_{36}. Note that if the ith interface is traction-free (i.e., z=H), then the $\beta's^{i+1}$ in Eqs. 4.52b and 4.54 are zero, but the $\beta's^i$ are eliminated as before. Also, if the total number of layers is even (Fig. 13) only traction-free conditions need to be satisfied at z=H for the last layer. Hence, in this case only β^i_{21} and β^i_{26} are eliminated.

Similar to σ_z, the interlaminar shear stress τ_{zx} (Eq. 4.17) can also be separated into 10 different sets of terms:

Term Set	Associated β's Present			Associated $T_i(y)$
1	β_{41}	β_{46}	β_{51}	$T_o(y)$
2	β_{56}	β_{61}	β_{66}	$T_o(y)$
3	β_{42}	β_{27}	β_{52}	$T_1(y)$
4	β_{57}	β_{62}	β_{67}	$T_1(y)$
5	β_{43}	β_{48}	β_{53}	$T_2(y)$
6	β_{58}	β_{63}	β_{68}	$T_2(y)$
7	β_{44}	β_{49}	β_{54}	$T_3(y)$
8	β_{59}	β_{64}	β_{69}	$T_3(y)$
9	β_{45}	β_{50}	β_{55}	$T_4(y)$
10	β_{60}	β_{65}	β_{70}	$T_4(y)$

In any layer i, to satisfy traction continuity at both interfaces, two β's are eliminated from each set.

Finally, in satisfying ε_x continuity, Eq. 4.23 is divided into 12 sets of terms:

Term Set	Associated β's Present		Associated Function of y
1	β_{71}	β_{76}	$T_o(y)$
2	β_{81}	β_{86}	$T_o(y)$
3	β_{72}	β_{77}	$T_1(y)$
4	β_{82}	β_{87}	$T_1(y)$
5	β_{73}	β_{78}	$T_2(y)$
6	β_{83}	β_{88}	$T_2(y)$
7	β_{74}	β_{79}	$T_3(y)$
8	β_{84}	β_{89}	$T_3(y)$
9	β_{75}	β_{80}	$T_4(y)$
10	β_{85}	β_{90}	$T_4(y)$
11	β_{91}	β_{92}	1
12	β_{93}	β_{94}	y

In any intermediate layer (e.g. layer 3 in Fig. 13), both β's are eliminated to satisfy ε_x continuity at both interfaces. However, at layer 1 (and layer 5 when NL=5), only one β is eliminated since continuity is required only at interface 1 (and interface 4 for NL=5).

Thus, many of the layer β's are eliminated to satisfy continuity and traction-free conditions. A laminate with NL layers, initially has 94 β's per layer; hence, for the entire TFQE:

$$\text{Total Betas} = 94\,NL \tag{4.55}$$

At each interface there are 3 traction continuity constraints (Eq. 4.10) and since there are 10 different sets of terms for each stress, 30 β's are eliminated. For NL-1 interfaces:

$$\left.\begin{array}{l}\text{Number of Betas Eliminated}\\ \text{from Traction Continuity}\\ \text{Conditions}\end{array}\right\} = 30\,(NL-1) \tag{4.56}$$

Also with 3 traction-free conditions at the two surfaces $z=\pm H$, one eliminates for the 10 sets

$$\left.\begin{array}{l}\text{Number of Betas Eliminated} \\ \text{(Traction-Free Conditions)}\end{array}\right\} = 30(2) = 60 \qquad (4.57)$$

Finally, for ε_x continuity at each interface, 12 β's are eliminated from the 12 sets of terms.

$$\left.\begin{array}{l}\text{Number of Betas Eliminated} \\ (\varepsilon_x \text{ Continuity})\end{array}\right\} = 12\,(NL-1) \qquad (4.58)$$

The total number of β's eliminated are obtained by summing Eqs. 4.56, 4.57, and 4.58:

$$\text{Total Betas Eliminated} = 42NL+18 \qquad (4.59)$$

Thus, after satisfying Eqs. 4.10 and 4.12, the independent β's left are (Eq. 4.55 minus Eq. 4.59)

$$N_\beta = 94NL - (42NL+18) = 52NL-18 \qquad (4.60)$$

For convenience, these β eliminations are summarized in the following tabulation:

Constraint Condition	At Each Surface or Interface			No. of Surfaces or Interfaces	Total Number of Conditions
	No. of Conditions	No. of Term Sets	Total per Surface or Interface		
Traction Continuity at Each Interface	3	10	30	NL-1	30(NL-1)
Traction Free Conditions at Two Surfaces: $z=\pm H$	3	10	30	2	60
ε_x Continuity at Each Interface	1	12	12	NL-1	12(NL-1)
Total Number of Conditions or β's Eliminated: $42(NL-1)+60$					
Remaining β's: $94NL - [42(NL-1)+60] = 52NL-18$					

The β elimination is done in alternate layers and this is shown in Fig. 13. This procedure allows the eliminated β coefficients to be dependent upon only the adjacent-layer coefficients. This reduces the band-width of the H-matrix (Eq. 3.6) because if coefficients are eliminated in every layer, the H-matrix will become fully populated. The savings in computer storage by "alternate-layer elimination" becomes significant with an increase in the number of layers. For a four-layer laminate (NL=4, N_β=190) for example, the H-matrix requires 16,417 words; the saving in storage space compared with the full population scheme is 9%. However, if NL=8(N_β=398), the storage required is 46,989 words, and the saving is 41%. Thus, β elimination in alternate layers significantly reduces the storage space required for the H-matrix. The maximum bandwidth of $\underset{\sim}{H}$ is 197.

4.5 Assumed Displacement Field

4.5.1 Selection Guidelines

Of principal interest in the present study are multilayer (composite laminated) plates which can be characterized as ranging from thin to moderately thick (roughly $\frac{b}{H} \underset{\sim}{>} 4$ using the nomenclature of Fig. 1). Since information of "fine detail" is needed in a region near a traction-free edge where (a) interlaminar stresses of significant magnitude and rapid variation can occur and (b) pronounced warping displacements can appear, the nodal control inplane displacements u^i and v^i are included at each layer interface at "free-edge" nodal stations A and B as well as at nodal stations C and F on the non-parallel sides of the TFQE as depicted in Fig. 6. These significant and rapidly varying stresses are confined roughly to a "boundary layer" region between the free edge (y=0) and along the y direction of about one laminate thickness 2H in extent; hence, considerable detail is needed in this region (ABCF) of the TFQE. In this important "free-edge effects region" ABCF of the TFQE, a lesser level of detail is needed for the w-displacement behavior since the interlaminar stresses are less sensitively affected by the variation through the thickness of the w displacement; accordingly, at nodal stations A,B,C, and F of the TFQE, control w-displacements are selected at the geometric midsurface as w^M, at

the bottom as w^B, and at the top surface as w^T, where respectively, z=0, z=-H, and z=+H.

Since it is intended that the TFQE be attached at nodal stations D and E (side DE) to another multilayer finite element of simpler but appropriate description such as MLP3K of Ref. 26, region CDEF of the TFQE is a transition region with a total of only 5 nodal control degrees of freedom defined at the z=0 location at node D by u^D, v^D, w^D, θ_y^D, and θ_x^D -- and similarly at node E. Next, it should be recalled that the Modified Principle of Complementary Energy, Eq. 3.1, upon which the present TFQE hybrid finite element is based requires for static loading problems assumed-displacement information only along the boundaries of the element. However, for dynamic response problems one must account for the inertia forces throughout the volume of the element; for this purpose, the variational statement given by Eq. 3.34 will be utilized.

Accordingly, the selections of the assumed displacements along the boundaries and in the interior of the TFQE are discussed in Subsections 4.5.2 and 4.5.3, respectively.

4.5.2 Boundary Displacements

As noted earlier, assumed displacement distributions are needed for the edge-boundary regions BC, CD, DE, EF, and FA (see Fig. 6). Along each of these regions the displacements u, v, and w are each assumed to vary linearly. For each (ith) layer u and v are defined in terms of (1) a coordinate $\bar{z}$ measured from the midthickness of the ith layer (which is of thickness $2h_i$) and (2) a normalized boundary coordinate s defined such that $0 \leq s \leq 1$.

Accordingly in the ith layer, $u^i(s,\bar{z})$ from station B to C is assumed to be

$$u^i(s,\bar{z}) = \left(0.5 + \frac{\bar{z}}{h_i}\right)(1-s)\,u_B^{i+1} + \left(0.5 - \frac{\bar{z}}{h_i}\right)(1-s)\,u_B^i + \left(0.5 + \frac{\bar{z}}{h_i}\right)s\,u_C^{i+1} + \left(0.5 - \frac{\bar{z}}{h_i}\right)s\,u_C^i \tag{4.61}$$

Similarly, $v^i(s,\bar{z})$ from B to C is assumed to be given by an expression like Eq. 4.61 with u_B^{i+1} and u_B^i replaced by v_B^{i+1} and v_B^i, and u_C^{i+1} and u_C^i replaced by v_C^{i+1} and v_C^i. Also, similar expressions apply for $u^i(s,\bar{z})$ and $v^i(s,\bar{z})$ from F to A, where one simply replaces nodal interface quantities having subscript B by F and C by A. Next, along BC the quadratic w-displacement through the thickness at each nodal station is assumed in turn to vary linearly from B to C as follows:

$$w^i(s,z) = (1-s)\, w_B(z) + s\, w_C(z) \tag{4.62}$$

where

$$w_B(z) = \tfrac{1}{2}\left(1+\frac{z}{H}\right)\frac{z}{H}\, w_B^T + \left(1-\frac{z^2}{H^2}\right) w_B^M - \tfrac{1}{2}\left(1-\frac{z}{H}\right)\frac{z}{H}\, w_B^B \tag{4.62a}$$

$$w_C(z) = \tfrac{1}{2}\left(1+\frac{z}{H}\right)\frac{z}{H}\, w_C^T + \left(1-\frac{z^2}{H^2}\right) w_C^M - \tfrac{1}{2}\left(1-\frac{z}{H}\right)\frac{z}{H}\, w_C^B \tag{4.62b}$$

and z is measured from the midplane of the entire multilayer configuration (see Fig. 6). From F to A, $w^i(s,z)$ is given by expressions like Eqs. 4.62, 4.62a, and 4.62b except that subscript B is replaced by F and C by A. This completes the assumed boundary displacement descriptions along boundary segments BC and FA.

Next, consider segments CD and EF. For the ith layer $u^i(s,\bar{z},z)$ for segment CD is assumed to be

$$u^i(s,\bar{z},z) = \left(0.5+\frac{\bar{z}}{h_i}\right)(1-s)\, u_C^{i+1} + \left(0.5-\frac{\bar{z}}{h_i}\right)(1-s)\, u_C^i + s\, u_D + sz\,\theta_y^D \tag{4.63}$$

where s the normalized boundary coordinate from C to D (or E to F) such that $0 \le s \le 1$. For $v^i(s,\bar{z},z)$, a similar expression applies with all u's

replaced by v's and θ_y^D replaced by $-\theta_x^D$. Similarly from E to F, an expression like Eq. 4.63 is used (for $u^i(x,\bar{z},z)$ and for $v^i(s,\bar{z},z)$) where label C is replaced by E and D by F. Finally, the $w^i(s,z)$ from C to D is assumed to be

$$w^i(s,z) = (1-s)\ w_C(z) + s\ w_D(z) \tag{4.64}$$

where

$$w_D(z) = w_D + \int \left(\frac{dw}{dz}\right)_C dz \tag{4.64a}$$

Note that since only 5 control degrees of freedom are used at node D, it is implied that $\varepsilon_z = 0$ at D (and in fact all along side DE); since the TFQE is a "three-dimensional" element, the stresses are very sensitive to this constraint and behave erratically if not "alleviated". Hence, it has been assumed that $\frac{dw}{dz}$ is a constant from C to D (and from E to F) with the value taken to be the $\frac{dw}{dz}$ computed at station C: $(\frac{dw}{dz})_C$ (or at station F: $(\frac{dw}{dz})_F$ when considering $w_E(z)$). This assumption is valid if (1) C (or F) is at least a distance of 2H away from the traction-free edge AB and (2) the distance CD (or EF) is small -- in which cases these interlaminar stresses in this region become negligible.

Finally, along side DE, $u^i(s,z)$ is assumed to vary linearly with s from D to E as follows:

$$u^i(s,z) = (1-s)\ u_D + s\ u_E + (1-s)z\ \theta_y^D + sz\ \theta_y^E \tag{4.65}$$

For $v^i(s,z)$ one uses an assumption similar to Eq. 4.65 where the u's are replaced by v's and θ_y^E is replaced by $-\theta_x^E$. Also,

$$w^i(s,z) = (1-s)\ w_D(z) + s\ w_E(z) \tag{4.66}$$

where $w_D(z)$ is given by Eq. 4.64a and $w_E(z)$ by

$$w_E(z) = w_E + \int \left(\frac{dw}{dz}\right)_F dz \tag{4.66a}$$

As pointed out earlier, the element has two restrictions on its geometry, without loss of generality: vertical planes through DE and CF must be parallel to the traction-free edge AB. These restrictions have been imposed since (a) otherwise, difficulties may arise because of element distortion effects and (b) the stresses in this region are essentially linear in x.

Collecting terms from Eqs. 4.61 to 4.66, the boundary displacements of the TFQE can be written in the matrix form of Eq. 3.4 as

$$\underset{\sim}{u}^{*} = \underset{\sim}{L}\,\underset{\sim}{q} \tag{3.4}$$

The terms $\underset{\sim}{q}$ in Eq. 3.4 represent the nodal degrees of freedom such as u_B^{i+1}, v_B^{i+1}, w_B^T etc., and the matrix $\underset{\sim}{L}$ is the interpolation function of $\underset{\sim}{q}$ along the element boundary.

Finally, note that along traction-free edge AB, no displacement variations need be assumed since the surface tractions are zero, and the integral in Eq. 3.7 vanishes on this edge.

4.5.3 Interior Displacements

In order to account for the inertia forces throughout the interior of the TFQE for dynamic analysis purposes, an internal assumed displacement field is needed -- to be used in conjunction with Eq. 3.34 for π_{DMC}.

For present purposes the internal displacement field u for the TFQE is constructed in two parts. Part 1 consists of ABCF, and part 2 is CDEF. In each part the nodal degrees of freedom at each node are interpolated bilinearly to provide an estimate of the interior displacements. The displacement field is thereby compatible across face CF.

First, consider region ABCF. At any given node, the displacements u, v, and w are functions of $\bar{z}$ and z as given by Eqs. 4.61 to 4.66 and/or equations of those forms. For example, at node B one may obtain $u_B(z)$ in the ith layer from Eq. 4.61 by setting s=0 thereby obtaining:

$$u_B^i(\bar{z}) = \left(0.5 + \frac{\bar{z}}{h_i}\right) u_B^{i+1} + \left(0.5 - \frac{\bar{z}}{h_i}\right) u_B^i \tag{4.67}$$

where u_B^{i+1} and u_B^i serve as two of the 2(NL+1)+3 generalized nodal displacement q_B where NL is the number of layers and

$$\underset{\sim}{q}_B = \left[u^1 v^1 u^2 v^2 u^3 v^3 \ldots\ldots\ldots u^{NL+1} v^{NL+1} w^B w^A w^T \right]^T \tag{4.68}$$

Similar generalized displacements apply at nodes A, C, and F. One may obtain $v_B^i(\bar{z})$ and $w_B(z)$ similarly. Next, the nodal values at nodes A, B, C, and F of $u_A^i(\bar{z})$, $v_A^i(\bar{z})$, and $w_A(z)$ at node A, for example, are used as control values for bilinear interpolation in terms of two normalized coordinates ξ and η defined such that $(\xi,\eta) = (0,0)$ for A, (1,0) for B, (1,1) for C, and (0,1) for F. Accordingly, the bilinear interpolation functions to be applied to the nodal functions of $\bar{z}$ and z at nodes A, B, C, and F, respectively are:

$$\begin{aligned} N_A(\xi,\eta) &= (1-\xi)(1-\eta) \\ N_B(\xi,\eta) &= (1-\eta)\xi \\ N_C(\xi,\eta) &= \xi\eta \\ N_F(\xi,\eta) &= (1-\xi)\eta \end{aligned} \tag{4.69}$$

Thus, one can write the element x,y coordinates in terms of the coordinates ξ and η by the following relations [30]:

$$\begin{aligned} x &= x_A N_A(\xi,\eta) + x_B N_B(\xi,\eta) + x_C N_C(\xi,\eta) + x_F N_F(\xi,\eta) \\ y &= y_A N_A(\xi,\eta) + y_B N_B(\xi,\eta) + y_C N_C(\xi,\eta) + y_F N_F(\xi,\eta) \end{aligned} \tag{4.70}$$

Hence, for example, one may express $u(x,y,\bar{z})$ or $u(\xi,\eta,\bar{z})$ in the interior of region ABCF by

$$u(\xi,\eta,\bar{z}) = u_A(\bar{z})N_A + u_B(\bar{z})N_B + u_C(\bar{z})N_C + u_F(\bar{z})N_F \tag{4.71}$$

where one portion of $u_B(\bar{z})$ is as given by Eq. 4.67. Similar expressions hold for $v(\xi,\eta,\bar{z})$ and $w(\xi,\eta,z)$.

Collecting Eqs. 4.67, 4.68, and 4.71 (and similar equations to provide all contributions to $u^i(\bar{z})$, $v^i(\bar{z})$, $w(z)$ at nodes A, B, C, and F), one may write the interior displacement field in matrix form as

$$\begin{bmatrix} u \\ v \\ w \end{bmatrix} = \underset{\sim}{N}(\xi,\eta,\bar{z},z)\ \underset{\sim}{q} \tag{4.72}$$

$3\times 1 \qquad 3\times(8NL+20) \qquad (8NL+20)\times 1$

For region CDEF, one proceeds in a similar fashion to construct an interior displacement field description analogous to Eq. 4.72.

4.6 Element Property Evaluations and Features

4.6.1 Evaluation of Element Quantities

The finite element quantities of final interest are $\underset{\sim}{k}$, $\underset{\sim}{Q}_M$, $\underset{\sim}{Q}_T$, and $\underset{\sim}{m}$ as given by Eqs. 3.14, 3.11, 3.15, and 3.36, respectively. The evaluation of $\underset{\sim}{m}$ involves a volume integration, $\underset{\sim}{k}$ and $\underset{\sim}{Q}_T$ require both volume and surface integration, but $\underset{\sim}{Q}_M$ involves only surface integration. Auxiliary quantities needed in some of these evaluations include $\underset{\sim}{H}$, $\underset{\sim}{G}$, $\underset{\sim}{H}_t$, $\underset{\sim}{G}_t$, and $\underset{\sim}{G}_o$ given by Eqs. 3.6, 3.7, 3.8, 3.9, and 3.10, respectively; $\underset{\sim}{H}$ and $\underset{\sim}{H}_t$ require volume integration, whereas $\underset{\sim}{G}$, $\underset{\sim}{G}_t$, and $\underset{\sim}{G}_o$ require only surface integration.

First, consider the quantities $\underset{\sim}{k}$, $\underset{\sim}{Q}_M$, $\underset{\sim}{Q}_T$, and the auxiliary quantities $\underset{\sim}{H}$, $\underset{\sim}{G}$, $\underset{\sim}{H}_t$, $\underset{\sim}{G}_t$, and $\underset{\sim}{G}_o$. In the volume integrals (Eqs. 3.6 and 3.8) the integration along x is carried out analytically but numerically along y using an eight-point Gaussian quadrature scheme [29,30]; the integration in $\bar{z}$ is uncoupled from x and y, and is done analytically. The surface integrals (Eqs. 3.7, 3.9, 3.10, and 3.15) are computed analytically along

DE, but along BD and EA an eight-point Gaussian quadrature scheme along s is used; the z and $\bar{z}$ integrations are done analytically.

Finally, the volume integration scheme used to evaluate the element mass matrix $\underset{\sim}{m}$ is with 3 by 3 Gaussian quadrature in the x,y plane and by analytical integration in $\bar{z}$.

Note that the $\underset{\sim}{H}$ matrix (Eq. 3.6) is a symmetric, positive-definite, banded matrix. In computing $\underset{\sim}{\beta}$ from Eq. 3.12b -- repeated below for convenience,

$$\underset{\sim}{\beta} = \underset{\sim}{H}^{-1}\,\underset{\sim}{G}\,\underset{\sim}{q} - \underset{\sim}{H}^{-1}\,\underset{\sim}{H}_t\,\underset{\sim}{\beta}_t \tag{3.12b}$$

the matrices $\underset{\sim}{H}^{-1}\underset{\sim}{G}$ and $\underset{\sim}{H}^{-1}\underset{\sim}{H}_t$ are obtained by the Gauss-Doolittle triple-decomposition/sequential solution method discussed in Subsection 3.1.2. This avoids computing $\underset{\sim}{H}^{-1}$; thus, computing time and memory storage space are reduced. Note that (following the procedure in Subsection 3.1.2) in computing $\underset{\sim}{H}^{-1}\underset{\sim}{G}$, the solution is stored so as to replace $\underset{\sim}{G}$ by $\underset{\sim}{H}^{-1}\underset{\sim}{G}$. Thus, $\underset{\sim}{G}$ is destroyed but one needs it to compute $\underset{\sim}{k}$ (Eq. 3.14). The direct approach would be to save $\underset{\sim}{G}$ at some temporary location $\underset{\sim}{G}_{save}$ before computing $\underset{\sim}{H}^{-1}\underset{\sim}{G}$. However, this imposes an additional storage burden which is significant since the $\underset{\sim}{G}$ matrix is large. As an example, a 3-layer laminate requires a storage space of 7452 words and this increases with more layers.

An alternate method as described below is used to avoid this excess storage. The $\underset{\sim}{H}$ matrix in factored form is

$$\underset{\sim}{H} = \underset{\sim}{L}\,\underset{\sim}{D}\,\underset{\sim}{L}^T \tag{4.73}$$

Similarly, $\underset{\sim}{H}^{-1}$ can be written as

$$H^{-1} = \left(\underset{\sim}{L}^T\right)^{-1}\,\underset{\sim}{D}^{-1}\,\left(\underset{\sim}{L}\right)^{-1} \tag{4.74}$$

Using Eq. 4.74, $\underset{\sim}{H}^{-1}\underset{\sim}{G}$ and $\underset{\sim}{k}$ can be written as

$$\underset{\sim}{H}^{-1}\underset{\sim}{G} = (\underset{\sim}{L}^T)^{-1}\underset{\sim}{D}^{-1}(\underset{\sim}{L})^{-1}\underset{\sim}{G} \tag{4.75a}$$

$$\underset{\sim}{k} = \underset{\sim}{G}^T(\underset{\sim}{L}^T)^{-1}\underset{\sim}{D}^{-1}(\underset{\sim}{L})^{-1}\underset{\sim}{G} \tag{4.75b}$$

Now let

$$\underset{\sim}{R} = \underset{\sim}{L}^{-1}\underset{\sim}{G} \tag{4.76}$$

Substituting Eq. 4.76 into Eq. 4.75, one obtains

$$\underset{\sim}{H}^{-1}\underset{\sim}{G} = (\underset{\sim}{L}^T)^{-1}\underset{\sim}{D}^{-1}\underset{\sim}{R} \tag{4.77a}$$

$$\underset{\sim}{k} = \underset{\sim}{R}^T\underset{\sim}{D}^{-1}\underset{\sim}{R} \tag{4.77b}$$

The matrix $\underset{\sim}{R}$ is easily obtained by forward substitution and is stored in $\underset{\sim}{G}$ (similar to Eq. 3.25). Next using Eq. 4.77b, $\underset{\sim}{k}$ is computed; then using Eqs. 3.27 and 3.28, the solution procedure for $\underset{\sim}{H}^{-1}\underset{\sim}{G}$ is completed and stored in $\underset{\sim}{G}$. Thus, all quantities are obtained without any extra storage space requirements. Using the computed matrix $\underset{\sim}{H}^{-1}\underset{\sim}{G}$, the thermal loads vector $\underset{\sim}{Q}_T$ is evaluated by substitution.

4.6.2 Kinematic Modes and Their Elimination

The strain energy, U, of an element can be written as (see Eq. 3.13)

$$U = \frac{1}{2}\underset{\sim}{q}^T\underset{\sim}{k}\underset{\sim}{q} \tag{4.78}$$

When the nodal displacements are the rigid-body modes of the element ($\underset{\sim}{q}_R$), the strain energy U should be zero, since no work is done. However, in the hybrid formulation, it is possible to have additional modes $\underset{\sim}{q}_K$ which also result in zero strain energy; these are called "Kinematic Modes" [26,42]. The presence of kinematic modes (like rigid body modes) renders the stiffness matrix $\underset{\sim}{k}$ singular. For example, if there are n_R rigid body

modes and n_K kinematic modes, an eigen analysis of $\underset{\sim}{k}$ would reveal n_R+n_K zero eigenvalues. Hence, the stiffness matrix $\underset{\sim}{k}$ to be nonsingular would require n_R+n_K appropriate constraints.

Kinematic modes like rigid body modes if suppressed by constraints will not affect the solution to any problem. However, if the constraints are insufficient, they render the assembled stiffness matrix $\underset{\sim}{K}$ singular and no solution is possible. These modes are a "pseudo effect", and can be eliminated by adding appropriate terms to the stress assumption (Eq. 3.2).

Kinematic modes occur when the assumed stresses do no work on the boundary for these modes. This work term in Eq. 3.1 is

$$W_B = \int_{\partial V_n} \underset{\sim}{T}^T \underset{\sim}{u}^* \, ds \tag{4.79}$$

= work done by boundary tractions

where $\underset{\sim}{T}$ is the boundary traction, $\underset{\sim}{u}^*$ is the boundary displacement vector and ∂V_n is the boundary surface of the nth element. In matrix form one can write W_B as (see Eq. 3.5 for this term)

$$W_B = \underset{\sim}{\beta}^T \underset{\sim}{G} \underset{\sim}{q} \tag{4.80}$$

Thus kinematic modes, $\underset{\sim}{q}_K$, by definition must satisfy

$$W_B = \underset{\sim}{\beta}^T \underset{\sim}{G} \underset{\sim}{q}_K = 0 \tag{4.81}$$

for all $\underset{\sim}{\beta}$. However, by adding appropriate stress terms, this pseudo condition can be corrected.

In formulating the stresses for the TFQE, initially 90 betas were assumed in each layer. These stresses are given in Subsection 4.2.3, neglecting β_{91} to β_{94}. However, an eigen analysis of the element stiffness matrix $\underset{\sim}{k}$ revealed 8 zero eigenvalues. Since the TFQE is a complete three dimensional element, there are 6 rigid body modes; this results in 6 zero eigenvalues in $\underset{\sim}{k}$. Thus, there were 2 kinematic modes.

In eliminating kinematic modes, two steps were taken:

1. Identify the nodal displacement vector $\underset{\sim}{q}_K$ of each mode.
2. Seek suitable additional terms in the stress assumption such that $W_B \neq 0$ for $\underset{\sim}{q}_K$ (Eq. 4.81).

In the eigenanalysis, along with the eigenvalues one can also compute eigenvectors $\underset{\sim}{q}_{EV}$. These vectors include (a) the rigid body modes $\underset{\sim}{q}_R$, and (b) the kinematic modes $\underset{\sim}{q}_K$. Thus,

$$\underset{\sim}{q}_{EV} = a_R \underset{\sim}{q}_R + b_K \underset{\sim}{q}_K \tag{4.82}$$

where a_R and b_K are constants. Separating the eigenvectors into $\underset{\sim}{q}_R$ and $\underset{\sim}{q}_K$ is difficult; hence, an alternate method was followed.

Before proceeding with the eigenanalysis, the following 6 nodal degrees of freedom in the TFQE (Fig. 6) were constrained:

$$u_E,\ v_E,\ w_E,\ \theta_{x_E},\ v_D \text{ and } w_D \tag{4.83}$$

These constraints suppress the 6 rigid body modes of the element. Thus, an eigenanalysis of the constrained $\underset{\sim}{k}$ gives the two kinematic modes of the element. These modes are functions of the nodal displacement $\underset{\sim}{v}$ only and are shown in Fig. 14. At A, B, C, and F the v is uniform through the thickness; that is, no warping occurs. Note that these modes are not uniquely distinguishable from each other. As an example, if both kinematic modes were subtracted from the rigid body translation mode in v (i.e., $\underset{\sim}{v}=1$), one would obtain $v_E=v_D=1$ and the remaining nodal displacements would be zero. Thus, two suitable stress terms to suppress both modes would be determined, but specific correlation of each term with a mode is not possible in this case.

The stress τ_{xy} does work because of the v displacements along sides BD and EA; also, the modes are equal on both of these faces. Hence, an unsymmetric term which is linear is x is required in τ_{xy} to suppress these modes. However, an inspection of τ_{xy} reveals that such terms are

present already. For example, from Eqs. 4.17 and 4.18a, there are terms like:

$$\times \int_y T_0(y)\, dy\, \beta_{61} \;,\; \times \int_y T_1(y)\, dy\, \beta_{62} \qquad etc. \tag{4.84}$$

But, a careful analysis shows the reason that these terms did not suppress the kinematic modes. The terms given in Eq. 4.84 are computed from τ_{zx} by the relation

$$\tau_{xy} = -\int \frac{\partial \tau_{zx}}{\partial \bar{z}}\, dy \tag{4.85}$$

from Eqs. 4.18a and 4.19, where $\bar{z}$ is the layer axis with its origin at the layer midplane. One can transform to the laminate axis z by the linear relation

$$z = C_0 + C_1 \bar{z} \tag{4.86}$$

Thus, the inplane shear stress can be written for the whole laminate as

$$\tau_{xy} = -c \int \frac{\partial \tau_{zx}}{\partial z}\, dy \tag{4.87}$$

where C is an appropriate constant. The kinematic displacements $\underset{\sim}{v}^*_K$ are independent of z; substituting τ_{xy} from Eq. 4.87 and $\underset{\sim}{v}^*_K$ for $\underset{\sim}{u}^*$ in Eq. 4.79, one finds

$$\begin{aligned} W_B &= \int_{\partial V_n} \tau_{xy}\, \underset{\sim}{v}^*_k\, ds \\ &= -c \int_{\partial V_n} \underset{\sim}{v}^*_k \int \frac{\partial \tau_{zx}}{\partial z}\, dy\, ds \end{aligned} \tag{4.88}$$

The integration in z is uncoupled and can be done first. Thus, one can write Eq. 4.88 as

$$W_B = -c \int_{\partial V_k} \bar{v}_k \int dy\, ds \int_{z=-H}^{H} \frac{\partial \tau_{zx}}{\partial z}\, dz$$

$$= -c \int_{\partial V_k} \bar{v}_k \int dy\, ds \left[\tau_{zx}\right]_{z=-H}^{H} = 0 \qquad (4.89)$$

since surfaces $z=\pm H$ are traction-free (Eq. 4.12). Thus, other terms are needed in τ_{xy} to suppress the kinematic modes.

The two appropriate terms are (see Eq. 4.23)

$$\sigma_x = x^2 \beta_{91} + x^2 y \beta_{93} \qquad (4.90)$$

and by Eqs. 4.24a and 4.25:

$$\tau_{xy} = -2xy \beta_{91} - xy^2 \beta_{93} \qquad (4.91)$$

In order to permit satisfying ε_x continuity at each interface, β_{92} and β_{94} have been added, but these are ineffective in suppressing the kinematic modes since they are odd functions of $\bar{z}$ and vanish during integration. Thus, the two kinematic modes have been eliminated.

Finally, as pointed out in Ref. 41 for a hybrid element, if "m" is the total number of independent β's, "n" is the total number of nodal displacements $\underset{\sim}{q}$, and "ℓ" is the number of rigid-body modes of the element, then a necessary* condition for avoiding kinematic modes is

$$m \geq n - \ell \qquad (4.92)$$

However, satisfying this condition does not ensure kinematic <u>stability</u>; accordingly, care must be taken not to omit important terms.

---

*But not a sufficient condition as the present study has demonstrated.

4.6.3 TFQE Region Proportions

There is one geometric parameter in the TFQE (Fig. 6) which should be carefully prescribed for each problem. This parameter is the distance AE' denoted by the distance "b". The width b should be sufficiently large such that as y increases the interlaminar stresses decay completely when plane CF is reached. This is important because at y=b no warping is allowed, and this would impose a pseudo constraint on the solution. In the $(0/90)_s$ and $(\pm 45)_s$ coupon problems discussed in Section 1, the boundary layer length is of the order of the thickness (2H) of the laminate; hence $b/(2H) \doteq 2$ is appropriate. However, other problems could require a larger (or smaller) b/(2H) ratio. Thus, a recommended rule is to use $[b/(2H)]_{trial}=2$ as an initial estimate; then from the interlaminar stress solution, the ratio can be increased or decreased accordingly. Note that it is also important to keep b a minimum, since the stress assumption will have difficulty representing zero interlaminar stress because of insufficient terms.

Based upon experience in the present study, the intermediate nodes C and F are located at y=0.95b. The distance E'F' (Fig. 6) is kept small because of the assumptions made in Subsection 4.5.2 (see Eq. 4.64a).

SECTION 5

TFQE EVALUATION AND APPLICATION TO THE STRESS ANALYSIS OF LAMINATED PLATES

Reported in this section are results predicted by using the traction-free edge quadrilateral element (TFQE) and comparison with available predictions for several illustrative problems in which severe interlaminar stresses occur at and near traction-free edges of mechanically-loaded or thermally-loaded multilayer laminated "plates". Principal attention is devoted to problems involving static loading. However, an illustrative example for a multilayer plate subjected to transient mechanical loading is included. The static and the transient response examples are discussed in Subsections 5.1 and 5.2, respectively.

5.1 Static Loading Problems

To illustrate the utility and accuracy of the TFQE element, relatively simple problems for which independent solutions were available were chosen. These consist of 4-layer laminated composite plates with the following symmetric layer stacking sequence: (a) $(0/90)_s$ and (b) $(\pm 45)_s$ as shown in Fig. 1. These two different ply orientations and stacking sequences are intended to show the TFQE prediction accuracy and to confirm the proper implementation of the analysis in the associated computer program. In addition, this assessment includes for each case the presence of (1) mechanical loads or (2) thermal loads since independent solutions are also available for each.

Another important physical situation where severe interlaminar stresses occur is that of cutouts or "windows" in multilayer composite plates and shells. Accordingly, this type of problem is investigated for two tension-loaded flat plates with a circular hole: (1) an isotropic plate and (2) a 4-layer $(0/90)_s$ laminated plate.

These six examples for both illustration and evaluation are discussed in Subsections 5.1.1 through 5.1.6.

An experimental investigation of the delamination behavior of layered composites was carried out by Harris and Orringer [4]. Two types of coupons were tested: (a) $[(\pm 26)_2/90]_s$ and (b) $[26/-26_2/26/90]_s$. Both specimens were analyzed by using the TFQE; the solutions are discussed in Subsection 5.1.7.

5.1.1 Tension-Loaded $(0/90)_s$ Coupon

This coupon specimen is depicted in Fig. 1. For the present example, its dimensions are 20h, 16h, and 4h along directions x, y, and z, respectively. Each layer of the symmetric 4-layer $(0/90)_s$ plate has a thickness h. For analysis, advantage has been taken of symmetry about both the x and the y axis; hence, only the quarter-plate has been modeled. Further, this quarter plate has been represented by a single TFQE element; accordingly, as indicated in Fig. 15 its dimensions are 10h, 8h, and 4h along the x, y, and z directions, respectively. On the four x or y boundaries, the conditions imposed are: (1) the entire faces at y = 8h and z = $\pm$H are traction free, (2) the symmetry displacement conditions u = 0 and v = 0 are imposed on the "entire face" at x = 0 and y = 0, respectively, and (3) a prescribed displacement of uniform u is applied at x = 10h such that $\varepsilon_x = 1.0$.[+] Finally, the principal material properties of each ply are:

$$E_L = 20 \times 10^6 \text{ psi}, \quad E_T = E_z = 2.1 \times 10^6 \text{ psi}$$

$$\nu_{LT} = \nu_{Lz} = \nu_{Tz} = 0.21$$

$$G_{LT} = G_{Lz} = G_{Tz} = 0.85 \times 10^6 \text{ psi}$$

Of particular interest is the normal stress σ_z at the symmetry-plane interface z = 0 between plies as a function of the distance y/b. The TFQE result is shown in Fig. 16 together with (a) the finite element result of Wang and Crossman [8] obtained by using assumed-displacements constant-

[+]This loading is equivalent to an applied stress, $\sigma_{x_\infty} = 1.1 \times 10^7$ psi.

strain triangles, (b) Pagano's prediction [12,13] by Reissner's approach, and (c) the assumed-displacement QUAD8 solution (Section 2). The TFQE prediction for σ_z agrees well with the other predictions and exhibits a very large σ_z stress with a steep gradient as the free edge is approached.

The shear stress τ_{yz} at the 0/90 interface where z = h is shown in Fig. 17 as a function of y/b. The solutions are in reasonable overall agreement but the location of the peak value of τ_{yz} predicted by the TFQE differs from the other approximate solutions shown. However, a finite difference solution by Pipes [1] shows a value of $(\tau_{yz})_{max} \doteq -0.11 \times 10^6$ psi which occurs near $y/b \doteq 0.875$; the TFQE solution indicates that $(\tau_{yz})_{max} \doteq -0.17 \times 10^6$ at $y/b \doteq 0.875$; and the solution by Pagano shows $(\tau_{yz})_{max} \doteq -0.23 \times 10^6$ at $y/b \doteq 0.975$. The QUAD8 prediction has not been plotted here because of stress violations of its solution on the 0°/90° interface near the free edge (see Section 2).

The σ_z and τ_{yz} solution obtained by a <u>single</u> TFQE element tends to oscillate about zero from y/b = 0 to about 0.5. This phenomenon exists because the stresses in the TFQE are assumed in polynomial form, but have an insufficient number of terms to represent zero exactly. However, these oscillations do not affect the significant portion of the stresses near the free edge, y = b.

The distribution of σ_z through the thickness is shown in Fig. 18. The maximum occurs at the midplane z = 0 and the stress is continuous across the 0/90 interface unlike the assumed-displacement QUAD8 solution discussed in Section 2. To check for convergence, each ply was represented by two layers (see Fig. 15); this solution (called 8-layer TFQE) is also shown. The solution appears to be converged.

In the other approaches (Refs. 8, 12, 13, and the QUAD8 solution), only the upper half of the laminate ($z \geq 0$) was considered because, the problem is symmetrical about z = 0. In spite of these advantages, the unknowns in each of these approaches are significantly large, and are tabulated below along with the modeling data for the TFQE solution:[+]

[+]The finite difference solution [1] is not included in the tabulation, because, the stresses did not converge at the free edge.

Method of Analysis	Portion of Laminate Thickness Modeled	Total Number of Unknowns
QUAD8 (Section 2)	Half Thickness ($z \geq 0$)	1490 degrees of freedom
Wang and Crossman [8]	Half Thickness ($z \geq 0$)	678 degrees of freedom
Pagano [11,12]	Half Thickness ($z \geq 0$)	138 unknowns
TFQE 4-layer	Total Thickness	62 degrees of freedom
TFQE 8-layer	Total Thickness	94 degrees of freedom

Thus, the TFQE is numerically very efficient compared with the other methods. Also note that the TFQE is a full 3-dimensional plate element which is applicable to more general problems.

5.1.2 Thermally-Loaded $(0/90)_s$ Coupon

This specimen is exactly the same as discussed in Subsection 5.1.1 and shown in Fig. 15, except that only thermal loading is present and is represented by a uniform temperature change $\Delta T = 1°F$; this configuration and thermal loading condition has also been analyzed by Wang and Crossman [45]. As discussed in Subsection 5.1.1, quarter-plate modeling by a single TFQE with NL = 4 has been used. For this case the boundary conditions are: (a) $v = 0$ at $y = 0$ (b) $u = 0$ at $x = 0$, and (c) the faces at $x = 10h$, $y = 8h$, and $z = \pm H$ are stress free. The principal material properties of each layer are the same as those cited in Subsection 5.1.1; in addition, the thermal expansion coefficients are $\alpha_L = 0.2 \times 10^{6}/°F$ and $\alpha_T = \alpha_z = 16 \times 10^{-6}/°F$.

The TFQE-predicted interlaminar normal stress σ_z at the midplane ($z = 0$) is shown in Fig. 19 as a function of y/b and is compared with the assumed-displacement constant-strain triangle finite-element solution of Wang and Crossman [45]. These two solutions are seen to compare well with each other.

The normal stress σ_z (Fig. 20) is shown as a function of location z through the thickness at fixed stations y at and/or near the free edge for: (1) the TFQE solution at y = b and y = 0.9b and (2) Wang and Crossman's solution at y = 0.999b. Note that both of these solutions satisfy the free-surface condtion $\sigma_z = 0$ at z = 2h; also at this location $\tau_{zx} = \tau_{zy} = 0$ and hence the z force-equilibrium equation

$$\frac{\partial \tau_{xz}}{\partial x} + \frac{\partial \tau_{yz}}{\partial y} + \frac{\partial \sigma_z}{\partial z} = 0$$

shows that $\frac{\partial \sigma_z}{\partial z} = 0$. This condition is satisfied exactly by the TFQE and appears to be satisfied approximately by the results of Ref. 45.

The TFQE solution for σ_z vs. z in Fig. 20 shows that σ_z satisfies the physically-correct stress-continuity condition at the 0/90 interface located at z = h and also varies smoothly throughout the depth including this interface. However, the Ref. 45 solution for σ_z vs. z is reminiscent of the assumed-displacement QUAD8 finite element solution shown in Fig. 12 where stress discontinuities are predicted at the 0/90 interface (from elements 220 and 221) and, accordingly, must be suspect.

Finally, the shear stress τ_{zy} at the 0/90 interface (z = h) for the TFQE solution and that of Ref. 45 are shown in Fig. 21 as a function of the y/b location. At the free edge, y/b = 1, the TFQE solution shows the correct result, $\tau_{zy} = 0$, as it must; however, the assumed-displacement finite-element solution of Ref. 45 appears to predict a large value of τ_{zy} at y/b = 1. Except near the free edge, these two solutions are in reasonable agreement.

Only these two solutions were found for this example problem; an exact solution has not been located.

5.1.3 Tension-Loaded $(\pm 45)_s$ Coupon

This coupon specimen is shown schematically in Fig. 1. For the present example, its dimensions are 100h, 16h, and 4h in directions x, y, and z, respectively. Each layer of the symmetric 4-layer plate (45/-45/-45/45 from bottom to top layer), has a thickness of h. It is

desired that "uniform x-direction tractions" be applied on the end faces $x = \pm 30h$ such that the stresses in the laminate will be independent of x as postulated by Pipes and Pagano [5] for a $(\pm 45)_s$ coupon of this type. For this type of laminate, Pipes and Pagano show that the u displacements vary considerably through the thickness-direction z from $z = -2h$ to $z = +2h$.

For analysis, advantage has been taken of symmetry about both the x and the y axis; hence, only the quarter-plate has been modeled. Accordingly, the dimensions of this quarter-plate model (see Fig. 22) are 50h, 8h, and 4h along directions x, y, and z, respectively. For convenience, this coupon has been "tension-loaded" by imposing a uniform x-displacement u over the entire face at $x = 50h$ so as to make $\varepsilon_x = 1.0$.[+] This "violates" the internal u-displacement conditions cited above for the Pipes/Pagano problem; however, by St. Venant's Principle, one expects to find the proper u displacement situation u(y,z) if one makes observations far enough from the "loaded end" which is located at $x = 50h$. Therefore, since stress conditions which are independent of x are sought in the present problem, the quarter-plate has been modeled by 5 TFQE elements along the x-direction, while in each case, each element spans the entire 8h y-dimension. On the four x,y boundaries, the conditions imposed are: (1) the entire face at $y = 8h$ is traction free, (2) the symmetry displacement conditions $u = 0$ and $v = 0$ are imposed on the "entire face" at $x = 0$ and $y = 0$, respectively, and (3) a prescribed displacement of uniform u is applied to the "entire face" at $x = 50h$ to make $\varepsilon_x = 1.0$. Hence, the solution where the stresses are independent of x was taken to be that at the midlength station $x = 25h$. Finally, the material properties of each layer are the same as those cited in Subsection 5.1.1.

The resulting TFQE solution for τ_{xz} as a function of y/b at the -45/+45 interface located at $z = +h$ (and at the midlength station $x = 25h$) is compared in Fig. 23 with three other solutions: (1) a finite-difference solution by Pipes and Pagano [5], (2) a 3-d assumed-stress finite element solution by Rybicki [7], and (3) an assumed-displacement solution by Wang and Crossman [8] obtained by using constant-strain triangles. It should be recalled that the latter two types of finite element solutions

[+]This loading is equivalent to an applied stress, $\sigma_{x_\infty} = 2.9 \times 10^6$ psi.

tend to bound the correct displacement solution [41]; the fact that the two solutions lie essentially on either side of the present TFQE solution is encouraging. That is, the analysis of Ref. 7 is based upon the Principle of Stationary Complementary Energy, that of Ref. 8 is based upon the Principle of Stationary Total Potential Energy, while the TFQE analysis is based upon the "intermediate" Principle of Modified Complementary Energy. However, one cannot claim that these other principles provide bounds on the stress solution. Also, the finite-difference solution of Ref. 5 is seen to be in reasonably good agreement with that of Ref. 8.

Another interesting aspect of the stress prediction for this example is τ_{zx} at the free edge y = b as a function of depthwise location z; the present TFQE prediction as well as those of Refs. 5 and 8 are shown in Fig. 24. They are in reasonable agreement.

5.1.4 Thermally-Loaded $(\pm 45)_s$ Coupon

This specimen is similar to that discussed in Subsection 5.1.3, except that (1) its total x-direction length is 220h and (2) only thermal loading as represented by a uniform temperature change $\Delta T = 1°F$ is employed; this type of example has also been analyzed by Wang and Crossman [45]. Modeling of the quarter-plate (see Fig. 22) was accomplished by using 11 equal-size 4-layer TFQE elements along the x-dimension, while each TFQE element spans the entire 8h y-dimension. For this case the boundary conditions used are (a) v = 0 at y = 0, (b) u = 0 at x = 0, and (c) the faces at x = 110h, y = 8h, and $z = \pm H$ are stress free. The principal material properties of each layer are the same as those cited in Subsection 5.1.2.

It is desired to examine the stresses for comparison with the predictions of Ref. 45 where the stresses are independent of x. Accordingly, the TFQE stress predictions at the "midspan station" x = 55h are discussed in the following. Plotted in Fig. 25 are σ_z, τ_{zx}, and τ_{xy} as a function of y/b at x = 55h and the -45/+45 interface (z = h) for comparison with the Wang and Crossman assumed-displacement finite element solution. Note that at and near the free edge y = b, the TFQE solution differs from that

of Wang and Crossman. Also at y = b, the stress free condition $\tau_{yx} = 0$ is satisfied exactly by the TFQE but is violated seriously by the Ref. 45 prediction. Recalling from the Subsection 1.1 discussion that τ_{zx} balances τ_{yx} at the free edge, the larger value predicted by Ref. 45 for τ_{zx} might very well have arisen from the violation of the stress free condition $\tau_{yx} = 0$ at y = b, and hence must be viewed skeptically.

The Ref. 45 predictions and the present TFQE predictions for various stresses are shown as a function of z as follows:

Figure	Stress	At y/b
26a	τ_{zx}	0.999 for Ref. 45
		1.0 for TFQE
26b	σ_x	0.999 for Ref. 45
		1.0 for TFQE

It is remarked in Ref. 45 that the stress behavior at z = h near y = b is (suggestive of) a singular point. The TFQE solution (Figs. 26a and 26b) does not show such a pronounced gradient, possibly because of the limited z terms in the stress assumption of the TFQE for each ply. To alleviate this, each ply could be subdivided into many layers; however, this was not carried out in the present study because of time and fund limitations. Both solutions show that $\tau_{xz} = 0$ at z = 2h and at the symmetry plane z = 0.

5.1.5 Uniaxial-Tension-Loaded Isotropic Plate with a Circular Hole

In classical elasticity theory, the analysis of uniaxial-tension-loaded plates with a circular hole (see Fig. 27a) is usually based upon the theory of generalized plane stress. However, if the ratio D/t of hole diameter D to plate thickness t is small (less than about 10), significant three-dimensional effects occur, and accordingly plane stress theory is inadequate. Alblas [22] has solved the three-dimensional elasticity problem by the use of complex eigenfunctions. Hence, to

AD-A071 910 MASSACHUSETTS INST OF TECH CAMBRIDGE AEROELASTIC AND--ETC F/G 20/11
A MULTILAYER, TRACTION-FREE EDGE, QUADRILATERAL, WARPING ELEMEN--ETC(U)
APR 79 A HARRIS, O ORRINGER, E A WITMER DAAG46-78-C-0015
UNCLASSIFIED ASRL-TR-193-1 AMMRC-TR-79-26 NL

2 OF 3
AD A071910

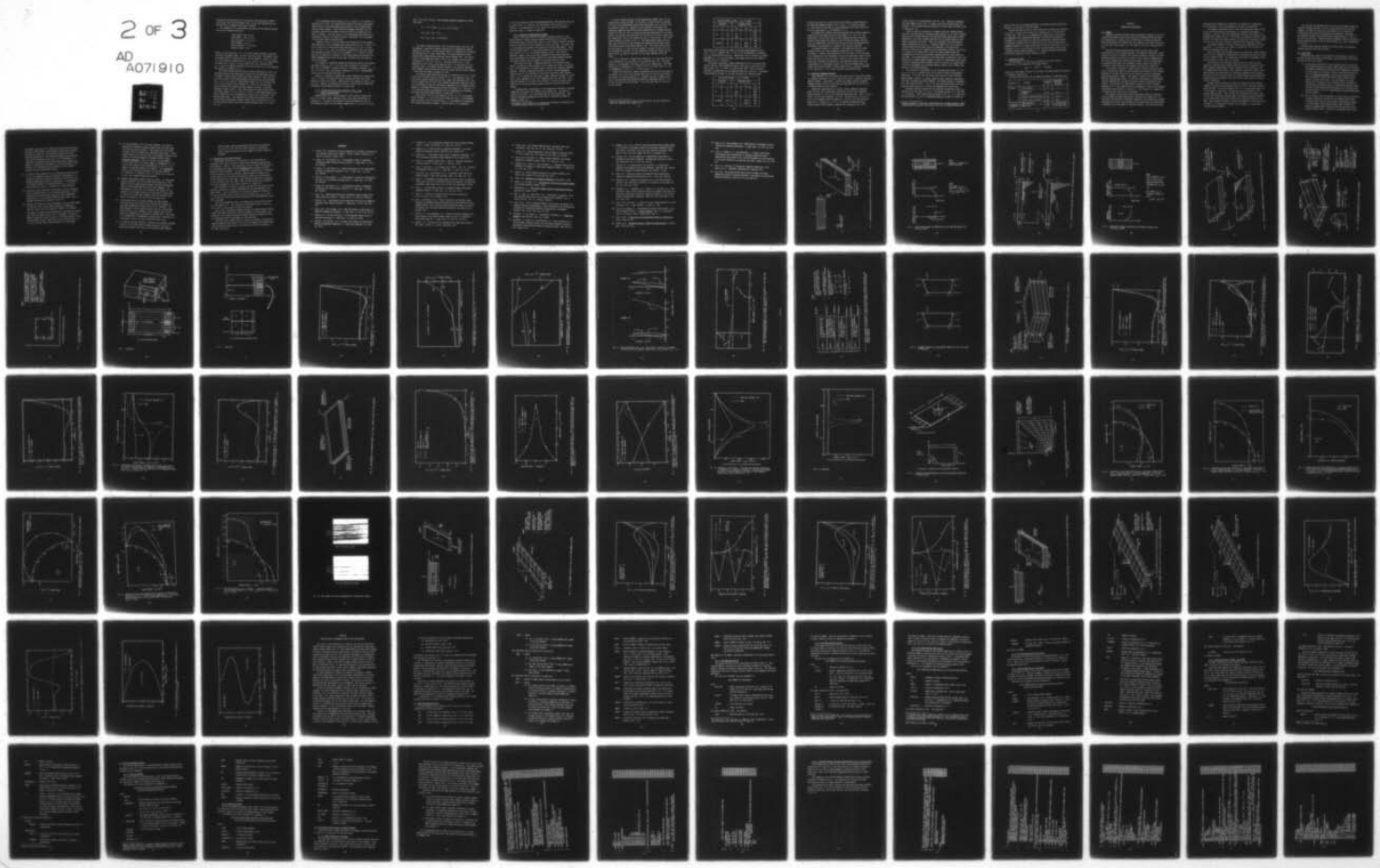

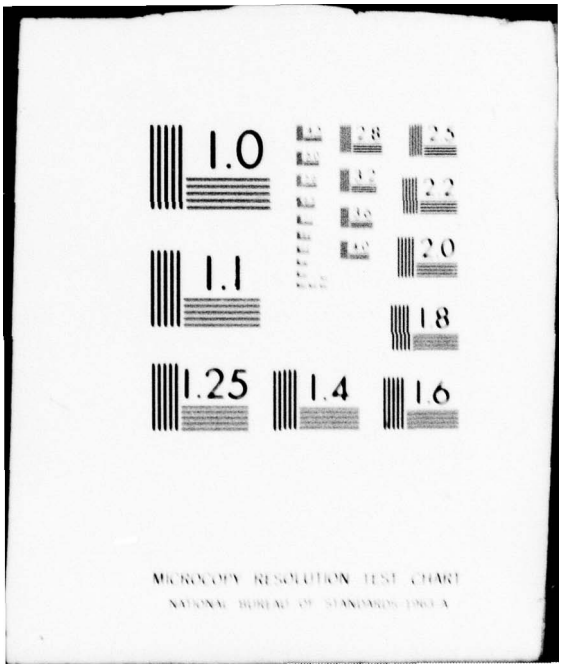
1.0
1.1
1.25
1.4
1.6
2.8
2.5
2.2
2.0
1.8
MICROCOPY RESOLUTION TEST CHART
NATIONAL BUREAU OF STANDARDS-1963-A

illustrate the applicability of the present three-dimensional TFQE to such a case, this type of problem (Fig. 27) has been analyzed and the results will be compared with those of Alblas.

The geometry of the configuration analyzed and the material properties of the isotropic plate are:

Plate Length = 2A = 8.0 in
Plate Width = 2B = 8.0 in
Plate Thickness = t = 0.5 in
Hole Diameter = 1.0 in
Elastic Modulus = E = 10^7 psi
Poisson's Ratio = 0.25

Hence, for this case (D/t) = 2. For finite element modeling, advantage was taken of symmetry about both the x and the y axis. Accordingly, only the quarter-plate as depicted in Fig. 27b was modeled. Along x = 0 and y = 0 the conditions imposed were $u = \theta_y = 0$ and $v = \theta_x = 0$, respectively. The edges at y = B and r = R were stress free, and a uniform stress $\sigma_x = 1.0$ psi was imposed uniformly on the entire face at x = A to simulate the uniform σ_x condition at $x \to \infty$.

The finite element modeling used is shown schematically in Fig. 28. Anticipating that three-dimensional effects will be significant only in a region of radial extent of about the plate thickness t near the hole, an initial width b of the TFQE elements surrounding the hole was taken as b = t = 0.5 in, and the "intermediate nodes C and F of the TFQE (see Fig. 6) were located at the distance b' = 0.4875 in; the resulting solution showed very rapidly decaying behavior such that no warping appeared at nodes C and F. Thus, TFQE elements of small radial width b were used; namely, b = 0.2 in and b' = 0.19 in. Eight TFQE elements were used to model the (3-d) circumferential region next to the hole in the quarter-plate model. The remainder of the plate was modeled with the hybrid-stress quadrilateral element, MLP3K [26] as indicated in Fig. 28; in each "radial sector" there were 24 MLP3K elements (NER = 24 -- see Fig. 28).

The interlaminar normal stress σ_z at r = R and z = 0 is shown as a function of θ in Fig. 29 as predicted by Alblas [22] and by the present TFQE analysis; the plotted TFQE points pertain to the circumferential center of each element. These predictions compare favorably, but the stresses predicted by the TFQE calculation tend to be larger by up to about 10 percent. Note also that σ_z is of significant magnitude over a substantial θ-sector, and should be taken into account in an assessment of the stress condition around holes.

Compared in Fig. 30 are the Alblas [22] prediction and the present TFQE prediction of the circumferential normal stress σ_θ at r = R and z = 0 as a function of θ; these predictions show that $\sigma_\theta = -1$ at $\theta = 0°$ and $\sigma_\theta = +3.0$ at $\theta = 90°$. Also, σ_θ exhibits a significant variation through the thickness as shown in Fig. 31, for example, at r = R and $\theta = 5.625°$ where σ_θ is plotted as a function of z/H; these results are plotted on a highly expanded stress scale and are seen to differ from each other by only a few percent.

At a station $z = \frac{H}{2}$ midway between the midsurface and the top surface, the shear stress $\tau_{z\theta}$ at r = R for the TFQE calculation is plotted in Fig. 32 as a function of angular position θ. Because of symmetry, $\tau_{z\theta} = 0$ at $\theta = 0°$ and $\theta = 90°$, and reaches a maximum at $\theta = 45°$. Corresponding results are not available from Ref. 22.

Finally, it should be remarked that Alblas compared his solution for (D/t) = 1.0 with 3-d elasticity results obtained by Green [24] using series in $\sin(n\theta)$ and $\cos(n\theta)$. Those results also agreed to within a few per cent. However, an examination of Refs. 22 and 24 does not show that convergence was definitely achieved in either case.

5.1.6 Uniaxial-Tension-Loaded Laminated $(0/90)_s$ Plate with a Circular Hole

Schematically, Fig. 27a also applies to this problem, except that this is a 4-layer $(0/90)_s$ symmetric plate, each layer of which has a thickness h. In terms of the geometric quantities defined in Fig. 27, the dimensions chosen for the present example are A = B = 8 in, R = 2 in,

and t = 2H = 4h = 0.02 in. The principal material properties of each layer are:

$$E_L = 30.7 \times 10^6 \text{ psi}, \quad E_T = E_z = 2.89 \times 10^6 \text{ psi}$$

$$\nu_{LT} = \nu_{Lz} = \nu_{Tz} = 0.21$$

$$G_{LT} = G_{Lz} = G_{Tz} = 0.723 \times 10^6 \text{ psi}$$

For finite element analysis, only the quarter-plate (see Fig. 27b) was modeled. Eight TFQE elements occupied the circumferential region adjacent to the hole. In each radial sector, the remainder of the plate was modeled with 14 "equal length" (NER = 14) MLP3K lamination theory hybrid stress quadrilateral multilayer plate elements [26]. The radial width b of each TFQE was chosen to be 0.1 in, whereas the total plate thickness is t = 2H = 4h = 0.02 in. This means that (b/t) = 5 was employed for this $(0/90)_s$ plate whereas (b/t) = 0.4 was chosen for the isotropic plate. The larger b-width required in the present laminated plate example stems from the fact that this plate exhibits severe warping -- with which the TFQE is designed to cope.

The present TFQE predictions for $\sigma_{z\theta}$ as a function of θ at r = R and at the 0/90 interface which is located at z = h are compared in Fig. 33 with finite element predictions by Levy, Armen, and Whiteside [46]. The finite elements used in Ref. 46 are assumed displacement elements consisting of alternating layers of orthotropic membranes and interlaminar shear regions, as developed originally by Puppo and Evenson [2]. From Fig. 33 it is seen that these $\tau_{z\theta}$ predictions are in reasonably good agreement. Note that this shear stress appears to peak near $\theta = 75°$.

Shown in Fig. 34 is σ_z as a function of θ at r = R at the midplane 90/90 interface (z = 0) for the present TFQE prediction; a corresponding result from Ref. 46 is not shown since $\sigma_z = 0$ was assumed in formulating the assumed displacement elements. Observe that σ_z is a maximum at

$\theta = 90°$ but is about an order of magnitude smaller* than the peak value for $\tau_{z\theta}$ seen on Fig. 33. However, the interlaminar normal stress, σ_z, is critical in the delamination [3] of certain ply stacking/orientation sequences; hence, it cannot be neglected.

5.1.7 Analysis of Experimental Coupons

Bogy [6] has shown that two dissimilar isotropic materials, when bonded together, develop singular stress distributions of the type $r^{-\alpha}$ at the interface near the free edge, where r is the "radial distance" measured from the intersection of the interface with the free edge. The power term α, in his solution, depends on the ratios of the two shear moduli, and of the two Poisson ratios. If the shear modulus of the two materials is the same, then $\alpha = 0$; i.e., no singular behavior occurs. This type of analysis, however, has not yet been extended to orthotropic materials; thus, the existence of singular behavior at interfaces between different orthotropic layers, does not appear to have been proved to date.

One should note that in composite materials the transverse shear moduli, G_{LZ} and G_{TZ} (resin property) do not change with fiber orientation. Thus, it is difficult to correlate Bogy's results with composite laminate behavior. However, numerical solutions [1,5,8] do indicate <u>possible</u> singularities at the interfaces of plies with dissimilar fiber orientations. In the analysis of the $(0/90)_s$ coupon, Wang and Crossman [8] found that σ_z was a maximum at the 0°/90° interface near the free edge. Also, Pipes and Pagano [1,5] using finite differences could not obtain convergence in the $(0/90)_s$ and $(\pm 45)_s$ coupon solutions even with very fine meshes.

An experimental investigation of the delamination behavior of layered composites was carried out by Harris and Orringer [4]. Two types of coupons were tested: (a) $[(\pm 26)_2/90]_s$ and (b) $[26/-26_2/26/90]_s$. Both types of specimens delaminated at the 26°/90° interface as shown, for example, in Fig. 35.

---

*Accordingly, the variation of σ_z through the thickness is believed to be of little interest, and is not plotted here.

A finite element analysis of the delamination coupons (Fig. 36) was carried out by using the TFQE. In the test, at each end of the specimen, 0.125-inch thick glass/epoxy loading tabs were bonded, and a tensile load was applied to each tab. Because of the stiffness of the tabs, this loading for numerical analysis has been represented by a clamped boundary condition at one end, and, an uniform prescribed displacement at the other. However, any loading inconsistencies will be seen only in the stresses near the loaded ends, and will not affect the rest of the solution. The finite element modeling is shown in Fig. 37. The TFQE elements model the free edge, and the interior of the laminate was modeled by multilayer lamination theory hybrid stress MLP3K elements [26]. The stress solution near the free edge at x = 0.25" for both coupons, is given in Figs. 38 to 41. The interlaminar stresses for both coupons are identical, except for the shear stress τ_{xz} which is sensitive to the layup sequence of the 26° plies.

It is of interest to examine the stresses at z = h near the free edge since delamination has occurred at this interface (Fig. 35). The shear stress τ_{xz} is negligible, but both σ_z and τ_{yz} are significant. The shear stress τ_{yz} is a maximum at y = 0.4875" (i.e., y = 0.975b*) and z = h; σ_z is a maximum at y = 0.5" (i.e., y = b*)[+] and z = 0.

Eleven $[26/-26_2/26/90]_s$ coupons delaminated [4] near the free edge in the region $-h \leq z \leq +h$ at an average axial load of 1979 lb; this load is equivalent to an axial strain of $\varepsilon_x = 0.00388$. For this "loading condition", the predicted interlaminar stresses are tabulated below at z = 0, $\frac{h}{2}$, and h at each of two y stations: (1) at the free edge (y = b*) and (2) at 0.975b*:

[+]Note that the plate half width is denoted here as b*; the y-direction width of a TFQE has been defined as b.

$[26/-26_2/26/90]_s$ Coupon: (ε_x = 0.00388)				
Location		Stresses (PSI)		
y	z	τ_{zx}	τ_{zy}	σ_z
b*	0	0	0	9778
	h/2	435	0	9312
	h	896	0	7411
0.975b*	0	0	0	889
	h/2	-10.4	-2429	830
	h	-29.9	-5975	788

Note that the most severe σ_z occurs at the free-edge midplane station (y,z) = (b*,0) ; however, for z > 0 at y = b* one observes the presence of a τ_{zx} contribution as well as a significant level of tensile σ_z stress. Although τ_{zy} = 0 at the free edge, a very large value of this stress is reached at (y,z) = (.975b*,h).

The eleven $[(\pm 26)_2/90]_s$ coupons delaminated [4] at an average axial load of 1583 lb; using lamination theory, this load is equivalent to an axial strain of ε_x = 0.00304. At this strain level, the interlaminar stresses at delamination can be computed from Figs. 38 and 39; accordingly, these predicted stresses at critical locations are tabulated below:

$[(\pm 26)_2/90]$ Coupon: (ε_x = 0.00304)				
Location		Stresses (PSI)		
y	z	τ_{zx}	τ_{zy}	σ_z
b*	0	0	0	7722
	h/2	-389	0	7358
	h	-812	0	5867
0.975b*	0	0	0	681
	h/2	1.3	-1903	635
	h	4.2	-4682	602

For this case also it is seen that the most severe σ_z stress occurs at the free-edge midplane station $(y,z) = (b^*,0)$. At a short distance $y = 975b^*$ from the free edge, σ_z has decreased by more than a factor of 10 but an appreciable τ_{zy} is observed at $z = h$.

The delamination coupons have been analyzed with a minimum number of layers used in the TFQE to model the thickness, i.e., NL = 10. The convergence of the solution has not been studied with more sublayers because storage space was limited in the IBM 370/168 computer used for numerical computation; time and fund constraints have not permitted the development of procedures to circumvent that current limitation.

No singular behavior is observed in the TFQE solutions for these specimens since the stress assumption (Subsection 4.2) includes no singularity. However, many researchers [1,3,8] believe in the existence of a singularity at the interfaces of plies with dissimilar fiber orientations; but this is yet to be proved. However, until this is done, one should also consider the possibility that delamination may arise from a combination of interlaminar tension (σ_z) and interlaminar shear (τ_{yz}), rather than from interlaminar tension alone since τ_{zy} reaches a maximum on the interface $z = h$ at a small distance from the free edge.

5.2 Transient Response Analysis

Many laminated plate structures with one or more traction-free edges are commonly subjected not only to static but also to transient externally-applied loading. Accordingly, a useful but simple transient response example has been chosen to illustrate the applicability and utility of the TFQE element for this purpose.

Chosen for illustration is a 4-layer $(0/90)_s$ symmetric laminated plate (see Fig. 42) of 900h span, 200h width, and 4h total thickness; having selected h = 0.01 in, the attendant dimensions are: span = 9.00 in, width = 2.00 in, and thickness = 0.04 in. The two ends at $x = \pm 4.50$ in are ideally clamped, while the edges at $y = \pm 1.00$ in are traction-free. Along the $y = 0$ plane at $x = 0.50$ in, a downward concentrated step function load P of 200 pounds is applied for a duration of 2×10^{-4}

seconds (that is, 200 microseconds; see Fig. 43b). Because of geometric and load symmetry about the y = 0 plane, only the half-width model was analyzed. The principal material properties of each layer are those cited in Subsection 5.1.1.

Since it might be instructive to compare transient response predictions for the same physical laminated-plate problem for (a) finite element modeling with the TFQE combined with laminated plate MLP3K hybrid stress elements vs. (b) finite element modeling with only MLP3K elements, both types of modelings were used. Figure 43a indicates the finite element modeling employed for case (a): 9 spanwise TFQE's of 0.08-in width are located along the free edge, while the remainder of the half plate consists of two rows of 9 spanwise equal-width MLP3K elements, and results in a total of 312 unknown DOF's; thus, the TFQE elements permit the accommodation of the very significant warping which can occur along the free edge. The second modeling of the half plate, as depicted in Fig. 43b, consists of 9 spanwise MLP3K elements in each of 3 equal-width rows; these "stiffer" lamination-theory elements involve a total of 144 unknown DOF's but do not accommodate the free-edge warping behavior that is taken into account in the former modeling.

The transient w-displacement at the load-application point (x = 0.5 in, y = 0, z = 0) is shown in Fig. 44 for each of these finite-element modelings. It is seen that the model which consists of both TFQE and MLP3K elements results in a larger predicted peak transient displacement than that utilizing only MLP3K elements. The former behaves, as expected, as a less stiff structure. Also, it is seen that beyond about 1300 μsec, these two predictions are in rather good agreement with each other.

Perhaps of greater interest is the transient interlaminar stress τ_{zx} located at the free edge y = 1.00 in, the midspan station x = 0, and the z = 0 interface. These predictions are shown in Fig. 45. It is seen that the peak positive τ_{zx} for the TFQE/MLP3K modeling is about 12 times[+] as

[+]Another calculation utilizing 5 equal-width rows of MLP3K elements showed a peak positive τ_{zx} about one-sixth of that for the TFQE/MLP3K modeling.

large as that for the all-MLP3K modeling; the former provides a much more realistic τ_{zx} prediction than the latter.

Another interesting facet of these predictions concerns the variation of τ_{zx} and σ_z through the thickness at a station (x,y) = (0,1.00 in) at t = 1200 μsec. This τ_{zx} vs. z information is shown in Fig. 46 for both the TFQE/MLP3K and the all-MLP3K modeling; the variations through the thickness of τ_{zx} are similar for these two predictions, though different in magnitude. Finally, Fig. 47 shows the σ_z vs. z profile only for the TFQE/MLP3K modeling; the peak values occur at the two interfaces at $z = \pm h$. Information on σ_z is not obtained from the all MLP3K model, since these lamination theory elements assume $\sigma_z \equiv 0$. Similar through-the-thickness profiles are observed at other instants in time.

5.3 Computation Times

The approximate CPU time (T_{CPU}) required on the IBM 370/168 to generate all of the properties of a single TFQE is

$$T_{CPU} = (NL)^{2.15} \quad \text{(Seconds)}$$

where NL is the number of layers of the TFQE. The above empirical equation is accurate to within 10%.

The CPU times required for the example problems are tabulated below:

Analysis	Problem	No. of Unknown q	Approximate CPU Time (Seconds)
Static	4-Ply Coupons	62	2
	Delamination Coupons	420	14.4
	Isotropic Plate with Hole	738	27.8
	$(0/90)_s$ Plate with Hole	909	40.9
Transient Response	TFQE and MLP3K	360	1.13/Time Step
	MLP3K Only	200	0.46/Time Step

SECTION 6

SUMMARY AND CONCLUSIONS

6.1 Summary

Laminated composites develop large interlaminar stresses at and near traction-free edges; often these stresses are significant and can cause ply delaminations. However, they are difficult to analyze and predict accurately because the stresses vary very rapidly over a small region near the free edge, whose extent is of the order of the total laminate thickness.

Previous solution methods have been able to solve only a very restricted class of free-edge problems. The numerical procedures (finite difference and finite element) are limited by computer storage; the other methods available are difficult to apply to more general problems which may involve complex edge geometries and loading. Also, an investigation of assumed displacement finite elements revealed severe violations of interlayer stress continuity and boundary traction-free conditions.

In the present research, a hybrid stress multilayer warping element with a traction-free edge has been developed for efficient finite element modeling at and near free edges, and is termed the Traction Free-Edge Quadrilateral Element (TFQE). The element is based on the Principle of Modified Complementary Energy, in which the requirements of interelement traction compatibility and applied boundary traction compatibility are relaxed. The stresses are independently assumed in terms of unknown parameters, $\underset{\sim}{\beta}$, in each element and are eliminated in terms of the boundary displacement nodal degrees of freedom, $\underset{\sim}{q}$. This results in a compact set of equations with only the $\underset{\sim}{q}$'s as unknowns.

The element stresses were selected from basic mechanics considerations including free-body equilibrium, traction-free conditions on the free edge, and interlayer continuity conditions. The stresses are assumed throughout each layer, and interlayer stress continuity and traction-free conditions at the free-edge are satisfied exactly. The resulting stress

distribution was examined for consistency as required by 3-dimensional stress functions. The stress assumption includes no singularity.

The assumed displacement field allows the traction-free edge to warp freely, and the transverse displacement w is quadratic through-the-thickness. However, since the interlaminar stresses decay rapidly (in a boundary-layer length which is of the order of a laminate thickness), away from the free-edge the element boundary is modeled by 5 degrees of freedom at each of its two nodal stations, consistent with lamination theory.

For dynamic analyses, a "hybrid semi-rational" mass matrix has been developed. It is based on the dynamic equivalent of the Principle of Modified Complementary Energy, π_{mc}.

Also for steady-state thermal analyses, an equivalent thermal loading vector has been computed by modifying the variational principle to include initial thermal strains. The temperature distribution is assumed to have been prescribed in each layer of the TFQE.

The interior of the laminate, away from the free edge, has been modeled by laminated-plate elements which are based on lamination theory. These elements (named MLP3K) include transverse shear deformation and are compatible with the TFQE. Thus, numerical results for general free-edge problems are obtained with an efficient lamination-theory element modeling of most of the structure, while TFQE elements provide additional warping degrees-of-freedom at and near the free edges where the warping effect is important.

Several static mechanically-loaded and thermally-loaded laminate examples, for which other numerical solutions exist, have been solved by using the TFQE. The results compare well, but a significant reduction in the number of unknowns of the equations has been achieved in the present TFQE solution. Also, several of the numerical procedures used in the "other solutions" violate some of the proper traction conditions. All of these stress conditions, however, are satisfied exactly by the TFQE. Even though the present illustrative examples are very restricted, the TFQE is a 3-dimensional element and, accordingly, is applicable to more general problems.

To illustrate the applicability and utility of the TFQE element for transient response analysis, a narrow laminated plate with both ends clamped, its other two sides free, and subjected to a w-direction concentrated step load of short duration was analyzed. Significant interlaminar stresses were predicted by the TFQE analysis to occur at and near the free edge. Lamination-theory analysis, however, resulted in a serious underestimation of one of these stresses τ_{zx}, and no information at all for σ_z.

Finally, some numerical methods for solving static and transient response equations have been reviewed.

6.2 Conclusions

Based upon this study of the analysis of interlaminar stresses at and near traction-free edges of multilayer laminated plates, the following conclusions can be stated:

(a) An efficient hybrid-stress finite element called the traction-free-edge-quadrilateral element (TFQE) based upon the Principle of Modified Complementary Energy has been developed successfully for the analysis of stresses, strains, and deflections at and near the traction-free edges of multilayer laminated plates where significant warping and severe rapidly varying interlaminar stresses often occur. The achievement of a given accuracy of interlaminar stress prediction with the TFQE for representative problems requires a substantially smaller number of final unknown generalized displacements $\tilde{q}$ in the governing equations than by the use of representative assumed-displacement finite elements.

(b) For the present class of problems, an exact solution upon which to base or guide the selection of the assumed stress field throughout each layer of the multilayer hybrid-stress element is not available, unlike hybrid-stress crack elements [47] where the assumed stress field is based upon the known exact solution around cracks. Therefore, the assumed stress field

throughout each layer of the TFQE has been selected from basic mechanics considerations, requirements arising from free-body equilibrium conditions, and consistency implied by stress function formulations. The resulting assumed-stress distribution selected throughout each layer of the TFQE appears to represent a reasonable spatial distribution while keeping the number of assumed-stress parameters β from being unduly large. However, more comprehensive distributions for the assumed stresses could be implemented readily.

(c) In hybrid stress elements when the interlaminar normal stress, $\sigma_z \neq 0$, the assumption that the transverse displacement w is a constant through the laminate thickness at any point in the boundary displacement field is inconsistent. This assumption is incorrect because the transverse strain, ε_z, is zero at those locations; also, σ_z is sensitive to this constraint.

(d) Interlayer stress continuity and boundary traction conditions can be satisfied exactly in the hybrid stress model. These conditions are enforced most efficiently when implemented analytically as in the present TFQE procedure rather than by Lagrange multipliers as reported in Ref. 20.

(e) Whereas, the number of stress parameters $\underset{\sim}{\beta}$ in each TFQE element is (52NL-18), the "final" nodal $\underset{\sim}{q}$ degrees of freedom are (8NL+30), where, NL is the number of layers in the element. The number of assumed-stress parameters β increases more rapidly than does the number of $\underset{\sim}{q}$'s as NL is increased. Further, no adverse (numerical) effect was seen in the TFQE solution of the tension-loaded $(0/90)_s$ coupon when NL was increased from 4 to 8; on the contrary both solutions appear to be converged.

(f) In the development of hybrid stress elements, care must be exercised to eliminate kinematic modes since such modes make the stiffness matrix singular. The present study has demonstrated a useful procedure for eliminating these modes. Demonstrated here also is the fact that the necessary condition cited in Ref. 42 for the avoidance of kinematic modes is not a sufficient condition. That is, the Ref. 42 requirement is $m \geq n-\ell$, where "m" is the total number of independent β's, "n" is the total number of nodal displacements $\underset{\sim}{q}$, and "ℓ" is the number of rigid-body modes of the element. In a preliminary version of the present formulation for the TFQE, however, $m = (52NL-18)$, $n = (8NL+30)$, and $\ell = 6$; hence, $m \geq n-\ell$ for all NL, but two kinematic modes were present.

(g) Assumed displacement elements tend to violate: (1) interlayer stress continuity and (2) traction-free conditions at free edges; this well-known general behavior has been demonstrated here for stress-free-edge multilayer plate examples. The deficiencies of such 2-d or 3-d elements when applied to the analysis of multilayer plates can be alleviated to some extent by the use of a great many elements (and the attendant large number of unknowns in the final governing equations).

(h) The uniaxial tests of 10-layer coupons of layup sequence $[26/-26_2/26/90]_s$ and $[(\pm 26)_2/90]_s$ by Harris and Orringer [4] show that delamination occurs at the 26°/90° interface. The TFQE analysis of these coupons predicts that the interlaminar shear stress τ_{zy} is a maximum at this interface near the free edge; also, significant σ_z stresses are present here. This leads to the possibility of delamination arising from a combination of interlaminar tension (σ_z) and interlaminar shear (τ_{zy}).

(i) In transient response problems, significant interlaminar stresses can occur at the free edges of laminated plates, and can be predicted plausibly with the use of the present TFQE elements.

These stresses cannot be predicted efficiently and accurately or even at all for certain of these stresses by lamination theory (and the associated finite element or finite difference analyses).

6.3 Suggestions for Future Research

The possible existence of a singularity at the interfaces of dissimilar plies near free edges of multilayer laminates needs further investigation. However, this singularity could be created "artificially" by the mathematical model, because mathematical ply properties change abruptly across interfaces. In real laminates, the material is two phase (resin and fiber), and ply properties change gradually; however, this could possibly lead to stress concentrations rather than singularities at the interface near free edges. When accurate information is obtained at ply interfaces near free edges, these stress features can be added to the stress assumption of the TFQE to improve its capability.

The continuity of strains ε_y and γ_{xy} (as well as the presently implemented ε_x continuity) at layer interfaces has not been enforced in the TFQE element. This is difficult in the present formulation because, ε_y and γ_{xy} are complex linear functions of the stresses, σ_x, σ_y, σ_z, and τ_{xy}. A method of satisfying strain continuity for these components needs to be developed.

The stress assumption used in the TFQE is for the most part linear in x and quartic in y. The influence of additional terms in either or both x and y on the solutions should be studied.

Most of the illustrative examples (except the tension-loaded $(0/90)_s$ coupon) have been studied with a minimum number of layers modeling the thickness. More detailed sublayered models should be analyzed to check for convergence and for improvement of the solutions.

The TFQE finite element should be tested on problems involving more complex geometries and loading. For such cases appropriate experimental and/or theoretical data should be obtained for testing the adequacy of the TFQE predictions.

REFERENCES

1. Pipes, R.B., "Solution of Certain Problems in the Theory of Elasticity for Laminated Anisotropic Systems", Doctor's Thesis, University of Texas at Arlington, Texas, 1972.

2. Puppo, A.H. and Evensen, H.A., "Interlaminar Shear in Laminated Composites under Generalized Plane Stress", J. Comp. Mat., 4, 1970, pp. 204-223.

3. Pagano, N.J. and Pipes, R.B., "Some Observations on the Interlaminar Strength of Composite Laminates", Int. J. Mech. Sci., 15, 1973, pp. 679-688.

4. Harris, A. and Orringer, O., "Investigation of Angle-Ply Delamination Specimen for Interlaminar Strength Test", J. Comp. Mat., 12, 1978, pp. 285-299.

5. Pipes, R.B. and Pagano, N.J., "Interlaminar Stresses in Composite Laminates under Uniform Axial Extension", J. Comp. Mat., 4, 1970, pp. 538-548.

6. Bogy, D.B., "Edge-Bonded Dissimilar Orthogonal Elastic Wedges under Normal and Shear Loading", J. Appl. Mech., 35, 1968, pp. 460-466.

7. Rybicki, E.F., "Approximate Three-Dimensional Solutions for Symmetric Laminates under Inplane Loading", J. Comp. Mat., 5, 1971, pp. 354-361.

8. Wang, A.S.D. and Crossman, F.W., "Some New Results on Edge Effect in Symmetric Composite Laminates", J. Comp. Mat., 11, 1977, pp. 92-106.

9. Pagano, N.J., "On the Calculation of Interlaminar Normal Stress in Composite Laminates", J. Comp. Mat., 8, 1974, pp. 65-82.

10. Whitney, J.M. and Sun, C.T., "A Higher Order Theory for Extensional Motion of Laminated Composites", J. Sound and Vibration, 30, 1973, pp. 85-97.

11. Reissner, E., "On a Variational Theorem for Finite Element Deformations", J. Math. and Physics, 32, 1953, pp. 129-135.

12. Pagano, N.J., "Stress Fields in Composite Laminates", Air Force Materials Laboratory Report AFML-TR-77-114, August 1977.

13. Pagano, N.J., "Free Edge Stress Fields in Composite Laminates", Air Force Materials Laboratory Report AFML-TR-77-113, August 1977.

14. Tang, S., "A Boundary Layer Theory - Part I: Laminated Composites in Plane Stress", J. Comp. Mat., 9, 1975, pp. 33-41.

15. Tang, S. and Levy, A., "A Boundary Layer Theory - Part II: Extension of Laminated Finite Strip", J. Comp. Mat., 9, 1975, pp. 42-52.

16. Friedrichs, K.O. and Dressler, R.F., "A Boundary Layer Theory for Elastic Plates", Comm. Pure and Appl. Math., 14, 1961, pp. 1-33.

17. Tang, S., "Interlaminar Stresses Around Circular Cutout of Composite Plates under Tension", Structures, Structural Dynamics, and Materials Conference, 18th, March 1977, pp. 251-259 (also AIAA Paper 77-409).

18. Tang, S., "Interlaminar Stresses of Uniformly Loaded Rectangular Composite Plates", J. Comp. Mat., 10, 1976, pp. 69-78.

19. Wang, S., "Fracture of Graphite Fiber Reinforced Composites", Doctor's Thesis, MIT, September 1974.

20. Mau, S. and Witmer, E.A., "Static, Vibration, and Thermal Stress Analyses of Laminated Plates and Shells by the Hybrid-Stress Finite-Element Method, with Transverse Shear Deformation Effects Included", Aeroelastic and Structures Research Laboratory, MIT ASRL TR 169-2, October 1972.

21. Rybicki, E.F. and Schmueser, D.W., "Effect of Stacking Sequence and Lay-up Angle on Free Edge Stresses Around a Hole in a Laminated Plate under Tension", J. Comp. Mat., 12, 1978, pp. 300-313.

22. Alblas, J.B., "Theorie Van De Driedimensionale Spanningstoestand In Een Plaat", Thesis, H.J. Paris, Amsterdam, 1957.

23. Green, A.E., "The Elastic Equilibrium of Isotropic Plates and Cylinders", Proc. Roy. Soc. A, 195, 1949, pp. 533-552.

24. Green, A.E., "Three-Dimensional Stress Systems in Isotropic Plates I", Phil. Trans. Roy. Soc. London A, 240, 1949, pp. 561-597.

25. Pian, T.H.H. and Tong, P., "Finite Element Methods in Continuum Mechanics", Advances in Appl. Mech., 12, 1972, pp. 1-58.

26. Spilker, R.L., Chou, S.C. and Orringer, O., "Alternate Hybrid-Stress Elements for Analysis of Multilayer Composite Plates", J. Comp. Mat., 11, 1977, pp. 51-70.

27. Harris, A., "Finite Element Analysis of a Contact Problem", M.S. Thesis, MIT, August 1974 (also ASRL TR 176-1).

28. Jones, R.M., Mechanics of Composite Materials, McGraw-Hill, 1975.

29. Desai, C.S. and Abel, J.F., Introduction to the Finite Element Method, Von Nostrand Reinhold Company, 1972.

30. Zienkiewicz, O.C., The Finite Element Method in Engineering Science, McGraw-Hill, London, 1971.

31. Tong, P., Mau, S.T. and Pian, T.H.H., "Derivation of Geometric Stiffness and Mass Matrices for Finite Element Hybrid Models", Int. J. Solids and Str., Vol. 10, 1974, pp. 919-932.

32. Pian, T.H.H., "Finite Element Methods by Variational Principles with Relaxed Continuity Requirements", Paper Presented at the International Conference on Variational Methods in Engineering, Southampton, England, Sept. 25-29, 1972, pp. 3/1-3/24.

33. Dahlquist, G. and Björck, A. (translated by Anderson, A.), Numerical Methods, Prentice-Hall, 1974, pp. 162-167.

34. Orringer, O., French, S.E. and Weinreich, M., "User's Guide for the Finite Element Analysis Library and the Element Generator Library", Aeroelastic and Structures Research Laboratory Report, ASRL TR 1024, MIT, January 1978.

35. Spilker, R.L. et al., "Use of the Hybrid-Stress Finite-Element Model for the Static and Dynamic Analysis of Multilayer Composite Plates and Shells", Aeroelastic and Structures Research Laboratory Report, ASRL TR 181-2, MIT (also AMMRC CTR 76-29), September 1976.

36. Nickell, R.E., "On the Stability of Approximation Operators in Problems of Structural Dynamics", International Journal of Solids and Structures, Vol. 7, 1971, pp. 301-319.

37. Geradin, M., "A Classification and Discussion of Integration Operators for Transient Structural Response", AIAA Paper No. 74-105, AIAA 12th Aerospace Sciences Meeting, Jan. 30-Feb. 1, 1974.

38. Park, K.C., "Practical Aspects of Numerical Time Integration", Journal of Computers and Structures, Vol. 7, 1977, pp. 343-353.

39. Newmark, N.N., "A Method of Computation for Structural Dynamics", Journal of the Engineering Mechanics, Proceedings of the ASCE, Vol. 85, July 1959, pp. 67-94.

40. Kotanchik, J.J., Yeghiayan, R.P., Witmer, E.A. and Berg, B.A., "The Transient Linear Elastic Response Analysis of Complex Thin Shells of Revolution Subjected to Arbitrary External Loadings, by the Finite-Element Program SABOR 5/DRASTIC", SAMSO TR 70-206 (MIT ASRL TR 146-10), April 1970.

41. Pian, T.H.H. and Tong, P., "Basis of Finite Element Methods for Solid Continua", Int. J. Num. Methods, 1, 1969, pp. 3-28.

42. Fraeijs de Veubeke, B., "Displacement and Equilibrium Models in the Finite Element Method", in Stress Analysis, (Ed. O.C. Zienkiewicz and G.S. Holister), Wiley, London, 1965, Chap. 9.

43. Love, A.E.H., A Treatise on the Mathematical Theory of Elasticity, Dover, 1944, pp. 88.

44. Snyder, M.A., Chebyshev Methods in Numerical Approximation, Prentice-Hall, 1966, pp. 20-21.

45. Wang, A.S.D. and Crossman, F.W., "Edge Effects on Thermally Induced Stresses in Composite Laminates", J. Comp. Mat., 11, 1977, pp. 300-312.

46. Levy, A., Armen Jr., H. and Whiteside, J., "Elastic and Plastic Interlaminar Shear Deformation in Laminated Composites under Generalized Plane Stress", Proc. of 3rd Conference on Matrix Methods in Structural Mechanics, Wright-Patterson AFB, October 1971, pp. 959-990.

47. Lin, K.Y., "Fracture of Filamentary Composite Materials", Ph.D. Thesis, M.I.T., Cambridge, Massachusetts, February 1977.

48. Lee, S.W., "An Assumed Stress Hybrid Finite Element for Three-Dimensional Elastic Structural Analysis", Aeroelastic and Structures Research Laboratory, ASRL TR 170-3, MIT, May 1974.

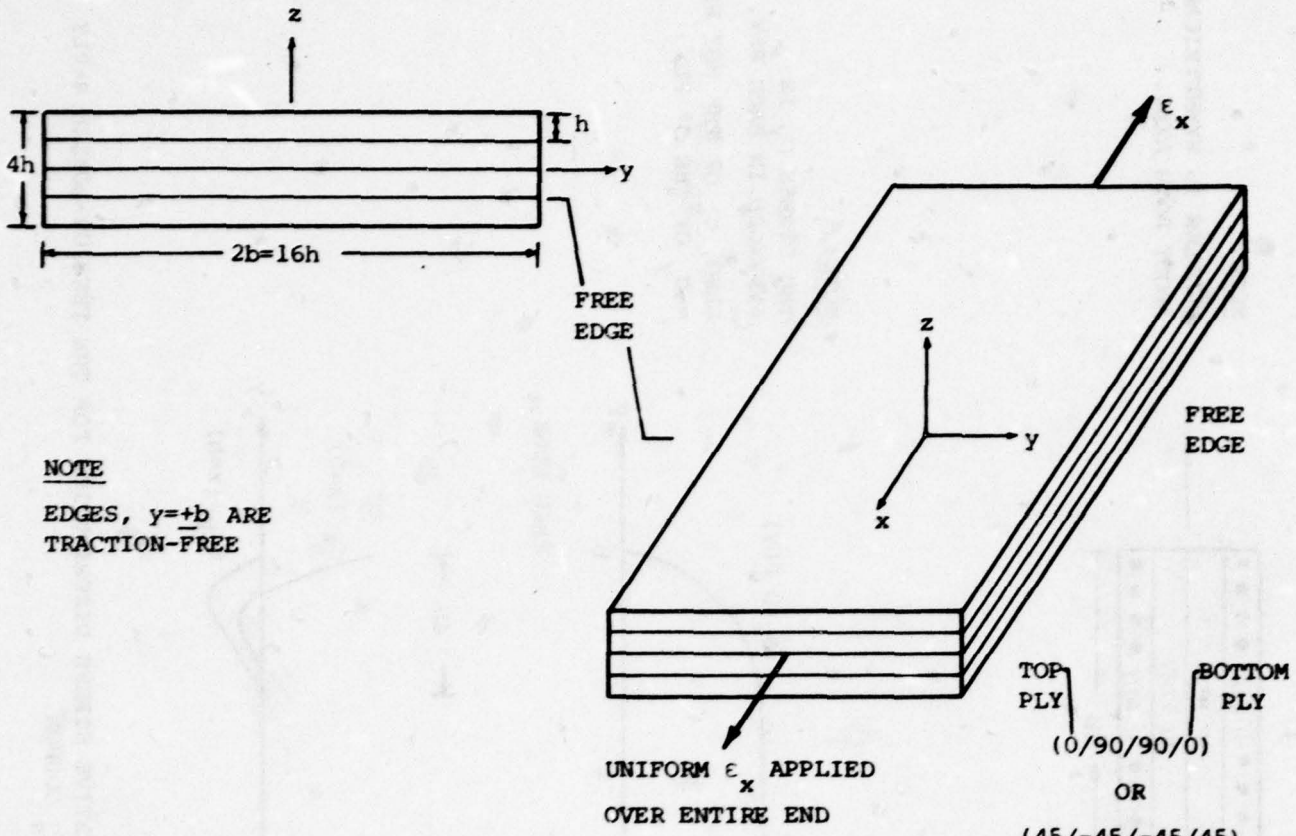

FIG. 1 NOMENCLATURE AND DEFINITION OF THE TENSION-LOADED 4-PLY COUPON

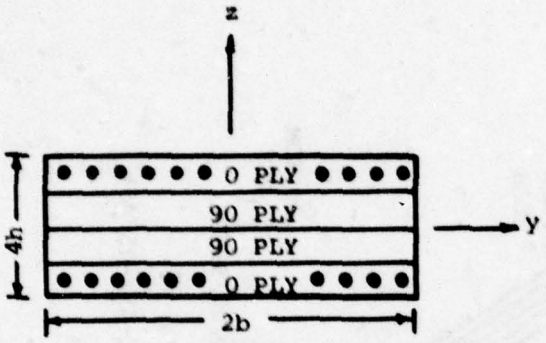

NOTE:

PROBLEM IS SYMMETRICAL ABOUT BOTH AXES.

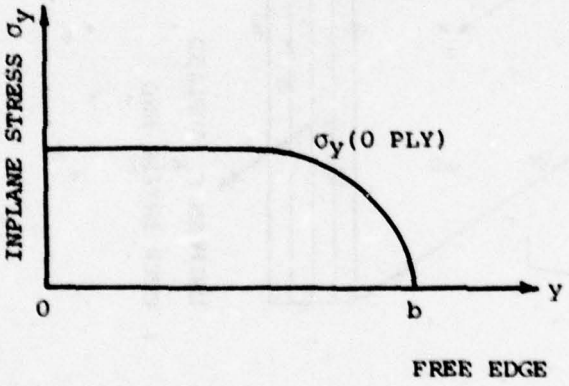

FREE EDGE

NOTE:

THE STRESS σ_y IS AVERAGED IN EACH PLY.

ALSO, σ_y OF THE 90° PLY $= -\sigma_y$ OF THE 0° PLY

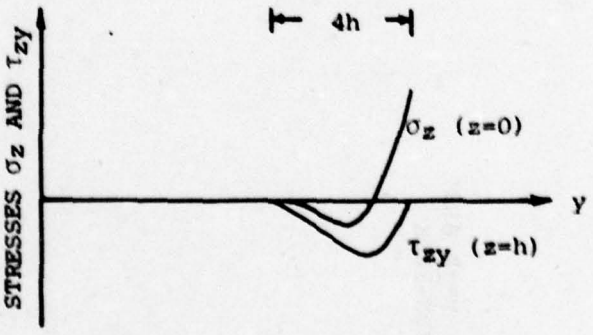

FIG. 2 QUALITATIVE STRESS DISTRIBUTION FOR THE TENSION-LOADED 4-PLY $(0/90)_s$ COUPON

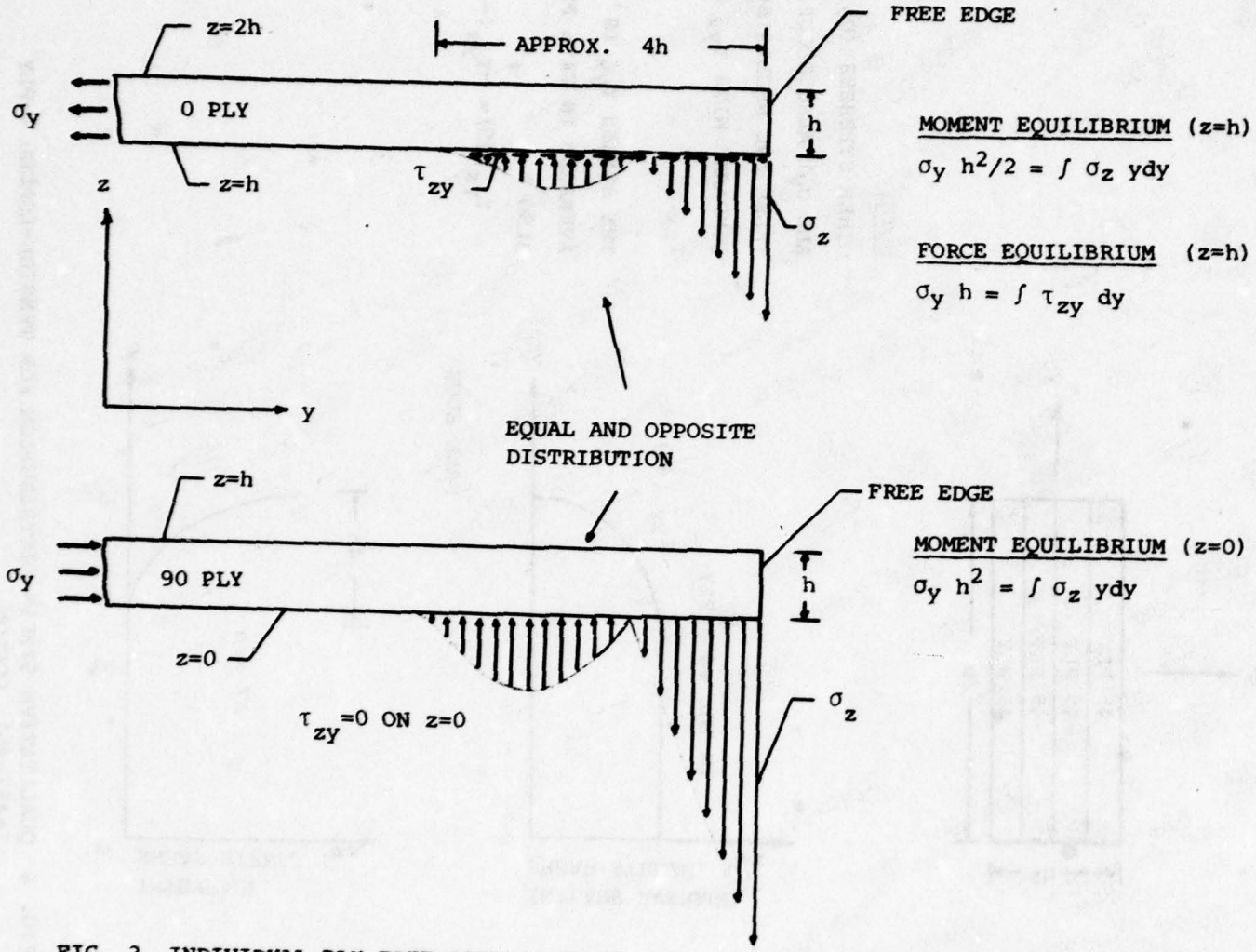

FIG. 3 INDIVIDUAL-PLY FREE-BODY DIAGRAMS FOR THE TENSION-LOADED 4-PLY $(0/90)_s$ COUPON

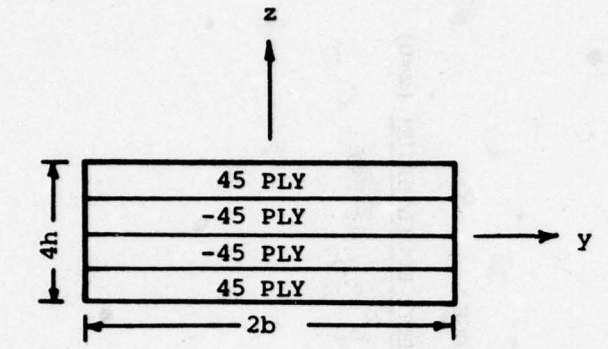

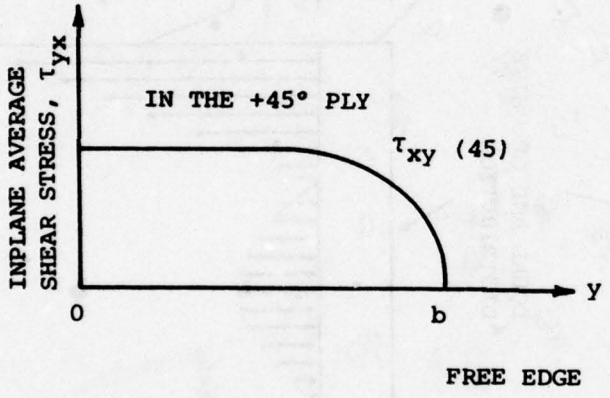

FREE EDGE

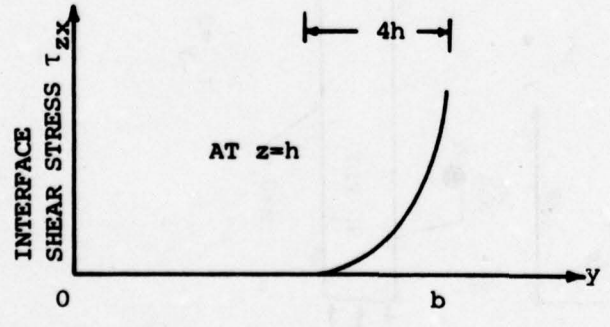

NOTE:

OTHER STRESSES (σ_z, τ_{zy}, AND σ_y) ALSO OCCUR. THESE ARE NEGLIGIBLE COMPARED WITH τ_{yx} AND τ_{zx}.

THE STRESS τ_{yx} IS AVERAGED IN EACH PLY. ALSO

$$\tau_{yx}(45) = -\tau_{yx}(-45)$$

FIG. 4 QUALITATIVE STRESS DISTRIBUTION FOR TENSION-LOADED 4-PLY $(+45/-45)_s$ COUPON

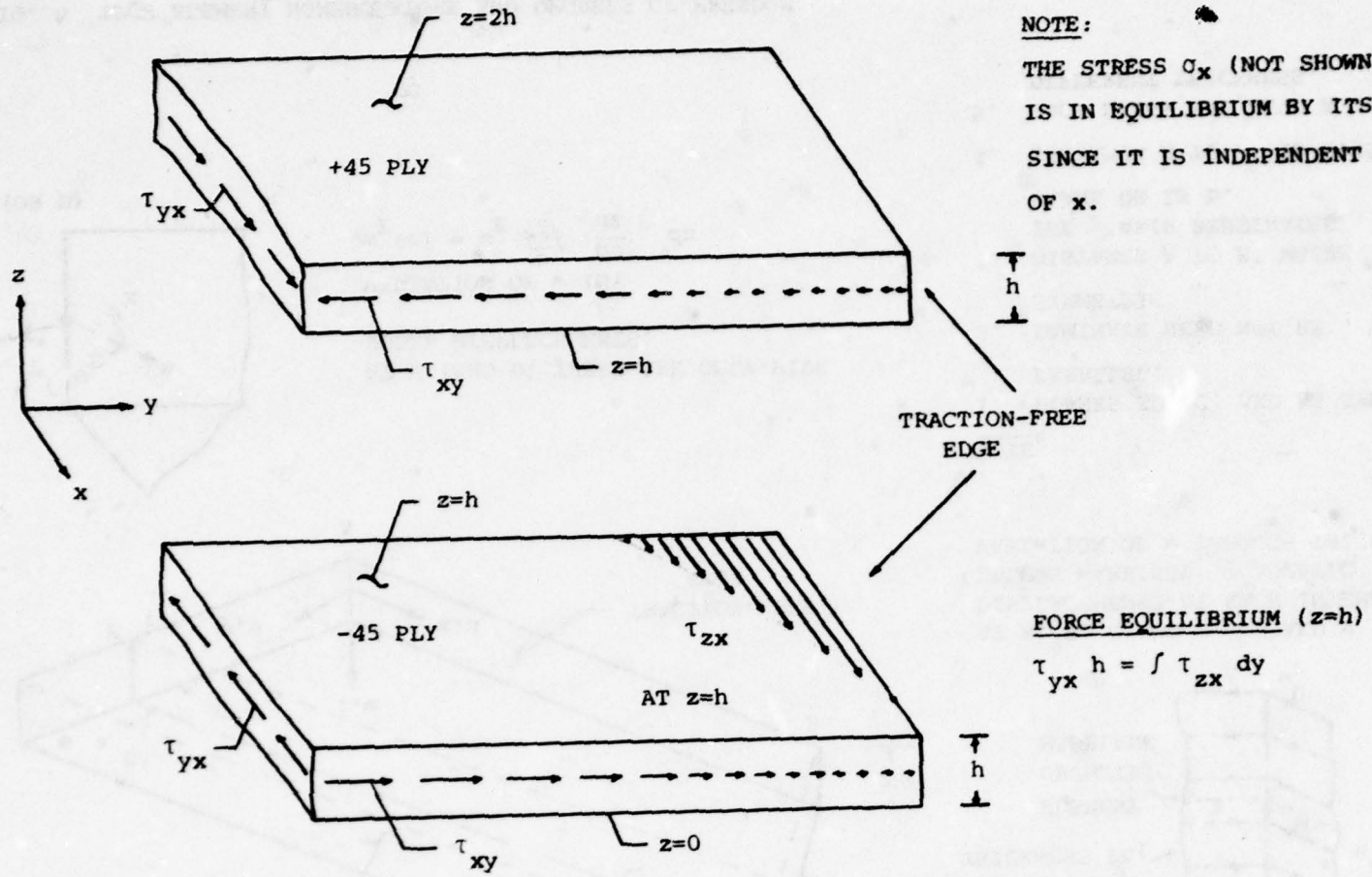

NOTE:
THE STRESS σ_x (NOT SHOWN)
IS IN EQUILIBRIUM BY ITSELF
SINCE IT IS INDEPENDENT
OF x.

FORCE EQUILIBRIUM (z=h)

$$\tau_{yx}\, h = \int \tau_{zx}\, dy$$

FIG. 5 INDIVIDUAL-PLY FREE-BODY DIAGRAMS FOR THE TENSION-LOADED 4-PLY $(+45/-45)_s$ COUPON

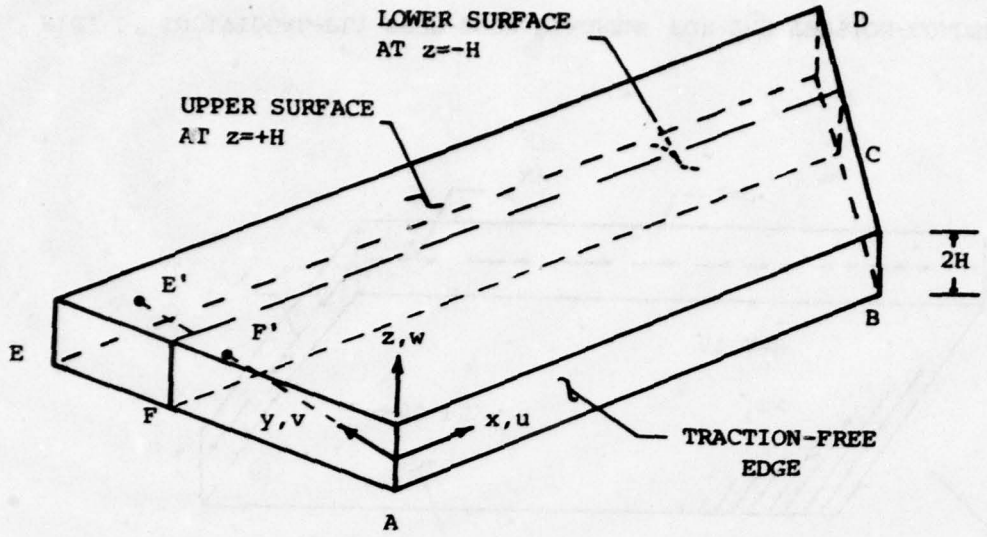

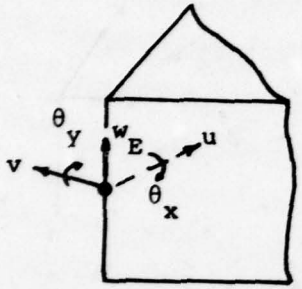

E(OR D)

AT E (AND D) THERE ARE ONLY FIVE NODAL DISPLACEMENTS.

VARIATION OF w IS:

$$w_E(z) = w_E + \int \left(\frac{dw}{dz}\right)_F dz$$

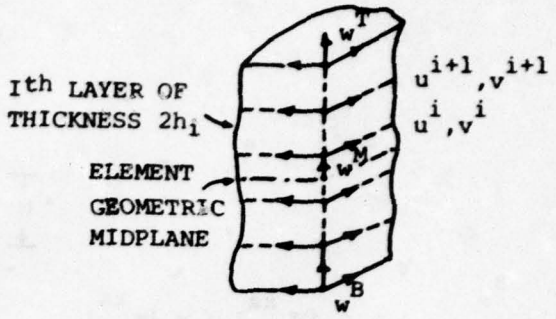

AT A, B, C AND F: u AND v DISPLACEMENTS AT EACH INTERFACE ALLOWS WARPING. QUADRATIC VARIATION OF w THROUGH THICKNESS.

NOTE

1. PLANES ED,FC, AND AB ARE PARALLEL.
2. LAMINATE NEED NOT BE SYMMETRIC.
3. DISTANCE A TO E' WHERE THE y AXIS PENETRATES PLANE DE IS b.
4. DISTANCE A TO F' IS 0.95b.
5. EACH LAYER MAY HAVE A DIFFERENT THICKNESS.

FIG. 6 TFQE ELEMENT NOMENCLATURE AND DEGREES OF FREEDOM

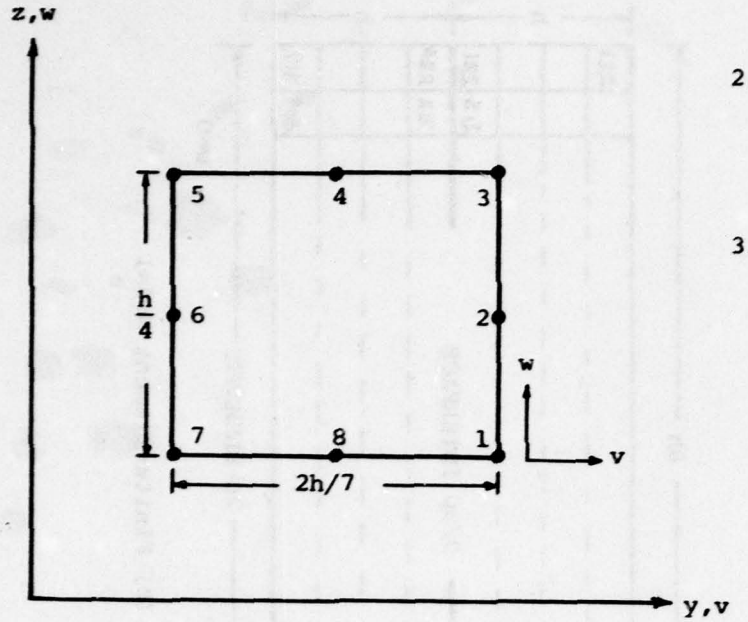

(a) QUAD8 DOF's and Nomenclature

NOTE:

1. QUAD8 IS A TWO-DIMENSIONAL MEMBRANE ASSUMED DISPLACEMENT ELEMENT; THE DISPLACEMENT FIELD IS BIQUADRATIC.
2. AT EACH OF THE EIGHT NODAL POINTS THERE ARE TWO DEGREES OF FREEDOM (DOF), v AND w. THIS RESULTS IN A TOTAL OF SIXTEEN DOF'S PER ELEMENT.
3. QUAD8 IS AN ISOPARAMETRIC ELEMENT. HENCE, ITS GEOMETRY IS NOT RESTRICTED TO A RECTANGLE.

FIG. 7 QUAD8 NOMENCLATURE AND FINITE ELEMENT MODELING FOR THE TENSION-LOADED 4-PLY $(0/90)_s$ COUPON

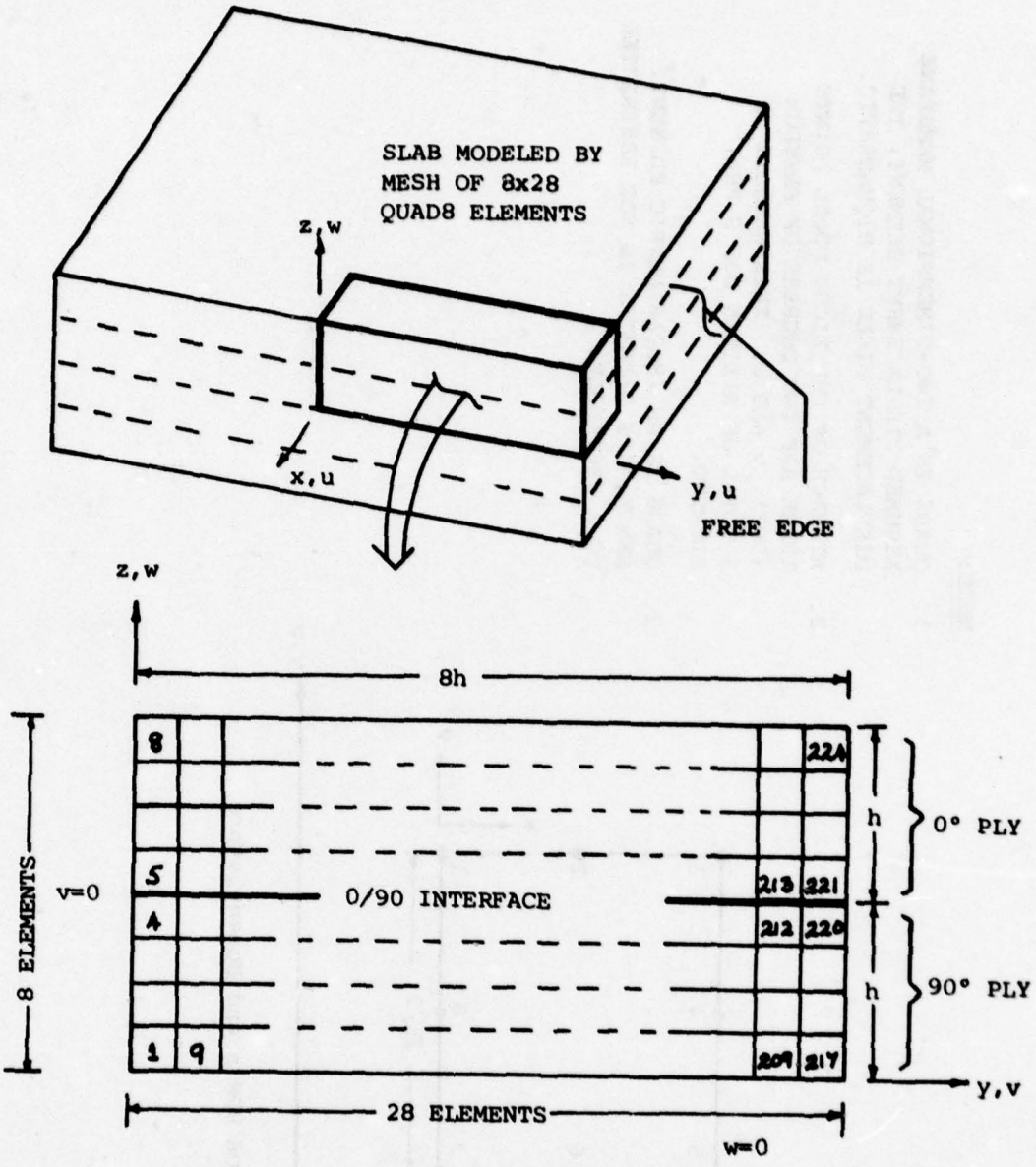

(b) Finite-Element Model

FIG. 7 CONTINUED

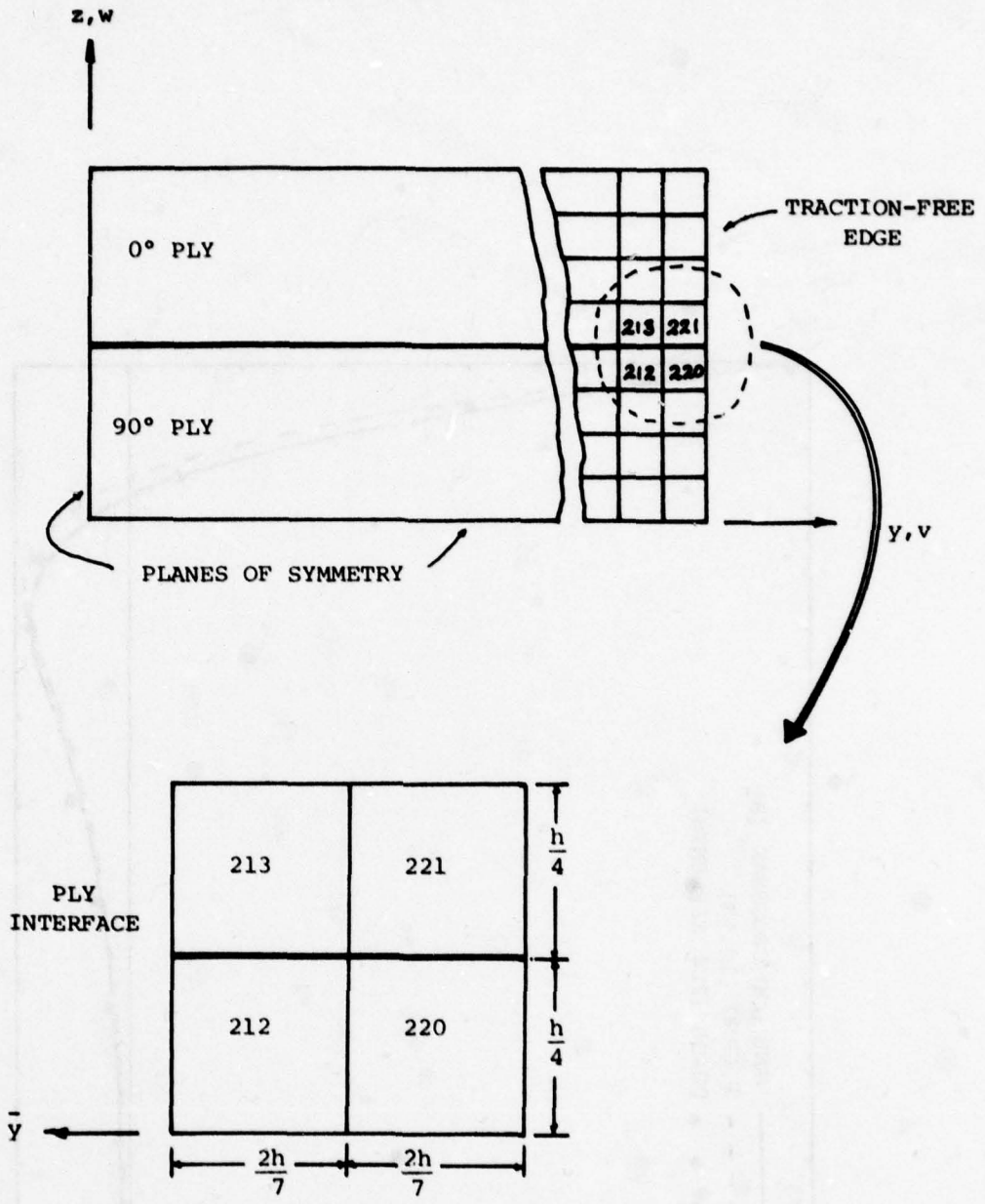

(c) Coordinates and Nomenclature

FIG. 7 CONCLUDED

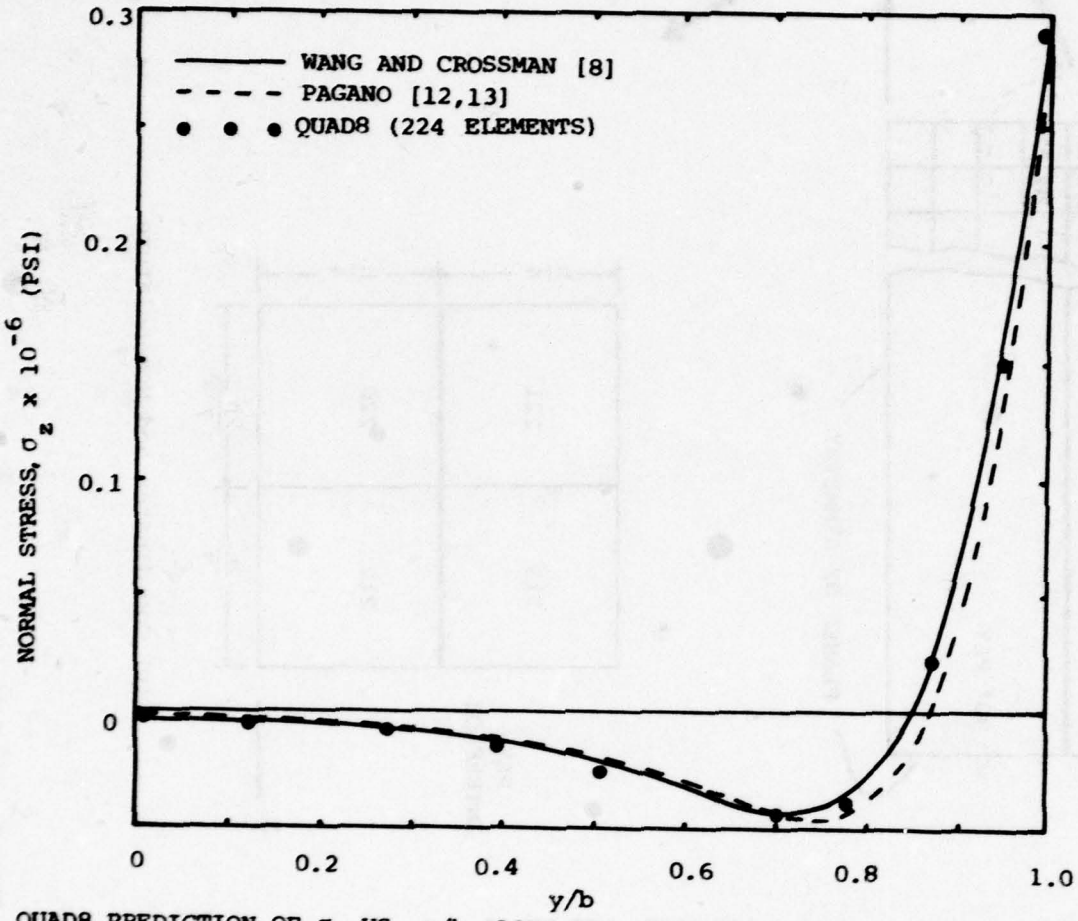

FIG. 8 QUAD8 PREDICTION OF σ_z VS. y/b ALONG THE MIDPLANE (z=0) FOR THE TENSION-LOADED 4-PLY $(0/90)_s$ COUPON ($\varepsilon_x = 1.0$)

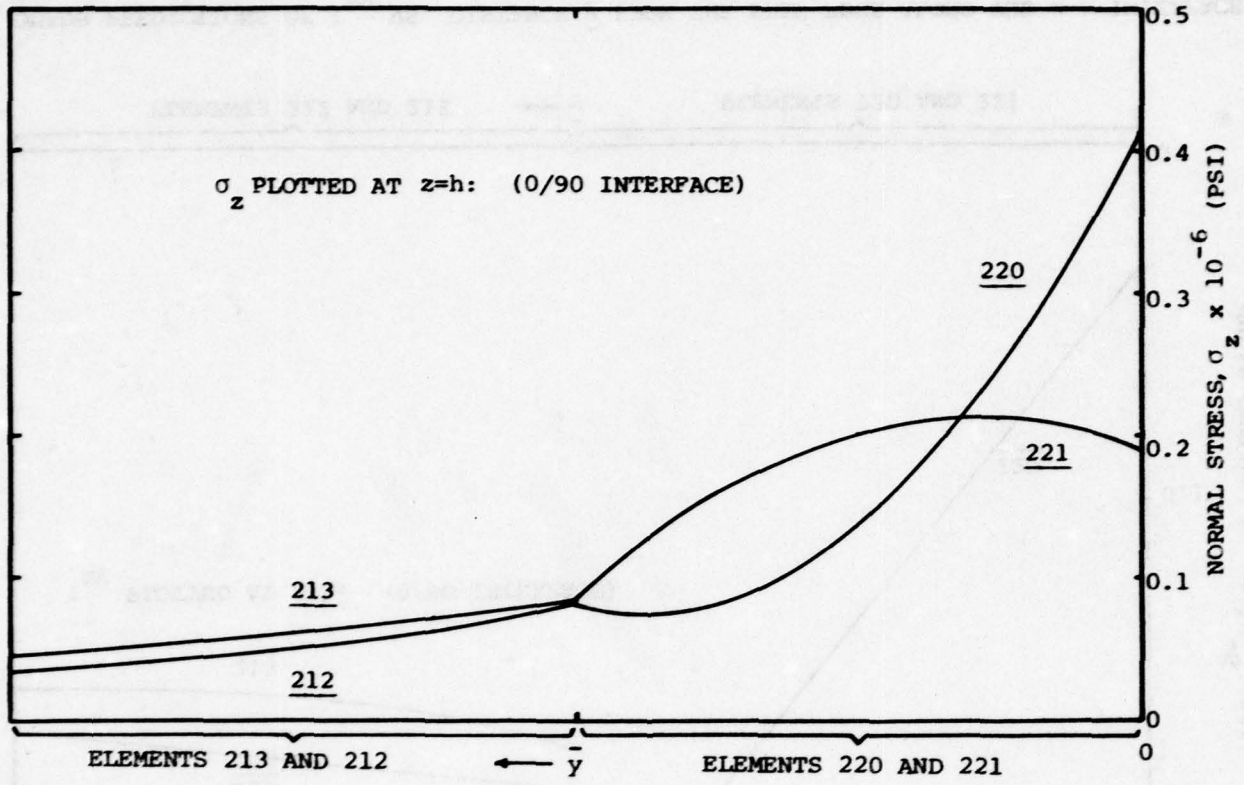

FIG. 9 QUAD8 PREDICTIONS OF σ_z VS. DISTANCE $\bar{y}$ FROM THE FREE EDGE ALONG THE z=h INTERFACE FOR THE TENSION-LOADED 4-PLY $(0/90)_s$ COUPON (ε_x = 1.0)

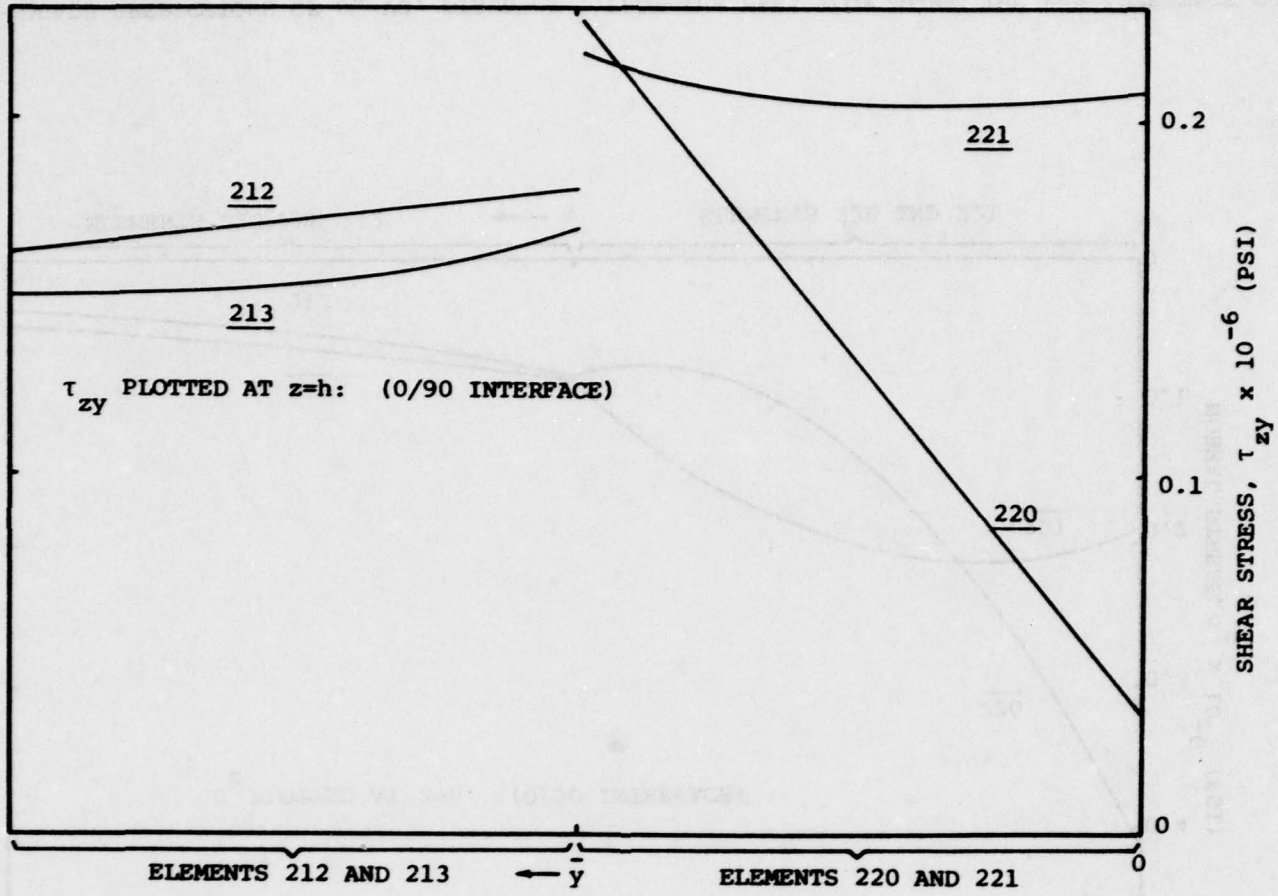

FIG. 10 QUAD8 PREDICTIONS OF τ_{zy} VS. DISTANCE $\bar{y}$ FROM THE FREE EDGE ALONG THE z=h INTERFACE FOR THE TENSION-LOADED 4-PLY $(0/90)_s$ COUPON ($\varepsilon_x = 1.0$)

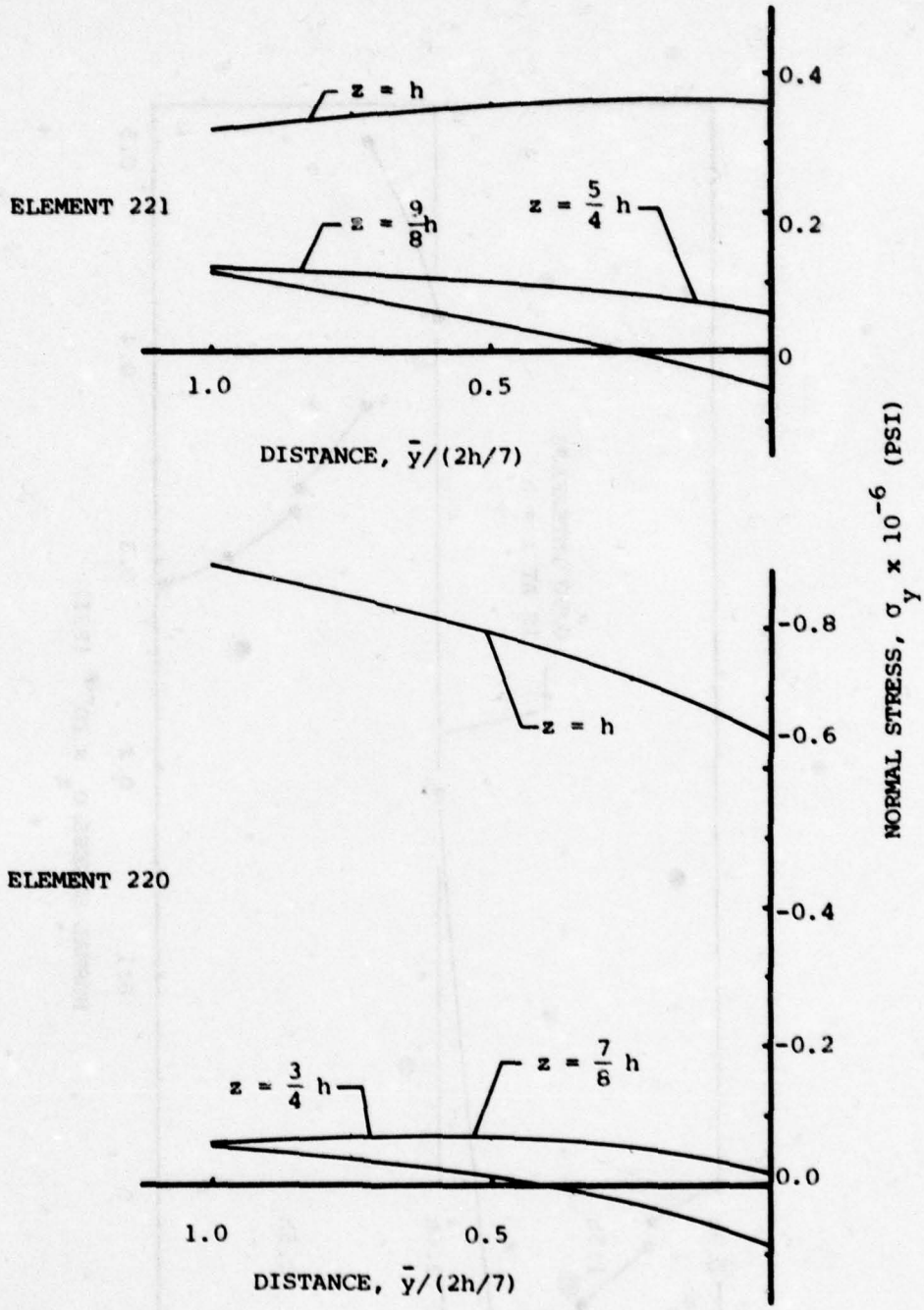

FIG. 11 QUAD8 PREDICTIONS OF σ_y VS. $\bar{y}$ AT VARIOUS z STATIONS IN ELEMENTS 220 AND 221 FOR THE TENSION LOADED 4-PLY $(0/90)_s$ COUPON ($\varepsilon_x = 1.0$)

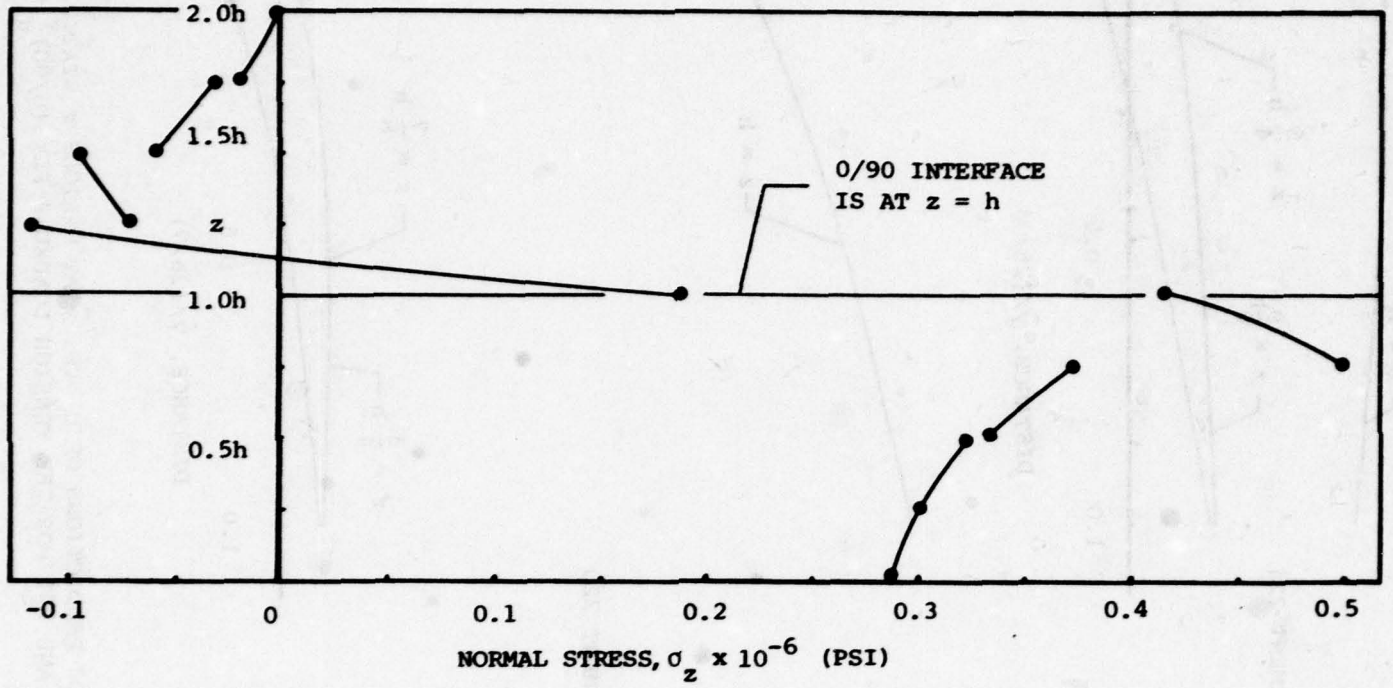

FIG. 12 QUAD8 PREDICTED DISTRIBUTION OF σ_z THROUGH THE LAMINATE THICKNESS AT THE FREE EDGE (y=b) FOR THE TENSION-LOADED 4-PLY $(0/90)_s$ COUPON (ϵ_x = 1.0)

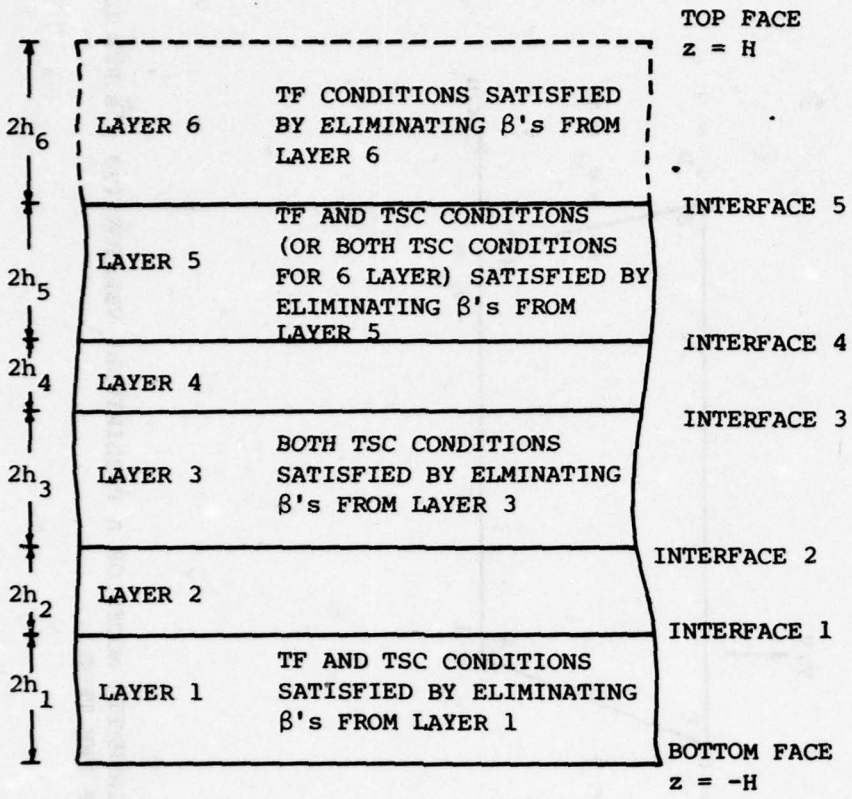

NOTE:

1. $\bar{z}$ IS THE LOCAL AXIS OF EACH LAYER. THE AXIS ORIGIN IS AT THE GEOMETRIC MIDPLANE OF THE LAYER.

2. z IS THE LAMINATE AXIS WITH ORIGIN AT THE GEOMETRIC MIDPLANE.

3. TRACTION AND STRAIN CONTINUITY (TSC) CONDITIONS AT THE ith INTERFACE ARE:

$$\sigma_z^i = \sigma_z^{i+1}; \quad \tau_{zy}^i = \tau_{zy}^{i+1}$$

$$\tau_{zx}^i = \tau_{zx}^{i+1}; \quad \varepsilon_x^i = \varepsilon_x^{i+1}$$

4. TRACTION-FREE (TF) CONDITIONS AT $z = \pm H$ ARE:

$$\sigma_z = \tau_{yz} = \tau_{xz} = 0.$$

FIG. 13 TYPICAL β-ELIMINATION PROCEDURE TO SATISFY TRACTION-FREE, TRACTION CONTINUITY, AND STRAIN CONTINUITY CONDITIONS AT SURFACES AND/OR INTERFACES FOR AN ODD (OR EVEN) LAYERED LAMINATE

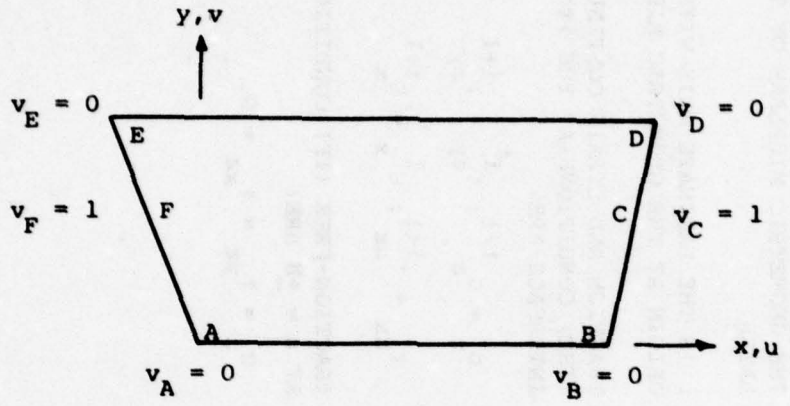

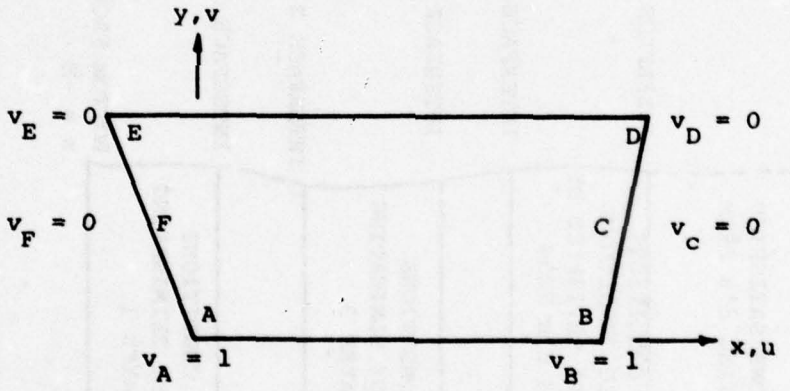

FIG. 14 KINEMATIC MODES OF A PRELIMINARY VERSION (90 β's PER LAYER) OF THE TFQE

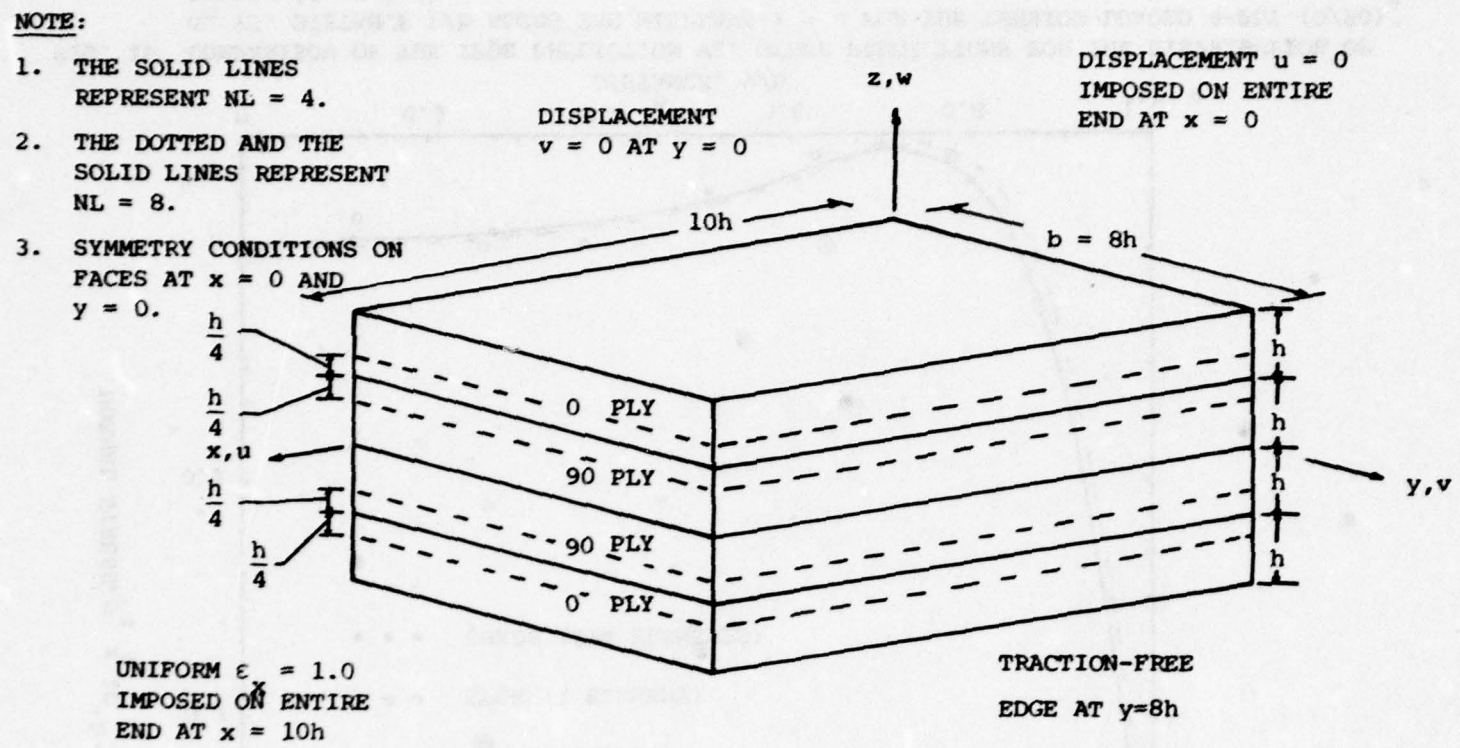

FIG. 15 MODELING OF ONE-QUARTER OF THE TENSION LOADED 4-PLY $(0/90)_s$ COUPON BY A SINGLE TFQE ELEMENT

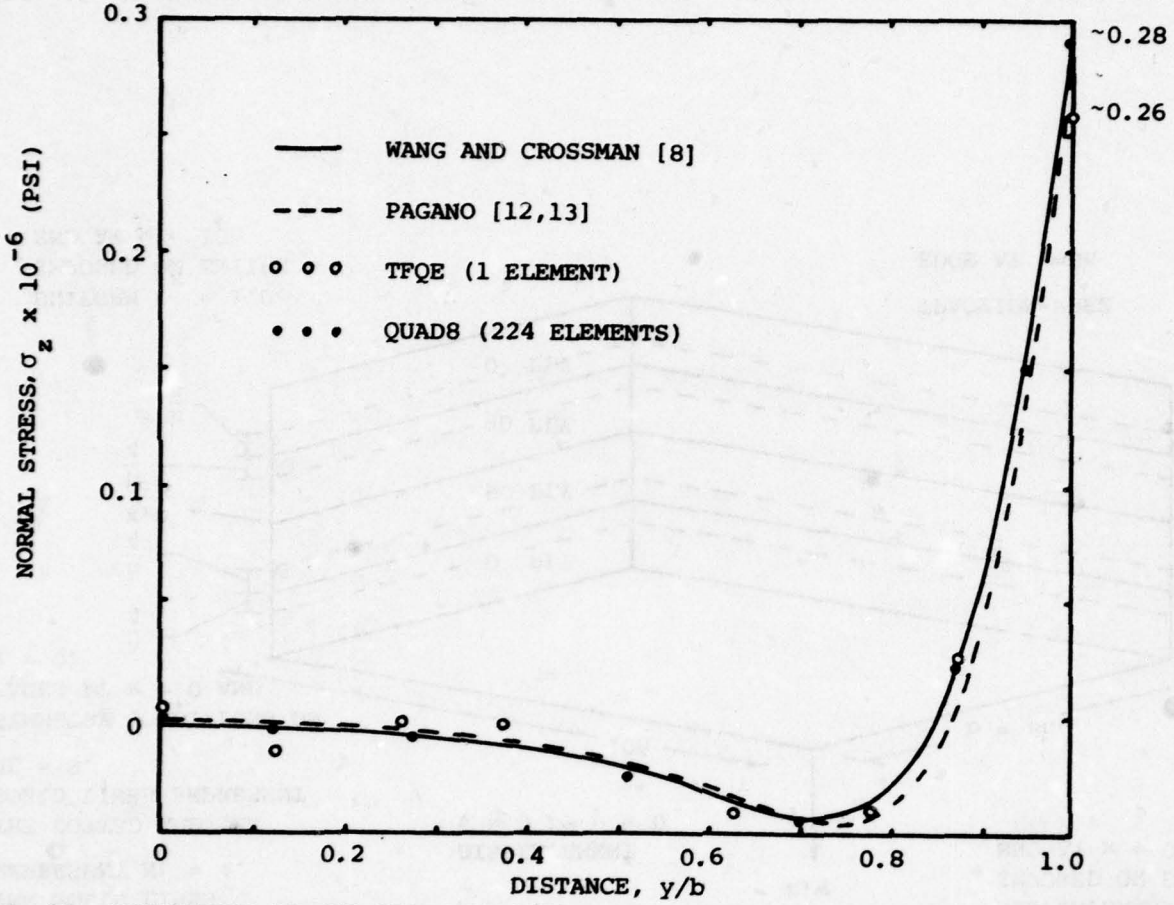

FIG. 16 COMPARISON OF THE TFQE PREDICTION VS. OTHER PREDICTIONS FOR THE DISTRIBUTION OF σ_z VS. DISTANCE y/b ALONG THE MIDPLANE z = 0 FOR THE TENSION-LOADED 4-PLY $(0/90)_s$ COUPON (ε_x = 1.0)

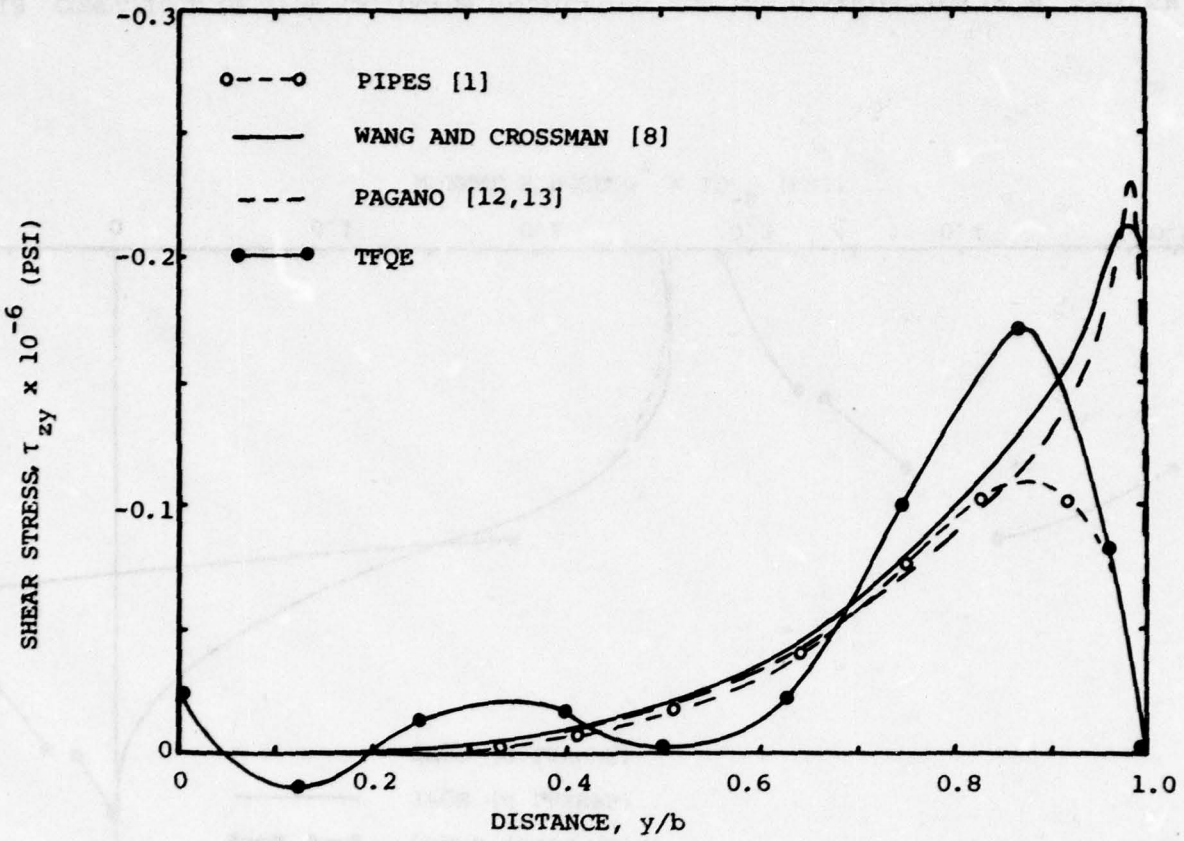

FIG. 17 COMPARISON OF THE TFQE PREDICTION VS. OTHER PREDICTIONS FOR THE DISTRIBUTION OF τ_{zy} VS. DISTANCE y/b ALONG THE 0/90 INTERFACE (z = h) FOR THE TENSION-LOADED 4-PLY $(0/90)_s$ COUPON (ε_x = 1.0)

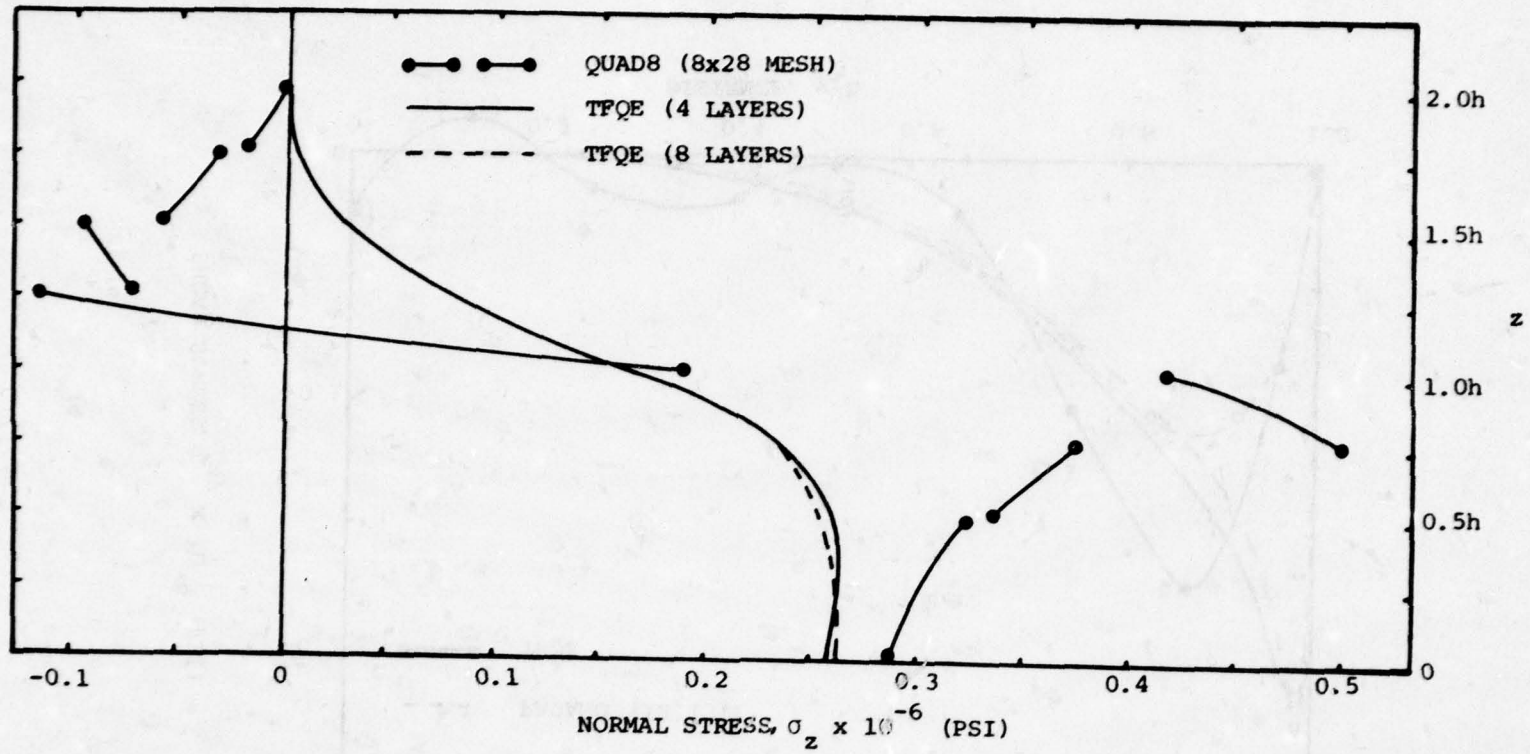

FIG. 18 COMPARISON OF TFQE VS. QUAD8 PREDICTIONS FOR THE DISTRIBUTION OF σ_z THROUGH THE THICKNESS AT THE FREE EDGE (y = b) FOR THE TENSION-LOADED 4-PLY $(0/90)_s$ COUPON ($\varepsilon_x = 1.0$)

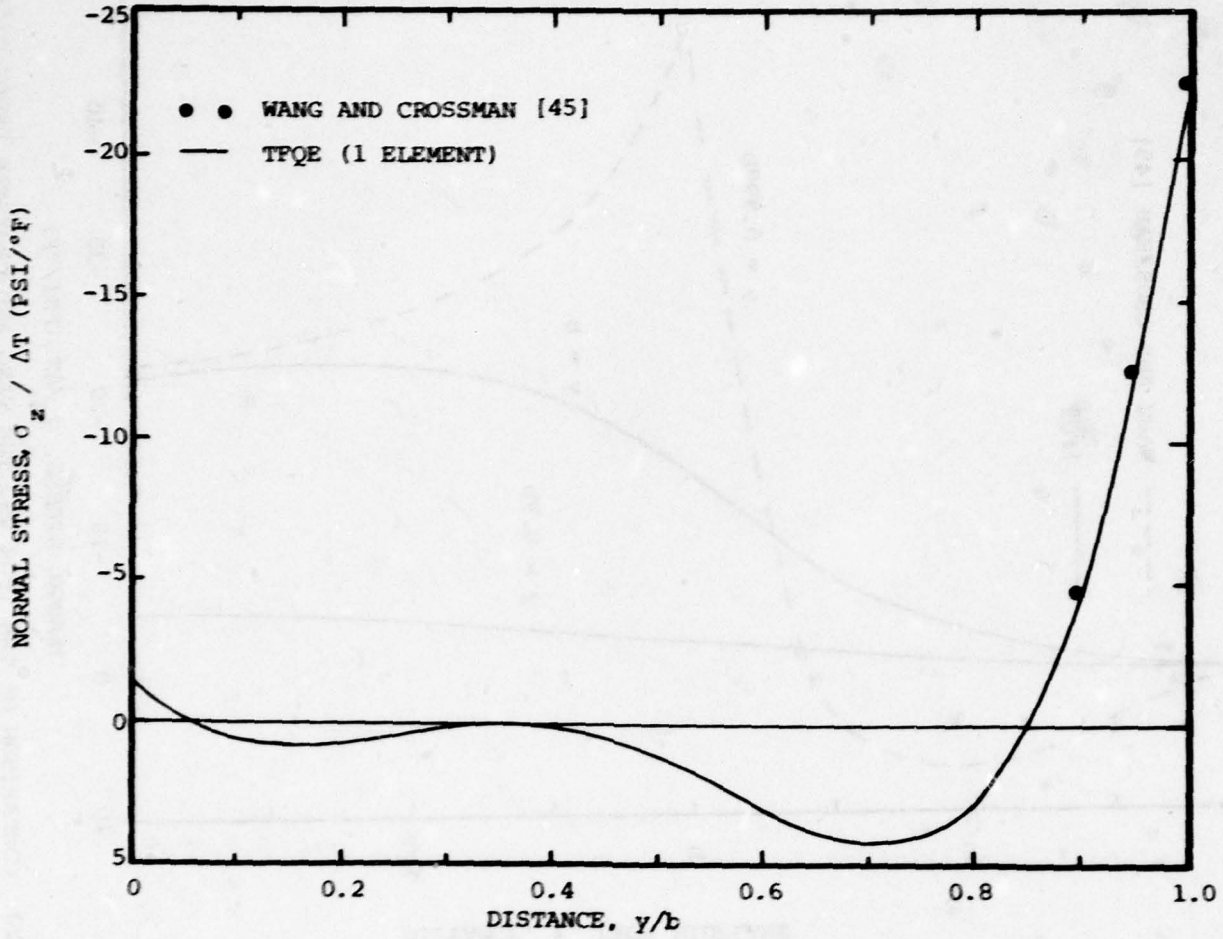

FIG. 19 COMPARISON OF THE TPQE VS. THE WANG AND CROSSMAN PREDICTION FOR THE DISTRIBUTION OF σ_z VS. DISTANCE y/b ALONG THE MIDPLANE (z = 0) FOR THE THERMALLY-LOADED 4-PLY $(0/90)_s$ COUPON (ΔT = 1°F)

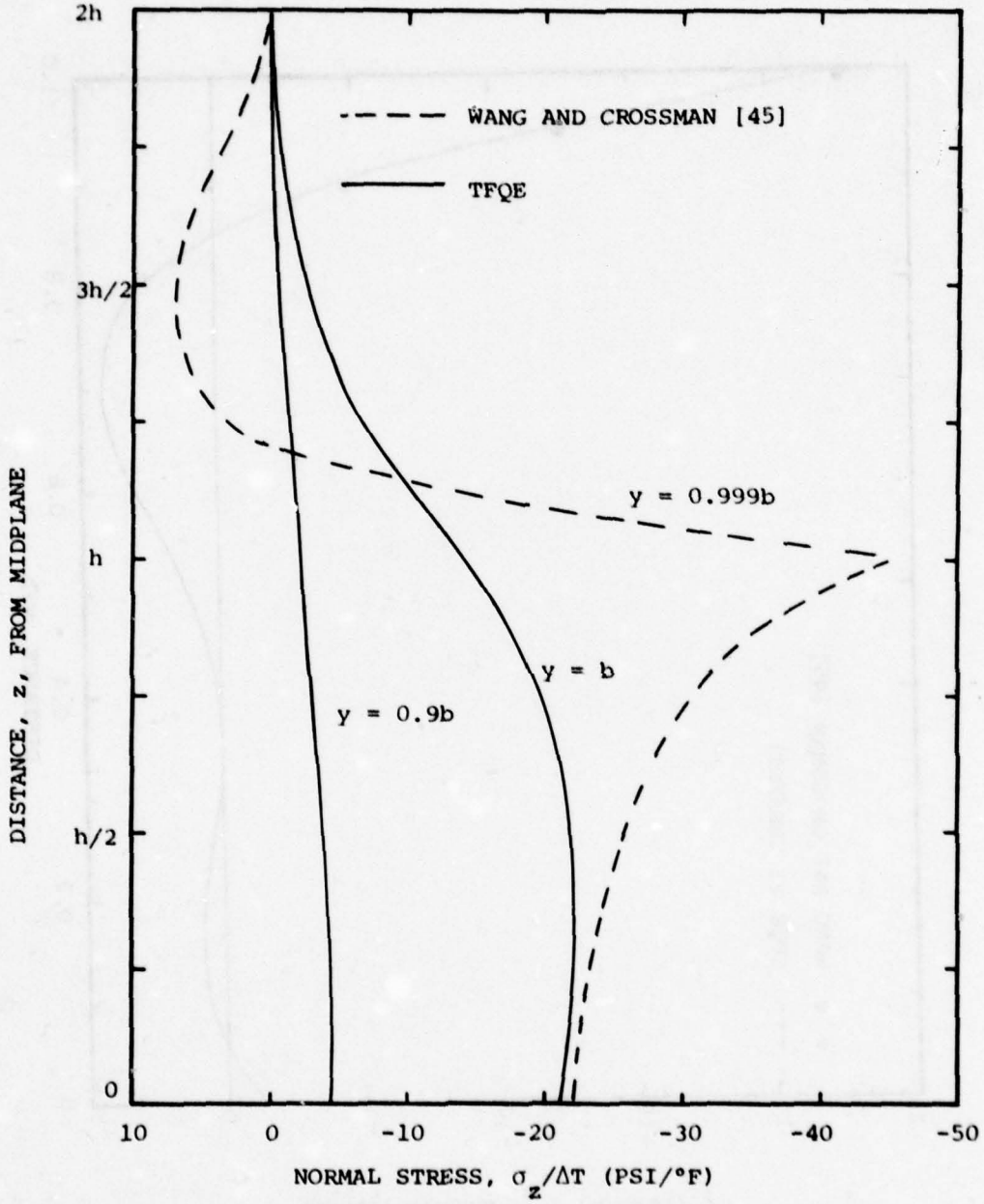

FIG. 20 COMPARISON OF THE TFQE VS. THE WANG AND CROSSMAN PREDICTION OF THE DISTRIBUTION THROUGH THE THICKNESS OF THE NORMAL STRESS σ_z AT FIXED y - STATIONS NEAR THE FREE EDGE OF THE THERMALLY-LOADED 4-PLY $(0/90)_s$ COUPON (ΔT = 1°F)

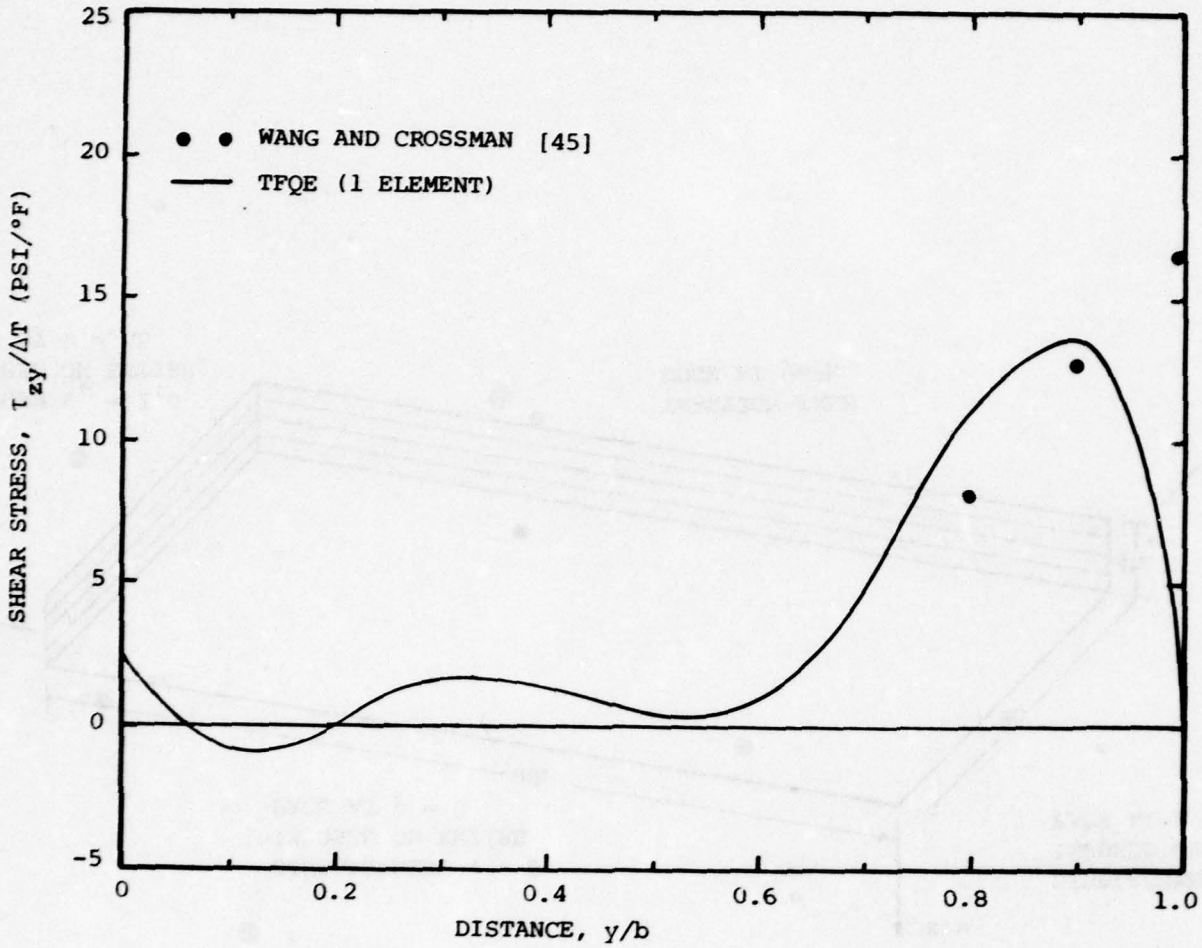

FIG. 21 COMPARISON OF THE TFQE VS. THE WANG AND CROSSMAN PREDICTION OF τ_{zy} VS. DISTANCE y/b ALONG THE MIDPLANE (z = 0) FOR THE THERMALLY-LOADED 4-PLY $(0/90)_s$ COUPON (ΔT = 1°F)

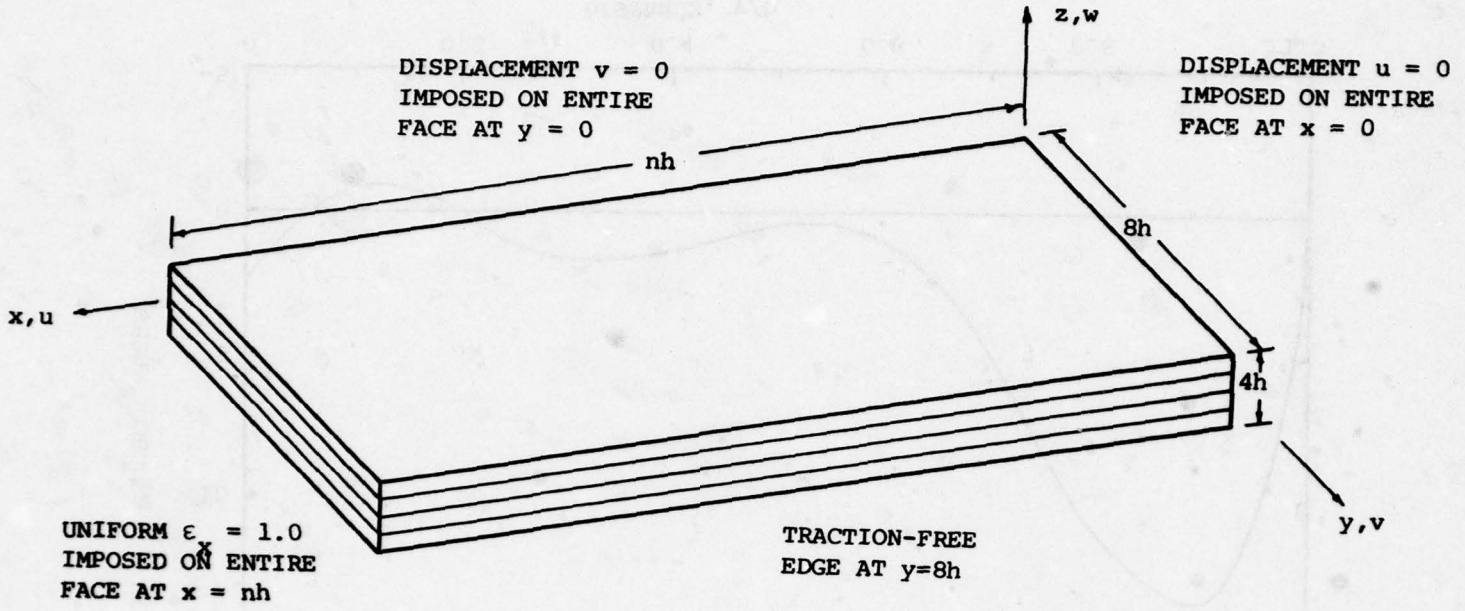

FIG. 22 ONE QUARTER OF THE TENSION-LOADED 4-PLY $(\pm 45)_s$ COUPON AS USED FOR TFQE MODELING

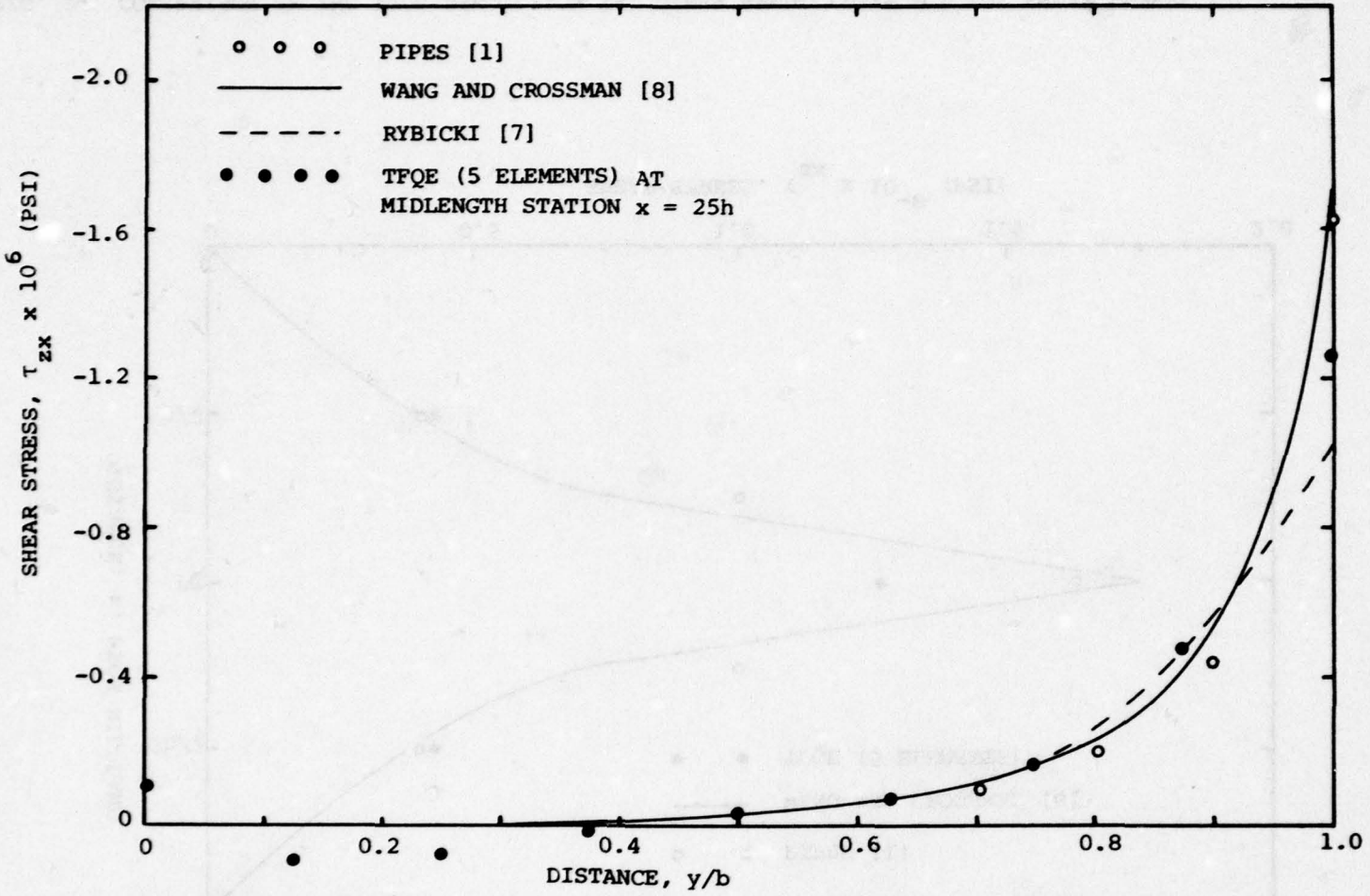

FIG. 23 COMPARISON OF THE TFQE PREDICTION VS. OTHER PREDICTIONS FOR THE DISTRIBUTION OF τ_{zx} DISTANCE y/b ALONG THE INTERFACE AT z = h FOR THE TENSION-LOADED 4-PLY $(\pm 45)_s$ COUPON ($\varepsilon_x = 1.0$)

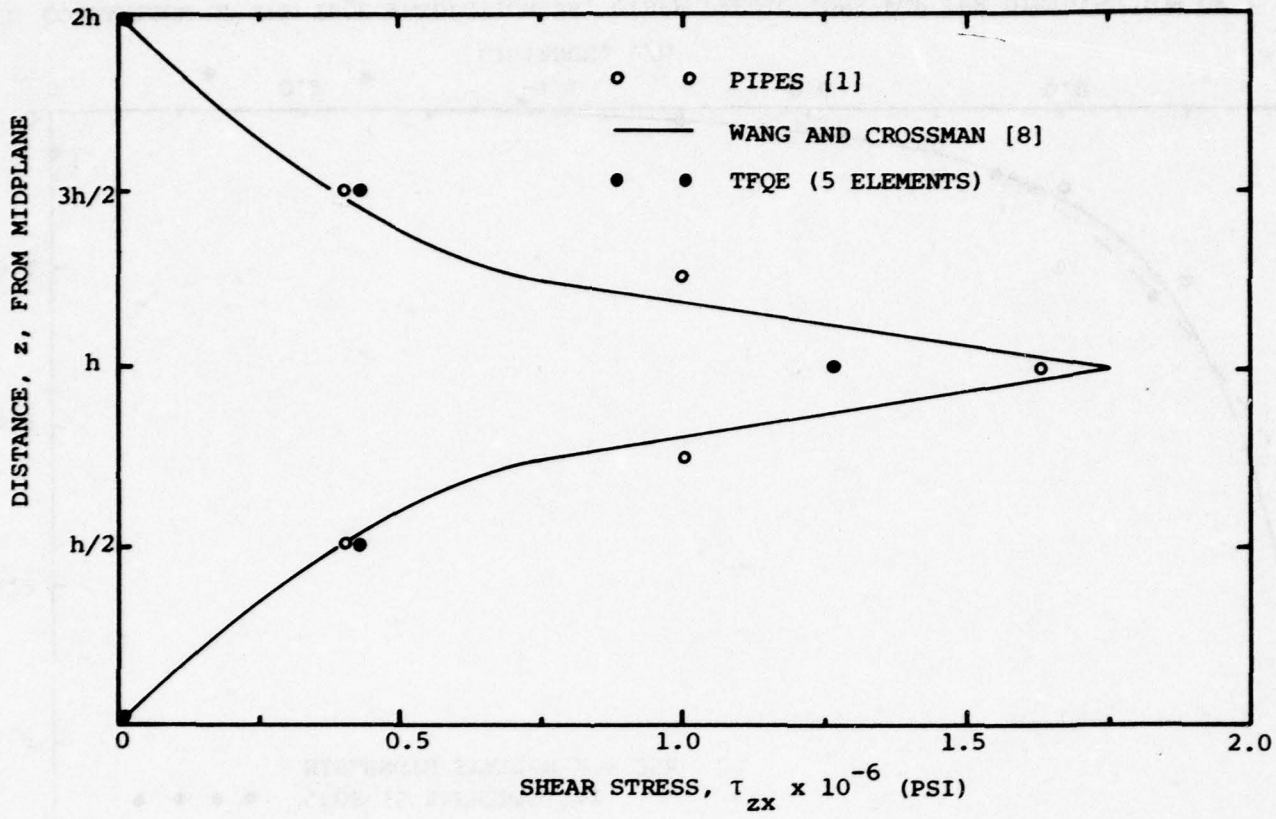

FIG. 24 COMPARISON OF THE TFQE PREDICTION VS. OTHER PREDICTIONS FOR THE SHEAR STRESS τ_{zx} THROUGH THE THICKNESS AT THE FREE EDGE y = 8h FOR THE TENSION-LOADED 4-PLY ($\pm$45) COUPON (ε_x = 1.0)

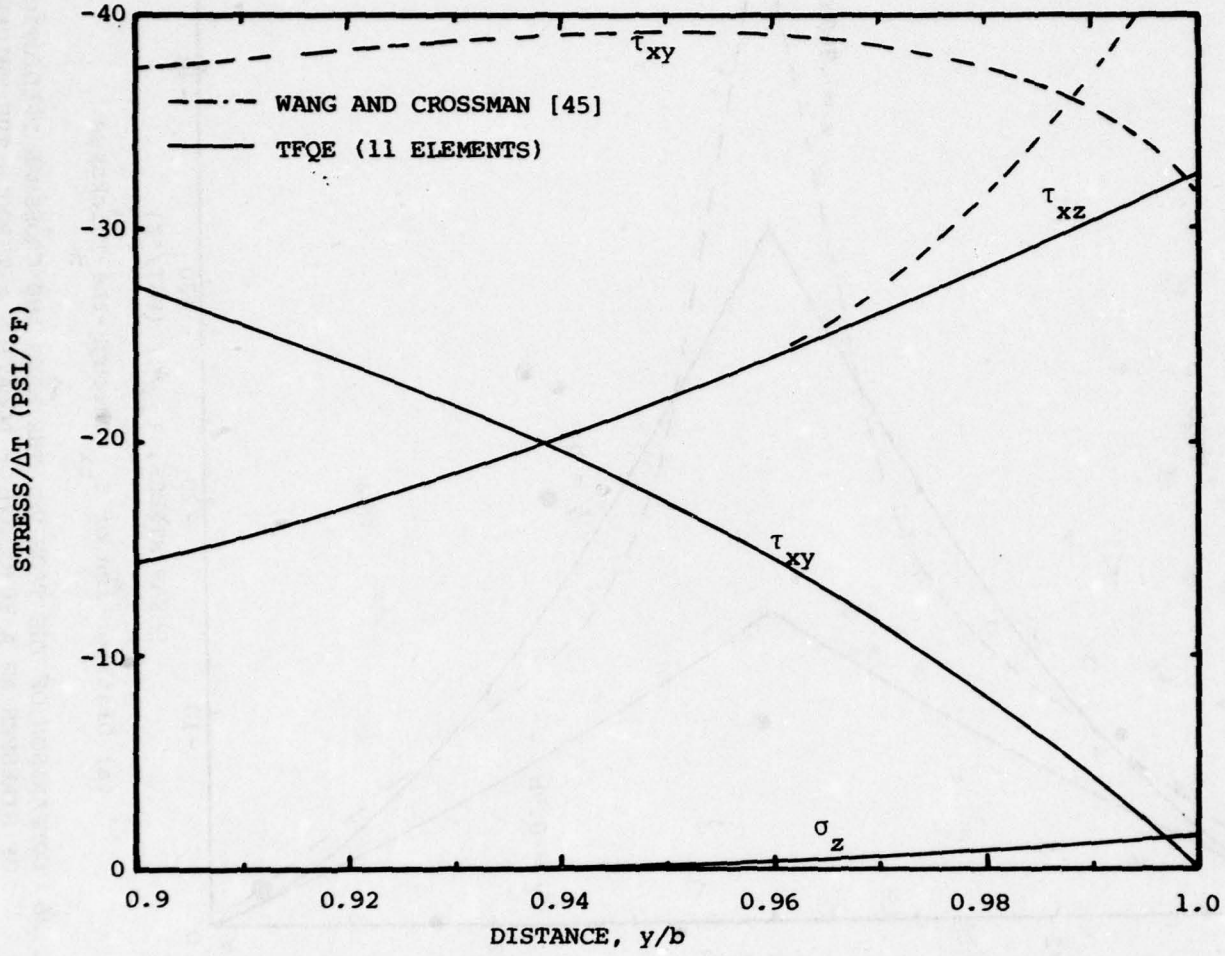

FIG. 25 COMPARISON OF THE TFQE PREDICTION FOR σ_z, τ_{zx}, AND τ_{xy} AS A FUNCTION OF DISTANCE y/b ALONG THE z = h INTERFACE VS. THE WANG AND CROSSMAN PREDICTION FOR THE THERMALLY-LOADED 4-PLY $(\pm 45)_s$ COUPON (ΔT = 1°F)

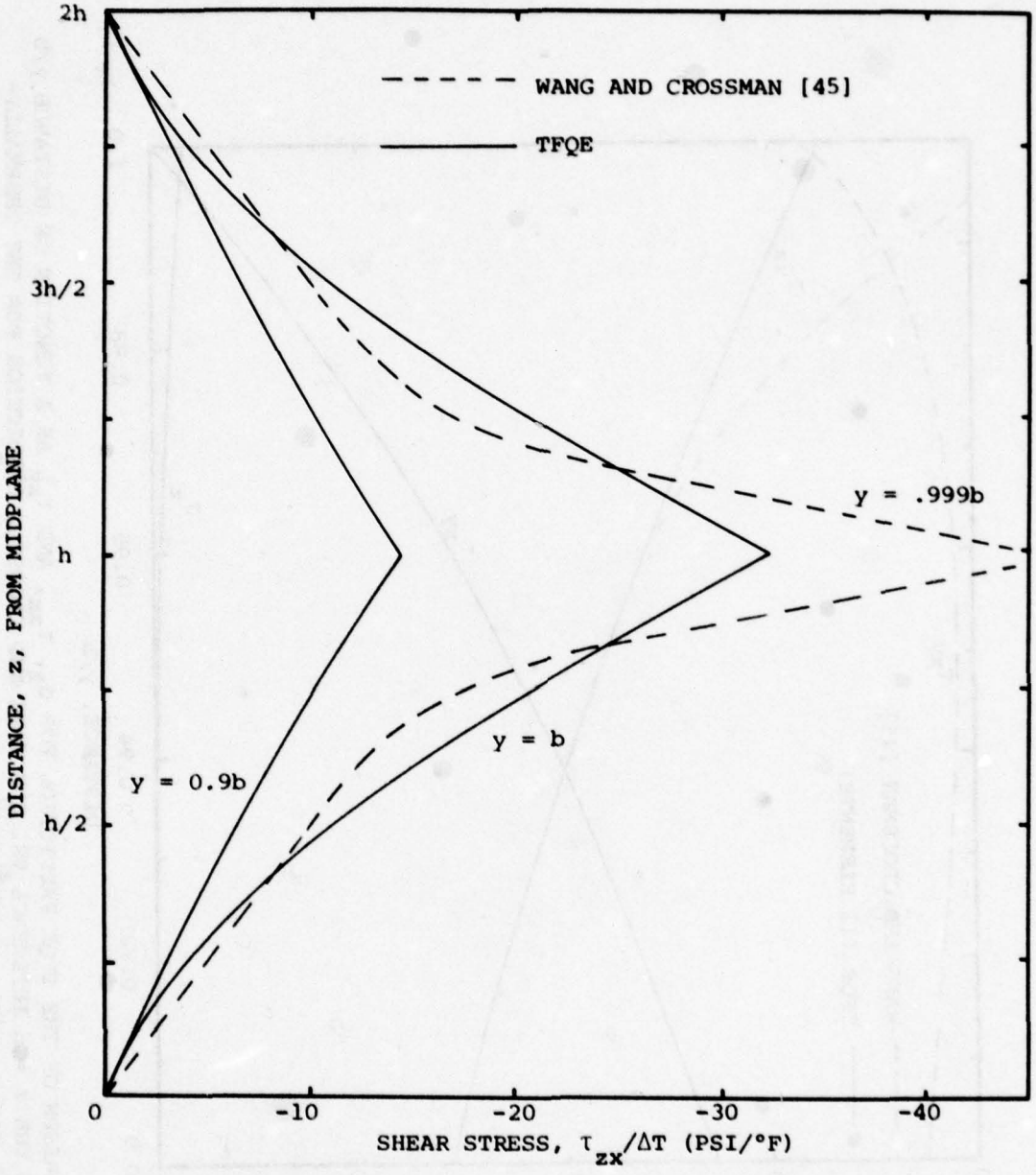

(a) Distribution of τ_{zx} Through-the-Thickness

FIG. 26 COMPARISON OF THE TFQE VS. THE WANG AND CROSSMAN PREDICTION OF STRESSES AS A FUNCTION OF LOCATION z THROUGH THE THICKNESS AT FIXED y-STATIONS NEAR THE FREE EDGE OF THE THERMALLY-LOADED 4-PLY $(\pm 45)_s$ COUPON ($\Delta T = 1°F$)

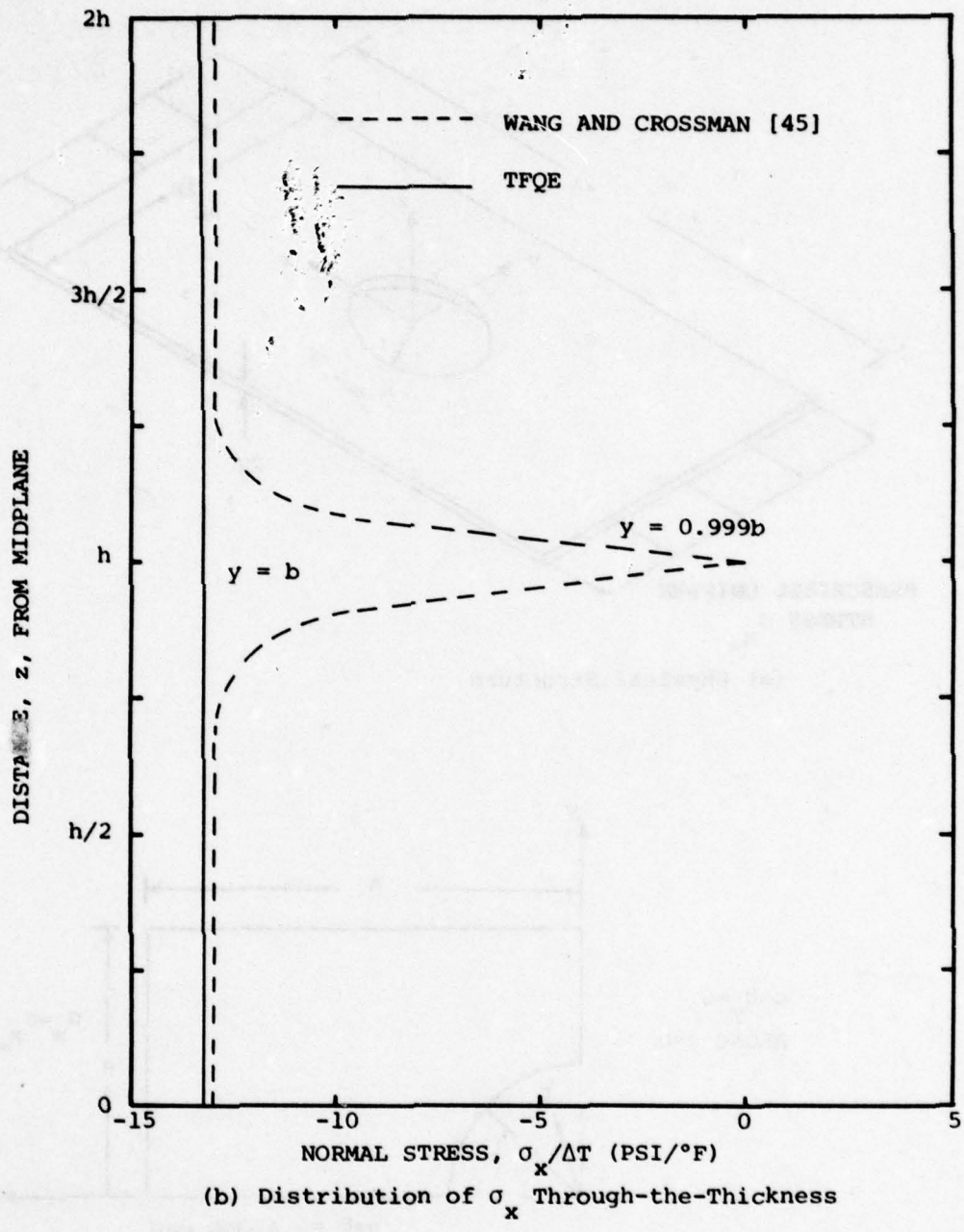

(b) Distribution of σ_x Through-the-Thickness

FIG. 26 CONCLUDED

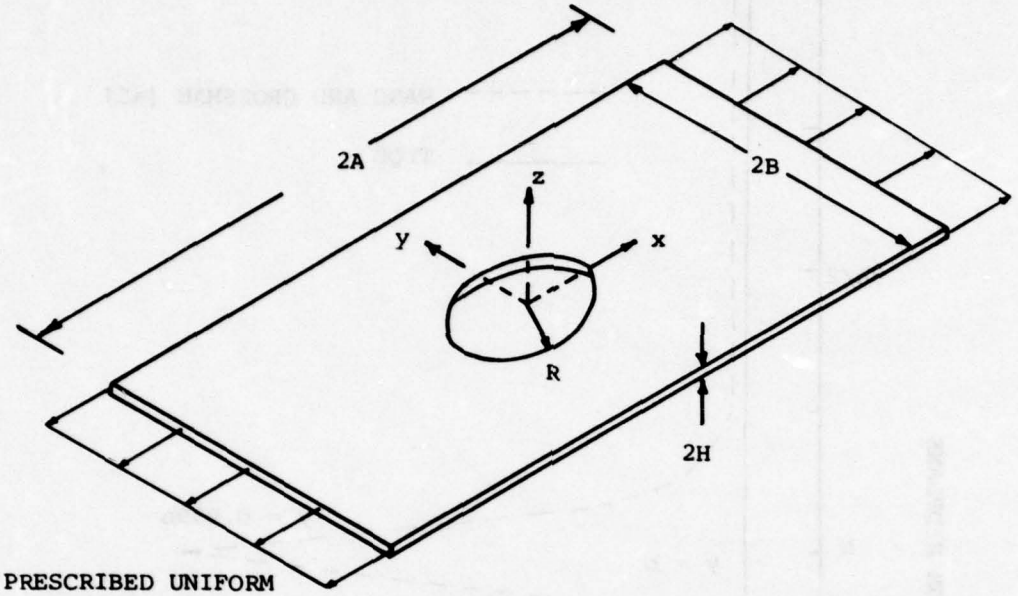

(a) Physical Structure

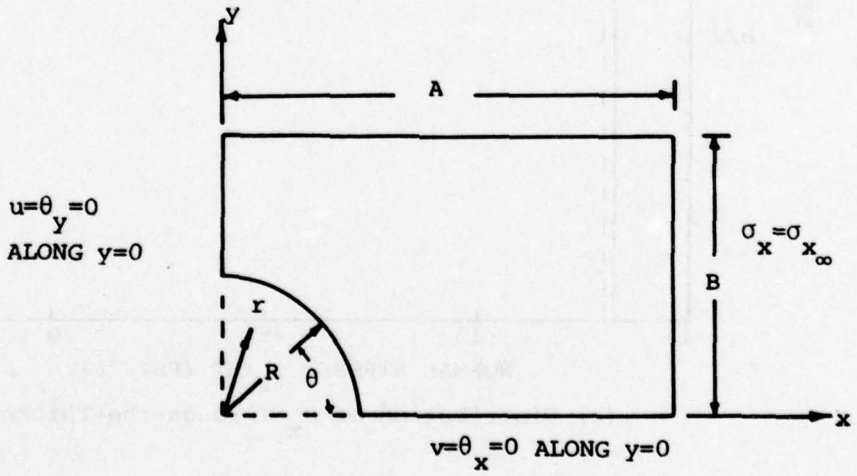

(b) Quadrant Isolated for Finite-Element Analysis

FIG. 27 GEOMETRY AND NOMENCLATURE OF THE TENSION-LOADED PLATE WITH A CIRCULAR HOLE

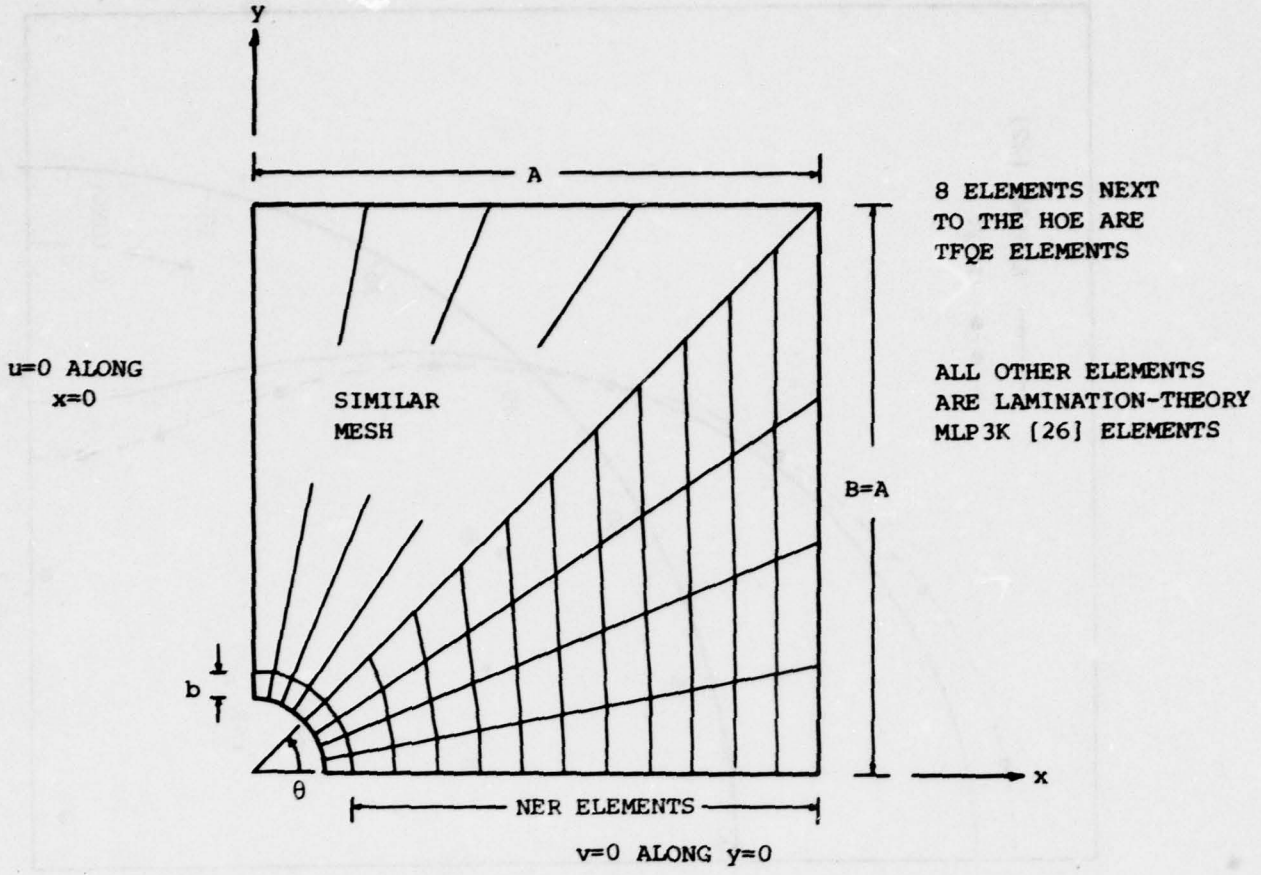

FIG. 28 SCHEMATIC OF FINITE ELEMENT MODELING OF ONE-QUARTER OF THE TENSION-LOADED PLATE WITH A CIRCULAR HOLE

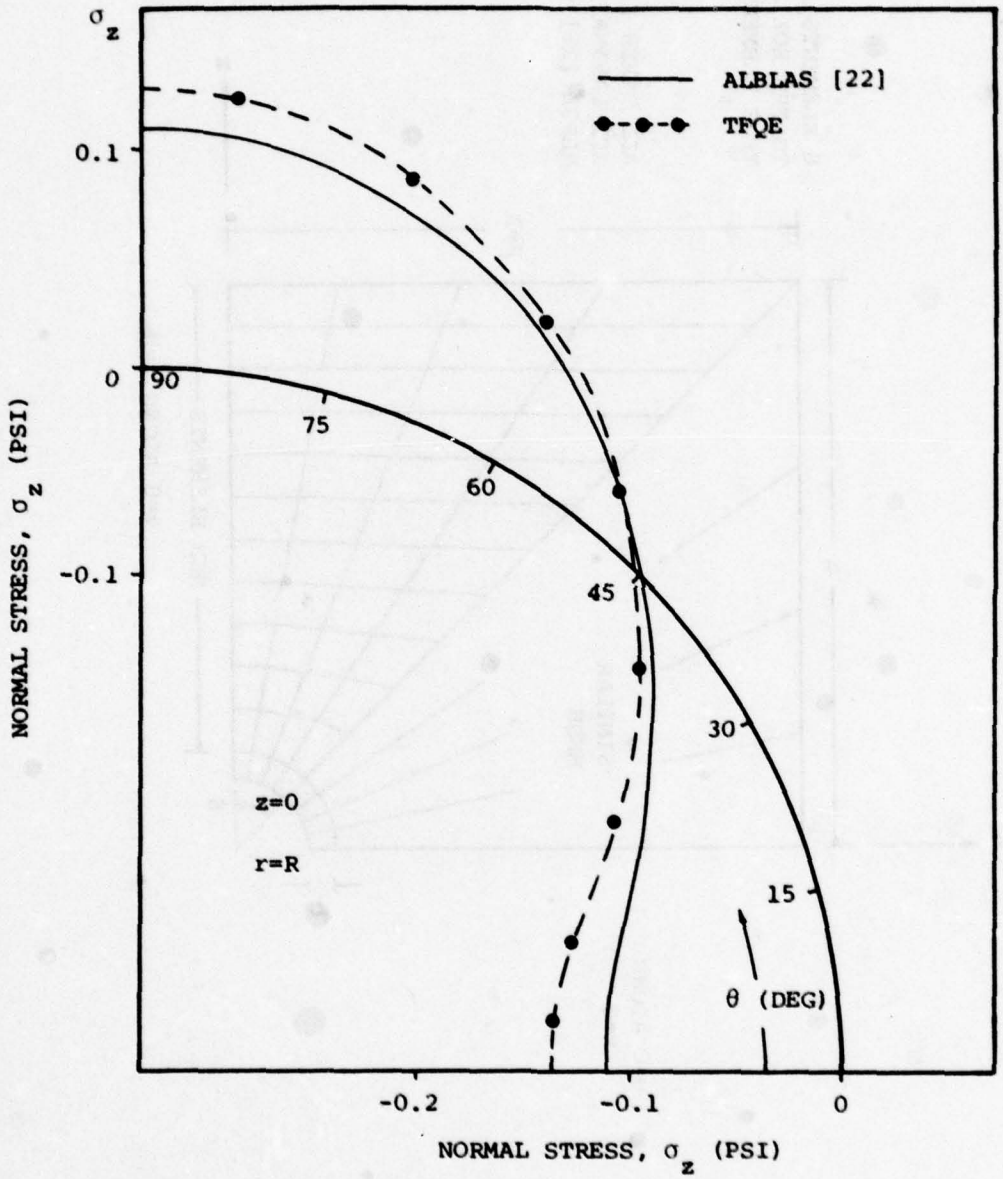

FIG. 29 COMPARISON OF THE TFQE PREDICTION VS. THE ALBLAS PREDICTION FOR σ_z VS. θ ALONG THE HOLE r = R AT THE MIDPLANE z = 0 FOR THE TENSION-LOADED ISOTROPIC PLATE WITH A CIRCULAR HOLE (σ_{x_∞} =1.0 PSI)

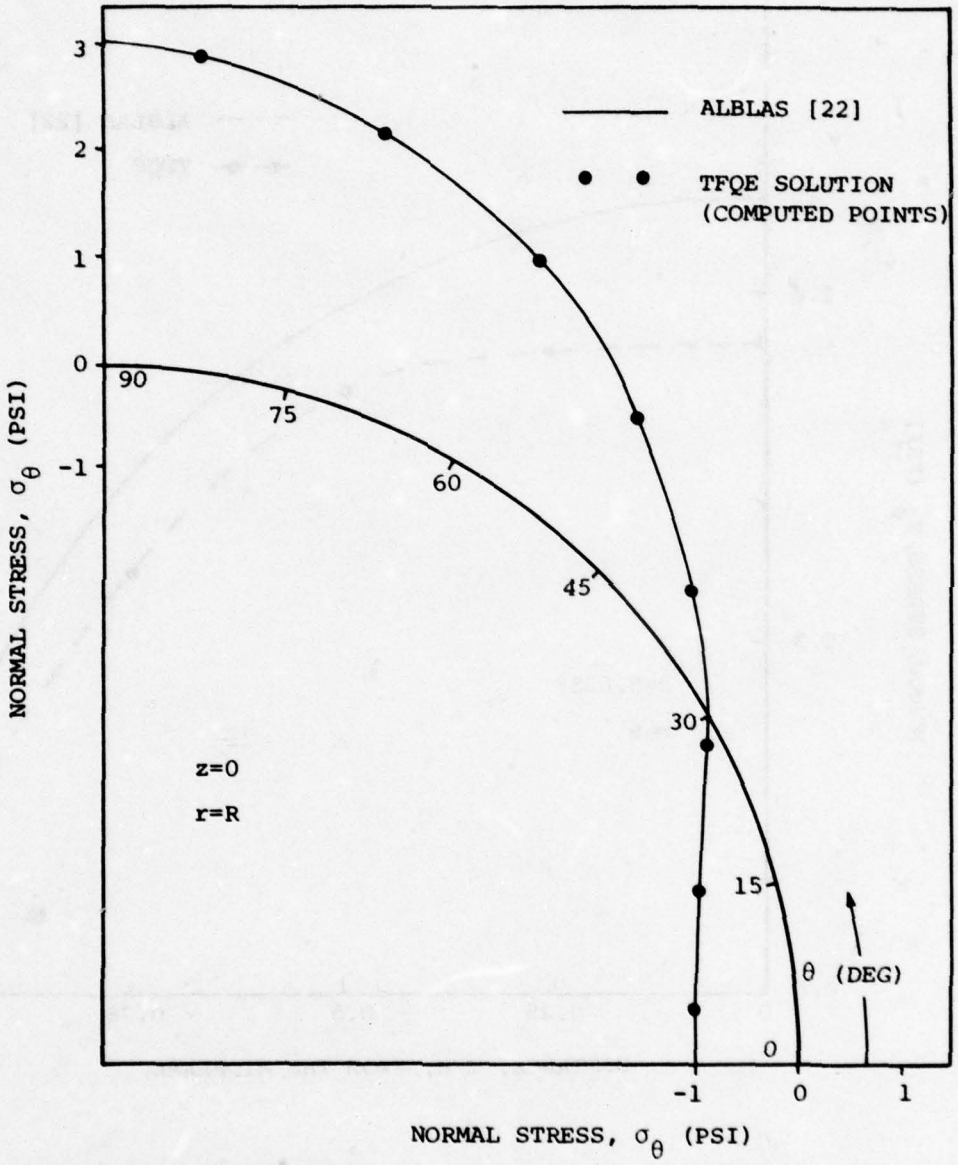

FIG. 30 COMPARISON OF THE TFQE PREDICTION VS. THE ALBLAS PREDICTION FOR σ_θ VS. θ ALONG THE HOLE r = R AT THE MIDPLANE z = 0 FOR THE TENSION-LOADED ISOTROPIC PLATE WITH A CIRCULAR HOLE (σ_{x_∞} =1.0 PSI)

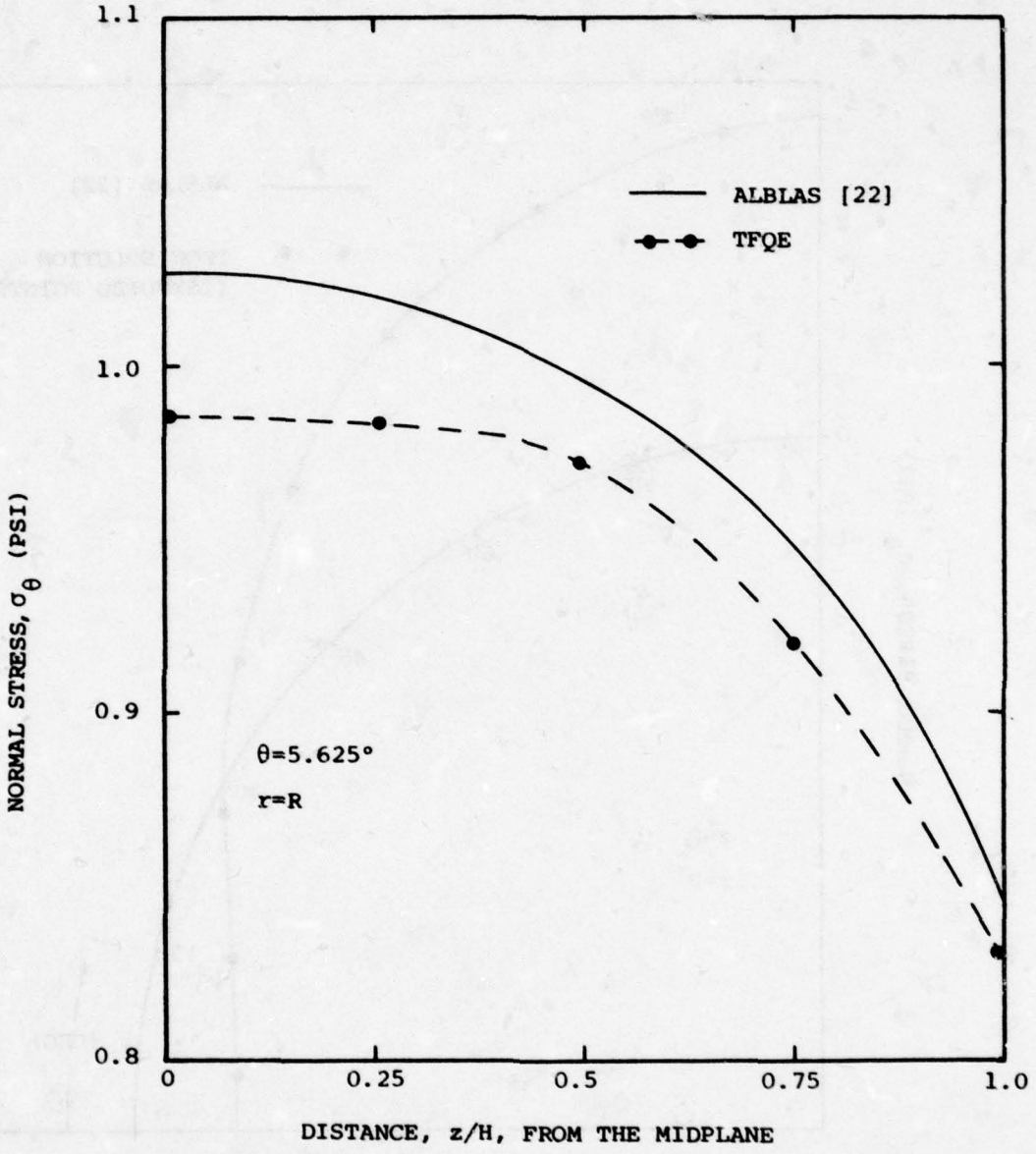

FIG. 31 COMPARISON OF THE TFQE PREDICTION VS. THE ALBLAS PREDICTION FOR σ_z AS A FUNCTION OF THE THROUGH-THE-THICKNESS LOCATION z/H AT r = R AND θ = 5.625° FOR THE TENSION-LOADED ISOTROPIC PLATE WITH A CIRCULAR HOLE (σ_{x_∞} = 1.0 PSI)

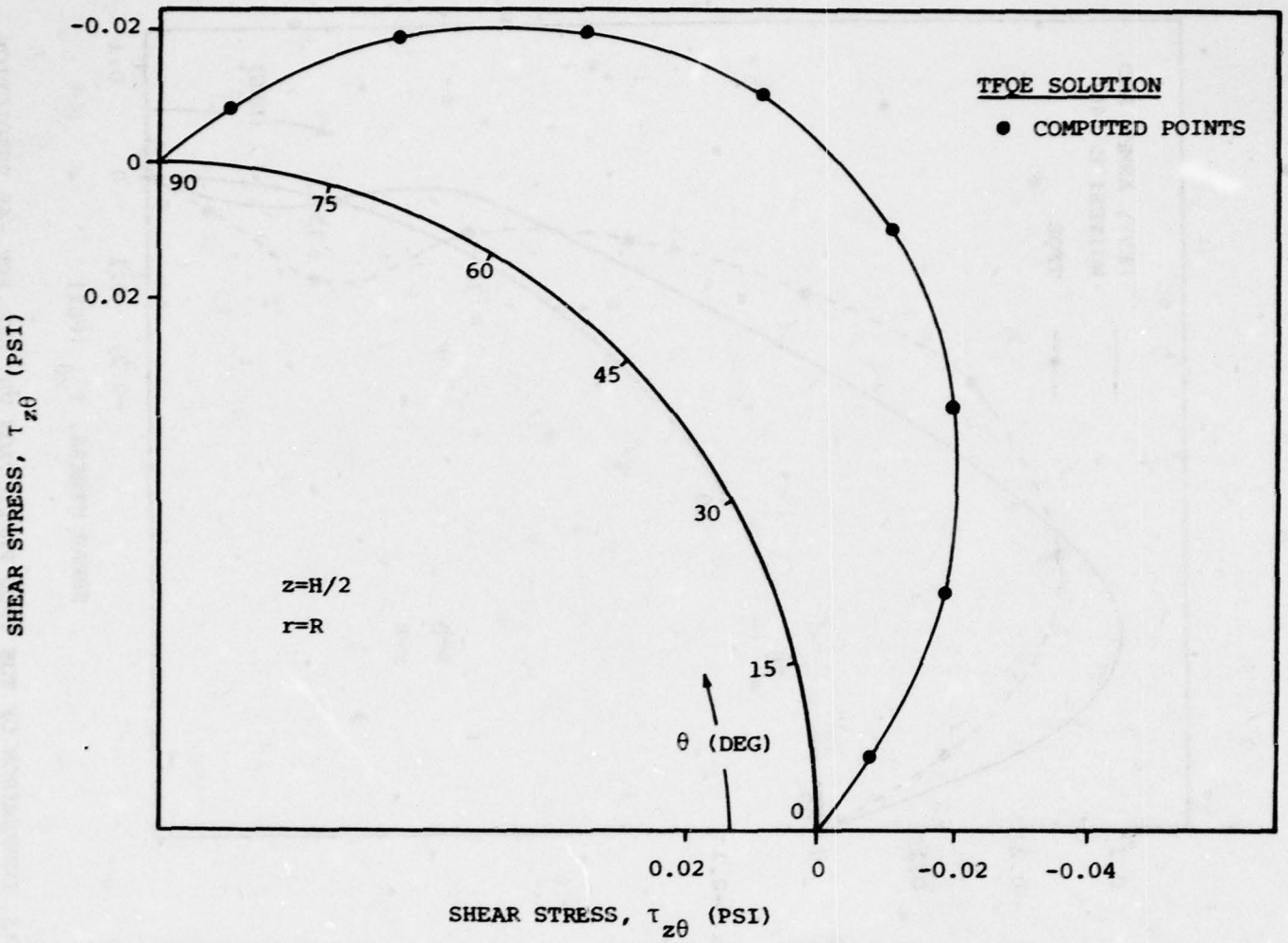

FIG. 32 TFQE PREDICTION FOR $\tau_{z\theta}$ VS. θ AT z = H/2 AND r = R FOR THE TENSION-LOADED ISOTROPIC PLATE WITH A CIRCULAR HOLE (σ_{x_∞} = 1.0 PSI)

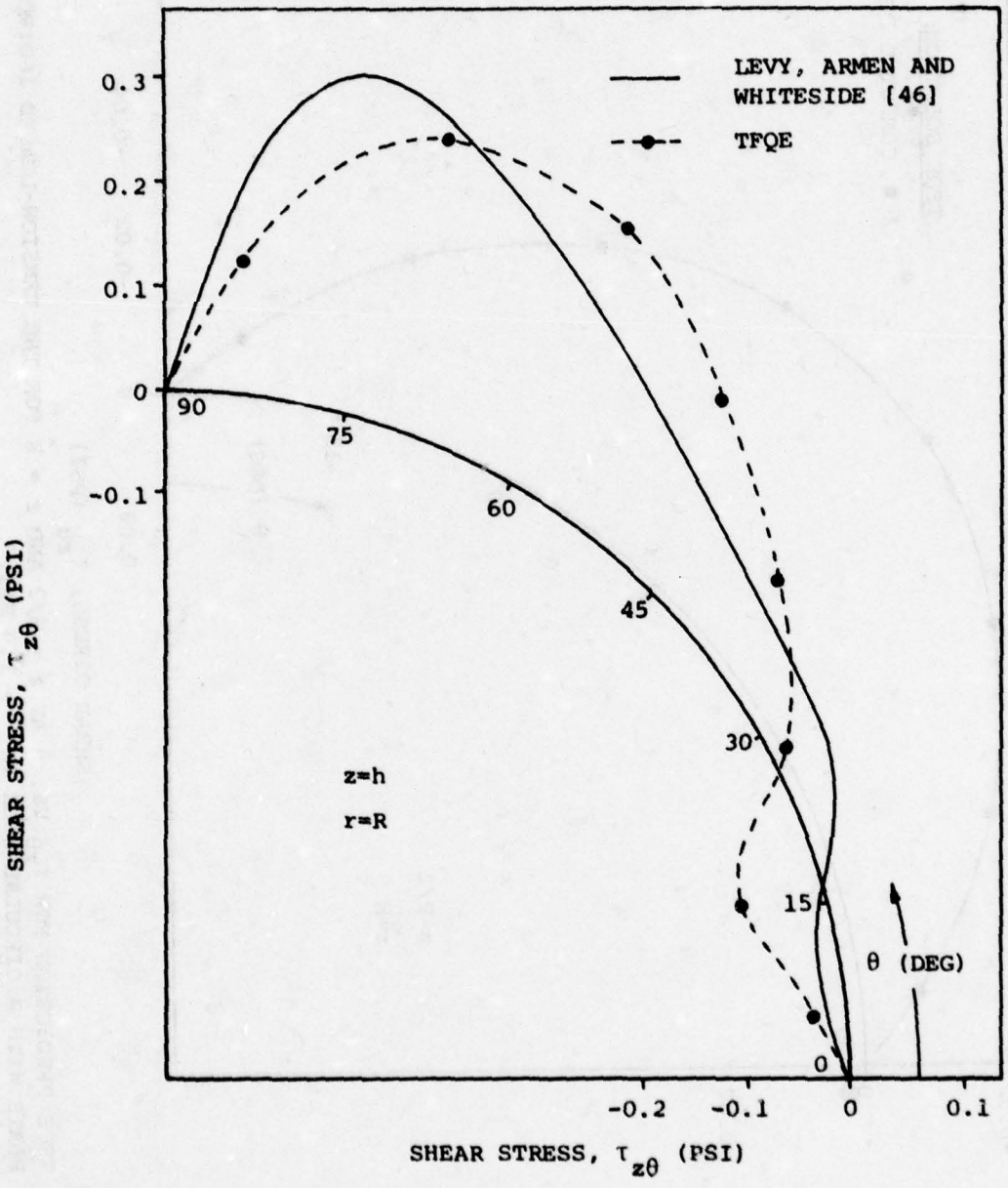

FIG. 33 COMPARISON OF THE TFQE PREDICTION VS. THE REF.-46 PREDICTION FOR $\tau_{z\theta}$ VS. θ AT r = R AND THE 0/90 INTERFACE AT z = h FOR THE TENSION-LOADED 4-PLY $(0/90)_s$ PLATE WITH A CIRCULAR HOLE (σ_{x_∞} = 1.0 PSI)

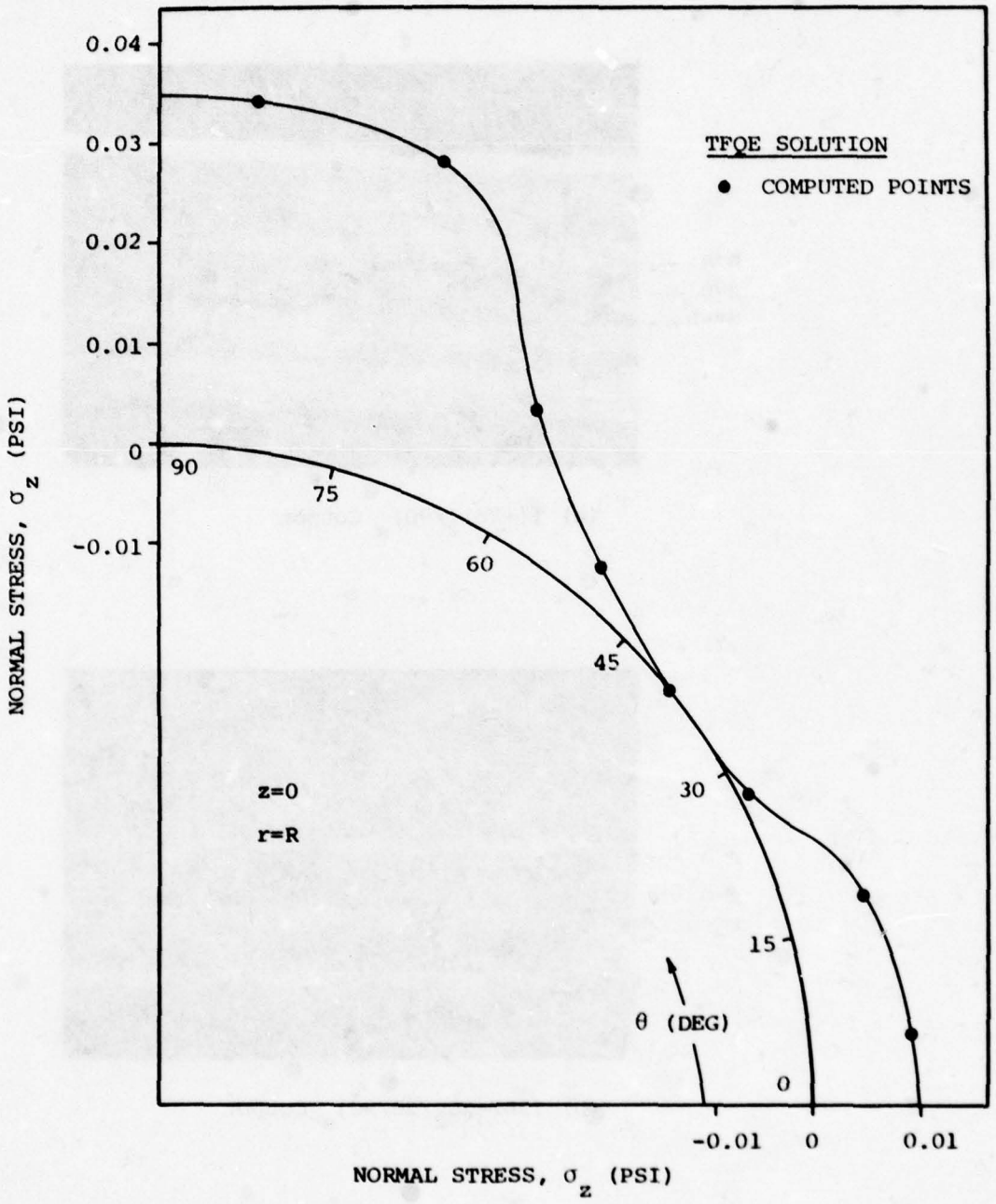

FIG. 34 TFQE PREDICTION OF σ_z VS. θ ALONG r = R AND THE MIDPLANE z = 0 FOR THE TENSION-LOADED 4-PLY $(0/90)_s$ PLATE WITH A CIRCULAR HOLE (σ_{x_∞} = 1.0 PSI)

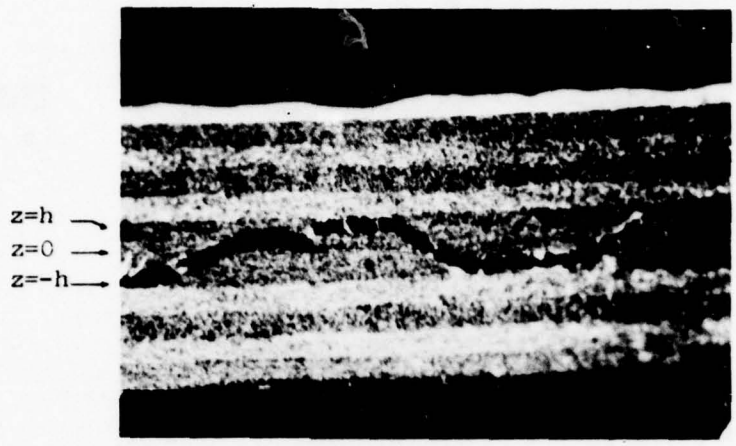

(a) $[(\pm 26)_2/90]_s$ Coupon

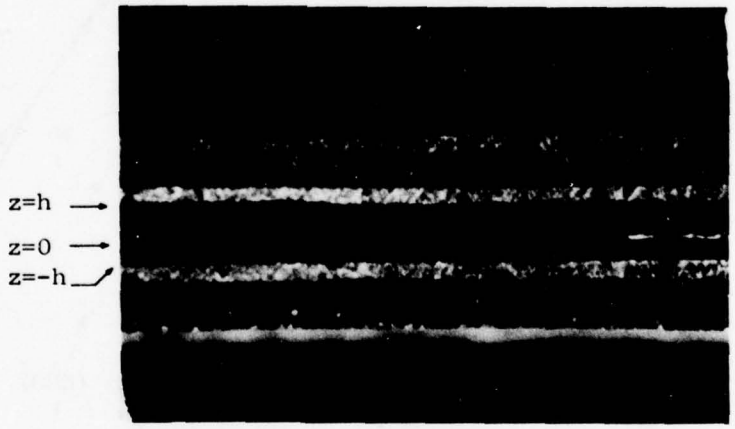

(b) $[26/-26_2/26/90]_s$ Coupon

FIG. 35 EDGE VIEWS OF TYPICAL DELAMINATIONS IN MULTILAYER COUPONS

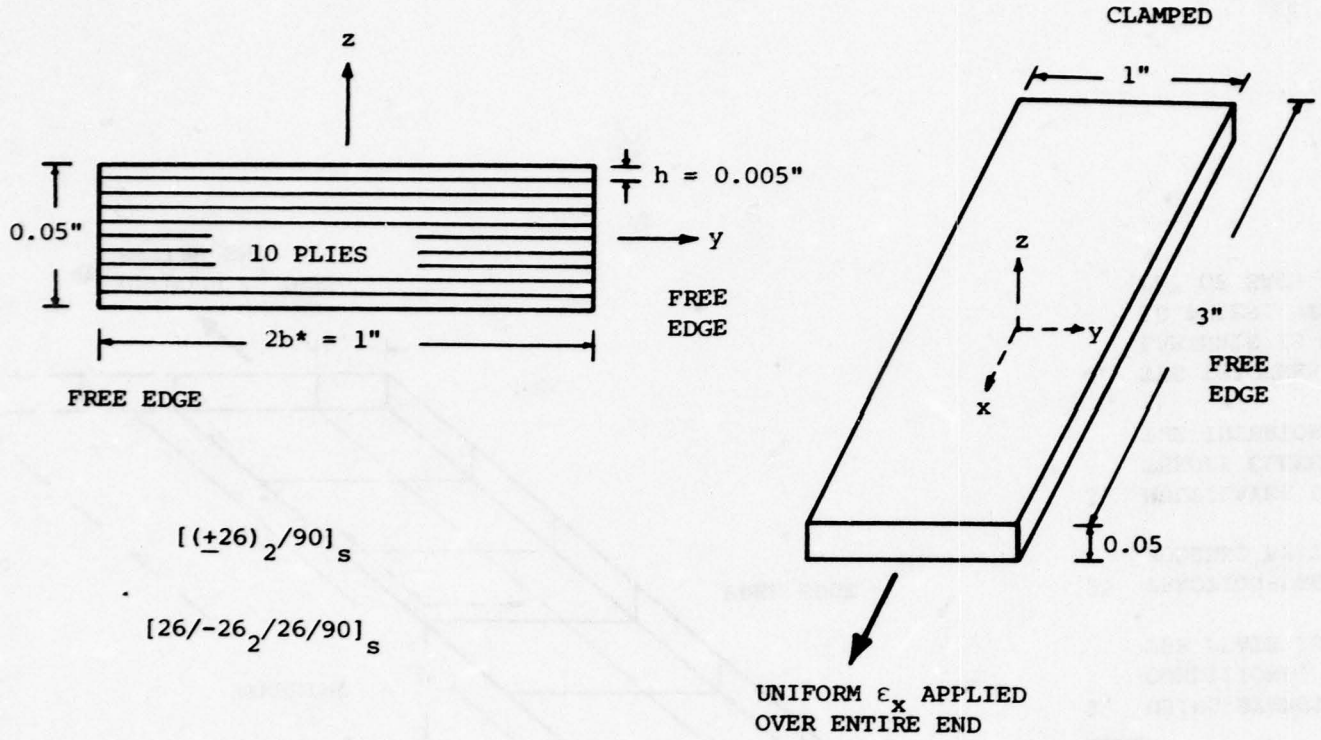

$[(\pm 26)_2/90]_s$

$[26/-26_2/26/90]_s$

FIG. 36 NOMENCLATURE AND DEFINITION OF THE 10-PLY EXPERIMENTAL COUPONS

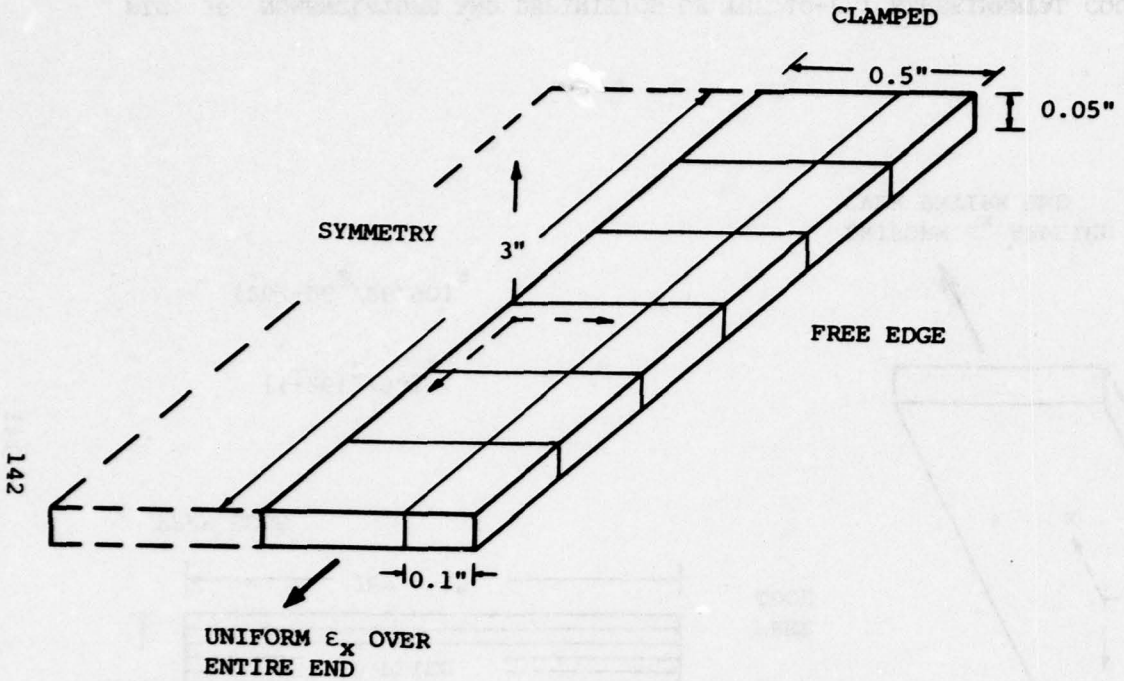

NOTE

1. USING SYMMETRY CONDITIONS, ONLY HALF THE PLATE IS ANALYZED.
2. TRACTION-FREE EDGE IS MODELED BY TFQE.
3. MULTILAYER LAMINATION THEORY ELEMENTS MODEL THE INTERIOR [26].
4. THE THICKNESS OF THE LAMINATE IS MADE UP OF 10 PLIES. THE THICKNESS "h" OF EACH PLY IS 0.005".

FIG. 37 FINITE ELEMENT MODELING OF THE 10-PLY EXPERIMENTAL COUPONS

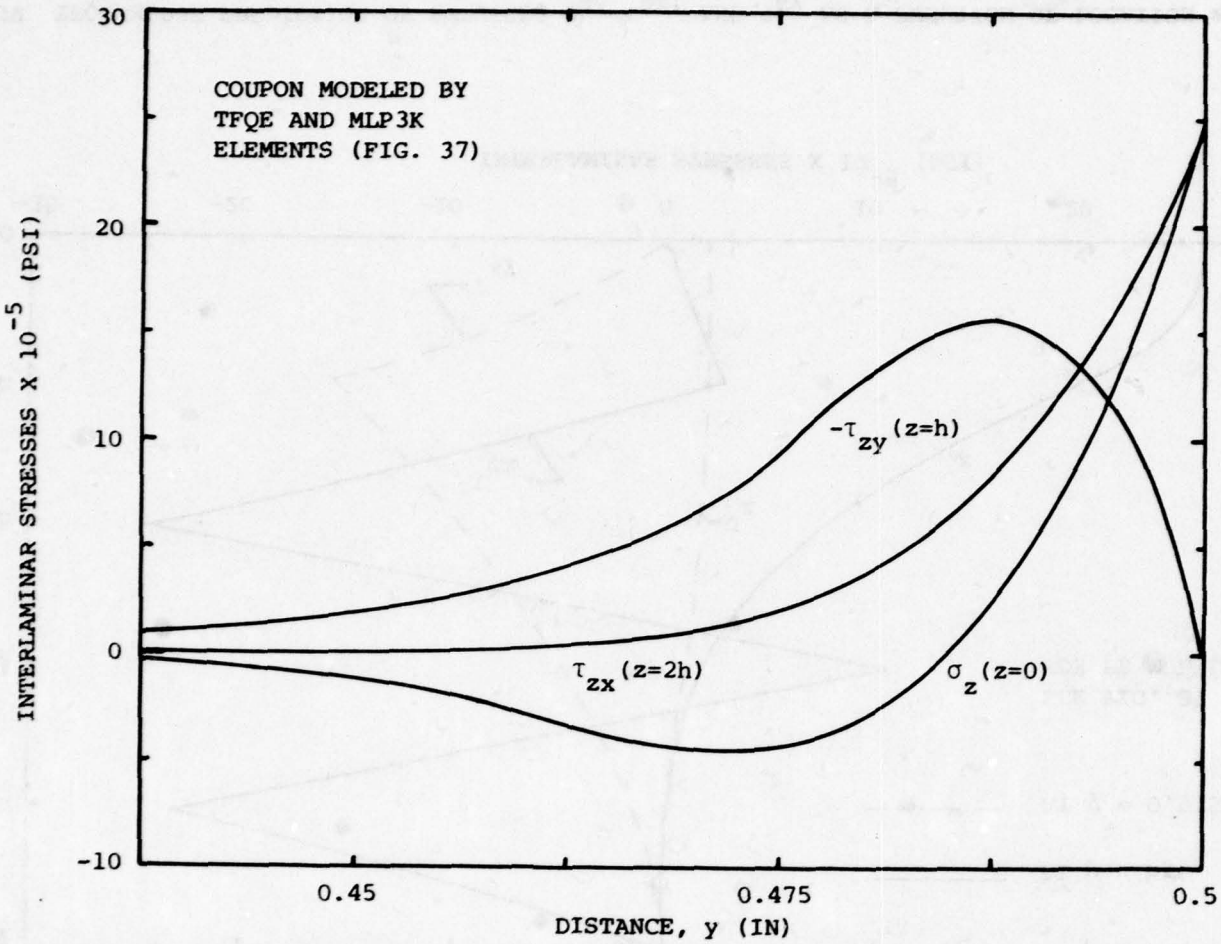

FIG. 38 TFQE/MLP3K PREDICTION OF THE INTERLAMINAR STRESSES σ_z, τ_{zx}, and τ_{zy} AS A FUNCTION OF DISTANCE y NEAR THE FREE EDGE ALONG INTERFACES z = 0, z = h, AND z = 2h OF THE TENSION-LOADED $[(\pm 26)_2/90]_s$ TESTED COUPON (ε_x = 1.0)

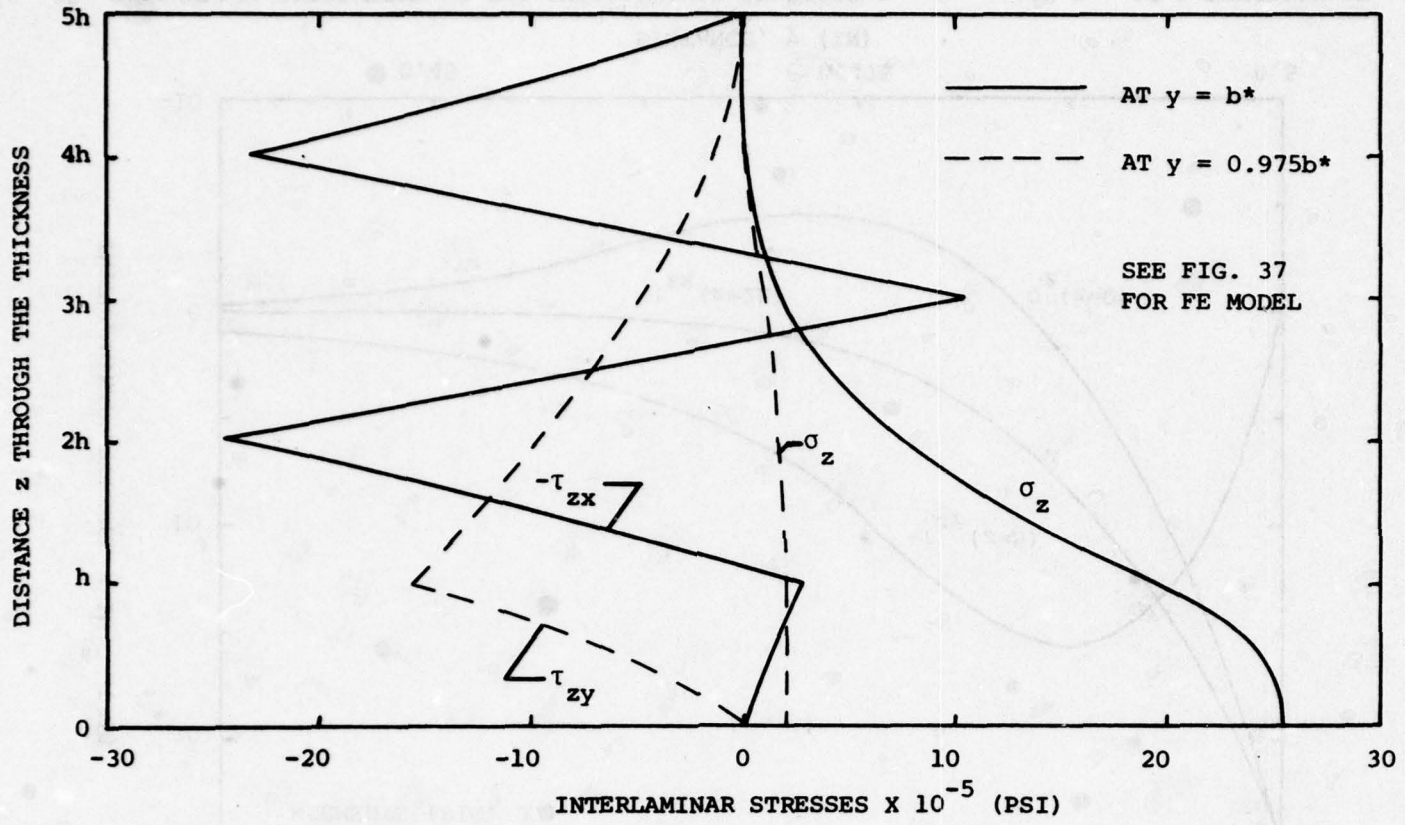

FIG. 39 TFQE/MLP3K PREDICTION OF STRESSES σ_z, τ_{zx}, AND τ_{zy} AS A FUNCTION OF LOCATION z THROUGH THE THICKNESS AT FIXED STATIONS y NEAR THE FREE EDGE OF THE TENSION-LOADED $[(\pm 26)_2/90]_s$ TESTED COUPON ($\varepsilon_x = 1.0$)

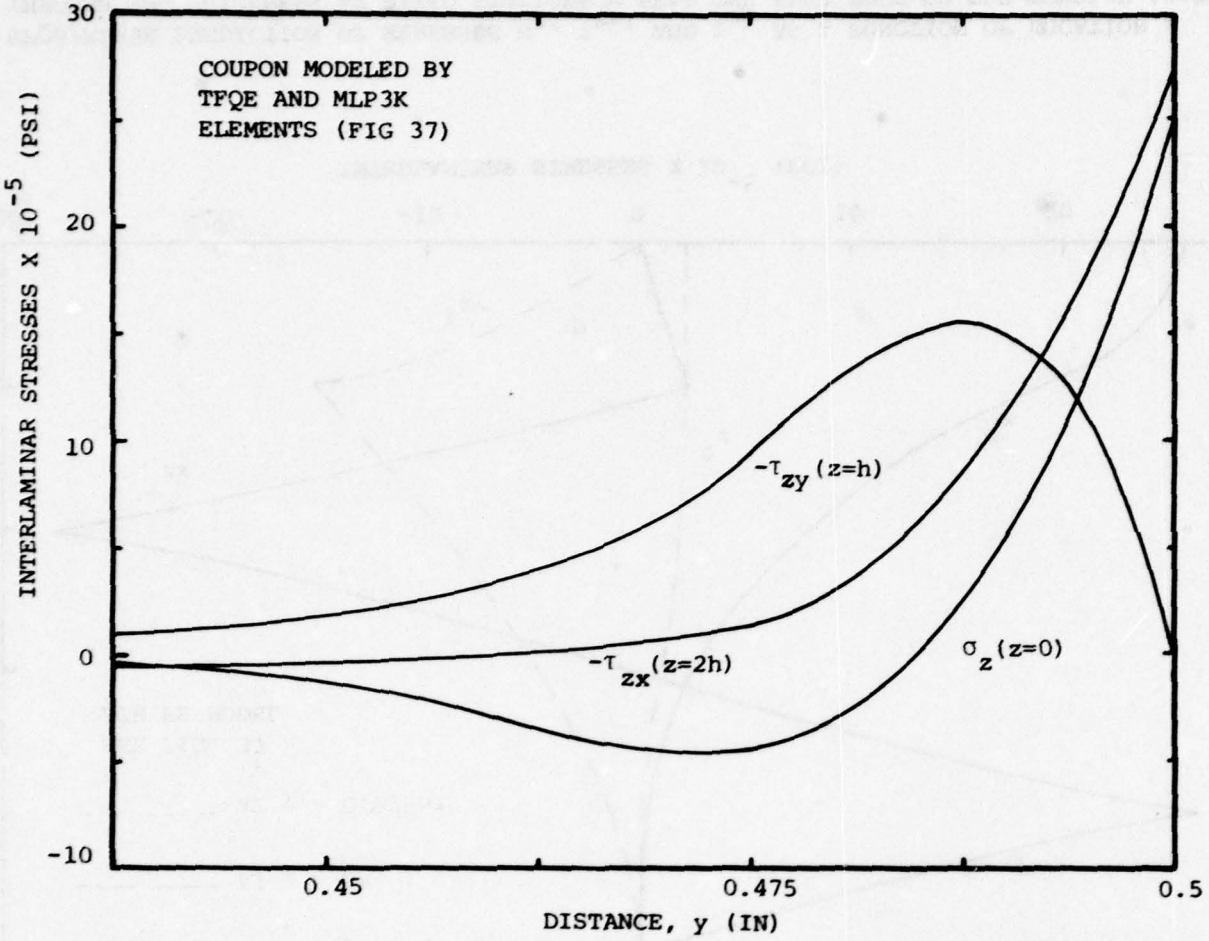

FIG. 40 TFQE/MLP3K PREDICTION OF THE INTERLAMINAR STRESSES σ_z, τ_{zx}, AND τ_{zy} AS A FUNCTION OF DISTANCE y NEAR THE FREE EDGE ALONG INTERFACES z = 0, z = h, AND z = 2h OF THE TENSION-LOADED $[(\pm 26)/(\pm 26)/90]_s$ TESTED COUPON ($\varepsilon_x = 1.0$)

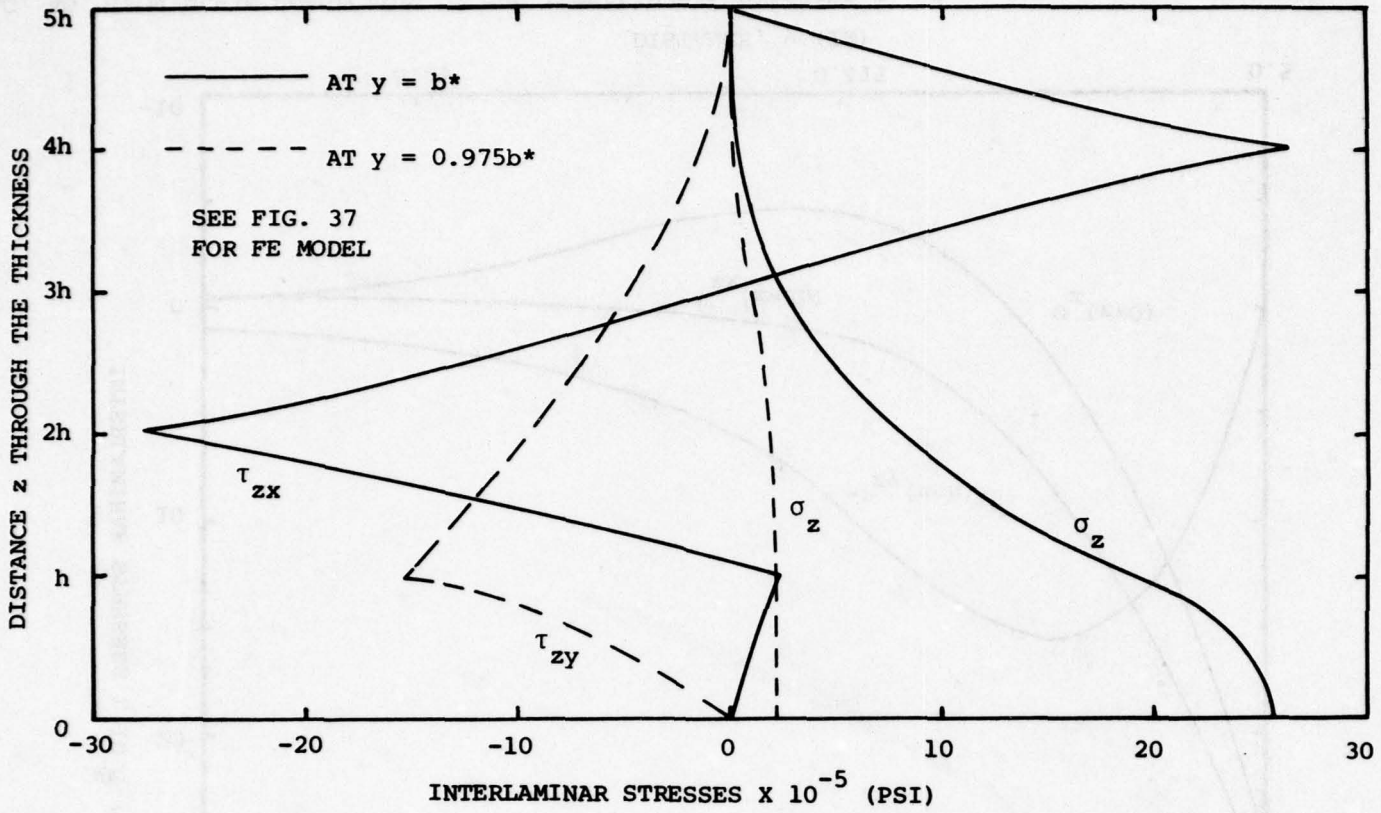

FIG. 41 TFQE/MLP3K PREDICTION OF STRESSES σ_z, τ_{zx}, AND τ_{zy} AS A FUNCTION OF LOCATION z THROUGH THE THICKNESS AT FIXED STATIONS y NEAR THE FREE EDGE OF THE TENSION-LOADED $[(\pm 26)/(\pm 26)/90]_s$ TESTED COUPON ($\varepsilon_x = 1.0$)

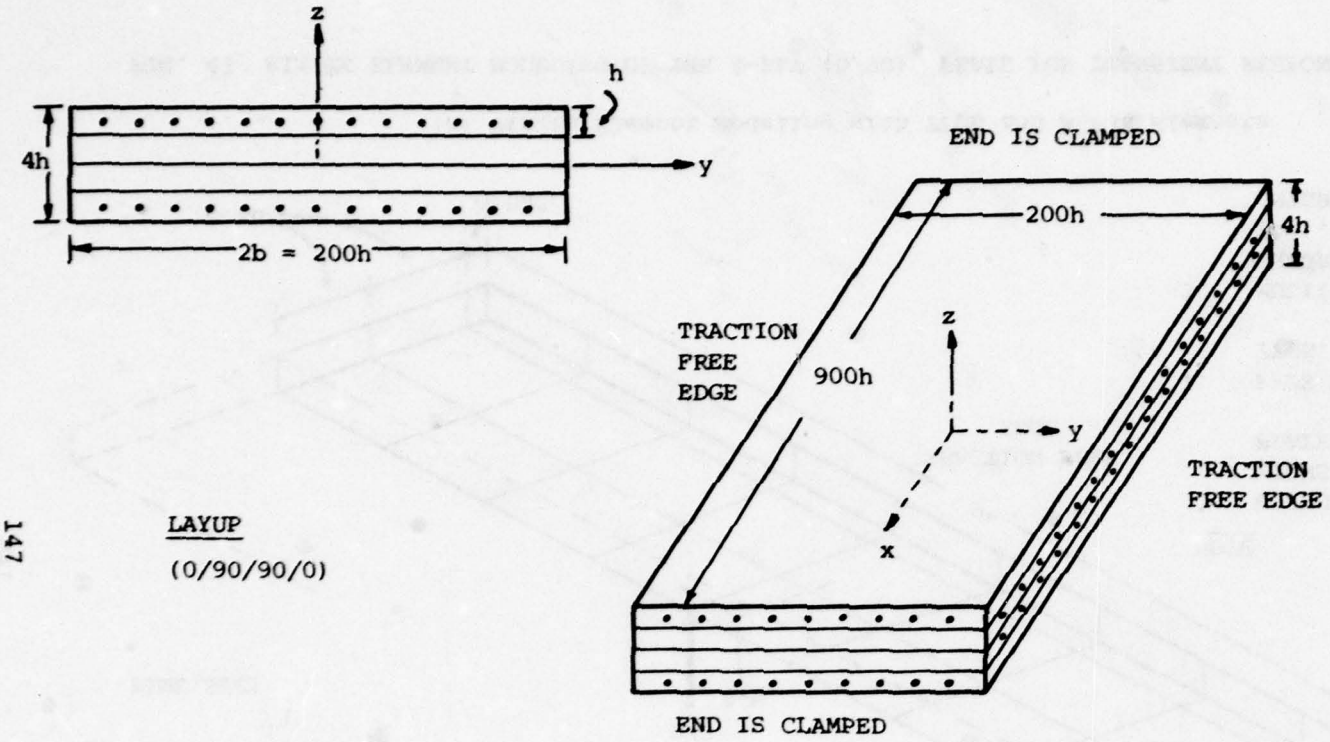

LAYUP

(0/90/90/0)

FIG. 42 DEFINITION AND NOMENCLATURE OF THE 4-PLY $(0/90)_s$ PLATE FOR TRANSIENT RESPONSE ANALYSIS

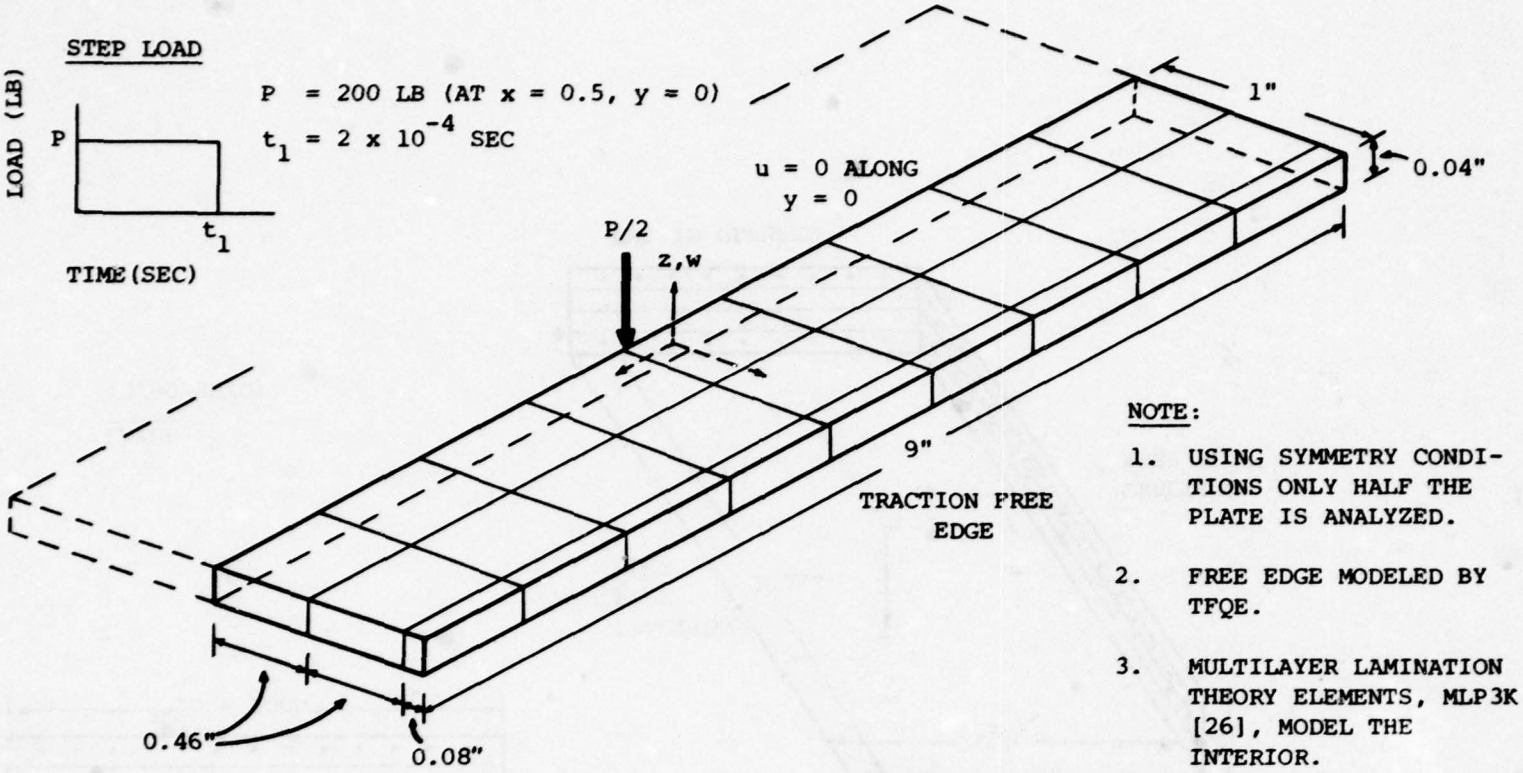

(a) Finite Element Modeling with TFQE and MLP3K Elements

FIG. 43 FINITE ELEMENT MODELING OF THE 4-PLY $(0/90)_s$ PLATE FOR TRANSIENT RESPONSE ANALYSIS

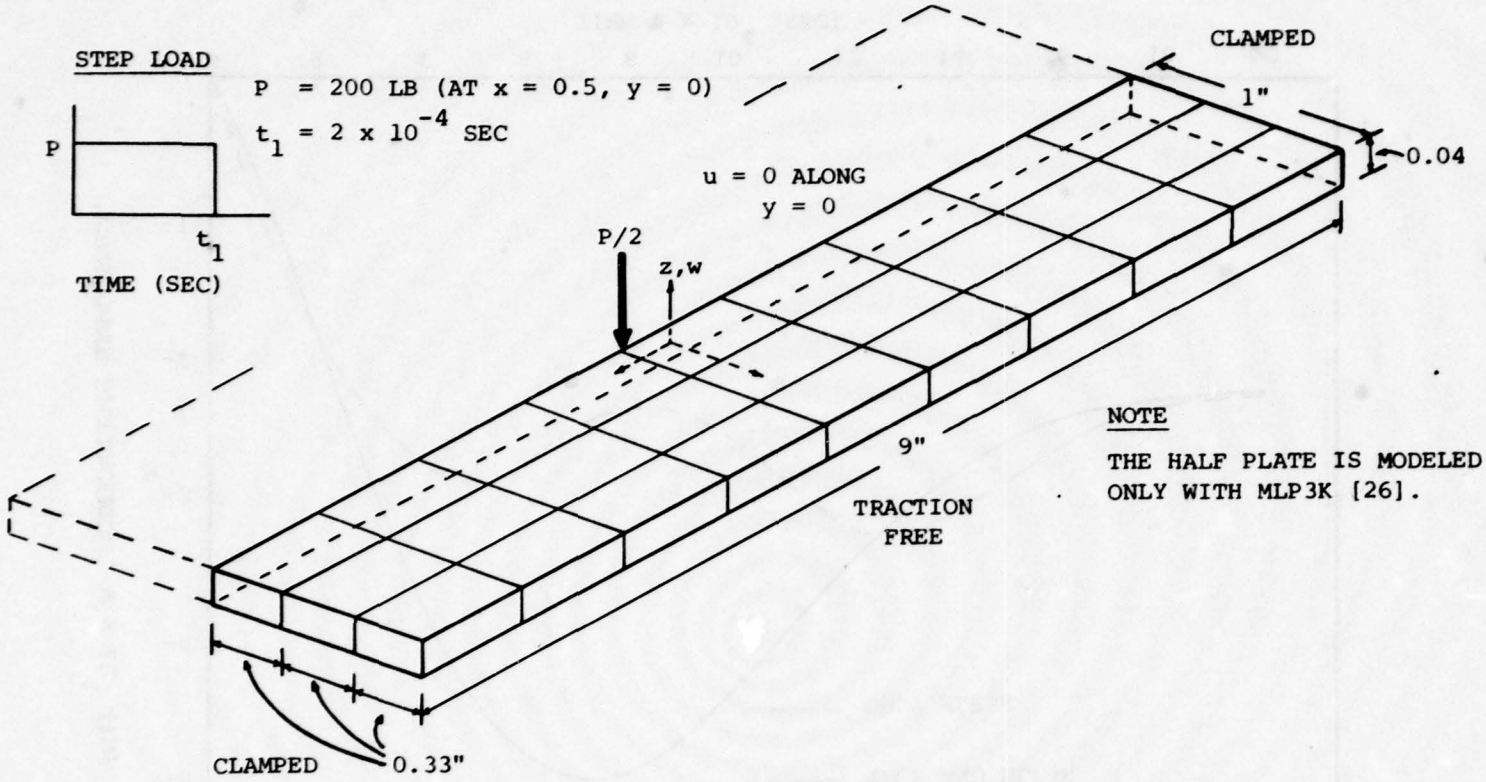

(b) Finite Element Modeling with MLP3K Elements Only

FIG. 43 CONCLUDED

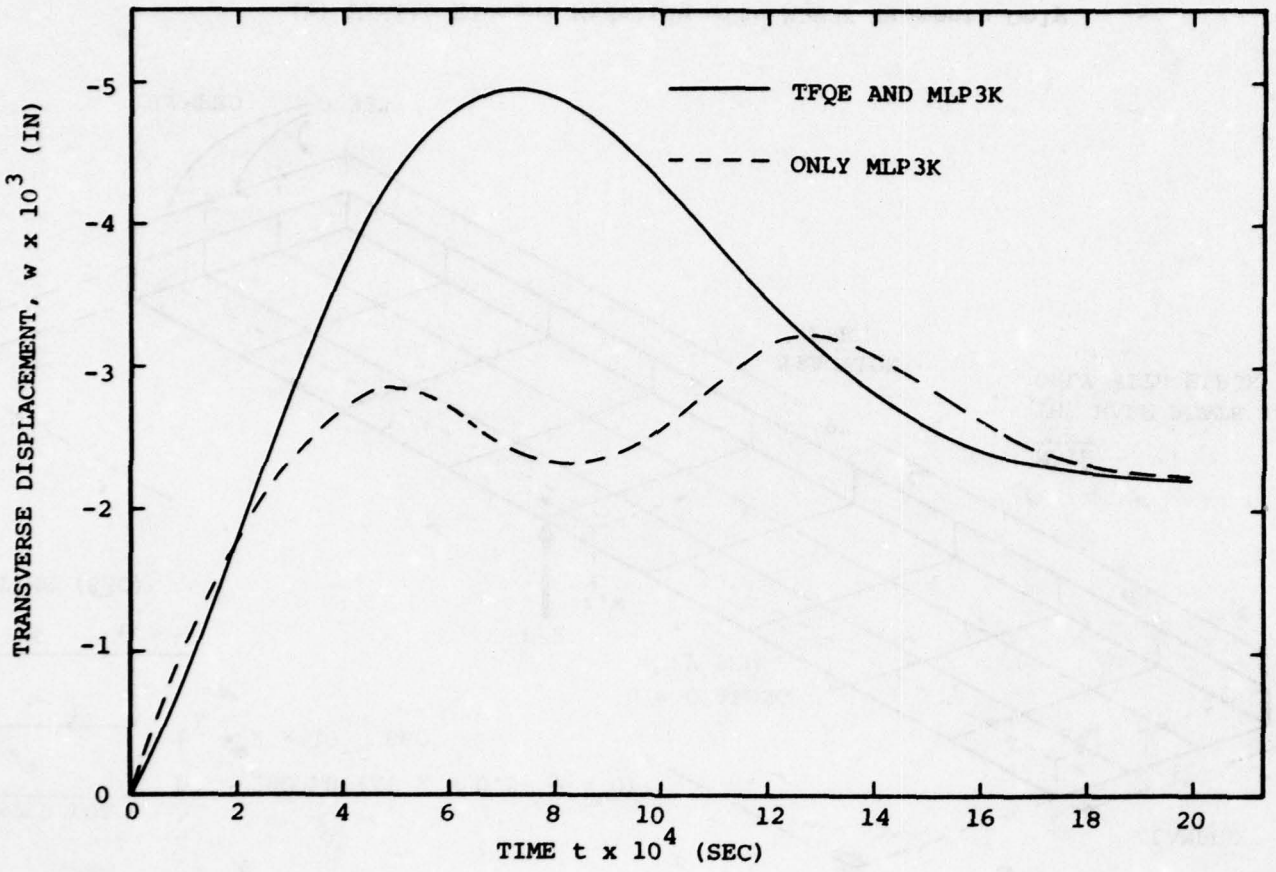

FIG. 44 PREDICTED TRANSVERSE DISPLACEMENT w AS A FUNCTION OF TIME AT THE LOAD-APPLICATION POINT (x = 0.5 IN, y = 0, z = 0)

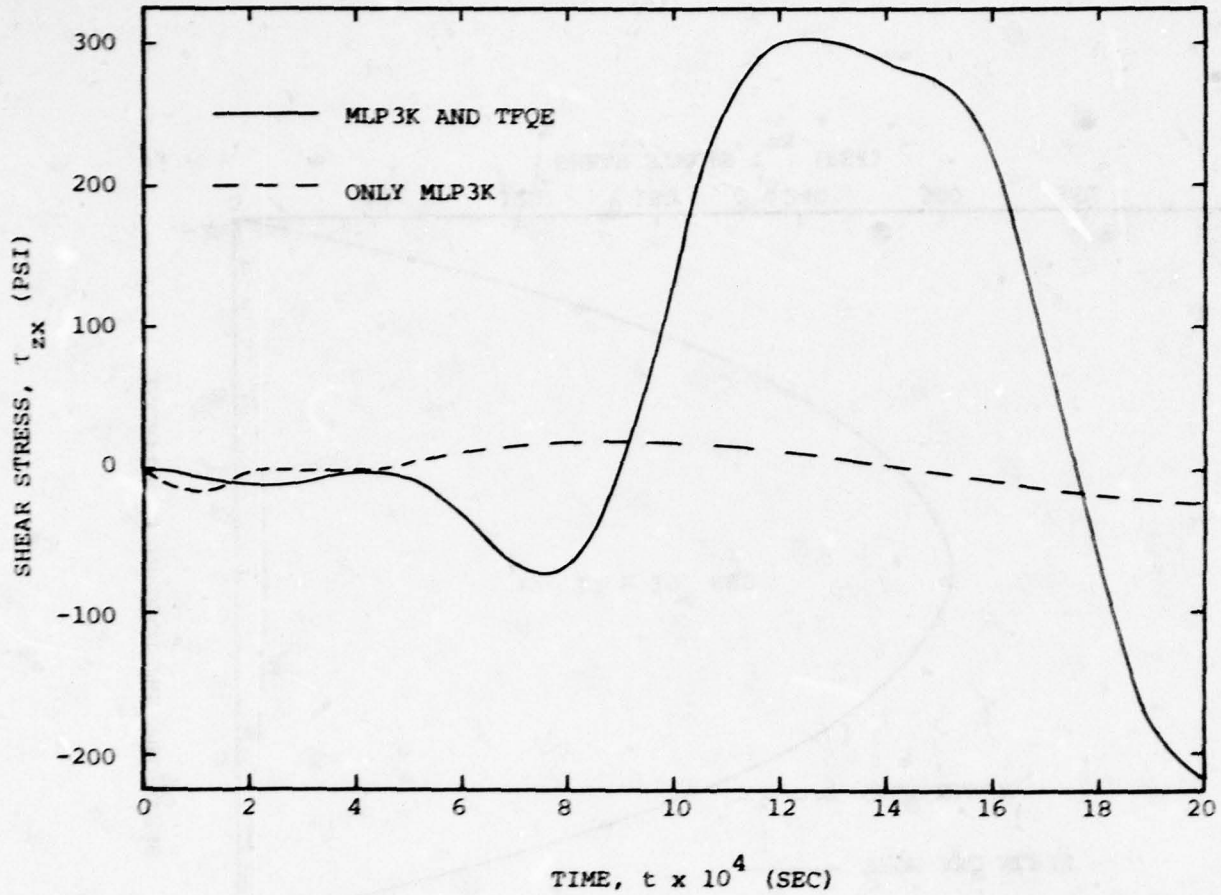

FIG. 45 PREDICTED TIME HISTORY OF THE INTERLAMINAR SHEAR STRESS τ_{zx} AT x = 0, y = 1.0 IN, z = 0

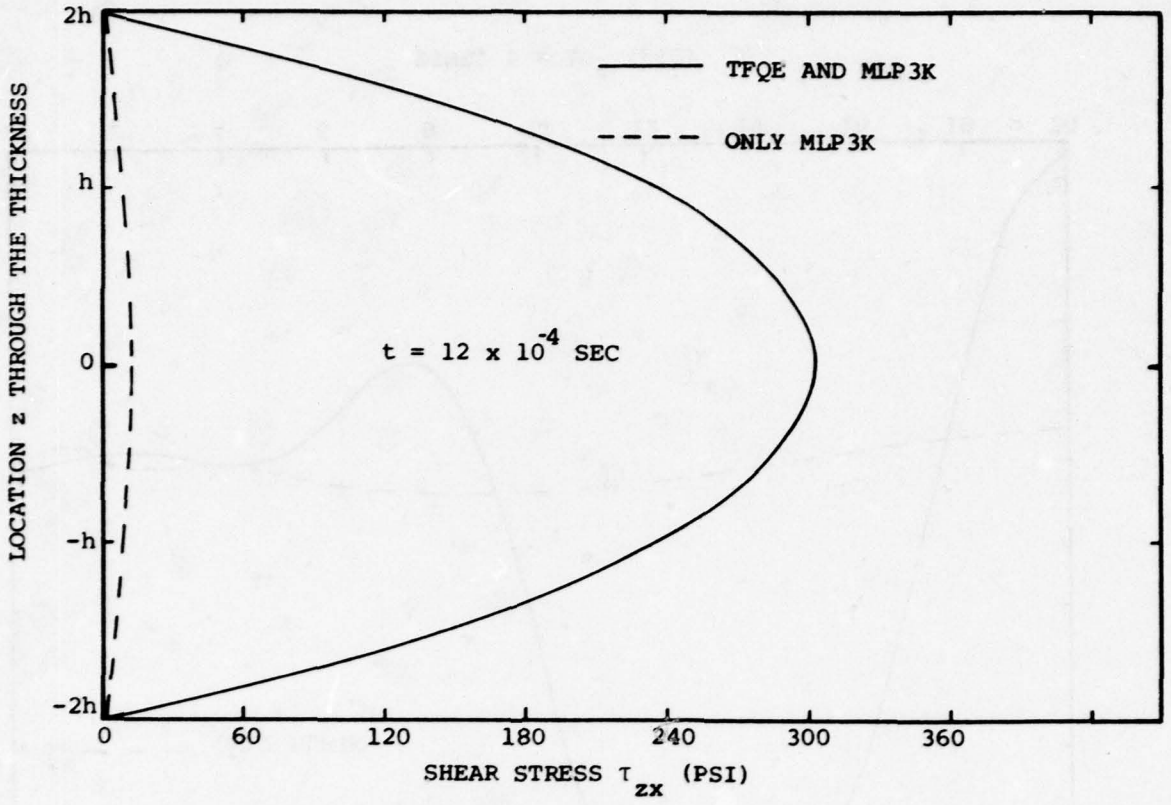

FIG. 46 PREDICTED DISTRIBUTION OF τ_{zx} THROUGH THE THICKNESS AT FREE-EDGE LOCATION (x = 0, y = 1.0 IN) AT t = 0.0012 SECOND

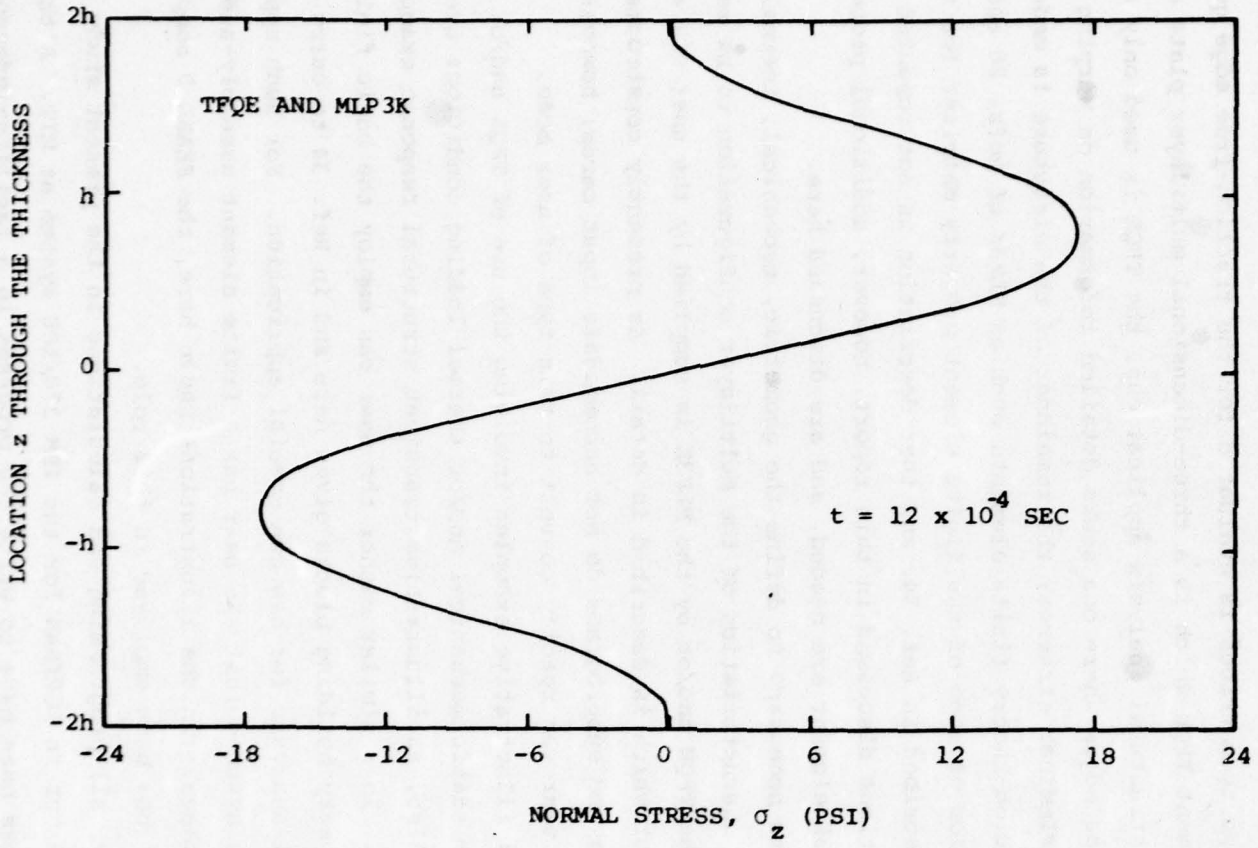

FIG. 47 PREDICTED DISTRIBUTION OF σ_z THROUGH THE THICKNESS AT FREE-EDGE LOCATION (x = 0, y = 1.0 IN) AT t = 0.0012 SECOND

APPENDIX

TFQE AND MLP3K PROGRAMMING DETAILS AND APPLICATIONS

The intent of this appendix is to describe how each of the finite-element property matrices is evaluated for the traction-free edge quadrilateral element TFQE which is a three-dimensional multilayer plate element. In typical structural analysis applications, the TFQE is used only along traction-free edges where one seeks detailed information on warping and severe interlaminar stresses; the remainder of the structure is modeled with lamination-theory finite elements such as MLP3K of Refs. 26 and 35. The evaluation of some of the finite element property matrices for the MLP3K is described in Ref. 34, and that description is not repeated here; for applications discussed in this report, however, additional properties for the MLP3K element are needed, and are discussed here.

The data necessary to define the geometric, mechanical, thermal, and/or mass characteristics of the multilayer configuration to be represented by the TFQE and/or by the MLP3K is supplied by the user via an argument list which is described in detail. As presently constructed, the programs and subprograms do not accommodate input cards; however, if desired the user can readily convert to this type of user mode.

Several illustrative examples involving the use of TFQE and/or MLP3K elements for static mechanical and/or thermal loading conditions are included. Also, an illustrative transient structural response example is included. In a similar manner the user can employ the basic finite element property building blocks given here and in Ref. 34 to carry out a structural analysis for his own special application. For such applications, it is assumed that the user has a finite element assembly-and-solution package. In the illustrations shown here, the FEABL 5 computer program [34] has been employed in this role.

Finally, all programming and calculations in the present study have been carried out in FORTRAN for the IBM 370/168 system at MIT. Although an attempt has been made to write the programs in a facility-independent fashion, the user should check to see what changes, if any, may be needed to enable these programs to be executed at his particular computer facility.

For structural analysis the four element quantities required are

(a) Mass Matrix, $\underset{\sim}{m}$ (Eq. 3.36)

(b) Stiffness Matrix, $\underset{\sim}{k}$ (Eq. 3.14)

(c) Thermal Loads Vector, $\underset{\sim}{Q}_T$ (Eq. 3.15)

(d) Mechanical Loads Vector, $\underset{\sim}{Q}_M$ (Eq. 3.11)

In addition, the stresses (Eq. 3.2) need to be computed from the displacement solution by using Eq. 3.19.

For the TFQE, $\underset{\sim}{m}$, $\underset{\sim}{k}$, and $\underset{\sim}{Q}_T$ are programmed as separate modules (consisting of a combination of selected subroutines) which can be accessed individually when needed. However, some interaction does occur between modules, because information developed in one module is required in another. The mechanical loads vector, $\underset{\sim}{Q}_M$ is computed analytically. The development and user information for obtaining these properties are discussed in Subsection A.1. The stress computation procedure is also included.

For MLP3K, the user information for $\underset{\sim}{m}$ and $\underset{\sim}{k}$ is given in Ref. 34 (p. 9-15). In the present effort, the stiffness matrix module has been modified to compute $\underset{\sim}{Q}_T$ also. The modified version for the $\underset{\sim}{k}$ for MLP3K is discussed in Subsection A.2. The mechanical loads vector, $\underset{\sim}{Q}_M$, is computed analytically similar to the procedure used for the TFQE. The MLP3K stress computation procedure is included in Subsection A.2.

In Subsection A.3, the applications of TFQE and MLP3K to the example problems described in Section 5 are discussed.

A.1 TFQE Programming Details

The TFQE properties are computed with the aid of the following alphabetically-listed subroutines:

ASG - Used by FHIGI for computing $\underset{\sim}{G}$ (Eq. 3.7) of each layer

ASGT - Used by THERM for computing $\underset{\sim}{G}_t$ (Eq. 3.9) of each layer

ASH - Used by FHIGI for computing $\underset{\sim}{H}$ (Eq. 3.6) of each layer

ASHT - Used by THERM for computing $\underset{\sim}{H}_t$ (Eq. 3.8) of each layer

DKRD - Reads

(a) NL, b, $\underset{\sim}{k}$ and $\underset{\sim}{m}$ if ISW = 1 using FORTRAN unit number 8 from disk dataset.

(b) $\underset{\sim}{Z}$, $\underset{\sim}{S}$ and $\underset{\sim}{H}^{-1}\underset{\sim}{G}$ if ISW = 2 using FORTRAN unit number 9 from disk dataset.

See subroutine DKW for definition of quantities.

DKRH - Reads

(a) $\underset{\sim}{Z}$, $\underset{\sim}{S}$ and $\underset{\sim}{H}^{-1}\underset{\sim}{G}$ if ISW = 1 using FORTRAN unit number 9 from disk dataset.

(b) NH, LNZ, LNR and IAD if ISW = 1 using FORTRAN unit number 10 from disk dataset.

(c) $\underset{\sim}{H}$ if ISW = 2 using FORTRAN unit number 10 from disk dataset.

See subroutine DKW for definition of quantities.

DKRS - Similar to DKRD except the mass matrix $\underset{\sim}{m}$ is not read.

DKW - Writes

(a) NL (integer value of the number of layers); b (element width in single precision); $\underset{\sim}{k}$ (element stiffness matrix in double precision); $\underset{\sim}{m}$ (element mass matrix in double precision) onto disk dataset using FORTRAN unit number 20.

(b) $\underset{\sim}{Z}$ (layer surface and/or interface coordinates in single precision); $\underset{\sim}{S}$ (material properties of each layer in single precision); $\underset{\sim}{H}^{-1}\underset{\sim}{G}$ (single precision array used to compute the betas, Eq. 3.12b) onto disk dataset using FORTRAN unit number 21.

(c) NH (integer value of H-matrix length); LNZ, LNR, IAD (integer arrays for the H-matrix since it is banded); $\underset{\sim}{H}$ (factored H-matrix in double precision) onto disk dataset using FORTRAN unit number 22.

ELM12 - Used by TFQEM to compute all xy-plane area integrals for the mass matrix $\underset{\sim}{m}$ (Eq. 3.36).

ELYM - Used by TFQEM to compute the mass matrix of each layer.

FHIGI - Computes $\underset{\sim}{G}$ (Eq. 3.7) and $\underset{\sim}{H}$ (Eq. 3.6) of each layer.

HGCON - Used by TFQEK to eliminate dependent β's and assemble $\underset{\sim}{G}$ (Eq. 3.7) and $\underset{\sim}{H}$ (Eq. 3.6) for entire element. Used similarly by TFQET to eliminate dependent β's and assemble $\underset{\sim t}{G}\underset{\sim t}{\beta}$ (Eq. 3.3 and 3.9) and $\underset{\sim t}{H}\underset{\sim t}{\beta}$ (Eq. 3.2 and 3.8) for entire element. Also used by STRESS to compute all 94 β's of each layer from the independent β's.

HIGK - Used by TFQEK to factor $\underset{\sim}{H}$ (Eq. 3.6) and compute $\underset{\sim}{k}$ (Eq. 3.14) and $\underset{\sim}{H}^{-1}\underset{\sim}{G}$ (Eq. 3.12b). Used by TFQET to compute $\underset{\sim}{H}^{-1}\underset{\sim t}{H}\underset{\sim t}{\beta}$ (Eq. 3.12b) using the factored form of $\underset{\sim}{H}$ (Eq. 4.73).

NUMINT - Computes all xy-plane area integrals and boundary integrals for $\underset{\sim}{G}$ (Eq. 3.7) and $\underset{\sim}{H}$ (Eq. 3.6).

PROP - Computes the compliance coefficients (Eq. 4.28) of each layer from ply orientation angles and material properties.

ROTATE - Transforms the element stiffness matrix and load vectors from element axes to global axes (Eq. 3.17). Also transforms the element displacement vector from global axes to element axes (Eq. 3.16). All transformations are in the xy-plane.

STRESS - Evaluates the stresses (Eq. 3.2) in each layer at coordinates specified by user.

TERMS - Computes $\underset{\sim o}{\beta}$ and $\underset{\sim t}{\beta}$ (Eq. 3.2).

TFQEK - Subroutine called by user to compute the element stiffness matrix $\underset{\sim}{k}$ (Eq. 3.14) and $\underset{\sim}{H}^{-1}\underset{\sim}{G}$ (Eq. 3.12b).

TFQEM - Subroutine called by user to compute the element mass matrix $\underset{\sim}{m}$ (Eq. 3.36).

TFQET - Subroutine called by user to compute the element thermal loads vector $\underset{\sim}{Q}_T$ (Eq. 3.15).

THERM - Used by TFQET to compute $\underset{\sim}{H}_t$ (Eq. 3.8) and $\underset{\sim}{G}_t$ (Eq. 3.9).

TMPSTR - Compute thermal quantities $\bar{\varepsilon}^o_x$, $\bar{\sigma}^o_y$, $\bar{\sigma}^o_z$ and $\bar{\tau}^o_{xy}$ (Eqs. 4.27 and 4.30) of each layer from ply geometrical, thermal, and material properties.

Each module of the TFQE is discussed individually in the following subsections.

A.1.1 The TFQE Mass Matrix

The program structure of the mass matrix is shown in Fig. A1. Subroutine TFQEM is called by the user, but ELM12 and ELYM are called by TFQEM to perform the specific computations shown in Fig. A1. The numerical computations are done in double precision and all real arguments are double precision.

The user call statement with the arguments is

```
CALL TFQEM(X,Y,Z,RHO,EM,NL)
```

where

X(4),Y(4) - Nodal coordinates of the four (4) corners in the order A, B, D, E (Fig. 6). Note that sides AB and DE must be parallel.

Z(NL+1) - Interface and/or surface coordinates of each layer with respect to the laminate axis z (not $\bar{z}$). Note that z(1) = -H (see Fig. 6).

RHO(NL) - Layer mass per unit volume.

NL - Number of Layers

are inputs supplied by user. The quantity

EM(*) - TFQE mass matrix in LTV form (Eq. 3.36).

---

* The array EM is used internally by TFQEM for other computations. Hence, add 750 words to the dimension given in Table A1.

is output by TFQEM. Since the mass matrix is symmetric, only the lower triangle (termed LTV form) is computed and supplied.

A.1.2 The TFQE Stiffness Matrix

The program structure of the stiffness matrix is shown in Fig. A2. Subroutine TFQEK is called by the user, but the others are called by TFQEK to perform the specific computations shown in Fig. A2. The numerical computations are done in double precision and all real arguments are double precision.

The user call statement with the arguments is

```
CALL TFQEK(X,Y,Z,S,HIG,ELK,NL,HMAT,LNZ,LNR,IAD)
```

where

X,Y,Z	-	Defined in Subsection A.1.1.
S(13,NL)	-	Elastic compliance coefficients (Eq. 4.28) of each layer. They are specified in the following order: S_{11}, S_{21}, S_{22}, S_{31}, S_{32}, S_{33}, S_{61}, S_{62}, S_{63}, S_{66}, S_{44}, S_{45}, and S_{55}. In Subsection A.1.6, subroutine PROP for computing the compliance properties is discussed.
NL	-	Number of layers.

are inputs supplied by user. The quantities

HIG(*)	-	Matrix $\underset{\sim}{H}^{-1}\underset{\sim}{G}$ (Eq. 3.12b).
ELK(*)	-	TFQE stiffness matrix in LTV form (Eq. 3.14).
HMAT(*)	-	trix $\underset{\sim}{H}$ in factored form (Eq. 4.73).
LNZ(NQ) LNR(NQ) IAD(NQ)	-	Pointers for $\underset{\sim}{H}$ since the matrix is banded. Need not be defined by user. Note NQ = 8NL+30.

*Refer to Table A1 for dimensions. The array ELK is used internally by TFQEK for other computations. Hence, the minimum dimension of ELK for TFQEK should be 8040 words.

are output by TFQEK. Since the stiffness matrix is symmetric, only the lower triangle (termed LTV form) is computed and supplied in the first NQ(NQ+1)/2 entries of ELK, where NQ = 8NL+30. Although ELK is dimensioned 8040, only part of it contains the stiffness matrix.

A.1.3 The TFQE Thermal Loads Vector

The program structure of the thermal loads vector is shown in Fig. A3. Subroutine TFQET is called by the user, but the others are called by TFQET to perform the specific computations shown in Fig. A3. Subroutine DKRH reads information from disk datasets on FORTRAN unit numbers[+] 9 and 10. Setting up the required information of disk datasets will be discussed in Subsection A.3. All arguments are double precision except Z and S.

The user call statement with the arguments is

```
CALL TFQET(STR,NL,NBETA,ELQ,S,X,Y,Z,TI,SGO,HT,LNZ,LNR,IAD)
```

where

STR(*)	-	Temporary storage in double precision.
NL	-	Number of layers.
NBETA	-	Number of independent betas, 52NL-18 (Eq. 4.60)
S,X,Y,Z	-	Defined in Subsection A.1.2.
TI(6,NL)	-	Temperature constants (Eq. 4.26) in each layer (ΔT_i, i = 1,6).
SGO(4,NL)	-	Thermal quantities $\bar{\varepsilon}^o_x$, $\bar{\sigma}^o_y$, $\bar{\sigma}^o_z$, and $\bar{\tau}^o_{xy}$ (Eqs. 4.27 and 4.30). In Subsection A.1.6, subroutine TMPSTR that computes SGO is discussed.
LNZ,LNR,IAD	-	Defined in Subsection A.1.2

are inputs supplied by user. The quantities

[+] The FORTRAN unit number (sometimes referred to as a hardware device code) is used to control input/output operations. The unit numbers 5 and 6 are commonly assigned to the card reader and line printer, respectively, on IBM and CDC systems.

[*] Same dimensions as HMAT in Table A1.

ELQ(NQ) - Thermal loads vector (Eq. 3.15) where NQ = 8NL+30.

HT(NBETA) - $\underset{\sim}{H}^{-1}\underset{\sim t}{H}\underset{\sim t}{\beta}$ (Eq. 3.12b). This is required by STRESS for computing stresses.

are output by TFQET.

A.1.4 The TFQE Mechanical Loads Vector

The mechanical loads vector $\underset{\sim}{Q}_M$ can be computed from Eq. 3.11. The nodal displacement interpolation function $\underset{\sim}{L}$ is discussed in Subsection 4.5.2. Thus, from the prescribed applied traction and known $\underset{\sim}{L}$, $\underset{\sim}{Q}_M$ can be computed analytically.

A.1.5 Stress Computation in the TFQE

The program structure of the stress computation and print procedure is shown in Fig. A4. Subroutine STRESS is called by the user, but HGCON and TERMS are called by STRESS to perform the specific computations shown in Fig. A4. Only the arguments HT,ELQ,TPI,SGO and BI are double precision.

The user call statement with the arguments is

```
CALL STRESS(LNUM,X,Y,ZZ,NSP,NL,S,HT,BI,HIG,ELQ,NZL,
NZC,TPI,SGO,ITMP,ISYM)
```

where

LNUM - User's global element number.

X(NSP)
Y(NSP+1) - xy-coordinates (w.r.t. element axes, Fig. 6) where stress output is desired. Also Y (NSP+1) = b (Fig. 6). At each of the NSP locations, the stresses and strains are computed in each layer from z = -H to z = H (Fig. 6).

ZZ(NL+1) - Interface and/or surface coordinates of each layer w.r.t. laminate axis z. Note that ZZ(1) = -H (Fig. 6). ZZ is also defined as Z in Subsection A.1.1.

NSP - Number of locations in the xy-plane where stresses and strains are to be computed.

NL - Number of layers.

S(13,NL) - Defined in Subsection A.1.2

HT(NBETA) - Defined in Subsection A.1.3. If there are no thermal effects, HT is not initialized.

HIG(*) - Defined in Subsection A.1.2.

ELQ(NQ) - Element nodal displacements w.r.t. element axes (Eq. 3.16). Note NQ = 8NL+30.

NZL - Number of z locations in each layer where stress and strain output is desired; must have NZL $\geq$ 2. For example if NZL = 5, the stresses and strains are computed and printed at the following 5 locations in each layer: 2 layer interfaces and 3 intermediate equally-spaced points. If NZL = 3, the stresses and strains are computed and printed at the layer interfaces and the layer midplane.

NZC - Portion of x,y plane NSP locations where stress and strain output is desired (at NZL locations). For location X(NZC+1), Y(NZC+1), NZL is set equal to 3; hence, at such locations stress and strain output are given at only 3 z-locations in each layer. Note that NZC $\leq$ NSP. These NZC locations are at X(1), Y(1)...X(NZC), Y(NZC). This provides flexibility to the user if detailed stress output is desired near the free edge.

TPI(6,NL) - Same as TI defined in Subsection A.1.3.

SGO(4,NL) - Defined in Subsection A.1.3.

ITMP - Pointer: ITMP = 1 when thermal effects occur; ITMP = 0 for no thermal effects.

ISYM - If the solution is symmetric about the element midplane z = 0, set ISYM = 1 to obtain stress and strain output only between $-H \leq z \leq 0$.

are inputs supplied by the user. The quantity

BI(94*NL) - Total betas of the TFQE (Eq. 4.55)

is output by STRESS.

A.1.6 Subroutines PROP, TMPSTR, and ROTATE

The above subroutines perform useful functions, essential to the TFQE. They will be discussed individually.

Subroutine PROP computes the compliance coefficients (Eq. 4.28) of each layer from the material properties and orientation angles of the plies. The coefficients are output in matrix S defined in Subsection A.1.2; these coefficients now are defined relative to the x,y,z axes of the whole laminate. All real arguments are double precision. The user call statement with arguments is

CALL PROP(S,XEL,ANG,NL,IPG)

where

XEL(12,NL) - Basic properties of each ply. They are specified in the following order: E_{11}, E_{22}, E_{33}, ν_{12}, ν_{23} ν_{31}, G_{12}, G_{23}, G_{31} (material properties) and α_1, α_2, α_3 (thermal properties). Subscripts 1, 2, and 3 refer to the material axes ξ,η,ζ of the ply (defined in Eq. 4.27).

ANG(NL) - Angle (positive) measured counterclockwise from x axis of the TFQE (Fig. 6) to the principal material 1-axis of each layer. ANG(NL) is specified in degrees.

NL - Number of layers

IPG - Pointer; if material and thermal properties of all layers are the same, set IPG = 1 and specify only the first layer properties in XEL. Also, the required dimension is XEL(12,1).

are inputs supplied by user. The quantity S(13,NL) -- defined in Subsection A.1.2 is output by PROP.

Subroutine TMPSTR computes the thermal quantities $\bar{\varepsilon}_x^o$, $\bar{\sigma}_y^o$, $\bar{\sigma}_z^o$, and $\bar{\tau}_{xy}^o$ (Eqs. 4.27 and 4.30) of each layer from ply geometrical, thermal, and material properties. The coefficients are output in matrix SGO, defined in Subsection A.1.3. Also, computed are $\bar{\varepsilon}_y^o$, and $\bar{\gamma}_{xy}^o$; these are used by MLP3K (discussed in Subsection A.2) to compute the thermal loads. The thermal strains are output in EPSO. All real arguments are double precision. The user call statement with arguments is

```
CALL TMPSTR(XEL,ANG,SGO,EPSO,NL,IPG)
```

where the inputs XEL, ANG, NL and IPG are defined in subroutine PROP. The quantities

SGO(4,NL) - Defined in Subsection A.1.3

EPSO(3,NL) - Equivalent thermal strains (Eq. 4.27a). They are defined in order as $\bar{\varepsilon}_x^o$, $\bar{\varepsilon}_y^o$, and $\bar{\gamma}_{xy}^o$.

are output by TMPSTR.

Subroutine ROTATE transforms the element stiffness matrix and loads vector from element coordinates to global coordinates (Eq. 3.17). It also transforms the element global displacement vector to element coordinates (Eq. 3.16). All transformations are in the xy-plane. All real arguments are double precision. The user call statement with arguments is

```
CALL ROTATE(ELKT,NL,ELKS,ELQ,INF,ANGLE,IK)
```

where the inputs are

ELKT(*) - Should contain the element stiffness matrix if IK = 1. It is undefined if IK = 2 and dimensioned ELKT(1) if IK = 0.

---

*Refer to Table A1 for dimensions.

NL - Number of layers.

ELKS(*) - Should contain the element stiffness matrix if IK = 2. It is undefined and dimensioned ELKS(1) if IK ≠ 2.

ELQ(NQ) - Input the thermal loads vector if IK ≠ 0. For IK = 0, should contain the element global displacement vector. Note: NQ = 8NL+30.

INF(4*NL+8) - Internal work array

ANGLE - Angle (positive measured counter clockwise) from global X axis to the x axis of the TFQE (Fig. 6). ANGLE is specified in degrees.

IK - Pointer: set IK = 0 for transforming the element global displacement vector to element axes (Eq. 3.16); set IK = 1 if EKLT contains the element stiffness matrix; set IK = 2 if ELKS contains the element stiffness matrix. This procedure is provided if one needs to compute $\underset{\sim}{k}$ global for various rotation angles from a master copy of $\underset{\sim}{k}$ element. By setting IK = 2, the $\underset{\sim}{k}$ element stored in ELKS is never destroyed.

The outputs by subroutine ROTATE are

IK = 0

ELQ(NQ) - Contains the element nodal displacement field w.r.t. element axes.

IK = 1 or 2

ELKT( ) - Contains the element stiffness matrix in global coordinates.

ELQ(NQ) - Contains the thermal loads vector in global coordinates.

---

* Refer to Table A1 for dimensions.

A.2 MLP3K Programming Details

The element nomenclature for lamination-theory element MLP3K is fully described in Ref. 34. In this subsection only the essential modifications to MLP3K will be discussed.

A.2.1 Subroutine MLP3K

All of the previous arguments given in Ref. 34 for MLP3K remain in the same order, but a few more have been added. These additional arguments are required to compute the thermal loads vector, $\underset{\sim}{Q}_T$.

The modified user call statement with arguments is

```
CALL MLP3K(EK,NLAY,XEL,Z,ALPHA,XX,YY,BETA,CMC,MAXL,
    NSIDE,OP,KW,ELQ,EPSO,TI,NPT,HT)
```

where

EK(210) - *

NLAY - Actual number of layers for current problem

XEL(MAXL,6) - Material properties, such that XEL(K,6) describes the Kth layer in order:

E_{11}, E_{22}, ν_{12}, ν_{23}, G_{12}, G_{23} if ØP = 0

E_L, E_T, ν_{LT}, ν_{23}, G_{LT}, G_{23} if ØP = 1

Z(MAXL+1) - Interface coordinates, such that Z(J) = location of Jth interface, including bottom and top surfaces.

ALPHA(MAXL) - Angle (positive counterclockwise) from global X-axis to the principal material 1-axis in degrees. ALPHA(K) = angle for Kth layer. See pg. 9-15 of Ref. 34.

XX(NSIDE) - X,Y coordinates of nodes

YY(NSIDE)

BETA(352) - *

CMC(MAXL,3,3) - *

---

*Element MLP3K returns EK = element stiffness matrix in LTV form. Vector BETA and matrix CMC are returned for stress analysis in MLP3S. These quantities must be saved in temporary storage for later use if stress analysis is to be executed.

MAXL - Maximum number of layers permitted using given dimensions

NSIDE - Number of element sides (=3 for triangle or 4 for quadrilateral)

ØP - Integer option parameter; set ØP = 0(1) if material properties are in tensor (handbook) form.

KW - FORTRAN unit number for on-line printer at user's facility.

ELQ(20) - Thermal loads vector

EPSO(3,NLAY) - Defined in Subsection A.1.6

TI(6,NLAY) - Defined in Subsection A.1.3

NPT - Set NPT = 1 if the thermal loads vector is desired.

HT(16) - Vector of length 16 created internally for later use in MLP3S.

A.2.2 Subroutine MLP3S

All of the previous arguments given in Ref. 34 for MLP3S remain in the same order, but a few more have been added. These additional arguments are required to include the thermal effects in the stresses.

The modified user call statement with arguments is

```
CALL MLP3S(LNUM,EQ,BETA,CMC,MAXL,Z,NLAY,NSIDE,NSP,
    XXP,YYP,XX,YY,XEL,ALPHA,ISDIR,KW,EPSO,TI,NPT,HT)
```

where

LNUM - User's element number

EQ(20) - Element displacement vector

BETA(352) - As defined by MLP3K

CMC(MAXL,3,3) - As defined by MLP3K

MAXL - Maximum number of layers permitted using given dimensions

Z(MAXL+1) - Interface coordinates

NLAY - Actual number of layers

NSIDE - 3 or 4

NSP - Number of points over the XY surface of the element at which stresses are to be calculated ($\leq$ 10). If NSP = 0, stresses will be calculated at the element geometric centroid.

XXP(10), YYP(10) - X,Y coordinates of stress-calculation points (need not be defined if NSP = 0).

XX(NSIDE), YY(NSIDE) - X,Y coordinates of nodes

XEL(MAXL,6) - Material properties

ALPHA(MAXL) - Layer of orientation angles

ISDIR - 0 for stress-strain results in global (XYZ) coordinates or 1 for results in material-axis (123) coordinates

KW - FORTRAN unit number for on-line printer at user's facility

EPSO(3,NLAY) - Defined in Subsection A.1.6

TI(6,NLAY) - Defined in Subsection A.1.3

NPT - Set NPT = 1 if temperature changes occur.

HT(16) - Vector of length 16 used internally. This was created in MLP3K.

A.3 Illustrative Applications of TFQE and MLP3K

The applications of TFQE and MLP3K to the example problems described in Section 5 are discussed in this subsection.

A.3.1 TFQE Generation and Storage

The TFQE mass, stiffness, and $\underset{\sim}{H}^{-1}\underset{\sim}{G}$ (used to compute stresses) matrices are computed first in any problem and are stored in disk datasets. Then during subsequent solutions, these quantities are read in from the datasets and may be reused whenever needed. This procedure saves computing time and storage.

The flow chart for the computer program is shown in Fig. A5, and the MAIN program is listed at the end of this subsection. The numerical computation is done in double precision. As an illustrative example, the dimensions of the various arrays have been set up for a four-layer TFQE. The ply properties in each layer are the same; hence, IPG = 1 and the array XEL is dimensioned only for the first layer (see Subsection A.1.6 for details). The thermal properties are not specified since they are required only by TMPSTR (Subsection A.1.6). The various inputs are clearly marked by comment cards. The integer value KWP is the FORTRAN unit number for the on-line printer at the user's facility. This is accessed by the TFQE (see GNST0200) through the COMMON block PRINT.

Subroutine DKW writes the TFQE properties into disk datasets in the following order:

(a) NL (integer value of the number of layers); WIDTH (element width in single precision); ELK (element stiffness matrix in double precision), and EM (element mass matrix in double precision) using FORTRAN unit number 20.

(b) SZ (layer surface and/or interface coordinates in single precision); SS (material properties of each layer in single precision), and SHIG (single precision array used to compute betas, Eq. 3.12b) using FORTRAN unit number 21.

(c) NH (integer value for length of the H-matrix); LNZ, LNR, IAD (integer arrays for the H-matrix since it is banded), and HMAT (factored H-matrix in double precision) using FORTRAN unit number 22.

It is emphasized that the TFQE is not restricted to a 4-layer laminate and the given geometry. The program listing that follows is an example case.

```
C                                                                       GNST0000
C THIS PROGRAM IS PART OF THE TRACTION FREE QUADRILATERAL ELEMENT (TFQE)GNST0010
C IT WAS WRITTEN BY ALEXANDER HARRIS AND PUBLISHED IN AEROELASTIC AND   GNST0020
C STRUCTURES RESEARCH LABORATORY TECHNICAL REPORT ASRL TR-193-1.        GNST0030
C   COPYRIGHT (C) MASSACHUSETTS INSTITUTE OF TECHNOLOGY FEBRUARY 27, 1979GNST0040
C                                                                       GNST0050
C  TFQE GENERATION AND STORAGE ON DISK DATASETS                         GNST0060
C                                                                       GNST0070
C  NUMERICAL COMPUTATION DONE IN DOUBLE PRECISION                       GNST0080
      IMPLICIT REAL*8(A-H,O-Z)                                          GNST0090
C                                                                       GNST0100
C  DIMENSION STATEMENTS                                                 GNST0110
C  PROP                                                                 GNST0120
      DIMENSION XEL(12,1),ANG(4)                                        GNST0130
C                                                                       GNST0140
C  TFQE                                                                 GNST0150
      DIMENSION LNZ(190),LNR(190),IAD(190)                              GNST0160
      DIMENSION HMAT(17000),HIG(12000),EM(3000),RHO(4)                  GNST0170
      DIMENSION S(13,4),X(4),Y(4),Z(5),ELK(8040)                        GNST0180
      REAL*4 SHIG(24000),SS(13,8),SZ(10),WIDTH                          GNST0190
      COMMON/PRINT/KWP                                                  GNST0200
      EQUIVALENCE (HIG(1),SHIG(1)),(S(1,1),SS(1,1))                     GNST0210
C                                                                       GNST0220
C                                                                       GNST0230
C  ****************************  INPUTS  ******************************GNST0240
C  ELEMENT XY COORDINATES                                               GNST0250
      DATA X/0.0,1.0,1.0,0.0/                                           GNST0260
      DATA Y/0.0,0.0,0.08,0.08/                                         GNST0270
C  LAYER SURFACE AND/OR INTERFACE COORDINATES                           GNST0280
      DATA Z/-0.02,-0.01,0.0,0.01,0.02/                                 GNST0290
C  LAYER ORIENTATION ANGLES                                             GNST0300
      DATA ANG/0.0,90.0,90.0,0.0/                                       GNST0310
C  LAYER DENSITIES (MASS PER UNIT VOLUME)                               GNST0320
      DATA RHO/4*0.056/                                                 GNST0330
C                                                                       GNST0340
C  PRINTER DEVICE CODE                                                  GNST0350
```

```
      KWP=6                                                              GNST0360
C     NUMBER OF LAYERS                                                   GNST0370
      NL=4                                                               GNST0380
C     POINTER FOR PROP                                                   GNST0390
      IPG=1                                                              GNST0400
C     BASIC PLY PROPERTIES                                               GNST0410
      E11=2.0D7                                                          GNST0420
      E22=2.1D6                                                          GNST0430
      GNU=0.21                                                           GNST0440
      GS=0.85D6                                                          GNST0450
      XEL(1,1)= E11                                                      GNST0460
      XEL(2,1)= E22                                                      GNST0470
      XEL(3,1)= E22                                                      GNST0480
      XEL(4,1)= GNU                                                      GNST0490
      XEL(5,1)= GNU                                                      GNST0500
      XEL(6,1)= XEL(4,1)*XEL(3,1)/XEL(1,1)                               GNST0510
      XEL(7,1)= GS                                                       GNST0520
      XEL(8,1)= GS                                                       GNST0530
      XEL(9,1)= GS                                                       GNST0540
C                                                                        GNST0550
C     ************************** END OF INPUTS  ***************************GNST0560
C                                                                        GNST0570
      WIDTH= Y(4)                                                        GNST0580
      NBETA=52*NL-18                                                     GNST0590
      NQ=8*NL+30                                                         GNST0600
      NZ=NL+1                                                            GNST0610
      NK=NQ*(NQ+1)/2                                                     GNST0620
      NHG=NBETA*NQ                                                       GNST0630
C                                                                        GNST0640
      CALL PROP(S,XEL,ANG,NL,IPG)                                        GNST0650
C                                                                        GNST0660
      CALL TPQEK(X,Y,Z,S,HIG,ELK,NL,HMAT,LNZ,LNR,IAD)                    GNST0670
      CALL TPQEM(X,Y,Z,RHO,EM,NL)                                        GNST0680
C                                                                        GNST0690
C     NOTE:  Z, S, AND HIG ARE STORED IN SINGLE PRECISION                GNST0700
C            HMAT,ELK AND EM ARE STORED IN DOUBLE PRECISION              GNST0710
```

```
C          THE H-MATRIX (HMAT) IS IN FACTORED FORM                        GNST0720
C                                                                         GNST0730
C  S.P. CONVERSION                                                        GNST0740
      DO 10 I=1,NZ                                                        GNST0750
   10 SZ(I)=Z(I)                                                          GNST0760
C                                                                         GNST0770
      DO 15 I=1,NL                                                        GNST0780
      DO 15 J=1,13                                                        GNST0790
   15 SS(J,I)=S(J,I)                                                      GNST0800
C                                                                         GNST0810
      DO 20 I=1,NHG                                                       GNST0820
   20 SHIG(I)=HIG(I)                                                      GNST0830
C                                                                         GNST0840
C  H-MATRIX LENGTH                                                        GNST0850
      NH= IAD(NBETA)+NBETA                                                GNST0860
C  WRITE ON DISK DATASETS                                                 GNST0870
      CALL DKW(NL,WIDTH,SS,SZ,EM,ELK,SHIG,HMAT,LNZ,LNR,IAD,NZ,NK,NHG,     GNST0880
     @         NBETA,NH)                                                  GNST0890
      STOP                                                                GNST0900
      END                                                                 GNST0910
```

A.3.2 A Uniaxial-Tension-Loaded Laminated Plate with a Circular Hole

This program can be used to solve both of the examples discussed in Subsections 5.1.5 and 5.1.6. The flow chart for the computer program is shown in Fig. A6, and the MAIN program is listed at the end of this subsection. Most of the numerical computation has been done in double precision.

This example is the tension loaded isotropic plate (Alblas problem) discussed in Subsection 5.1.5. The dimensions of the various arrays have been set up for a 4-layer TFQE and a 1-layer MLP3K.

The program can be used to analyze any axial-tension-loaded laminated plate with a hole. The only restriction is that the problem should be symmetric about the x and y axes (see Fig. 27) and the plate is square; i.e., A = B.

```
C                                                                       HOLE0000
C THIS PROGRAM IS PART OF THE TRACTION FREE QUADRILATERAL ELEMENT (TFQE) HOLE0010
C IT WAS WRITTEN BY ALEXANDER HARRIS AND PUBLISHED IN AEROELASTIC AND   HOLE0020
C STRUCTURES RESEARCH LABORATORY TECHNICAL REPORT ASRL TR-193-1.        HOLE0030
C   COPYRIGHT (C) MASSACHUSETTS INSTITUTE OF TECHNOLOGY FEBRUARY 27,1979HOLE0040
C                                                                       HOLE0050
C  PLATE WITH A HOLE PROBLEM (ISOTROPIC PLATE; ALBLAS PROBLEM)          HOLE0060
C                                                                       HOLE0070
      REAL*8 ELKD,RANGLE,TPI,SGO,ELQ,RE                                 HOLE0080
      INTEGER HLONG                                                     HOLE0090
C                                                                       HOLE0100
C  FEABL                                                              HOLE0110
      DIMENSION RE(70000),IN(70000)                                     HOLE0120
      EQUIVALENCE (RE(1),IN(1))                                         HOLE0130
```

```
C                                                                       HOLE0140
C  TPQE AND MLP3K                                                       HOLE0150
      DIMENSION S(13,4),XS(11),YS(12),ELKD(2000),ELKS(4000)             HOLE0160
      DIMENSION INF(40),ELQ(62),X(5),Y(5),BETA(352),XSP(5),YSP(5)       HOLE0170
      DIMENSION ELK(210),XR(1),XEL(1,6),HI(5),CMC(1,3,3),H(2)           HOLE0180
      DIMENSION TPI(6,1),SGO(4,1),LOWEL(6)                              HOLE0190
      EQUIVALENCE (ELKD(1),ELKS(1))                                     HOLE0200
C                                                                       HOLE0210
      COMMON /IO/ KR, KW, KP, KT1, KT2, KT3                             HOLE0220
      COMMON /SIZE/ NET, NDT                                            HOLE0230
      COMMON /BEGIN/ ICON,IKOUNT,ILNZ,IMASTR,IQ,IK                      HOLE0240
      COMMON /END/ LCON,LKOUNT,LLNZ,LMASTR,LQ,LK                        HOLE0250
      COMMON/PRINT/KWP                                                  HOLE0260
C                                                                       HOLE0270
      DATA PI/3.141593/                                                 HOLE0280
      DATA LOWEL/2,1,10,19,20,11/                                       HOLE0290
C                                                                       HOLE0300
C ********************************* INPUTS ********************************HOLE0310
C  DATA INPUT (CARDS) DEVICE CODE                                       HOLE0320
      KR = 5                                                            HOLE0330
C  PRINTER DEVICE CODE                                                  HOLE0340
      KW = 6                                                            HOLE0350
      KWP= KW                                                           HOLE0360
C  LENGTH OF FEABL DATA VECTOR                                          HOLE0370
      LENGTH=70000                                                      HOLE0380
C  NUMBER OF STRESS POINTS WHERE STRESS PRINTOUT IS DESIRED IN TPQE     HOLE0390
      NSTRS=11                                                          HOLE0400
C  NUMBER OF LAYERS IN MLP3K                                            HOLE0410
      NLM=1                                                             HOLE0420
C  NUMBER OF LAYERS IN TPQE                                             HOLE0430
      NLY=4                                                             HOLE0440
C  INPUT CARD FORMAT                                                    HOLE0450
  500 FORMAT(8E10.3)                                                    HOLE0460
C  INPUT RADIUS OF HOLE AND HALF LENGTH OF SQUARE PLATE SIDE            HOLE0470
      READ (KR,500) RADIUS, A                                           HOLE0480
C  INPUT FOR MLP3K                                                      HOLE0490
```

```
C  PLY ANGLE, PLY THICKNESS, PLY PROPERTIES                              HOLE0500
C  ALSO COMPUTE TOTAL THICKNESS OF PLATE                                 HOLE0510
      HTOT=0.0                                                           HOLE0520
      DO 1 I = 1,NLM                                                     HOLE0530
      READ (KR,500) XR(I), H(I+1), (XEL(I,J), J = 1,6)                   HOLE0540
    1 HTOT=HTOT+H(I+1)                                                   HOLE0550
C  APPLIED AXIAL STRESS                                                  HOLE0560
      SXXI= 1.0E6                                                        HOLE0570
C  POINTER USED BY STRESS. SET ISYM=1 IF SOLUTION IS SYMMETRIC IN Z.     HOLE0580
C  STRESSES ARE PRINTED FROM Z=-H TO Z=0.                                HOLE0590
      ISYM=1                                                             HOLE0600
C ********************************* END OF INPUTS ************************HOLE0610
      NQ=8*NLY+30                                                        HOLE0620
      DO 100 I = 1,NQ                                                    HOLE0630
  100 ELQ(I) = 0.                                                        HOLE0640
      NBETA=52*NLY-18                                                    HOLE0650
      NLY1=NLY+1                                                         HOLE0660
      KLONG=NQ*(NQ+1)/2                                                  HOLE0670
      HLONG=NQ*NBETA                                                     HOLE0680
      NDPEH=NQ                                                           HOLE0690
      KT1=KW                                                             HOLE0700
      B=A                                                                HOLE0710
C  READ NL,WIDTH,ELK FROM DISK                                           HOLE0720
      CALL DKRS(NLY,WIDTH,S,HI,ELKD,ELK,NLY1,KLONG,HLONG,1)              HOLE0730
      REWIND 8                                                           HOLE0740
C  COMPUTE STRESS PRINTOUT LOCATIONS                                     HOLE0750
      XL=PI*RADIUS/32.                                                   HOLE0760
      DI=WIDTH/(NSTRS-1)                                                 HOLE0770
      DO 101 I=1,NSTRS                                                   HOLE0780
      XS(I)= XL                                                          HOLE0790
  101 YS(I)= DI*(I-1)                                                    HOLE0800
      YS(NSTRS+1)= WIDTH                                                 HOLE0810
C MESH SIZING CALCULATIONS & AUXILIARY COUNTERS                          HOLE0820
      R=RADIUS+WIDTH                                                     HOLE0830
      EDGE = PI*R/16.                                                    HOLE0840
      EE = (B-R)/EDGE+0.5                                                HOLE0850
```

```
      NER = EE                                                          HOLE0860
C ADD 1 TO THE NUMBER OF ELEMENTS IN THE RADIAL DIRECTION.              HOLE0870
      NER=NER+1                                                         HOLE0880
      NNR = NER+1                                                       HOLE0890
      NET = 8*NER                                                       HOLE0900
      NNT = 9*(NNR+1)                                                   HOLE0910
      NDPN = 5                                                          HOLE0920
      NDT=NDPN*NNT+2*NLY*18                                             HOLE0930
      NCON = 4*NNR+4*NLY+34                                             HOLE0940
      NDOFT = 9*NDPN                                                    HOLE0950
      NDPE = 4*NDPN                                                     HOLE0960
C  DEFINE THE NUMBER OF DOF PER TFQE WARPING NODE                       HOLE0970
      NDPNH=2*NLY+5                                                     HOLE0980
C INCREASE LENGTH OF ASSEMBLY LIST BY ADDING NO. OF ENTRIES FOR TFQP ELEHOLE0990
      LIST=(NET-8)*(NDPE+1)+8*(1+NDPEH)                                 HOLE1000
      NDOFB = 5*NDPN                                                    HOLE1010
      WRITE (KW,801) ICASE, RADIUS, A, R, NLY                           HOLE1020
  801 FORMAT(15H1INPUT FOR CASE,I4,//,9H RADIUS =,E10.3,/,4H A =,E10.3,/HOLE1030
     &4H R =,E10.3,/,5H NLY=,I2)                                        HOLE1040
      WRITE (KW,802) NLM                                                HOLE1050
  802 FORMAT(15H0PROPERTIES FOR,I3,7H LAYERS,/,1X,10HROTN ANGLE,1X,10HTHHOLE1060
     &ICKNESS ,5X,2HE1,9X,2HE2,8X,4HNU12,7X,4HNU23,7X,4HG 12,7X,4HG 23,/HOLE1070
     &,8(1X,10H----------))                                             HOLE1080
      H(1) = -0.5*HTOT                                                  HOLE1090
      DO 83 I = 1,NLM                                                   HOLE1100
      WRITE (KW,803) XR(I), H(I+1), (XEL(I,J), J = 1,6)                 HOLE1110
   83 H(I+1)= H(I)+H(I+1)                                               HOLE1120
  803 FORMAT(11(1X,E10.3))                                              HOLE1130
      WRITE (KW,804) NER, NET, NNT, NDPN, NDT, NCON, NDOFT,NDOFB,LIST   HOLE1140
  804 FORMAT(21H0MESH SIZING RESULTS:,//,7H   NER=,I6,/,                HOLE1150
     @                                7H   NET=,I6,/,7H   NNT=,I6,/,7H  NDHOLE1160
     &PN=,I6,/,7H   NDT=,I6,/,7H  NCON=,I6,/,7H NDOFT=,I6,/,7H NDOFB=,I6HOLE1170
     &,/,7H  LIST=,I6)                                                  HOLE1180
      CALL DSETUP(LENGTH,NCON,LIST,RE,IN)                               HOLE1190
C ASSEMBLY LIST IN DATA VECTOR; STORE ELEMENT COORDINATES, TYPE AND     HOLE1200
C CENTROID IN FILE 20                                                   HOLE1210
```

```
      REWIND 20                                                          HOLE1220
      LP = IMASTR                                                        HOLE1230
      L = LP+NET                                                         HOLE1240
C  ADD 8 TFQE ELEMENTS ON INSIDE OF HOLE                                 HOLE1250
      DO 220 LNUM=1,8                                                    HOLE1260
      IN(LP)=L                                                           HOLE1270
      LNUMM1=LNUM-1                                                      HOLE1280
      LOWDOF=18*NDPNH                                                    HOLE1290
      DO 218 INODE=1,6                                                   HOLE1300
      NODENO=LOWEL(INODE)+LNUMM1                                         HOLE1310
      IF(INODE .EQ. 4 .OR. INODE .EQ. 5) GO TO 212                       HOLE1320
C NODE HAS 2*NLY+5 DOFS.                                                 HOLE1330
      NUMDF=NDPNH                                                        HOLE1340
      KEND=(NODENO-1)*NDPNH                                              HOLE1350
      GO TO 214                                                          HOLE1360
C NODE HAS 5 DOFS.                                                       HOLE1370
 212  NUMDF=5                                                            HOLE1380
      KEND=LOWDOF+5*(NODENO-19)                                          HOLE1390
 214  DO 216 I=1,NUMDF                                                   HOLE1400
 216  IN(L+I-1)=KEND+I                                                   HOLE1410
      L=L+NUMDF                                                          HOLE1420
 218  CONTINUE                                                           HOLE1430
      LP=LP+1                                                            HOLE1440
 220  CONTINUE                                                           HOLE1450
      NERM1=NER-1                                                        HOLE1460
      DO 5 I=1,NERM1                                                     HOLE1470
      DO 5 J = 1,8                                                       HOLE1480
      T2 = J*PI/16.                                                      HOLE1490
      T1 = T2-PI/16.                                                     HOLE1500
      IF (J .GT. 4) GO TO 2                                              HOLE1510
      IF (J .GT. 4) GO TO 2                                              HOLE1520
      SR1 = (B/COS(T1)-R)/NERM1                                          HOLE1530
      SR2 = (B/COS(T2)-R)/NERM1                                          HOLE1540
      GO TO 3                                                            HOLE1550
    2 SR1 = (B/SIN(T1)-R)/NERM1                                          HOLE1560
      SR2 = (B/SIN(T2)-R)/NERM1                                          HOLE1570
```

AD-A071 910 MASSACHUSETTS INST OF TECH CAMBRIDGE AEROELASTIC AND--ETC F/G 20/11
A MULTILAYER, TRACTION-FREE EDGE, QUADRILATERAL, WARPING ELEMEN--ETC(U)
APR 79 A HARRIS, O ORRINGER, E A WITMER DAAG46-78-C-0015
UNCLASSIFIED ASRL-TR-193-1 AMMRC-TR-79-26 NL

3 OF 3
AD A071910

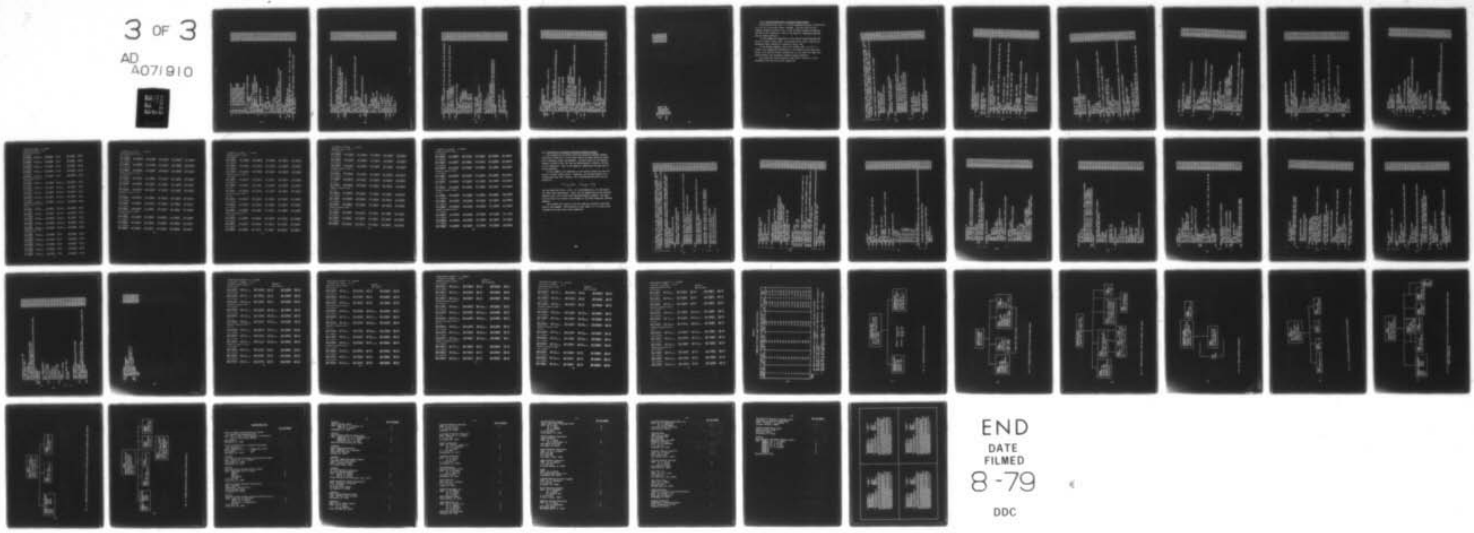

END
DATE FILMED
8-79
DDC

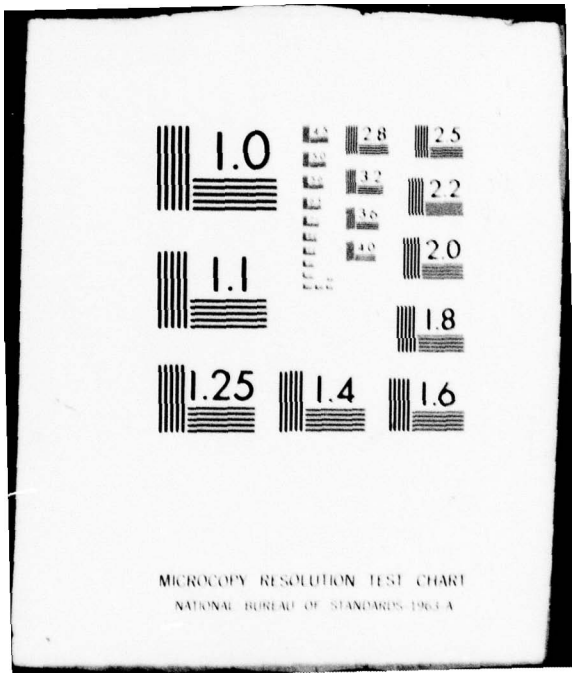
1.0
1.1
1.25
1.4
1.6
2.8
3.2
3.6
2.5
2.2
2.0
1.8
MICROCOPY RESOLUTION TEST CHART
NATIONAL BUREAU OF STANDARDS 1963 A

```
      3 X(1)  =  (R+(I-1)*SR1)*COS(T1)                                  HOLE1580
        X(2)  =  (R+I*SR1)*COS(T1)                                      HOLE1590
        X(3)  =  (R+I*SR2)*COS(T2)                                      HOLE1600
        X(4)  =  (R+(I-1)*SR2)*COS(T2)                                  HOLE1610
        Y(1)  =  (R+(I-1)*SR1)*SIN(T1)                                  HOLE1620
        Y(2)  =  (R+I*SR1)*SIN(T1)                                      HOLE1630
        Y(3)  =  (R+I*SR2)*SIN(T2)                                      HOLE1640
        Y(4)  =  (R+(I-1)*SR2)*SIN(T2)                                  HOLE1650
        IN(LP) = L                                                      HOLE1660
        KH1 =  (I-1)*NDOFT+(J-1)*NDPN+LOWDOF                            HOLE1670
        DO 4 K = 1,NDPN                                                 HOLE1680
        IN(L+K-1) = KH1+K                                               HOLE1690
        IN(L+NDPN+K-1) = KH1+NDOFT+K                                    HOLE1700
        IN(L+2*NDPN+K-1) = KH1+NDOFT+NDPN+K                             HOLE1710
        IN(L+3*NDPN+K-1) = KH1+NDPN+K                                   HOLE1720
      4 CONTINUE                                                        HOLE1730
        LIST = KH1+NDOFT+2*NDPN                                         HOLE1740
        WRITE (20) X, Y                                                 HOLE1750
        LP = LP+1                                                       HOLE1760
      5 L = L+NDPE                                                      HOLE1770
        IF (KT1 .EQ. KW) GO TO 15                                       HOLE1780
        LP = IMASTR                                                     HOLE1790
        L=IN(LP)                                                        HOLE1800
        LIST=IN(LP+1)-1                                                 HOLE1810
        DO 14 I = 1,NET                                                 HOLE1820
        IF(I.EQ.NET) LIST=LMASTR                                        HOLE1830
        WRITE (KW,600) IN(LP), (IN(J), J = L,LIST)                      HOLE1840
    600 FORMAT(1X,26I5/6X,25I5/6X,25I5/6X,25I5)                         HOLE1850
        LP = LP+1                                                       HOLE1860
        L=IN(LP)                                                        HOLE1870
     14   LIST=IN(LP+1)-1                                               HOLE1880
       15 CALL DORK(LENGTH,RE,IN)                                       HOLE1890
      805 FORMAT(18HOSTORAGE ESTIMATE:,//,6H    IK=,I6,/,6H    LK=,I6,/) HOLE1900
        WRITE (KW,805) IK, LK                                           HOLE1910
C ROTATE AND ASSEMBLE THE 8 TFQE ELEMENTS ON INSIDE OF HOLE.            HOLE1920
        DO 152 IEL=1,8                                                  HOLE1930
```

```
      CALL DKRS(NLY,WIDTH,S,HI,ELKD,ELK,NLY1,KLONG,HLONG,1)          HOLE1940
      REWIND 8                                                       HOLE1950
      I=IEL-8                                                        HOLE1960
      RANGLE=-5.625+I*11.25                                          HOLE1970
C ROTATE THE ELKD MATRIX (NOTE: ELKD IS IN D.P.)                     HOLE1980
      CALL ROTATE(ELKD,NLY,ELK,ELQ,INF,RANGLE,1)                     HOLE1990
      CALL DASMLT(IEL,NDPEM,ELKD,ELQ,RE,IN)                          HOLE2000
  152 CONTINUE                                                       HOLE2010
C ASSEMBLY; STOR B-MATRICES IN FILE 21                               HOLE2020
      REWIND 20                                                      HOLE2030
      REWIND 21                                                      HOLE2040
      DO 16 L = 9,NET                                                HOLE2050
      READ (20) X, Y                                                 HOLE2060
      CALL MLP3K(ELK,NLM,XEL,H,XR,X,Y,BETA,CMC,NLM,4,1,KW)           HOLE2070
      WRITE (21) BETA, CMC                                           HOLE2080
      DO 153 I=1,210                                                 HOLE2090
  153 ELKD(I)=ELK(I)                                                 HOLE2100
      CALL DASMLT(L,NDPE,ELKD,ELQ,RE,IN)                             HOLE2110
   16 CONTINUE                                                       HOLE2120
C CONSTRAINTS ALGORITHM                                              HOLE2130
      NNT = 2                                                        HOLE2140
      L = ICON                                                       HOLE2150
      DO 17 I=1,NER                                                  HOLE2160
      KM1 = NDPN*(I-1)*9                                             HOLE2170
      KM1=KM1+LOWDOF                                                 HOLE2180
      K = NDPN*(9*(I-1)+8)                                           HOLE2190
      K=K+LOWDOF                                                     HOLE2200
      DO 17 J = 2,NNT,2                                              HOLE2210
      IN(L) = KM1+J                                                  HOLE2220
      IN(L+1) = K+J-1                                                HOLE2230
C CONSTRAIN THETA X                                                  HOLE2240
      IN(L+2) = KM1+J+2                                              HOLE2250
C CONSTRAIN THETA Y                                                  HOLE2260
      IN(L+3) = K+J+3                                                HOLE2270
   17 L = L+4                                                        HOLE2280
      KEND=2*NLY1                                                    HOLE2290
```

```
      DO 191 I=2,KEND,2                                                 HOLE2300
C CONSTRAIN THE V DISPLACEMENT AT THE FIRST TWO NODES ALONG HORIZONTAL. HOLE2310
      IN(L)=I                                                           HOLE2320
      IN(L+NLY1)= I+9*NDPNH                                             HOLE2330
C CONSTRAIN THE U DISPLACEMENT AT THE FIRST TWO NODES ALONG VERTICAL.   HOLE2340
      IN(L+2*NLY1)= I+8*NDPNH-1                                         HOLE2350
      IN(L+3*NLY1)= I+17*NDPNH-1                                        HOLE2360
 191  L=L+1                                                             HOLE2370
C  CONSTRAIN MIDPLANE W'S AT HOLE                                       HOLE2380
      NN= 3*NLY1                                                        HOLE2390
      IN(L+NN)= NDPNH-1                                                 HOLE2400
      IN(L+NN+1)= 9*NDPNH-1                                             HOLE2410
      IN(L+NN+2)= 10*NDPNH-1                                            HOLE2420
      IN(L+NN+3)= 18*NDPNH-1                                            HOLE2430
      IN(L+NN+4)= NDT-2                                                 HOLE2440
      IN(L+NN+5)= NDT-22                                                HOLE2450
      IN(L+NN+6)= NDT-42                                                HOLE2460
C                                                                       HOLE2470
C  COMPUTE AXIAL LOAD                                                   HOLE2480
      APLD= SXXI*HTOT                                                   HOLE2490
 4949 FORMAT(1H0,' LOAD=',E12.4)                                        HOLE2500
      WRITE(KW,4949) APLD                                               HOLE2510
C                                                                       HOLE2520
      DO 192 I=1,4                                                      HOLE2530
      ANG1=I*PI/16.0                                                    HOLE2540
      ANG0=(I-1)*PI/16.0                                                HOLE2550
      DIST=A*(TAN(ANG1)-TAN(ANG0))                                      HOLE2560
      RE(IQ+NDT+I*5-50)=RE(IQ+NDT+I*5-50)+APLD*DIST/2.0                 HOLE2570
      RE(IQ+NDT+I*5-45)=RE(IQ+NDT+I*5-45)+APLD*DIST/2.0                 HOLE2580
  192 CONTINUE                                                          HOLE2590
C                                                                       HOLE2600
      CALL DBCON(RE,IN)                                                 HOLE2610
      ISGN=1                                                            HOLE2620
      CALL DFACT(ISGN,RE,IN)                                            HOLE2630
      WRITE(KW,850)                                                     HOLE2640
C  SOLVE                                                                HOLE2650
```

```
      KT1=0                                                              HOLE2660
      CALL DSIMUL(EE,RE,IN)                                              HOLE2670
C STRESS CALCULATIONS.                                                   HOLE2680
  850 FORMAT(1H1)                                                        HOLE2690
  860 FORMAT(1H0,'DISPLACEMENTS',/,(10D13.4))                            HOLE2700
      K1=NDPEH+1                                                         HOLE2710
      K2= KLONG/2                                                        HOLE2720
C  READ S,Z,HIG FROM DISK DATA SET                                       HOLE2730
      CALL DKRS(NLY,WIDTH,S,HI,ELKD,RE(IK),NLY1,KLONG,HLONG,2)           HOLE2740
      DO 241 IEL=1,8                                                     HOLE2750
      CALL DXTRAC(IEL,NDPEH,ELQ,RE,IN)                                   HOLE2760
      WRITE(KW,850)                                                      HOLE2770
      WRITE(KW,860)  (ELQ(I),I=1,NDPEH)                                  HOLE2780
      I=IEL-8                                                            HOLE2790
      RANGLE=-5.625+I*11.25                                              HOLE2800
C ROTATE DISPLACEMENTS FOR THIS ELEMENT.                                 HOLE2810
      CALL ROTATE(ELKD,NLY,ELK,ELQ,INF,RANGLE,0)                         HOLE2820
      WRITE(KW,860)  (ELQ(I),I=1,NDPEH)                                  HOLE2830
      CALL STRESS(IEL,XS,YS,HI,NSTRS,NLY,S,ELKD(K1),ELKD(K2),RE(IK),     HOLE2840
     @ ELQ,3,1,TPI,SG0,0,ISYM)                                           HOLE2850
C  PRINT BETAS                                                           HOLE2860
      CALL RITE(NLY,ELKD(K1),ELKD(K2))                                   HOLE2870
  241 CONTINUE                                                           HOLE2880
      WRITE(KW,850)                                                      HOLE2890
C USE ONLY TENSOR PROPERTIES.                                            HOLE2900
      ISDIR = 0                                                          HOLE2910
      NNT = NLY+1                                                        HOLE2920
      REWIND 20                                                          HOLE2930
      REWIND 21                                                          HOLE2940
      DO 25 L = 9,NET                                                    HOLE2950
      READ (20) X, Y                                                     HOLE2960
      READ (21) BETA, CMC                                                HOLE2970
      CALL DXTRAC(L,NDPE,ELQ,RE,IN)                                      HOLE2980
      DO 242 I=1,20                                                      HOLE2990
  242 ELK(I)=ELQ(I)                                                      HOLE3000
      CALL MLP3S(L,ELK,BETA,CMC,NLM,H,NLM,4,0,XSP,YSP,X,Y,XEL,XR,ISDIR,  HOLE3010
```

```
      HOLE3020
      HOLE3030
      HOLE3040
      HOLE3050
      HOLE3060
      HOLE3070
      HOLE3080
      HOLE3090
```

```
     +KW)
  25 CONTINUE
  30 CONTINUE
       REWIND 8
       REWIND 9
1000 CONTINUE
       RETURN
         END
```

A.3.3 Tension-Loaded and/or Thermally-Loaded Coupons

This program can be used to solve the examples discussed in Subsections 5.1.1 to 5.1.4, and other coupon problems. The flow chart for the computer program is shown in Fig. A7 and the MAIN program is listed at the end of this subsection. Most of the numerical computation has been done in double precision.

In this example the dimensions of the various arrays have been set up for a 4-layer $(0/90)_s$ TFQE. The program can be used to analyze any laminated coupon subjected to thermal or axial load.

In the present example, there is no thermal load, i.e. $\Delta T = 0$. However, any temperature distribution in the laminate can be described by Eq. 4.26, and the fitting constants ΔT_i in each layer are input into array TI(6,NL) (see statements COUP0920 through COUP0950).

The stress and strain printout at the first 5 locations is also included at the very end of this subsection.

```
C                                                                       COUP0000
C THIS PROGRAM IS PART OF THE TRACTION FREE QUADRILATERAL ELEMENT (TFQE)COUP0010
C IT WAS WRITTEN BY ALEXANDER HARRIS AND PUBLISHED IN AEROELASTIC AND   COUP0020
C STRUCTURES RESEARCH LABORATORY TECHNICAL REPORT ASRL TR-193-1.        COUP0030
C   COPYRIGHT (C) MASSACHUSETTS INSTITUTE OF TECHNOLOGY FEBRUARY 27,1979COUP0040
C                                                                       COUP0050
C  COUPON TEST PROBLEM (EXAMPLE CASE SET UP FOR 4 LAYERS)               COUP0060
C                                                                       COUP0070
C  DOUBLE PRECISION ARRAYS                                              COUP0080
      REAL*8 REAL,ELK,ELQ                                               COUP0090
      REAL*8 BI,HT,XD,YD                                                COUP0100
      REAL*8 XEL,ANG,SG0,EPS0,TI                                        COUP0110
C                                                                       COUP0120
C  FEABL                                                                COUP0130
      DIMENSION REAL(22000),INTGR(22000)                                COUP0140
      EQUIVALENCE (REAL(1),INTGR(1))                                    COUP0150
C                                                                       COUP0160
C  TFQE                                                                 COUP0170
      DIMENSION LNZ(190),LNR(190),IAD(190)                              COUP0180
      DIMENSION XEL(12,1),ANG(4),SG0(4,4),EPS0(3,4),TI(6,4)             COUP0190
      DIMENSION ELK(2000),ELQ(64)                                       COUP0200
      DIMENSION S(13,4),X(12),Y(12),Z(5)                                COUP0210
      DIMENSION HT(190),BI(400),XD(6),YD(6)                             COUP0220
      EQUIVALENCE (X(1),XD(1)),(Y(1),YD(1))                             COUP0230
C                                                                       COUP0240
C                                                                       COUP0250
C  INITIALIZE ARRAYS                                                    COUP0260
      DATA HT,BI/590*0.0/                                               COUP0270
      DATA XD/6*0.0/                                                    COUP0280
      DATA YD/6*0.0/                                                    COUP0290
      DATA ELQ/64*0.0D0/                                                COUP0300
C                                                                       COUP0310
C  FEABL COMMON BLOCKS                                                  COUP0320
      COMMON/IO/KR,KW,KP,KT1,KT2,KT3                                    COUP0330
      COMMON/SIZE/NET,NDT                                               COUP0340
```

```
      COMMON/BEGIN/ICON,IKOUNT,ILNZ,IMASTR,IQ,IK                        COUP0350
      COMMON/END/LCON,LKOUNT,LLNZ,LMASTR,LQ,LK                          COUP0360
C  TFQE COMMON BLOCK                                                    COUP0370
      COMMON/PRINT/KWP                                                  COUP0380
C                                                                       COUP0390
  600 FORMAT(1H0,20I6)                                                  COUP0400
  610 FORMAT(1H0,' IK=',I5)                                             COUP0410
  620 FORMAT(1H1)                                                       COUP0420
C                                                                       COUP0430
C ********************************** INPUTS ****************************COUP0440
C  LAYERS ORIENTATION ANGLES                                            COUP0450
      DATA ANG/0.0,90.0,90.0,0.0/                                       COUP0460
C  NUMBER OF LAYERS                                                     COUP0470
      NL=4                                                              COUP0480
C  POINTER FOR PROP.  SET IPG=1 IF BASIC PROPERTIES IS THE SAME FOR     COUP0490
C  ALL LAYERS.                                                          COUP0500
      IPG=1                                                             COUP0510
C  NUMBER OF TFQE ELEMENTS ALONG SPAN                                   COUP0520
      NROW=1                                                            COUP0530
C  SET IREFNE=1 IF STRESS DETAIL IS REQUIRED ONLY NEAR THE FREE EDGE    COUP0540
      IREFNE=0                                                          COUP0550
C  PRINTER DEVICE CODE FOR FEABL AND TFQE                               COUP0560
      KW=6                                                              COUP0570
      KWP=KW                                                            COUP0580
C  LENGTH OF FEABL DATA VECTOR                                          COUP0590
      LENGTH=22000                                                      COUP0600
C  NUMBER OF STRESS POINTS WHERE PRINTOUT IS DESIRED                    COUP0610
      NSP=11                                                            COUP0620
C                                                                       COUP0630
C  WANG AND CROSSMAN TEST CASE PROPERTIES                               COUP0640
      XEL(1,1)= 20.0D6                                                  COUP0650
      XEL(2,1)= 2.1D6                                                   COUP0660
      XEL(3,1)= 2.1D6                                                   COUP0670
      XEL(4,1)= 0.21                                                    COUP0680
      XEL(5,1)= 0.21                                                    COUP0690
      XEL(6,1)= XEL(4,1)*XEL(3,1)/XEL(1,1)                              COUP0700
```

```
      XEL(7,1)= 0.85D6                                                    COUP0710
      XEL(8,1)= 0.85D6                                                    COUP0720
      XEL(9,1)= 0.85D6                                                    COUP0730
C  THERMAL PROPERTIES(HIGH STRENGTH GR/EP) IN/IN/DEGREE F                 COUP0740
      XEL(10,1)=-0.21E-6                                                  COUP0750
      XEL(11,1)= 0.16E-4                                                  COUP0760
      XEL(12,1)= 0.16E-4                                                  COUP0770
C                                                                         COUP0780
C  ELEMENT GEOMETRY                                                       COUP0790
      XL=1.0                                                              COUP0800
      XD(2)=XL                                                            COUP0810
      XD(3)=XL                                                            COUP0820
      YD(3)=0.08                                                          COUP0830
      YD(4)=0.08                                                          COUP0840
C  THERMAL POINTER.  SET ITHP=0 IF NO TEMPERATURE CHANGES OCCUR.          COUP0850
      ITHP=0                                                              COUP0860
C  SET IFIX=0 IF COUPON IS FREE TO EXPAND AXIALLY.                        COUP0870
      IFIX=1                                                              COUP0880
C  MECHANICAL LOADING (EPSILON-X = 1)                                     COUP0890
C  NOTE: SET IFIX=1 IF PDU IS NOT ZERO                                    COUP0900
      PDU=XL*NROW                                                         COUP0910
C  THERMAL LOAD (DELTA-T = 0)                                             COUP0920
      DO 10 I=1,NL                                                        COUP0930
      DO 10 J=1,6                                                         COUP0940
   10 TI(J,I)=0.0                                                         COUP0950
C ***********************************END OF INPUTS ************************COUP0960
C                                                                         COUP0970
C  NUMBER OF BOUNDARY NODAL DISPLACEMENTS                                 COUP0980
      NQ=8*NL+30                                                          COUP0990
C  NUMBER OF INDPENDENT BETAS                                             COUP1000
      NBETA=52*NL-18                                                      COUP1010
C                                                                         COUP1020
C  COMPUTE THERMAL LOADS IF ITHP=1                                        COUP1030
      IF(ITHP.NE.1) GO TO 90                                              COUP1040
      CALL THPSTH(XEL,ANG,SG0,EPS0,NL,IPG)                                COUP1050
      CALL TPQET(NEAL,NL,NBETA,ELQ,S,XD,YD,Z,TI,SG0,HT,LNZ,LNR,IAD)       COUP1060
```

```
   90 CONTINUE                                                          COUP1070
C                                                                       COUP1080
C  READ NL,WIDTH,ELK FROM DISK                                          COUP1090
      NZ=NL+1                                                           COUP1100
      NK=NQ*(NQ+1)/2                                                    COUP1110
      NHG=NBETA*NQ                                                      COUP1120
      CALL DKRS(NL,WIDTH,S,Z,ELK,REAL,NZ,NK,NHG,1)                      COUP1130
C                                                                       COUP1140
C  ASSEMBLY AND SOLUTION                                                COUP1150
      KT1=KW                                                            COUP1160
      NET= NROW                                                         COUP1170
      NQR= 4*NL+15                                                      COUP1180
      NDT= (NROW+1)*NQR                                                 COUP1190
      NCON= 3*NROW+4*NL+15                                              COUP1200
      IF(IPIV.EQ.0 .AND. ITMP.EQ.1) NCON=NCON-2*NL-4                    COUP1210
      MASTRL= NROW*(NQ+1)                                               COUP1220
      NDPE= 2*NL+5                                                      COUP1230
      CALL DSETUP(LENGTH,NCON,MASTRL,REAL,INTGR)                        COUP1240
C                                                                       COUP1250
C  MASTER ASSEMBLY LIST                                                 COUP1260
      IM= IMASTR                                                        COUP1270
      DO 100 IROW=1,NROW                                                COUP1280
      LP1= IMASTR+NET+(IROW-1)*NQ                                       COUP1290
      INTGR(IM)= LP1                                                    COUP1300
      DO 110 I=1,NDPE                                                   COUP1310
      INTGR(LP1+I-1)= (IROW-1)*NQR+I                                    COUP1320
      INTGR(LP1+I-1+NDPE)= IROW*NQR+I                                   COUP1330
      INTGR(LP1+I-1+2*NDPE)= IROW*NQR+I+NDPE                            COUP1340
      INTGR(LP1+I+9+3*NDPE)= (IROW-1)*NQR+I+NDPE                        COUP1350
  110 CONTINUE                                                          COUP1360
      DO 120 I=1,2                                                      COUP1370
      DO 120 J=1,5                                                      COUP1380
  120 INTGR(LP1+3*NDPE+(I-1)*5+J-1)= (IROW-I+1)*NQR+J+2*NDPE            COUP1390
  100 IM=IM+1                                                           COUP1400
      WRITE(KW,600)  (INTGR(I),I=IMASTR,LMASTR)                         COUP1410
C                                                                       COUP1420
```

```
      CALL DORK(LENGTH,REAL,INTGR)                                      COUP1430
      WRITE(KW,610)  IK                                                 COUP1440
      KT1=0                                                             COUP1450
C  ASSEMBLY ELEMENT STIFFNESS MATRIX                                    COUP1460
      DO 200 IROW=1,NROW                                                COUP1470
  200 CALL DASHLT(IROW,NQ,ELK,ELQ,REAL,INTGR)                           COUP1480
C  INPUT CONSTRAINTS                                                    COUP1490
      NN=0                                                              COUP1500
      NL1=NL+1                                                          COUP1510
      DO 300 II=1,2                                                     COUP1520
      ISP=(II-1)*(NDT-NQR)                                              COUP1530
      DO 305 I=1,2                                                      COUP1540
      NN=NN+1                                                           COUP1550
      NS=ISP+I*NDPE-1                                                   COUP1560
      INTGR(NN)= NS                                                     COUP1570
      REAL(NS+IQ-1)= 0.0                                                COUP1580
      IF(IFIX.EQ.0 .AND. ITMP.EQ.1 .AND. II.EQ.2) GO TO 305             COUP1590
      DO 310 J=1,NL1                                                    COUP1600
      NS=(J-1)*2+(I-1)*NDPE+1+ISP                                       COUP1610
      NN=NN+1                                                           COUP1620
      REAL(NS+IQ-1)= 0.0                                                COUP1630
      IF(II.EQ.2)  REAL(NS+IQ-1)= PDU                                   COUP1640
  310 INTGR(NN)= NS                                                     COUP1650
  305 CONTINUE                                                          COUP1660
      IF(IFIX.EQ.0 .AND. ITMP.EQ.1 .AND. II.EQ.2) GO TO 300             COUP1670
      DO 320 I=1,2                                                      COUP1680
      NN=NN+1                                                           COUP1690
      NS=2*NDPE+(I-1)*4+1+ISP                                           COUP1700
      REAL(NS+IQ-1)= 0.0                                                COUP1710
      IF(II.EQ.2 .AND. I.EQ.1)  REAL(NS+IQ-1)= PDU                      COUP1720
      INTGR(NN)= NS                                                     COUP1730
  320 CONTINUE                                                          COUP1740
  300 CONTINUE                                                          COUP1750
      N1= NROW+1                                                        COUP1760
      DO 330 I=1,N1                                                     COUP1770
      DO 330 J=1,3                                                      COUP1780
```

```
      NN=NN+1                                                          COUP1790
      NS= I*NQR-4+J                                                    COUP1800
      REAL(NS+IQ-1)= 0.0                                               COUP1810
  330 INTGR(NN)= NS                                                    COUP1820
C                                                                      COUP1830
C  APPLY CONSTRAINTS                                                   COUP1840
      CALL DBCON(REAL,INTGR)                                           COUP1850
C  FACTOR GLOBAL K                                                     COUP1860
      ISGN=1                                                           COUP1870
      CALL DFACT(ISGN,REAL,INTGR)                                      COUP1880
C  SOLVE                                                               COUP1890
      CALL DSIMUL(ENERGY,REAL,INTGR)                                   COUP1900
C  READ Z,S,HIG FROM DISK                                              COUP1910
      CALL DKRS(NL,WIDTH,S,Z,ELK,REAL(IK),NZ,NK,NHG,2)                 COUP1920
C  DETERMINE STRESSES                                                  COUP1930
      DI= WIDTH/(NSP-1)                                                COUP1940
      IF(IRFNE.EQ.1) DI=DI/10.0                                        COUP1950
      XMP= XL/2.0                                                      COUP1960
      DO 510 I=1,NSP                                                   COUP1970
      X(I)=XMP                                                         COUP1980
  510 Y(I)= (I-1)*DI                                                   COUP1990
      Y(NSP+1)= WIDTH                                                  COUP2000
C                                                                      COUP2010
      DO 520 IROW=1,NROW                                               COUP2020
      WRITE(KW,620)                                                    COUP2030
C                                                                      COUP2040
C                                                                      COUP2050
      LNUM=IROW                                                        COUP2060
      CALL DXTRAC(LNUM,NQ,ELQ,REAL,INTGR)                              COUP2070
      CALL STRESS(LNUM,X,Y,Z,NSP,NL,S,HT,BI,REAL(IK),ELQ,5,1,TI,SG0,   COUP2080
     @ ITMP,0)                                                         COUP2090
  520 CONTINUE                                                         COUP2100
  550 CONTINUE                                                         COUP2110
      STOP                                                             COUP2120
      END                                                              COUP2130
```

STRESS OUTPUT FOR ELEMENT 1 AT 11 LOCATIONS

AT LOCATION 1 X= 0.500E+00 Y= 0.0

STRESSES AND STRAINS IN LAYER 1

AT Z=-0.200E-01

SXX= 0.200E+08 SYY= 0.0 SZZ=-0.223E-01 TXY= 0.0 TXZ= 0.166E-05 TYZ= 0.0
EXX= 0.100E+01 EYY=-0.210E+00 EZZ=-0.210E+00 EXY= 0.0 EXZ= 0.195E-11 EYZ= 0.0

AT Z=-0.175E-01

SXX= 0.200E+08 SYY= 0.0 SZZ= 0.546E+04 TXY= 0.0 TXZ= 0.145E+00 TYZ= 0.0
EXX= 0.100E+01 EYY=-0.211E+00 EZZ=-0.207E+00 EXY= 0.0 EXZ= 0.170E-06 EYZ= 0.0

AT Z=-0.150E-01

SXX= 0.200E+08 SYY= 0.0 SZZ= 0.281E+05 TXY= 0.0 TXZ= 0.270E+00 TYZ= 0.0
EXX= 0.100E+01 EYY=-0.213E+00 EZZ=-0.197E+00 EXY= 0.0 EXZ= 0.318E-06 EYZ= 0.0

AT Z=-0.125E-01

SXX= 0.200E+08 SYY= 0.0 SZZ= 0.772E+05 TXY= 0.0 TXZ= 0.393E+00 TYZ= 0.0
EXX= 0.100E+01 EYY=-0.218E+00 EZZ=-0.173E+00 EXY= 0.0 EXZ= 0.462E-06 EYZ= 0.0

AT Z=-0.100E-01

SXX= 0.200E+08 SYY= 0.0 SZZ= 0.162E+06 TXY= 0.0 TXZ= 0.490E+00 TYZ= 0.0
EXX= 0.100E+01 EYY=-0.227E+00 EZZ=-0.133E+00 EXY= 0.0 EXZ= 0.576E-06 EYZ= 0.0

STRESSES AND STRAINS IN LAYER 2

AT Z=-0.100E-01

SXX= 0.213E+07 SYY= 0.0 SZZ= 0.162E+06 TXY= 0.0 TXZ= 0.488E+00 TYZ= 0.0
EXX= 0.100E+01 EYY=-0.241E-01 EZZ=-0.136E+00 EXY= 0.753E-07 EXZ= 0.575E-06 EYZ= 0.0

AT Z=-0.750E-02

SXX= 0.215E+07 SYY= 0.0 SZZ= 0.236E+06 TXY= 0.0 TXZ= 0.444E+00 TYZ= 0.0
EXX= 0.100E+01 EYY=-0.251E-01 EZZ=-0.102E+00 EXY= 0.780E-07 EXZ= 0.522E-06 EYZ= 0.0

AT Z=-0.500E-02

SXX= 0.215E+07 SYY= 0.0 SZZ= 0.262E+06 TXY= 0.0 TXZ= 0.403E+00 TYZ= 0.0
EXX= 0.100E+01 EYY=-0.254E-01 EZZ=-0.906E-01 EXY= 0.789E-07 EXZ= 0.474E-06 EYZ= 0.0

AT Z=-0.250E-02

SXX= 0.215E+07 SYY= 0.0 SZZ= 0.261E+06 TXY= 0.0 TXZ= 0.355E+00 TYZ= 0.0
EXX= 0.100E+01 EYY=-0.254E-01 EZZ=-0.910E-01 EXY= 0.789E-07 EXZ= 0.418E-06 EYZ= 0.0

AT Z= 0.373E-08

SXX= 0.215E+07 SYY= 0.0 SZZ= 0.256E+06 TXY= 0.0 TXZ= 0.295E+00 TYZ= 0.0
EXX= 0.100E+01 EYY=-0.253E-01 EZZ=-0.933E-01 EXY= 0.787E-07 EXZ= 0.347E-06 EYZ= 0.0

STRESSES AND STRAINS IN LAYER 3

AT Z= 0.0

SXX= 0.215E+07 SYY= 0.0 SZZ= 0.256E+06 TXY= 0.0 TXZ= 0.294E+00 TYZ= 0.0
EXX= 0.100E+01 EYY=-0.253E-01 EZZ=-0.933E-01 EXY= 0.787E-07 EXZ= 0.346E-06 EYZ= 0.0

AT Z= 0.250E-02

SXX= 0.215E+07 SYY= 0.0 SZZ= 0.261E+06 TXY= 0.0 TXZ= 0.165E+00 TYZ= 0.0
EXX= 0.100E+01 EYY=-0.254E-01 EZZ=-0.910E-01 EXY= 0.789E-07 EXZ= 0.194E-06 EYZ= 0.0

AT Z= 0.500E-02

SXX= 0.215E+07 SYY= 0.0 SZZ= 0.262E+06 TXY= 0.0 TXZ= 0.481E-01 TYZ= 0.0
EXX= 0.100E+01 EYY=-0.254E-01 EZZ=-0.906E-01 EXY= 0.789E-07 EXZ= 0.566E-07 EYZ= 0.0

AT Z= 0.750E-02

SXX= 0.215E+07 SYY= 0.0 SZZ= 0.236E+06 TXY= 0.0 TXZ=-0.620E-01 TYZ= 0.0
EXX= 0.100E+01 EYY=-0.251E-01 EZZ=-0.102E+00 EXY= 0.780E-07 EXZ=-0.729E-07 EYZ= 0.0

AT Z= 0.100E-01

SXX= 0.213E+07 SYY= 0.0 SZZ= 0.162E+06 TXY= 0.0 TXZ=-0.175E+00 TYZ= 0.0
EXX= 0.100E+01 EYY=-0.241E-01 EZZ=-0.136E+00 EXY= 0.753E-07 EXZ=-0.206E-06 EYZ= 0.0

STRESSES AND STRAINS IN LAYER 4

AT Z= 0.100E-01

SXX= 0.200E+08 SYY= 0.0 SZZ= 0.162E+06 TXY= 0.0 TXZ=-0.176E+00 TYZ= 0.0
EXX= 0.100E+01 EYY=-0.227E+00 EZZ=-0.133E+00 EXY= 0.0 EXZ=-0.207E-06 EYZ= 0.0

AT Z= 0.125E-01

SXX= 0.200E+08 SYY= 0.0 SZZ= 0.772E+05 TXY= 0.0 TXZ=-0.154E+00 TYZ= 0.0
EXX= 0.100E+01 EYY=-0.218E+00 EZZ=-0.173E+00 EXY= 0.0 EXZ=-0.182E-06 EYZ= 0.0

AT Z= 0.150E-01

SXX= 0.200E+08 SYY= 0.0 SZZ= 0.281E+05 TXY= 0.0 TXZ=-0.114E+00 TYZ= 0.0
EXX= 0.100E+01 EYY=-0.213E+00 EZZ=-0.197E+00 EXY= 0.0 EXZ=-0.135E-06 EYZ= 0.0

AT Z= 0.175E-01

SXX= 0.200E+08 SYY= 0.0 SZZ= 0.546E+04 TXY= 0.0 TXZ=-0.465E-01 TYZ= 0.0
EXX= 0.100E+01 EYY=-0.211E+00 EZZ=-0.207E+00 EXY= 0.0 EXZ=-0.782E-07 EYZ= 0.0

AT Z= 0.200E-01

SXX= 0.200E+08 SYY= 0.0 SZZ=-0.438E-01 TXY= 0.0 TXZ=-0.490E-03 TYZ= 0.0
EXX= 0.100E+01 EYY=-0.210E+00 EZZ=-0.210E+00 EXY= 0.0 EXZ=-0.576E-09 EYZ= 0.0

AT LOCATION 2 X= 0.530E+00 Y= 0.800E-02

STRESSES AND STRAINS IN LAYER 1

AT Z=-0.200E-01

SXX= 0.200E+08 SYY= 0.359E+05 SZZ= 0.108E-02 TXY= 0.135E+01 TXZ= 0.661E-03 TYZ= 0.110E-01
EXX= 0.100E+01 EYY=-0.193E+00 EZZ=-0.214E+00 EXY= 0.124E-05 EXZ= 0.777E-09 EYZ= 0.130E-07

AT Z=-0.150E-01

SXX= 0.200E+08 SYY= 0.869E+05 SZZ= 0.847E+04 TXY= 0.154E+00 TXZ= 0.264E+00 TYZ=-0.627E+05
EXX= 0.100E+01 EYY=-0.170E+00 EZZ=-0.215E+00 EXY= 0.181E-06 EXZ= 0.310E-06 EYZ=-0.737E-01

AT Z=-0.100E-01

SXX= 0.200E+08 SYY= 0.138E+06 SZZ= 0.283E+05 TXY=-0.744E+00 TXZ= 0.465E+00 TYZ=-0.167E+06
EXX= 0.100E+01 EYY=-0.148E+00 EZZ=-0.211E+00 EXY=-0.876E-06 EXZ= 0.547E-06 EYZ=-0.197E+00

STRESSES AND STRAINS IN LAYER 2

AT Z=-0.100E-01

SXX= 0.210E+07 SYY=-0.215E+06 SZZ= 0.283E+05 TXY=-0.920E-03 TXZ= 0.465E+00 TYZ=-0.167E+06
EXX= 0.100E+01 EYY=-0.331E-01 EZZ=-0.194E+00 EXY= 0.106E-06 EXZ= 0.547E-06 EYZ=-0.197E+00

AT Z=-0.500E-02

SXX= 0.211E+07 SYY=-0.869E+05 SZZ= 0.481E+05 TXY= 0.533E-01 TXZ= 0.414E+00 TYZ=-0.279E+05
EXX= 0.100E+01 EYY=-0.270E-01 EZZ=-0.187E+00 EXY= 0.149E-06 EXZ= 0.487E-06 EYZ=-0.329E-01

AT Z= 0.0

SXX= 0.211E+07 SYY= 0.412E+05 SZZ= 0.566E+05 TXY= 0.130E+00 TXZ= 0.311E+00 TYZ= 0.167E+06
EXX= 0.100E+01 EYY=-0.207E-01 EZZ=-0.185E+00 EXY= 0.191E-06 EXZ= 0.366E-06 EYZ= 0.196E-06

STRESSES AND STRAINS IN LAYER 3

AT Z= 0.0

SXX= 0.211E+07 SYY= 0.412E+05 SZZ= 0.566E+05 TXY= 0.261E+00 TXZ= 0.311E+00 TYZ= 0.994E-01
EXX= 0.100E+01 EYY=-0.207E-01 EZZ=-0.185E+00 EXY= 0.371E-06 EXZ= 0.366E-06 EYZ= 0.117E-06

AT Z= 0.500E-02

SXX= 0.211E+07 SYY=-0.869E+05 SZZ= 0.481E+05 TXY= 0.216E+00 TXZ= 0.166E+00 TYZ= 0.279E+05
EXX= 0.100E+01 EYY=-0.270E-01 EZZ=-0.187E+00 EXY= 0.341E-06 EXZ= 0.195E-06 EYZ= 0.329E-01

AT Z= 0.100E-01

SXX= 0.210E+07 SYY=-0.215E+06 SZZ= 0.283E+05 TXY= 0.172E+00 TXZ= 0.710E-01 TYZ= 0.167E+06
EXX= 0.100E+01 EYY=-0.331E-01 EZZ=-0.194E+00 EXY= 0.310E-06 EXZ= 0.835E-07 EYZ= 0.197E+00

STRESSES AND STRAINS IN LAYER 4

AT Z= 0.100E-01

SXX= 0.200E+08 SYY= 0.138E+06 SZZ= 0.283E+05 TXY=-0.206E+00 TXZ= 0.714E-01 TYZ= 0.167E+06
EXX= 0.100E+01 EYY=-0.148E+00 EZZ=-0.211E+00 EXY=-0.242E-06 EXZ= 0.840E-07 EYZ= 0.197E+00

AT Z= 0.150E-01

SXX= 0.200E+08 SYY= 0.869E+05 SZZ= 0.847E+04 TXY= 0.692E+00 TXZ= 0.490E-02 TYZ= 0.627E+05
EXX= 0.100E+01 EYY=-0.170E+00 EZZ=-0.215E+00 EXY= 0.814E-06 EXZ= 0.576E-08 EYZ= 0.737E-01

AT Z= 0.230E-01

SXX= 0.200E+08 SYY= 0.359E+05 SZZ= 0.323E-02 TXY= 0.159E+01 TXZ=-0.416E-03 TYZ=-0.175E-01
EXX= 0.100E+01 EYY=-0.193E+00 EZZ=-0.214E+00 EXY= 0.187E-05 EXZ=-0.490E-09 EYZ=-0.206E-07

AT LOCATION 3 X= 0.900E+00 Y= 0.160E-01

STRESSES AND STRAINS IN LAYER 1

AT Z=-0.200E-01

SXX= 0.203E+08	SYY= 0.122E+06	SZZ= 0.126E-02	TXY= 0.202E+01	TXZ= 0.447E-03	TYZ= 0.729E-01
EXX= 0.100E+01	EYY=-0.152E+00	EZZ=-0.222E+00	EXY= 0.338E-05	EXZ= 0.526E-09	EYZ= 0.853E-07

AT Z=-0.150E-01

SXX= 0.203E+08	SYY= 0.216E+06	SZZ=-0.211E+04	TXY= 0.120E+00	TXZ= 0.266E+00	TYZ=-0.651E+05
EXX= 0.100E+01	EYY=-0.107E+00	EZZ=-0.233E+00	EXY= 0.142E-06	EXZ= 0.312E-06	EYZ=-0.766E-01

AT Z=-0.100E-01

SXX= 0.201E+08	SYY= 0.310E+06	SZZ=-0.260E+05	TXY=-0.177E+01	TXZ= 0.497E+00	TYZ=-0.138E+06
EXX= 0.100E+01	EYY=-0.602E-01	EZZ=-0.254E+00	EXY=-0.209E-05	EXZ= 0.584E-06	EYZ=-0.163E+00

STRESSES AND STRAINS IN LAYER 2

AT Z=-0.100E-01

SXX= 0.20ME+07	SYY=-0.480E+06	SZZ=-0.260E+05	TXY= 0.143E-01	TXZ= 0.496E+00	TYZ=-0.138E+06
EXX= 0.100E+01	EYY=-0.456E-01	EZZ=-0.216E+00	EXY= 0.168E-06	EXZ= 0.584E-06	EYZ=-0.163E+00

AT Z=-0.500E-02

SXX= 0.209E+07	SYY=-0.216E+06	SZZ=-0.397E+05	TXY= 0.112E+00	TXZ= 0.385E+00	TYZ=-0.460E+05
EXX= 0.103E+01	EYY=-0.323E-01	EZZ=-0.225E+00	EXY= 0.237E-06	EXZ= 0.453E-06	EYZ=-0.542E-01

AT Z= 0.0

SXX= 0.209E+07	SYY= 0.481E+05	SZZ=-0.317E+05	TXY= 0.207E+00	TXZ= 0.235E+00	TYZ= 0.940E-01
EXX= 0.103E+01	EYY=-0.193E-01	EZZ=-0.225E+00	EXY= 0.304E-06	EXZ= 0.276E-06	EYZ= 0.111E-06

STRESSES AND STRAINS IN LAYER 3

AT Z= 0.0

SXX= 0.209E+07	SYY= 0.481E+05	SZZ=-0.317E+05	TXY= 0.324E+00	TXZ= 0.233E+00	TYZ= 0.154E+00
EXX= 0.103E+01	EYY=-0.193E-01	EZZ=-0.225E+00	EXY= 0.441E-06	EXZ= 0.275E-06	EYZ= 0.181E-06

AT Z= 0.500E-02

SXX= 0.209E+07	SYY=-0.216E+06	SZZ=-0.397E+05	TXY= 0.249E+00	TXZ= 0.174E+00	TYZ= 0.460E+05
EXX= 0.103E+01	EYY=-0.323E-01	EZZ=-0.225E+00	EXY= 0.398E-06	EXZ= 0.204E-06	EYZ= 0.542E-01

AT Z= 0.100E-01

SXX= 0.208E+07	SYY=-0.480E+06	SZZ=-0.260E+05	TXY= 0.170E+00	TXZ= 0.153E+00	TYZ= 0.138E+06
EXX= 0.103E+01	EYY=-0.456E-01	EZZ=-0.216E+00	EXY= 0.351E-06	EXZ= 0.180E-06	EYZ= 0.163E+00

STRESSES AND STRAINS IN LAYER 4

AT Z= 0.100E-01

SXX= 0.201E+08	SYY= 0.310E+06	SZZ=-0.260E+05	TXY=-0.574E+00	TXZ= 0.153E+00	TYZ= 0.138E+06
EXX= 0.100E+01	EYY=-0.602E-01	EZZ=-0.254E+00	EXY=-0.675E-06	EXZ= 0.180E-06	EYZ= 0.163E+00

AT Z= 0.150E-01

SXX= 0.200E+08	SYY= 0.216E+06	SZZ=-0.211E+04	TXY= 0.132E+01	TXZ= 0.596E-01	TYZ= 0.651E+05
EXX= 0.100E+01	EYY=-0.107E+00	EZZ=-0.233E+00	EXY= 0.155E-05	EXZ= 0.701E-07	EYZ= 0.766E-01

AT Z= 0.200E-01

SXX= 0.200E+08	SYY= 0.122E+06	SZZ= 0.366E-12	TXY= 0.322E+01	TXZ=-0.447E-03	TYZ=-0.753E-01
EXX= 0.100E+01	EYY=-0.152E+00	EZZ=-0.222E+00	EXY= 0.379E-05	EXZ=-0.526E-09	EYZ=-0.886E-07

AT LOCATION 4 X= 0.500E+00 Y= 0.240E-01

STRESSES AND STRAINS IN LAYER 1

AT Z=-0.200E-01

SXX= 0.203E+08	SYY= 0.219E+06	SZZ= 0.173E-02	TXY= 0.305E+01	TXZ= 0.495E-03	TYZ=-0.279E-01
EXX= 0.100E+01	EYY=-0.106E+00	EZZ=-0.232E+00	EXY= 0.359E-05	EXZ= 0.582E-09	EYZ=-0.328E-07

AT Z=-0.150E-01

SXX= 0.201E+08	SYY= 0.296E+06	SZZ=-0.629E+04	TXY= 0.662E-01	TXZ= 0.247E+00	TYZ=-0.446E+05
EXX= 0.100E+01	EYY=-0.689E-01	EZZ=-0.243E+00	EXY= 0.779E-07	EXZ= 0.290E-06	EYZ=-0.525E-01

AT Z=-0.100E-01

SXX= 0.201E+08	SYY= 0.373E+06	SZZ=-0.341E+05	TXY=-0.291E+01	TXZ= 0.497E+00	TYZ=-0.631E+05
EXX= 0.100E+01	EYY=-0.296E-01	EZZ=-0.264E+00	EXY=-0.343E-05	EXZ= 0.584E-06	EYZ=-0.742E-01

STRESSES AND STRAINS IN LAYER 2

AT Z=-0.100E-01

SXX= 0.208E+07	SYY=-0.566E+06	SZZ=-0.341E+05	TXY= 0.147E+00	TXZ= 0.496E+00	TYZ=-0.631E+05
EXX= 0.100E+01	EYY=-0.498E-01	EZZ=-0.218E+00	EXY= 0.339E-06	EXZ= 0.583E-06	EYZ=-0.742E-01

AT Z=-0.500E-02

SXX= 0.208E+07	SYY=-0.296E+06	SZZ=-0.540E+05	TXY= 0.260E+00	TXZ= 0.307E+00	TYZ=-0.487E+05
EXX= 0.100E+01	EYY=-0.361E-01	EZZ=-0.231E+00	EXY= 0.424E-06	EXZ= 0.361E-06	EYZ=-0.573E-01

AT Z= 0.0

SXX= 0.209E+07	SYY=-0.272E+05	SZZ=-0.523E+05	TXY= 0.369E+00	TXZ= 0.975E-01	TYZ= 0.397E-01
EXX= 0.100E+01	EYY=-0.227E-01	EZZ=-0.233E+00	EXY= 0.506E-06	EXZ= 0.115E-06	EYZ= 0.467E-07

STRESSES AND STRAINS IN LAYER 3

AT Z= 0.0

SXX= 0.209E+07	SYY=-0.272E+05	SZZ=-0.523E+05	TXY= 0.226E+00	TXZ= 0.965E-01	TYZ=-0.395E-01
EXX= 0.100E+01	EYY=-0.227E-01	EZZ=-0.233E+00	EXY= 0.338E-06	EXZ= 0.113E-06	EYZ=-0.464E-07

AT Z= 0.500E-02

SXX= 0.209E+07	SYY=-0.296E+06	SZZ=-0.540E+05	TXY= 0.144E+00	TXZ= 0.118E+00	TYZ= 0.487E+05
EXX= 0.100E+01	EYY=-0.361E-01	EZZ=-0.231E+00	EXY= 0.288E-06	EXZ= 0.139E-06	EYZ= 0.573E-01

AT Z= 0.100E-01

SXX= 0.208E+07	SYY=-0.566E+06	SZZ=-0.341E+05	TXY= 0.580E-01	TXZ= 0.161E+00	TYZ= 0.631E+05
EXX= 0.100E+01	EYY=-0.498E-01	EZZ=-0.218E+00	EXY= 0.233E-06	EXZ= 0.189E-06	EYZ= 0.742E-01

STRESSES AND STRAINS IN LAYER 4

AT Z= 0.100E-01

SXX= 0.201E+08	SYY= 0.373E+06	SZZ=-0.341E+05	TXY=-0.135E+01	TXZ= 0.159E+00	TYZ= 0.631E+05
EXX= 0.100E+01	EYY=-0.296E-01	EZZ=-0.264E+00	EXY=-0.124E-05	EXZ= 0.188E-06	EYZ= 0.742E-01

AT Z= 0.150E-01

SXX= 0.201E+08	SYY= 0.296E+06	SZZ=-0.629E+04	TXY= 0.192E+01	TXZ= 0.810E-01	TYZ= 0.446E+05
EXX= 0.100E+01	EYY=-0.689E-01	EZZ=-0.243E+00	EXY= 0.226E-05	EXZ= 0.953E-07	EYZ= 0.525E-01

AT Z= 0.200E-01

SXX= 0.203E+08	SYY= 0.219E+06	SZZ=-0.108E-01	TXY= 0.490E+01	TXZ=-0.648E-05	TYZ= 0.333E-01
EXX= 0.100E+01	EYY=-0.106E+00	EZZ=-0.232E+00	EXY= 0.576E-05	EXZ=-0.762E-11	EYZ= 0.391E-07

AT LOCATION 5 X= 0.500E+00 Y= 0.320E-01

STRESSES AND STRAINS IN LAYER 1

AT Z=-0.200E-01

SXX= 0.201E+08	SYY= 0.298E+06	SZZ=-0.177E-01	TXY= 0.421E+01	TXZ= 0.202E-03	TYZ= 0.297E-01
EXX= 0.100E+01	EYY=-0.689E-01	EZZ=-0.240E+00	EXY= 0.496E-05	EXZ= 0.237E-09	EYZ= 0.349E-07

AT Z=-0.150E-01

SXX= 0.201E+08	SYY= 0.324E+06	SZZ=-0.633E+04	TXY= 0.621E-01	TXZ= 0.192E+00	TYZ=-0.226E+05
EXX= 0.100E+01	EYY=-0.557E-01	EZZ=-0.246E+00	EXY= 0.731E-07	EXZ= 0.225E-06	EYZ=-0.266E-01

AT Z=-0.100E-01

SXX= 0.201E+08	SYY= 0.351E+06	SZZ=-0.217E+05	TXY=-0.408E+01	TXZ= 0.420E+00	TYZ=-0.132E+05
EXX= 0.100E+01	EYY=-0.416E-01	EZZ=-0.256E+00	EXY=-0.480E-05	EXZ= 0.494E-06	EYZ=-0.155E-01

STRESSES AND STRAINS IN LAYER 2

AT Z=-0.100E-01

SXX= 0.209E+07	SYY=-0.506E+06	SZZ=-0.217E+05	TXY= 0.395E+00	TXZ= 0.420E+00	TYZ=-0.132E+05
EXX= 0.100E+01	EYY=-0.470E-01	EZZ=-0.213E+00	EXY= 0.620E-06	EXZ= 0.494E-06	EYZ=-0.155E-01

AT Z=-0.500E-02

SXX= 0.209E+07	SYY=-0.324E+06	SZZ=-0.350E+05	TXY= 0.490E+00	TXZ= 0.179E+00	TYZ=-0.388E+05
EXX= 0.100E+01	EYY=-0.377E-01	EZZ=-0.222E+00	EXY= 0.701E-06	EXZ= 0.211E-06	EYZ=-0.456E-01

AT Z= 0.0

SXX= 0.209E+07	SYY=-0.142E+06	SZZ=-0.393E+05	TXY= 0.585E+00	TXZ=-0.672E-01	TYZ= 0.322E-02
EXX= 0.100E+01	EYY=-0.286E-01	EZZ=-0.226E+00	EXY= 0.781E-06	EXZ=-0.791E-07	EYZ= 0.379E-08

STRESSES AND STRAINS IN LAYER 3

AT Z= 0.0

SXX= 0.209E+07	SYY=-0.142E+06	SZZ=-0.393E+05	TXY=-0.286E-01	TXZ=-0.682E-01	TYZ=-0.169E+00
EXX= 0.100E+01	EYY=-0.286E-01	EZZ=-0.226E+00	EXY= 0.988E-07	EXZ=-0.802E-07	EYZ=-0.199E-06

AT Z= 0.500E-02

SXX= 0.209E+07	SYY=-0.324E+06	SZZ=-0.350E+05	TXY=-0.902E-01	TXZ= 0.348E-01	TYZ= 0.388E+05
EXX= 0.100E+01	EYY=-0.377E-01	EZZ=-0.222E+00	EXY= 0.176E-07	EXZ= 0.409E-07	EYZ= 0.456E-01

AT Z= 0.100E-01

SXX= 0.208E+07	SYY=-0.506E+06	SZZ=-0.217E+05	TXY=-0.154E+00	TXZ= 0.144E+00	TYZ= 0.132E+05
EXX= 0.100E+01	EYY=-0.470E-01	EZZ=-0.213E+00	EXY=-0.256E-07	EXZ= 0.169E-06	EYZ= 0.155E-01

STRESSES AND STRAINS IN LAYER 4

AT Z= 0.100E-01

SXX= 0.201E+08	SYY= 0.351E+06	SZZ=-0.217E+05	TXY=-0.166E+01	TXZ= 0.143E+00	TYZ= 0.132E+05
EXX= 0.100E+01	EYY=-0.416E-01	EZZ=-0.256E+00	EXY=-0.195E-05	EXZ= 0.168E-06	EYZ= 0.155E-01

AT Z= 0.150E-01

SXX= 0.201E+08	SYY= 0.324E+06	SZZ=-0.633E+04	TXY= 0.248E+01	TXZ= 0.902E-01	TYZ= 0.226E+05
EXX= 0.100E+01	EYY=-0.557E-01	EZZ=-0.246E+00	EXY= 0.292E-05	EXZ= 0.106E-06	EYZ= 0.266E-01

AT Z= 0.200E-01

SXX= 0.201E+08	SYY= 0.298E+06	SZZ=-0.214E-01	TXY= 0.662E+01	TXZ=-0.308E-03	TYZ=-0.201E-01
EXX= 0.100E+01	EYY=-0.689E-01	EZZ=-0.240E+00	EXY= 0.779E-05	EXZ=-0.363E-09	EYZ=-0.236E-07

A.4 Illustration of Transient Structural Response Analysis

This program can be used to solve the transient response example discussed in Subsection 5.2 and other similar problems involving plates with a different layup and geometry. The flow chart for the computer program is shown in Fig. A8, and the MAIN program is listed at the end of this subsection. Most of the numerical computation has been done in single precision.

In this example, the dimensions of the various arrays have been set up for a 4-layer $(0/90)_s$ plate. Presently, the forcing function is a concentrated step load. However, for a distributed load which can be written as

$$F(x,y,t) = \bar{F}(x,y)\ T(t)$$

one can substitute $\bar{F}(x,y)$ in Eq. 3.11 (see Subsection A.1.4) and obtain the nodal force distribution. Then, one can compute the forcing function portion of Eq. 3.41 at each time step and proceed as before. The equations of motion are solved by the Newmark $\beta = \frac{1}{4}$ finite-difference timewise operator.

The stresses and strains at the free edge are printed at each time step in this example. The printouts at time steps 2, 4, 6, 8 and 10 are included at the very end of this subsection.

```
C                                                                       TRNS0000
C THIS PROGRAM IS PART OF THE TRACTION FREE QUADRILATERAL ELEMENT (TFQE) TRNS0010
C IT WAS WRITTEN BY ALEXANDER HARRIS AND PUBLISHED IN AEROELASTIC AND   TRNS0020
C STRUCTURES RESEARCH LABORATORY TECHNICAL REPORT ASRL TR-193-1.        TRNS0030
C   COPYRIGHT (C) MASSACHUSETTS INSTITUTE OF TECHNOLOGY FEBRUARY 27,1979TRNS0040
C                                                                       TRNS0050
C  TRANSIENT RESPONSE ANALYSIS (0/90 SYMMETRIC COUPON UNDER STEP LOAD)  TRNS0060
C  TIMEWISE FINITE DIFFERENCE PROCEDURE USING THE NEWMARK BETA EQUAL    TRNS0070
C  ONE-QUARTER METHOD                                                   TRNS0080
      REAL*8 ELK,ELM                                                    TRNS0090
      REAL*8 HT,BI,ELQD,TPI,SG0                                         TRNS0100
C  FEABL                                                              TRNS0110
      DIMENSION REAL(30000),INTGR(30000)                                TRNS0120
      EQUIVALENCE (REAL(1),INTGR(1))                                    TRNS0130
C                                                                       TRNS0140
C  TFQE                                                               TRNS0150
      DIMENSION ELK(2000),ELKS1(3400),ELQ(64),S(13,4),X(12),Y(13),Z(5)  TRNS0160
      DIMENSION TPI(6,1),SG0(4,1)                                       TRNS0170
      DIMENSION HT(200),BI(400),HIG(12000),ELQD(64)                     TRNS0180
      DIMENSION ELQ0(64),ELQ1(64)                                       TRNS0190
      DIMENSION ELM(2000),ELMS1(2000)                                   TRNS0200
C                                                                       TRNS0210
C  MLP3K                                                              TRNS0220
      DIMENSION ELKS2(300),XEL(4,6),ALPHA(4),BETA(352),CMC(4,3,3)       TRNS0230
      DIMENSION ELMS2(300),DENS(4)                                      TRNS0240
      DIMENSION XXP(1),YYP(1)                                           TRNS0250
C                                                                       TRNS0260
      EQUIVALENCE (ELM(1),ELMS1(1)),(ELM(1701),ELMS2(1))                TRNS0270
      EQUIVALENCE (ELK(1),ELKS1(1)),(ELK(1701),ELKS2(1))                TRNS0280
C                                                                       TRNS0290
C  XY COORDINATES OF THE MLP3K ELEMENTS                                 TRNS0300
      DATA X/0.0,1.0,1.0,9*0.0/                                         TRNS0310
      DATA Y/0.0,0.0,2*0.46,9*0.0/                                      TRNS0320
      DATA Z/-0.02,-0.01,0.0,0.01,0.02/                                 TRNS0330
C                                                                       TRNS0340
```

```
C  LAYER DENSITIES FOR HLP3M                                          TRNS0350
      DATA DENS/4*0.056/                                              TRNS0360
C  INITIALIZE                                                         TRNS0370
      DATA ELQ/64*0.0/                                                TRNS0380
C  PLY ANGLES                                                         TRNS0390
      DATA ALPHA/0.0,90.0,90.0,0.0/                                   TRNS0400
C                                                                     TRNS0410
C  FEABL COMMON BLOCKS                                                TRNS0420
      COMMON/IO/KR,KW,KP,KT1,KT2,KT3                                  TRNS0430
      COMMON/SIZE/NET,NDT                                             TRNS0440
      COMMON/BEGIN/ICON,IKOUNT,ILNZ,IMASTR,IQ,IK                      TRNS0450
      COMMON/END/LCON,LKOUNT,LLNZ,LMASTR,LQ,LK                        TRNS0460
C  COMMON BLOCKS USED BY SUBROUTINE FORCE                             TRNS0470
      COMMON/PNTRS/IQ0,LQ0,IQ1,LQ1,NDPE                               TRNS0480
      COMMON/DYN/TSTEP2                                               TRNS0490
C  PRINTER DEVICE CODE USED BY TPQE                                   TRNS0500
      COMMON/PRINT/KWP                                                TRNS0510
C                                                                     TRNS0520
C  PRINT FORMATS                                                      TRNS0530
  600 FORMAT(1HC,20I6)                                                TRNS0540
  610 FORMAT(1H0,' IQ=',I5)                                           TRNS0550
  615 FORMAT(1H0,' LK=',I5)                                           TRNS0560
  620 FORMAT(1H1)                                                     TRNS0570
  625 FORMAT(1H0,'TIME INCREMENT',E12.4,5X,'NSTEP',I4,5X,'NFH=',I3,   TRNS0580
     @ 5X,'FORCE=',E12.4)                                             TRNS0590
  630 FORMAT(1H0,'ELEMENT',I2,1X,'NODAL DISPLACEMENTS',/,(10E13.4))   TRNS0600
  635 FORMAT(1H0,' LQ1=',I5)                                          TRNS0610
  640 FORMAT(1H0,'TIME STEP',I3,/,1X,'TRANSVERSE DISPLACEMENTS',3E15.4) TRNS0620
  645 FORMAT(1HC,'PRINT-OUT NODES',3I5)                               TRNS0630
C                                                                     TRNS0640
C ********************************** INPUTS ****************************TRNS0650
C  NUMBER OF ELEMENT ROWS ALONG THE SPAN                              TRNS0660
      NROW=9                                                          TRNS0670
C  TIME INCREMENT                                                     TRNS0680
      TSTEP=0.2E-3                                                    TRNS0690
C  NUMBER OF TIME STEPS                                               TRNS0700
```

```
      NSTEP=10                                                          TRNS0710
C     STEP LOAD                                                         TRNS0720
      FORCE=-100.0                                                      TRNS0730
C     NUMBER OF TIME STEPS FORCE ACTS ON THE PLATE                      TRNS0740
      NFM=10                                                            TRNS0750
C     PRINTER DEVICE CODE                                               TRNS0760
      KW=6                                                              TRNS0770
      KWP=KW                                                            TRNS0780
C     LENGTH OF FEABL DATA VECTOR                                       TRNS0790
      LENGTH=30000                                                      TRNS0800
C     NUMBER OF STRESS POINTS WHERE PRINTOUT IS DESIRED.                TRNS0810
      NSP=12                                                            TRNS0820
C     NUMBER OF LAYERS                                                  TRNS0830
      NL=4                                                              TRNS0840
C     MATERIAL PROPERTIES FOR MLP3K                                     TRNS0850
      E11= 20.0E6                                                       TRNS0860
      E22= 2.10E6                                                       TRNS0870
      GS= 0.85E6                                                        TRNS0880
    5 GNU=0.21                                                          TRNS0890
      XEL(1,1)= E11                                                     TRNS0900
      XEL(1,2)= E22                                                     TRNS0910
      XEL(1,3)= GNU                                                     TRNS0920
      XEL(1,4)= GNU                                                     TRNS0930
      XEL(1,5)= GS                                                      TRNS0940
      XEL(1,6)= GS                                                      TRNS0950
      DO 10 I=2,NL                                                      TRNS0960
      DO 10 J=1,6                                                       TRNS0970
   10 XEL(I,J)= XEL(1,J)                                                TRNS0980
C     ********************************* END OF INPUTS ********************TRNS0990
C                                                                       TRNS1000
      WRITE(KW,625) TSTEP,NSTEP,NFM,FORCE                               TRNS1010
C                                                                       TRNS1020
C     READ NL,WIDTH,S,Z,ELK,HIG FROM DISK                               TRNS1030
      NQ=8*NL+30                                                        TRNS1040
      NBETA=52*NL-18                                                    TRNS1050
      NZ=NL+1                                                           TRNS1060
```

```
      NK=NQ*(NQ+1)/2                                                    TRNS1070
      NHG=NBETA*NQ                                                      TRNS1080
      CALL DKRD(NL,WIDTH,S,Z,ELM,ELK,HIG,NZ,NK,NHG,1)                   TRNS1090
      CALL DKRD(NL,WIDTH,S,Z,ELM,ELK,HIG,NZ,NK,NHG,2)                   TRNS1100
      DO 15 I=1,NK                                                      TRNS1110
      ELMS1(I)=ELM(I)                                                   TRNS1120
   15 ELKS1(I)=ELK(I)                                                   TRNS1130
C  COMPUTE MLP3K STIFFNESS AND MASS MATRICES                           TRNS1140
      CALL MLP3K(ELKS2,NL,XEL,Z,ALPHA,X,Y,BETA,CHC,NL,4,0,6)            TRNS1150
      CALL MLP3M(ELMS2,NL,X,Y,Z,DENS,1,4)                               TRNS1160
C                                                                       TRNS1170
C  ASSEMBLY AND SOLUTION                                               TRNS1180
      KT1=KW                                                            TRNS1190
      ISYM=1                                                            TRNS1200
      NET= NROW*3                                                       TRNS1210
      NQR= 4*NL+25                                                      TRNS1220
      NDT= (NROW+1)*NQR                                                 TRNS1230
      NCON= NROW*3+NL*8+57                                              TRNS1240
      IF(ISYM.EQ.1) NCON=NCON-NROW+1                                    TRNS1250
      MASTRL= NROW*(NQ+43)                                              TRNS1260
      NDPE= 2*NL+5                                                      TRNS1270
      CALL SETUP(LENGTH,NCON,MASTRL,REAL,INTGR)                         TRNS1280
C                                                                       TRNS1290
      IM= IMASTR                                                        TRNS1300
      DO 100 IROW=1,NROW                                                TRNS1310
      LP1= IMASTR+NET+(IROW-1)*(NQ+40)                                  TRNS1320
      LP2= LP1+NQ                                                       TRNS1330
      LP3= LP2+20                                                       TRNS1340
      INTGR(IM)= LP1                                                    TRNS1350
      INTGR(IM+1)= LP2                                                  TRNS1360
      INTGR(IM+2)= LP3                                                  TRNS1370
      DO 110 I=1,NDPE                                                   TRNS1380
      INTGR(LP1+I-1)= (IROW-1)*NQR+I                                    TRNS1390
      INTGR(LP1+I-1+NDPE)= IROW*NQR+I                                   TRNS1400
      INTGR(LP1+I-1+2*NDPE)= IROW*NQR+I+NDPE                            TRNS1410
      INTGR(LP1+I+9+3*NDPE)= (IROW-1)*NQR+I+NDPE                        TRNS1420
```

```
  110 CONTINUE                                                          TRNS1430
      DO 120 I=1,2                                                      TRNS1440
      DO 120 J=1,5                                                      TRNS1450
      INTGR(LP1+3*NDPE+(I-1)*5+J-1)= (IROW-I+1)*NQR+J+2*NDPE            TRNS1460
      INTGR(LP2+(I-1)*5+J-1)= (IROW+I-2)*NQR+2*NDPE+J                   TRNS1470
      INTGR(LP2+(I-1)*5+J+9)= (IROW-I+1)*NQR+J+2*NDPE+5                 TRNS1480
      INTGR(LP3+(I-1)*5+J-1)= (IROW+I-2)*NQR+2*NDPE+J+5                 TRNS1490
  120 INTGR(LP3+(I-1)*5+J+9)= (IROW-I+1)*NQR+J+2*NDPE+10                TRNS1500
  100 IM=IM+3                                                           TRNS1510
C                                                                       TRNS1520
      WRITE(6,600) (INTGR(I),I=IMASTR,LMASTR)                           TRNS1530
      CALL ORK(LENGTH,REAL,INTGR)                                       TRNS1540
      IQ0=LK+1                                                          TRNS1550
      LQ0=LK+NDT                                                        TRNS1560
      IQ1=LQ0+1                                                         TRNS1570
      LQ1=LQ0+NDT                                                       TRNS1580
C                                                                       TRNS1590
      WRITE(KW,610) IQ                                                  TRNS1600
      WRITE(KW,635) LQ1                                                 TRNS1610
      KT1=0                                                             TRNS1620
C  INPUT CONSTRAINTS                                                    TRNS1630
      NN=0                                                              TRNS1640
      NL1=NL+1                                                          TRNS1650
      DO 300 II=1,2                                                     TRNS1660
      ISP=(II-1)*(NDT-NQR)                                              TRNS1670
      DO 310 I=1,2                                                      TRNS1680
      NS=ISP+I*NDPE-1                                                   TRNS1690
      NN=NN+2                                                           TRNS1700
      INTGR(NN-1)=NS-1                                                  TRNS1710
      INTGR(NN)=NS+1                                                    TRNS1720
      NN=NN+1                                                           TRNS1730
      INTGR(NN)= NS                                                     TRNS1740
      DO 310 J=1,NL1                                                    TRNS1750
      NS=(J-1)*2+(I-1)*NDPE+1+ISP                                       TRNS1760
      NN=NN+1                                                           TRNS1770
      INTGR(NN)=NS+1                                                    TRNS1780
```

```
      NN=NN+1                                                                  TRNS1790
  310 INTGR(NN)= NS                                                            TRNS1800
      DO 320 I=1,3                                                             TRNS1810
      NS= 2*NDPE+ISF+(I-1)*5                                                   TRNS1820
      IF(I.NE.3) NN=NN+2                                                       TRNS1830
      IF(I.NE.3) INTGR(NN-1)= NS+2                                             TRNS1840
      IF(I.NE.3) INTGR(NN)= NS+4                                               TRNS1850
      DO 320 J=1,3                                                             TRNS1860
      IF(I.EQ.3 .AND. J.EQ.2) GO TO 320                                        TRNS1870
      NN=NN+1                                                                  TRNS1880
      NS=(I-1)*5+2*NDPE+(J-1)*2+1+ISF                                          TRNS1890
      INTGR(NN)= NS                                                            TRNS1900
  320 CONTINUE                                                                 TRNS1910
  300 CONTINUE                                                                 TRNS1920
      N1= NROW+1                                                               TRNS1930
      DO 330 I=1,N1                                                            TRNS1940
      DO 330 J=1,3                                                             TRNS1950
      IF(ISYM.EQ.1 .AND. I.NE.1 .AND. I.NE.N1 .AND. J.EQ.2) GO TO 330          TRNS1960
      NN=NN+1                                                                  TRNS1970
      NS= I*NQR-4+J                                                            TRNS1980
      INTGR(NN)= NS                                                            TRNS1990
  330 CONTINUE                                                                 TRNS2000
C                                                                              TRNS2010
C                                                                              TRNS2020
C  PREPARE STIFFNESS MATRICES FOR ASSEMBLY                                     TRNS2030
      TSTEP2=TSTEP**2                                                          TRNS2040
      DO 340 I=1,210                                                           TRNS2050
  340 ELKS2(I)=ELKS2(I)*0.25*TSTEP2                                            TRNS2060
      DO 350 I=1,NK                                                            TRNS2070
  350 ELKS1(I)=ELKS1(I)*0.25*TSTEP2                                            TRNS2080
C  ASSEMBLY                                                                    TRNS2090
      DO 360 IROW=1,NROW                                                       TRNS2100
      DO 360 I=1,2                                                             TRNS2110
      LNUM=IROW*3+I-2                                                          TRNS2120
      CALL ASMLTV(LNUM,20,ELMS2,ELQ,REAL,INTGR)                                TRNS2130
  360 CALL ASMLTV(LNUM,20,ELKS2,ELQ,REAL,INTGR)                                TRNS2140
```

```
C                                                                       TRNS2150
      DO 370 IROW=1,NROW                                                TRNS2160
      LNUM=IROW*3-2                                                     TRNS2170
      CALL ASMLTV(LNUM,NQ,ELMS1,ELQ,REAL,INTGR)                         TRNS2180
  370 CALL ASMLTV(LNUM,NQ,ELKS1,ELQ,REAL,INTGR)                         TRNS2190
C                                                                       TRNS2200
C                                                                       TRNS2210
      CALL BCON(REAL,INTGR)                                             TRNS2220
      ISGN=1                                                            TRNS2230
      CALL FACT(ISGN,REAL,INTGR)                                        TRNS2240
      IF(TSTEP.EQ.0.0) STOP                                             TRNS2250
C                                                                       TRNS2260
C  STARTING PROCEDURE (N=1)                                             TRNS2270
      FINC=0.25*TSTEP2*FORCE                                            TRNS2280
C  DOF AT WHICH STEP LOAD ACTS                                          TRNS2290
      NQF=(NROW/2+1)*NQR-3+IQ                                           TRNS2300
C  INTERMEDIATE NODES AT WHICH DISPLACEMENTS ARE PRINTED                TRNS2310
      NQA=(NROW/4+1)*NQR-3+IQ                                           TRNS2320
      NQB=(3*NROW/4+1)*NQR-3+IQ                                         TRNS2330
C                                                                       TRNS2340
      WRITE(KW,645) NQA,NQF,NQB                                         TRNS2350
C  FORCE INPUT FOR THE STARTING PROCEDURE                               TRNS2360
      REAL(NQF)=REAL(NQF)+FINC*2.0                                      TRNS2370
C                                                                       TRNS2380
      CALL SIMULQ(ENERGY,REAL,INTGR)                                    TRNS2390
      KT1=6                                                             TRNS2400
      ISTEP=1                                                           TRNS2410
      WRITE(KW,640) ISTEP,REAL(NQA),REAL(NQF),REAL(NQB)                 TRNS2420
C  STORE DISPLACEMENTS                                                  TRNS2430
      DO 400 I=1,NDT                                                    TRNS2440
      REAL(IQ0+I-1)=0.0                                                 TRNS2450
      REAL(IQ1+I-1)=REAL(IQ+I-1)                                        TRNS2460
  400 REAL(IQ+I-1)=0.0                                                  TRNS2470
C                                                                       TRNS2480
C  INTEGRATE IN TIME USING NEWMARK BETA EQUAL 1/4 METHOD                TRNS2490
      DO 1000 ISTEP=2,NSTEP                                             TRNS2500
```

```
C                                                                       TRNS2510
C  PRINT CONTROL                                                        TRNS2520
      ITFQE=1                                                           TRNS2530
C     IF(4*(ISTEP/4).EQ.ISTEP) ITFQE=1                                  TRNS2540
C                                                                       TRNS2550
C  COMPUTE R.H.S.                                                       TRNS2560
C  TFQE                                                                 TRNS2570
      NDPE=NQ                                                           TRNS2580
      DO 410 IROW=1,NROW                                                TRNS2590
      LNUM=IROW*3-2                                                     TRNS2600
  410 CALL FORCES(LNUM,ELMS1,ELKS1,ELQ,ELQ0,ELQ1,REAL,INTGR)            TRNS2610
C                                                                       TRNS2620
C  MLP3K                                                                TRNS2630
      NDPE=20                                                           TRNS2640
      DO 420 IROW=1,NROW                                                TRNS2650
      DO 420 I=1,2                                                      TRNS2660
      LNUM=IROW*3+I-2                                                   TRNS2670
  420 CALL FORCES(LNUM,ELMS2,ELKS2,ELQ,ELQ0,ELQ1,REAL,INTGR)            TRNS2680
C                                                                       TRNS2690
C  APPLIED LOAD                                                         TRNS2700
      IF(ISTEP.LE.NFM) REAL(NQF)=REAL(NQF)+FINC                         TRNS2710
      IF(ISTEP.LE.NFM+1) REAL(NQF)=REAL(NQF)-FINC*1.75                  TRNS2720
      IF(ISTEP.LE.NFM+2) REAL(NQF)=REAL(NQF)+FINC                       TRNS2730
C                                                                       TRNS2740
C  ZERO OUT CONSTRAINTS                                                 TRNS2750
      DO 430 I=1,NCON                                                   TRNS2760
      NN=INTGR(I)                                                       TRNS2770
      IF(NN.GT.0) REAL(IQ+NN-1)=0.0                                     TRNS2780
  430 CONTINUE                                                          TRNS2790
C                                                                       TRNS2800
C  SOLVE                                                                TRNS2810
      CALL SIMULQ(ENERGY,REAL,INTGR)                                    TRNS2820
      WRITE(KW,640) ISTEP,REAL(NQA),REAL(NQF),REAL(NQB)                 TRNS2830
C  DETERMINE STRESSES                                                   TRNS2840
      NN=NROW/2+1                                                       TRNS2850
      IF(ITFQE.EQ.0) GO TO 550                                          TRNS2860
```

```
      IF(ITFQE.EQ.1) GO TO 505                                          TRNS2870
      DO 500 IROW=1,NN,2                                                TRNS2880
      DO 500 I=1,2                                                      TRNS2890
      LNUM= 3*IROW+I-2                                                  TRNS2900
      CALL XTRACT(LNUM,20,ELQ,REAL,INTGR)                               TRNS2910
      WRITE(KW,630) LNUM,(ELQ(I),I=1,20)                                TRNS2920
      CALL MLP3S(LNUM,ELQ,BETA,CMC,NL,Z,NL,4,0,XXP,YYP,X,Y,XEL,         TRNS2930
     @ ALPHA,0,6)                                                       TRNS2940
  500 CONTINUE                                                          TRNS2950
  505 CONTINUE                                                          TRNS2960
C                                                                       TRNS2970
      DI= WIDTH/(NSP-4)                                                 TRNS2980
      XMP= X(2)/2.0                                                     TRNS2990
      DO 510 I=5,NSP                                                    TRNS3000
  510 Y(I)= (I-4)*DI                                                    TRNS3010
      Y(1)=0.0                                                          TRNS3020
      Y(2)=DI/4.0                                                       TRNS3030
      Y(3)=DI/2.0                                                       TRNS3040
      Y(4)=DI*0.75                                                      TRNS3050
      DO 515 I=1,NSP                                                    TRNS3060
  515 X(I)=XMP                                                          TRNS3070
      NSP=1                                                             TRNS3080
      Y(NSP+1)= WIDTH                                                   TRNS3090
C                                                                       TRNS3100
C     DO 520 IROW=1,NN,2                                                TRNS3110
      IROW=NN                                                           TRNS3120
C                                                                       TRNS3130
C                                                                       TRNS3140
      LNUM=IROW*3-2                                                     TRNS3150
      CALL XTRACT(LNUM,NQ,ELQ,REAL,INTGR)                               TRNS3160
      DO 521 I=1,NQ                                                     TRNS3170
  521 ELQD(I)=ELQ(I)                                                    TRNS3180
      WRITE(KW,630) LNUM,(ELQ(I),I=1,NQ)                                TRNS3190
      CALL STRESS(LNUM,X,Y,Z,NSP,NL,S,HT,BI,HIG,ELQD,3,1,TPI,SGO,0,0)   TRNS3200
      WRITE(KW,620)                                                     TRNS3210
  520 CONTINUE                                                          TRNS3220
```

```
  550 CONTINUE                                                          TRNS3230
C  UPDATE DISPLACEMENTS                                                TRNS3240
      DO 560 I=1,NDT                                                    TRNS3250
      REAL(IQ0+I-1)=REAL(IQ1+I-1)                                       TRNS3260
      REAL(IQ1+I-1)=REAL(IQ+I-1)                                        TRNS3270
  560 REAL(IQ+I-1)=0.0                                                  TRNS3280
 1000 CONTINUE                                                          TRNS3290
      STOP                                                              TRNS3300
      END                                                               TRNS3310
```

STRESS OUTPUT FOR ELEMENT 13 AT 1 LOCATIONS

AT LOCATION 1 X= 0.500E+00 Y= 0.0

TIME STEP = 2

TIME = 0.04 E-02

STRESSES AND STRAINS IN LAYER 1

AT Z=-0.200E-01

SXX=-0.820E+01	SYY= 0.0	SZZ= 0.308E-06	TXY= 0.0	TXZ=-0.288E-03	TYZ= 0.0
EXX=-0.210E-04	EYY= 0.441E-05	EZZ= 0.441E-05	EXY= 0.0	EXZ=-0.338E-09	EYZ= 0.0

AT Z=-0.150E-01

SXX=-0.966E+03	SYY= 0.0	SZZ= 0.893E+01	TXY= 0.0	TXZ= 0.234E+03	TYZ= 0.0
EXX=-0.484E-04	EYY= 0.925E-05	EZZ= 0.144E-04	EXY= 0.0	EXZ= 0.276E-03	EYZ= 0.0

AT Z=-0.100E-01

SXX=-0.151E+04	SYY= 0.0	SZZ= 0.191E+02	TXY= 0.0	TXZ= 0.284E+03	TYZ= 0.0
EXX=-0.758E-04	EYY= 0.140E-04	EZZ= 0.250E-04	EXY= 0.0	EXZ= 0.334E-03	EYZ= 0.0

STRESSES AND STRAINS IN LAYER 2

AT Z=-0.100E-01

SXX=-0.155E+03	SYY= 0.0	SZZ= 0.191E+02	TXY= 0.0	TXZ= 0.284E+03	TYZ= 0.0
EXX=-0.758E-04	EYY= 0.143E-05	EZZ= 0.246E-04	EXY=-0.458E-11	EXZ= 0.334E-03	EYZ= 0.0

AT Z=-0.500E-02

SXX=-0.766E+02	SYY= 0.0	SZZ= 0.141E+02	TXY= 0.0	TXZ= 0.307E+03	TYZ= 0.0
EXX=-0.379E-04	EYY= 0.656E-06	EZZ= 0.144E-04	EXY=-0.212E-11	EXZ= 0.361E-03	EYZ= 0.0

AT Z= 0.0

SXX= 0.166E-02	SYY= 0.0	SZZ= 0.210E-02	TXY= 0.0	TXZ= 0.313E+03	TYZ= 0.0
EXX= 0.578E-09	EYY=-0.394E-10	EZZ= 0.834E-09	EXY= 0.116E-15	EXZ= 0.368E-03	EYZ= 0.0

STRESSES AND STRAINS IN LAYER 3

AT Z= 0.0

SXX= 0.134E-02	SYY= 0.0	SZZ= 0.209E-02	TXY= 0.0	TXZ= 0.313E+03	TYZ= 0.0
EXX= 0.424E-09	EYY=-0.358E-10	EZZ= 0.855E-09	EXY= 0.105E-15	EXZ= 0.368E-03	EYZ= 0.0

AT Z= 0.500E-02

SXX= 0.766E+02	SYY= 0.0	SZZ=-0.141E+02	TXY= 0.0	TXZ= 0.307E+03	TYZ= 0.0
EXX= 0.379E-04	EYY=-0.656E-06	EZZ=-0.144E-04	EXY= 0.212E-11	EXZ= 0.361E-03	EYZ= 0.0

AT Z= 0.100E-01

SXX= 0.155E+03	SYY= 0.0	SZZ=-0.191E+02	TXY= 0.0	TXZ= 0.284E+03	TYZ= 0.0
EXX= 0.758E-04	EYY=-0.143E-05	EZZ=-0.246E-04	EXY= 0.458E-11	EXZ= 0.334E-03	EYZ= 0.0

STRESSES AND STRAINS IN LAYER 4

AT Z= 0.100E-01

SXX= 0.151E+04	SYY= 0.0	SZZ=-0.191E+02	TXY= 0.0	TXZ= 0.284E+03	TYZ= 0.0
EXX= 0.758E-04	EYY=-0.140E-04	EZZ=-0.250E-04	EXY= 0.0	EXZ= 0.334E-03	EYZ= 0.0

AT Z= 0.150E-01

SXX= 0.966E+03	SYY= 0.0	SZZ=-0.892E+01	TXY= 0.0	TXZ= 0.234E+03	TYZ= 0.0
EXX= 0.484E-04	EYY=-0.925E-05	EZZ=-0.144E-04	EXY= 0.0	EXZ= 0.276E-03	EYZ= 0.0

AT Z= 0.200E-01

SXX= 0.820E+03	SYY= 0.0	SZZ=-0.113E-05	TXY= 0.0	TXZ=-0.322E-03	TYZ= 0.0
EXX= 0.210E-04	EYY=-0.441E-05	EZZ=-0.441E-05	EXY= 0.0	EXZ=-0.379E-09	EYZ= 0.0

STRESS OUTPUT FOR ELEMENT 13 AT 1 LOCATIONS

AT LOCATION 1 X= 0.500E+00 Y= 0.0

TIME STEP = 4

STRESSES AND STRAINS IN LAYER 1

TIME = 0.08 E-02

AT Z=-0.200E-01

SXX=-0.258E+05	SYY= 0.0	SZZ=-0.152E-03	TXY= 0.0	TXZ= 0.268E-03	TYZ= 0.0
EXX=-0.129E-02	EYY= 0.271E-03	EZZ= 0.271E-03	EXY= 0.0	EXZ= 0.316E-09	EYZ= 0.0

AT Z=-0.150E-01

SXX=-0.167E+05	SYY= 0.0	SZZ= 0.193E+02	TXY= 0.0	TXZ= 0.340E+03	TYZ= 0.0
EXX=-0.835E-03	EYY= 0.173E-03	EZZ= 0.184E-03	EXY= 0.0	EXZ= 0.400E-03	EYZ= 0.0

AT Z=-0.100E-01

SXX=-0.758E+04	SYY= 0.0	SZZ= 0.401E+02	TXY= 0.0	TXZ= 0.421E+03	TYZ= 0.0
EXX=-0.379E-03	EYY= 0.756E-04	EZZ= 0.987E-04	EXY= 0.0	EXZ= 0.495E-03	EYZ= 0.0

STRESSES AND STRAINS IN LAYER 2

AT Z=-0.100E-01

SXX=-0.788E+03	SYY= 0.0	SZZ= 0.401E+02	TXY= 0.0	TXZ= 0.421E+03	TYZ= 0.0
EXX=-0.379E-03	EYY= 0.786E-05	EZZ= 0.979E-04	EXY=-0.249E-10	EXZ= 0.495E-03	EYZ= 0.0

AT Z=-0.500E-02

SXX=-0.392E+03	SYY= 0.0	SZZ= 0.311E+02	TXY= 0.0	TXZ= 0.417E+03	TYZ= 0.0
EXX=-0.190E-03	EYY= 0.379E-05	EZZ= 0.540E-04	EXY=-0.121E-10	EXZ= 0.490E-03	EYZ= 0.0

AT Z= 0.0

SXX=-0.238E-02	SYY= 0.0	SZZ=-0.211E-01	TXY= 0.0	TXZ= 0.411E+03	TYZ= 0.0
EXX= 0.972E-09	EYY= 0.246E-09	EZZ=-0.979E-08	EXY=-0.693E-15	EXZ= 0.484E-03	EYZ= 0.0

STRESSES AND STRAINS IN LAYER 3

AT Z= 0.0

SXX=-0.228E-02	SYY= 0.0	SZZ=-0.215E-01	TXY= 0.0	TXZ= 0.411E+03	TYZ= 0.0
EXX= 0.106E-08	EYY= 0.250E-09	EZZ=-0.100E-07	EXY=-0.702E-15	EXZ= 0.484E-03	EYZ= 0.0

AT Z= 0.500E-02

SXX= 0.392E+03	SYY= 0.0	SZZ=-0.311E+02	TXY= 0.0	TXZ= 0.417E+03	TYZ= 0.0
EXX= 0.190E-03	EYY=-0.379E-05	EZZ=-0.540E-04	EXY= 0.121E-10	EXZ= 0.490E-03	EYZ= 0.0

AT Z= 0.100E-01

SXX= 0.788E+03	SYY= 0.0	SZZ=-0.401E+02	TXY= 0.0	TXZ= 0.421E+03	TYZ= 0.0
EXX= 0.379E-03	EYY=-0.786E-05	EZZ=-0.979E-04	EXY= 0.249E-10	EXZ= 0.495E-03	EYZ= 0.0

STRESSES AND STRAINS IN LAYER 4

AT Z= 0.100E-01

SXX= 0.758E+04	SYY= 0.0	SZZ=-0.401E+02	TXY= 0.0	TXZ= 0.421E+03	TYZ= 0.0
EXX= 0.379E-03	EYY=-0.756E-04	EZZ=-0.987E-04	EXY= 0.0	EXZ= 0.495E-03	EYZ= 0.0

AT Z= 0.150E-01

SXX= 0.167E+05	SYY= 0.0	SZZ=-0.193E+02	TXY= 0.0	TXZ= 0.340E+03	TYZ= 0.0
EXX= 0.835E-03	EYY=-0.173E-03	EZZ=-0.185E-03	EXY= 0.0	EXZ= 0.400E-03	EYZ= 0.0

AT Z= 0.200E-01

SXX= 0.258E+05	SYY= 0.0	SZZ= 0.127E-03	TXY= 0.0	TXZ=-0.360E-04	TYZ= 0.0
EXX= 0.129E-02	EYY=-0.271E-03	EZZ=-0.271E-03	EXY= 0.0	EXZ=-0.424E-10	EYZ= 0.0

STRESS OUTPUT FOR ELEMENT 13 AT 1 LOCATIONS

AT LOCATION 1 X= 0.500E+00 Y= 0.0

TIME STEP = 6

STRESSES AND STRAINS IN LAYER 1

TIME = 0.12 E-02 SEC.

AT Z=-0.200E-01

SXX=-0.282E+04	SYY= 0.0	SZZ= 0.178E-03	TXY= 0.0	TXZ=-0.331E-03	TYZ= 0.0
EXX=-0.141E-03	EYY= 0.296E-04	EZZ= 0.296E-04	EXY= 0.0	EXZ=-0.389E-09	EYZ= 0.0

AT Z=-0.150E-01

SXX= 0.904E+04	SYY= 0.0	SZZ=-0.231E+02	TXY= 0.0	TXZ=-0.356E+03	TYZ= 0.0
EXX= 0.452E-03	EYY=-0.926E-04	EZZ=-0.106E-03	EXY= 0.0	EXZ=-0.419E-03	EYZ= 0.0

AT Z=-0.100E-01

SXX= 0.209E+05	SYY= 0.0	SZZ=-0.652E+02	TXY= 0.0	TXZ=-0.695E+03	TYZ= 0.0
EXX= 0.105E-02	EYY=-0.213E-03	EZZ=-0.250E-03	EXY= 0.0	EXZ=-0.818E-03	EYZ= 0.0

STRESSES AND STRAINS IN LAYER 2

AT Z=-0.100E-01

SXX= 0.218E+04	SYY= 0.0	SZZ=-0.652E+02	TXY= 0.0	TXZ=-0.695E+03	TYZ= 0.0
EXX= 0.105E-02	EYY=-0.222E-04	EZZ=-0.249E-03	EXY= 0.703E-10	EXZ=-0.818E-03	EYZ= 0.0

AT Z=-0.500E-02

SXX= 0.109E+04	SYY= 0.0	SZZ=-0.570E+02	TXY= 0.0	TXZ=-0.850E+03	TYZ= 0.0
EXX= 0.523E-03	EYY=-0.108E-04	EZZ=-0.136E-03	EXY= 0.343E-10	EXZ=-0.100E-02	EYZ= 0.0

AT Z= 0.0

SXX=-0.493E-01	SYY= 0.0	SZZ=-0.132E+00	TXY= 0.0	TXZ=-0.915E+03	TYZ= 0.0
EXX=-0.103E-07	EYY= 0.190E-08	EZZ=-0.578E-07	EXY=-0.547E-14	EXZ=-0.108E-02	EYZ= 0.0

STRESSES AND STRAINS IN LAYER 3

AT Z= 0.0

SXX=-0.457E-01	SYY= 0.0	SZZ=-0.131E+00	TXY= 0.0	TXZ=-0.915E+03	TYZ= 0.0
EXX=-0.865E-08	EYY= 0.186E-08	EZZ=-0.579E-07	EXY=-0.534E-14	EXZ=-0.108E-02	EYZ= 0.0

AT Z= 0.500E-02

SXX=-0.109E+04	SYY= 0.0	SZZ= 0.568E+02	TXY= 0.0	TXZ=-0.850E+03	TYZ= 0.0
EXX=-0.523E-03	EYY= 0.108E-04	EZZ= 0.136E-03	EXY=-0.343E-10	EXZ=-0.100E-02	EYZ= 0.0

AT Z= 0.100E-01

SXX=-0.218E+04	SYY= 0.0	SZZ= 0.650E+02	TXY= 0.0	TXZ=-0.695E+03	TYZ= 0.0
EXX=-0.105E-02	EYY= 0.222E-04	EZZ= 0.249E-03	EXY=-0.703E-10	EXZ=-0.818E-03	EYZ= 0.0

STRESSES AND STRAINS IN LAYER 4

AT Z= 0.100E-01

SXX=-0.209E+05	SYY= 0.0	SZZ= 0.650E+02	TXY= 0.0	TXZ=-0.695E+03	TYZ= 0.0
EXX=-0.105E-02	EYY= 0.213E-03	EZZ= 0.250E-03	EXY= 0.0	EXZ=-0.818E-03	EYZ= 0.0

AT Z= 0.150E-01

SXX=-0.904E+04	SYY= 0.0	SZZ= 0.229E+02	TXY= 0.0	TXZ=-0.356E+03	TYZ= 0.0
EXX=-0.452E-03	EYY= 0.926E-04	EZZ= 0.106E-03	EXY= 0.0	EXZ=-0.419E-03	EYZ= 0.0

AT Z= 0.200E-01

SXX= 0.282E+04	SYY= 0.0	SZZ=-0.142E-03	TXY= 0.0	TXZ=-0.294E-03	TYZ= 0.0
EXX= 0.141E-03	EYY=-0.296E-04	EZZ=-0.296E-04	EXY= 0.0	EXZ=-0.346E-09	EYZ= 0.0

STRESS OUTPUT FOR ELEMENT 13 AT 1 LOCATIONS

AT LOCATION 1 X= 0.500E+00 Y= 0.0

STRESSES AND STRAINS IN LAYER 1 TIME STEP = 8

TIME = 0.16 E-02 SEC.

AT Z=-0.200E-01

SXX= 0.690E+04 SYY= 0.0 SZZ=-0.589E-04 TXY= 0.0 TXZ=-0.207E-03 TYZ= 0.0
EXX= 0.345E-03 EYY=-0.724E-04 EZZ=-0.724E-04 EXY= 0.0 EXZ=-0.244E-09 EYZ= 0.0

AT Z=-0.150E-01

SXX= 0.152E+05 SYY= 0.0 SZZ=-0.799E+01 TXY= 0.0 TXZ=-0.253E+03 TYZ= 0.0
EXX= 0.762E-03 EYY=-0.159E-03 EZZ=-0.164E-03 EXY= 0.0 EXZ=-0.297E-03 EYZ= 0.0

AT Z=-0.100E-01

SXX= 0.236E+05 SYY= 0.0 SZZ=-0.175E+02 TXY= 0.0 TXZ=-0.598E+03 TYZ= 0.0
EXX= 0.118E-02 EYY=-0.246E-03 EZZ=-0.256E-03 EXY= 0.0 EXZ=-0.704E-03 EYZ= 0.0

STRESSES AND STRAINS IN LAYER 2

AT Z=-0.100E-01

SXX= 0.287E+04 SYY= 0.0 SZZ=-0.175E+02 TXY= 0.0 TXZ=-0.598E+03 TYZ= 0.0
EXX= 0.118E-02 EYY=-0.258E-04 EZZ=-0.256E-03 EXY= 0.813E-10 EXZ=-0.704E-03 EYZ= 0.0

AT Z=-0.500E-02

SXX= 0.124E+04 SYY= 0.0 SZZ=-0.139E+02 TXY= 0.0 TXZ=-0.653E+03 TYZ= 0.0
EXX= 0.590E-03 EYY=-0.120E-04 EZZ=-0.130E-03 EXY= 0.405E-10 EXZ=-0.768E-03 EYZ= 0.0

AT Z= 0.0

SXX=-0.106E+03 SYY= 0.0 SZZ=-0.217E+00 TXY= 0.0 TXZ=-0.698E+03 TYZ= 0.0
EXX=-0.299E-07 EYY= 0.300E-08 EZZ=-0.928E-07 EXY=-0.985E-14 EXZ=-0.821E-03 EYZ= 0.0

STRESSES AND STRAINS IN LAYER 3

AT Z= 0.0

SXX=-0.115E+00 SYY= 0.0 SZZ=-0.217E+00 TXY= 0.0 TXZ=-0.698E+03 TYZ= 0.0
EXX=-0.295E-07 EYY= 0.339E-08 EZZ=-0.929E-07 EXY=-0.902E-14 EXZ=-0.821E-03 EYZ= 0.0

AT Z= 0.500E-02

SXX=-0.124E+04 SYY= 0.0 SZZ= 0.135E+02 TXY= 0.0 TXZ=-0.653E+03 TYZ= 0.0
EXX=-0.590E-03 EYY= 0.120E-04 EZZ= 0.130E-03 EXY=-0.405E-10 EXZ=-0.768E-03 EYZ= 0.0

AT Z= 0.100E-01

SXX=-0.287E+04 SYY= 0.0 SZZ= 0.169E+02 TXY= 0.0 TXZ=-0.598E+03 TYZ= 0.0
EXX=-0.118E-02 EYY= 0.258E-04 EZZ= 0.255E-03 EXY=-0.814E-10 EXZ=-0.704E-03 EYZ= 0.0

STRESSES AND STRAINS IN LAYER 4

AT Z= 0.100E-01

SXX=-0.236E+05 SYY= 0.0 SZZ= 0.169E+02 TXY= 0.0 TXZ=-0.598E+03 TYZ= 0.0
EXX=-0.118E-02 EYY= 0.246E-03 EZZ= 0.256E-03 EXY= 0.0 EXZ=-0.704E-03 EYZ= 0.0

AT Z= 0.150E-01

SXX=-0.152E+05 SYY= 0.0 SZZ= 0.767E+01 TXY= 0.0 TXZ=-0.253E+03 TYZ= 0.0
EXX=-0.762E-03 EYY= 0.159E-03 EZZ= 0.164E-03 EXY= 0.0 EXZ=-0.297E-03 EYZ= 0.0

AT Z= 0.200E-01

SXX=-0.690E+04 SYY= 0.0 SZZ= 0.648E-04 TXY= 0.0 TXZ=-0.207E-03 TYZ= 0.0
EXX=-0.345E-03 EYY= 0.724E-04 EZZ= 0.724E-04 EXY= 0.0 EXZ=-0.244E-09 EYZ= 0.0

STRESS OUTPUT FOR ELEMENT 13 AT 1 LOCATIONS

AT LOCATION 1 X= 0.500E+00 Y= 0.0

TIME STEP = 10

TIME = 0.2 E-02 SEC.

STRESSES AND STRAINS IN LAYER 1

AT Z=-0.200E-01

SXX=-0.159E+05	SYY= 0.0	SZZ=-0.673E-04	TXY= 0.0	TXZ= 0.300E-03	TYZ= 0.0
EXX=-0.793E-03	EYY= 0.166E-03	EZZ= 0.166E-03	EXY= 0.0	EXZ= 0.353E-09	EYZ= 0.0

AT Z=-0.150E-01

SXX=-0.118E+05	SYY= 0.0	SZZ= 0.269E+02	TXY= 0.0	TXZ= 0.268E+03	TYZ= 0.0
EXX=-0.593E-03	EYY= 0.122E-03	EZZ= 0.137E-03	EXY= 0.0	EXZ= 0.315E-03	EYZ= 0.0

AT Z=-0.100E-01

SXX=-0.784E+04	SYY= 0.0	SZZ= 0.555E+02	TXY= 0.0	TXZ= 0.276E+03	TYZ= 0.0
EXX=-0.393E-03	EYY= 0.768E-04	EZZ= 0.109E-03	EXY= 0.0	EXZ= 0.325E-03	EYZ= 0.0

STRESSES AND STRAINS IN LAYER 2

AT Z=-0.100E-01

SXX=-0.813E+03	SYY= 0.0	SZZ= 0.555E+02	TXY= 0.0	TXZ= 0.276E+03	TYZ= 0.0
EXX=-0.393E-03	EYY= 0.795E-05	EZZ= 0.108E-03	EXY=-0.253E-10	EXZ= 0.325E-03	EYZ= 0.0

AT Z=-0.500E-02

SXX=-0.404E+03	SYY= 0.0	SZZ= 0.415E+02	TXY= 0.0	TXZ= 0.283E+03	TYZ= 0.0
EXX=-0.196E-03	EYY= 0.380E-05	EZZ= 0.601E-04	EXY=-0.121E-10	EXZ= 0.332E-03	EYZ= 0.0

AT Z= 0.0

SXX=-0.172E+00	SYY= 0.0	SZZ=-0.291E+00	TXY= 0.0	TXZ= 0.281E+03	TYZ= 0.0
EXX=-0.528E-07	EYY= 0.486E-08	EZZ=-0.121E-06	EXY=-0.142E-13	EXZ= 0.330E-03	EYZ= 0.0

STRESSES AND STRAINS IN LAYER 3

AT Z= 0.0

SXX=-0.172E+00	SYY= 0.0	SZZ=-0.292E+00	TXY= 0.0	TXZ= 0.281E+03	TYZ= 0.0
EXX=-0.527E-07	EYY= 0.487E-08	EZZ=-0.122E-06	EXY=-0.142E-13	EXZ= 0.330E-03	EYZ= 0.0

AT Z= 0.500E-02

SXX= 0.403E+03	SYY= 0.0	SZZ=-0.421E+02	TXY= 0.0	TXZ= 0.283E+03	TYZ= 0.0
EXX= 0.196E-03	EYY=-0.379E-05	EZZ=-0.604E-04	EXY= 0.121E-10	EXZ= 0.332E-03	EYZ= 0.0

AT Z= 0.100E-01

SXX= 0.813E+03	SYY= 0.0	SZZ=-0.564E+02	TXY= 0.0	TXZ= 0.276E+03	TYZ= 0.0
EXX= 0.393E-03	EYY=-0.794E-05	EZZ=-0.108E-03	EXY= 0.252E-10	EXZ= 0.325E-03	EYZ= 0.0

STRESSES AND STRAINS IN LAYER 4

AT Z= 0.100E-01

SXX= 0.784E+04	SYY= 0.0	SZZ=-0.564E+02	TXY= 0.0	TXZ= 0.276E+03	TYZ= 0.0
EXX= 0.393E-03	EYY=-0.767E-04	EZZ=-0.109E-03	EXY= 0.0	EXZ= 0.325E-03	EYZ= 0.0

AT Z= 0.150E-01

SXX= 0.118E+05	SYY= 0.0	SZZ=-0.274E+02	TXY= 0.0	TXZ= 0.268E+03	TYZ= 0.0
EXX= 0.593E-03	EYY=-0.122E-03	EZZ=-0.137E-03	EXY= 0.0	EXZ= 0.315E-03	EYZ= 0.0

AT Z= 0.200E-01

SXX= 0.159E+05	SYY= 0.0	SZZ= 0.160E-04	TXY= 0.0	TXZ=-0.750E-03	TYZ= 0.0
EXX= 0.793E-03	EYY=-0.166E-03	EZZ=-0.166E-03	EXY= 0.0	EXZ=-0.882E-09	EYZ= 0.0

TABLE A1

DIMENSIONS OF VARIOUS ARRAYS USED BY THE TFQE

Number of Layers [NL]	Nodal DOF [NQ = 8NL+30]	Independent Betas [NB = 52NL-18]	EM and ELK Matrices [NKM = NQ(NQ+1)/2]	HIG [NHG = NQ*NB]	HMAT [NH]
3	54	138	1,485	7,452	9,107
4	62	190	1,953	11,780	16,517
5	70	242	2,485	16,940	24,343
6	78	294	3,081	22,932	31,753
7	86	346	3,741	29,756	39,579
8	94	398	4,465	37,412	46,989
9	102	450	5,253	45,900	54,815
10	110	502	6,105	55,220	62,225
11	118	554	7,021	65,372	70,051
12	126	606	8,001	76,356	77,461
13	134	658	9,045	88,172	85,287
14	142	710	10,153	100,820	92,697
15	150	762	11,325	114,300	100,523
16	158	814	12,561	128,612	107,933
17	166	866	13,861	143,756	115,759
18	174	918	15,225	159,732	123,169

NOTE:

1. The TFQE has been programmed for a minimum of 3 layers through the thickness.
2. The array EM is used internally by TFQEM for other computations. Hence, add 750 words to the dimension in this table.
3. The array ELK is used internally by TFQEK for other computations. Hence, the minimum dimension of ELK for TFQEK should be 8040 words.

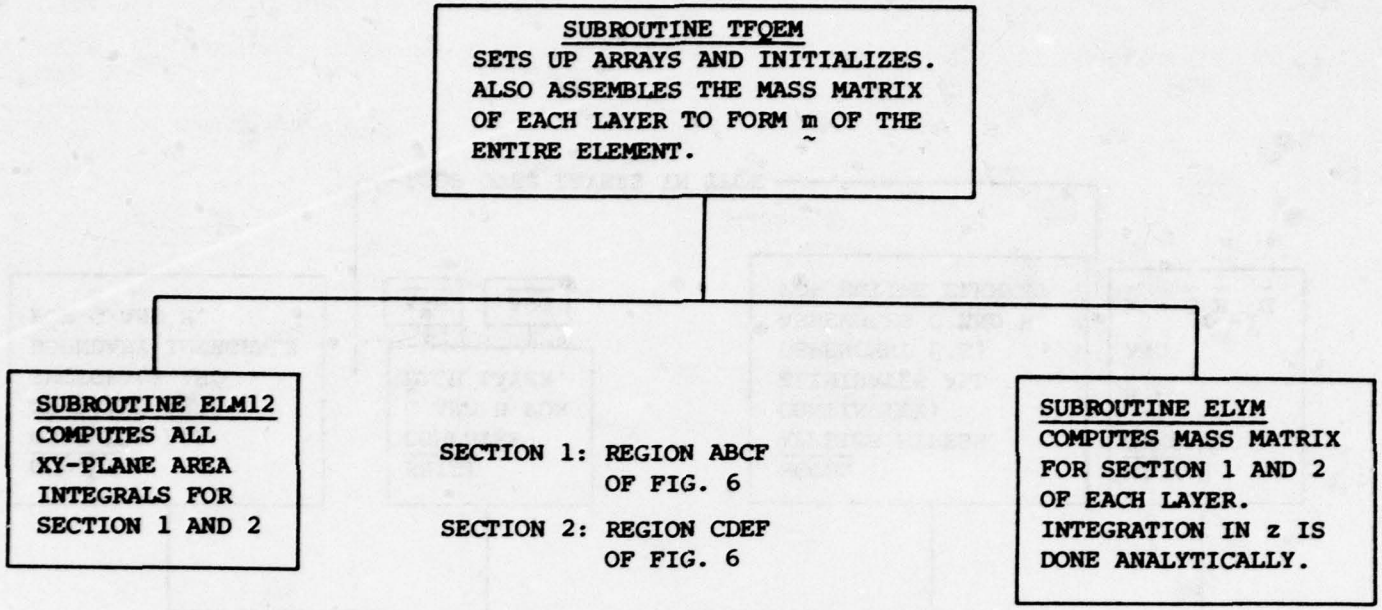

FIG. A1 PROGRAM STRUCTURE OF THE TFQE MASS MATRIX

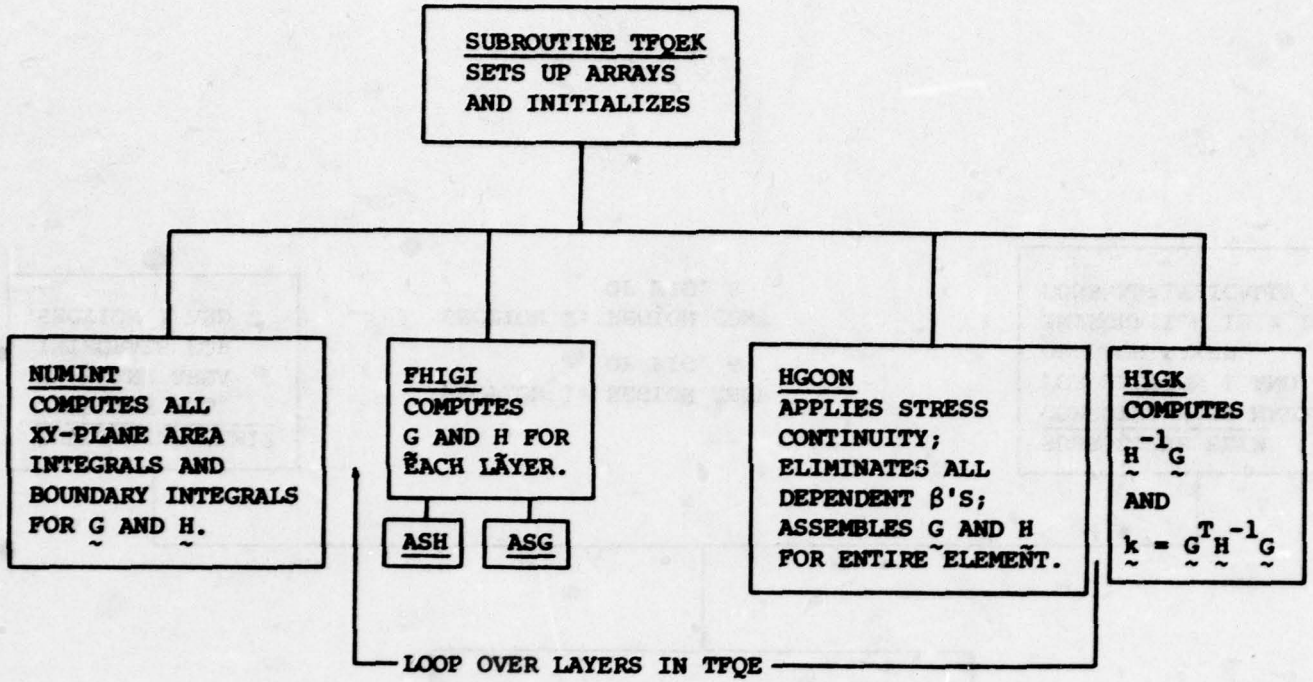

FIG. A2 PROGRAM STRUCTURE OF THE TFQE STIFFNESS MATRIX

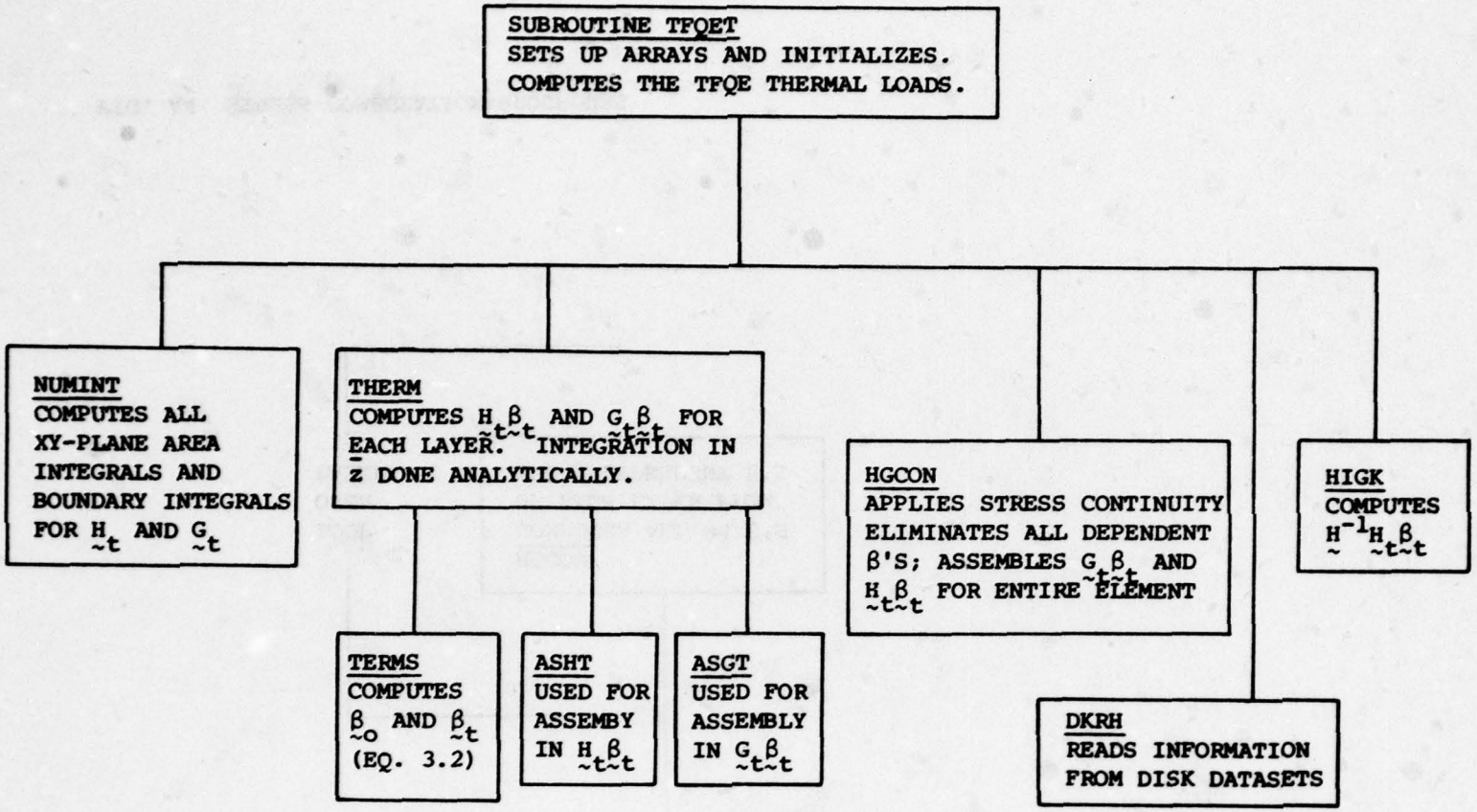

FIG. A3 PROGRAM STRUCTURE OF THE TFQE THERMAL LOADS VECTOR

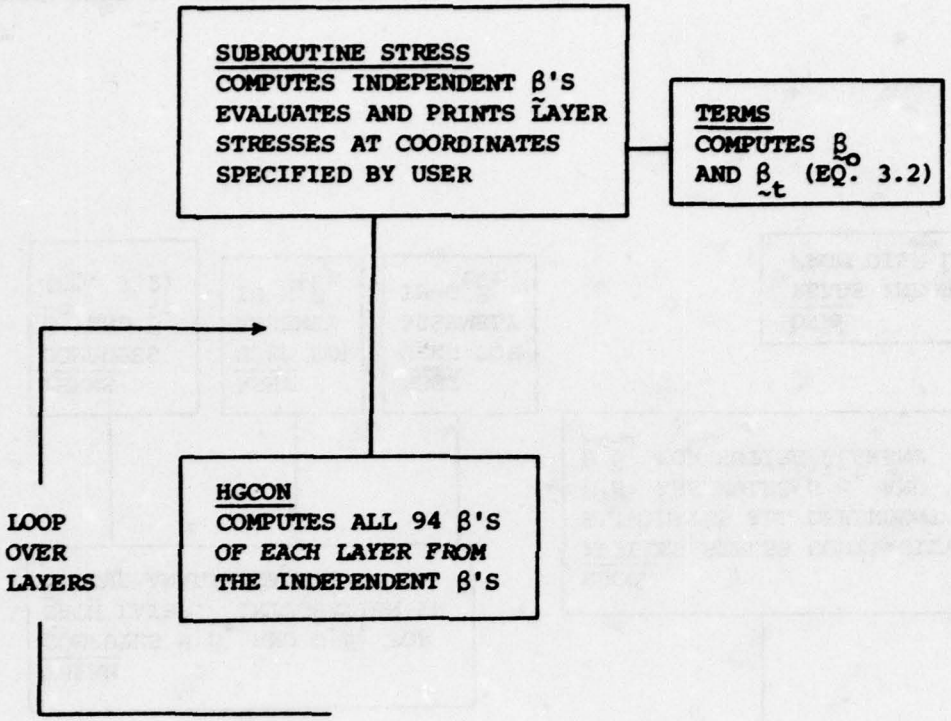

FIG. A4 STRESS COMPUTATION PROCEDURE

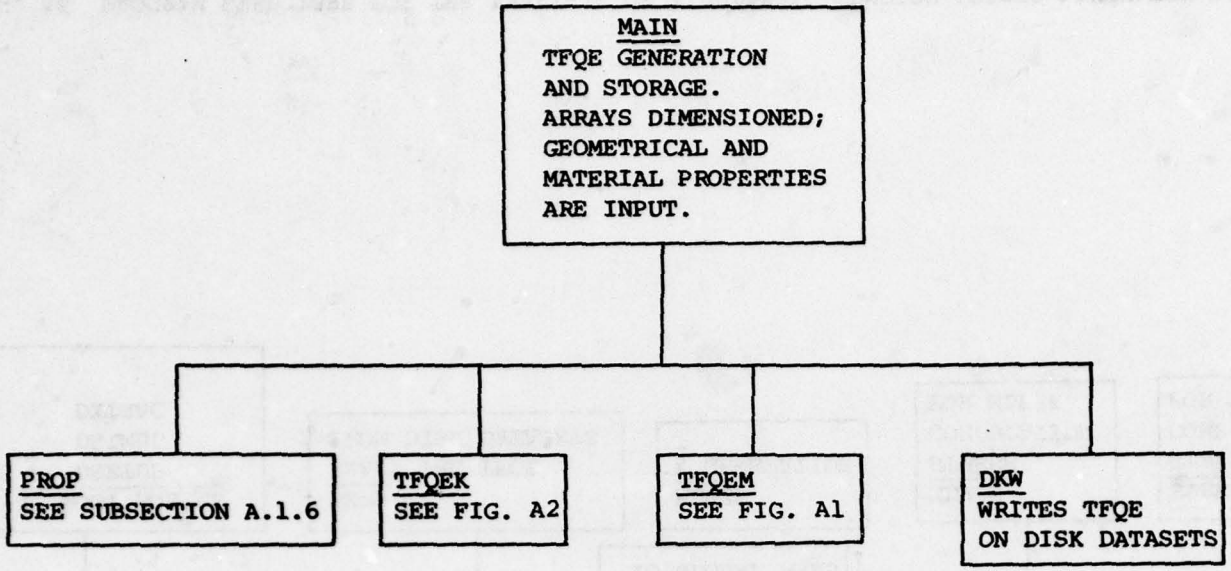

FIG. A5 THE TFQE GENERATION AND STORAGE ON DISK DATASETS

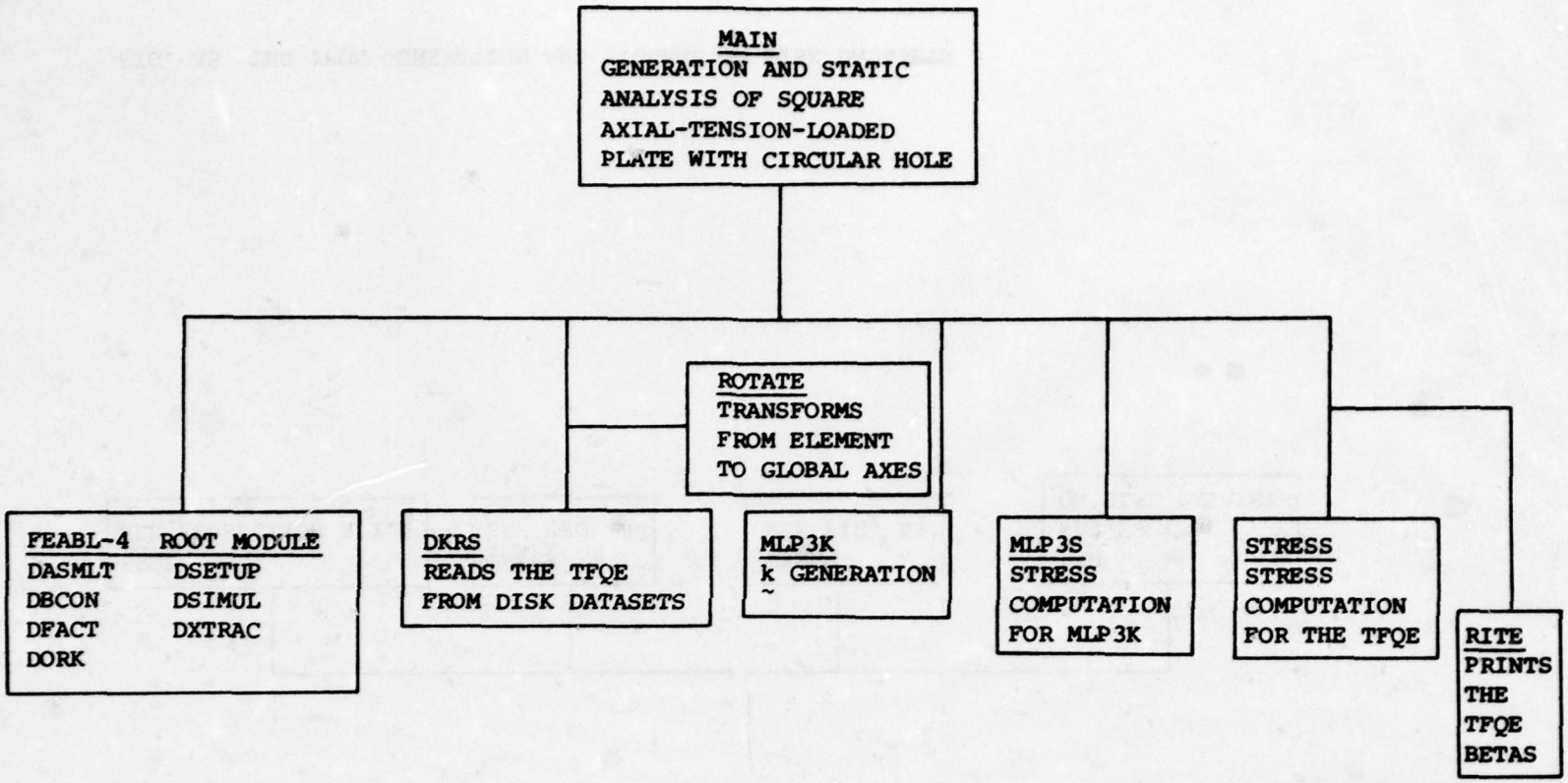

FIG. A6 PROGRAM STRUCTURE FOR THE ANALYSIS OF A UNIAXIAL-TENSION-LOADED LAMINATED PLATE WITH A CIRCULAR HOLE

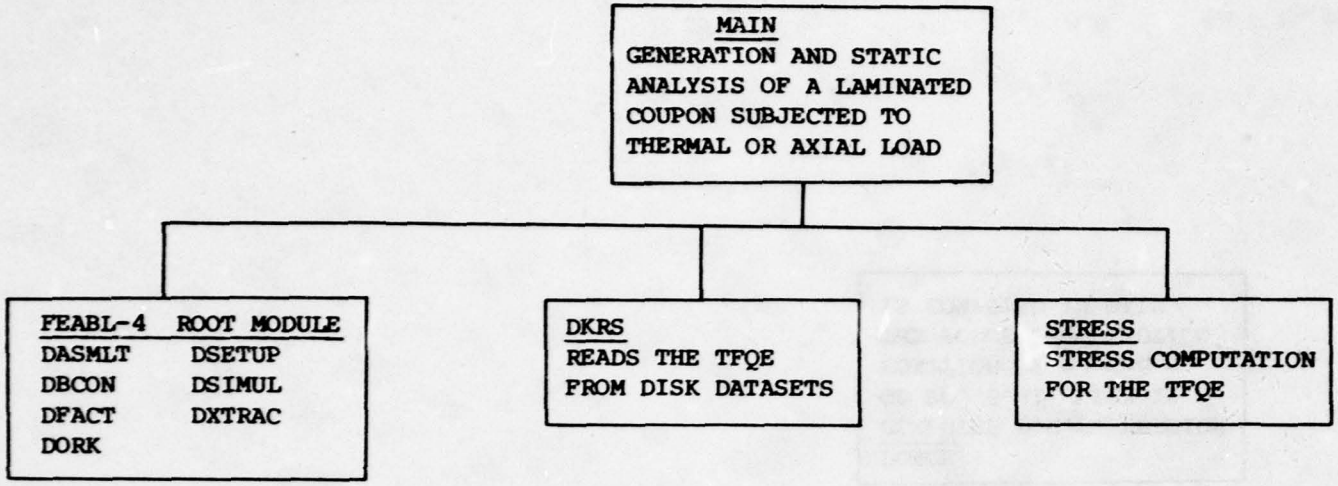

FIG. A7 PROGRAM STRUCTURE FOR THE ANALYSIS OF TENSION-LOADED AND/OR THERMALLY-LOADED COUPONS

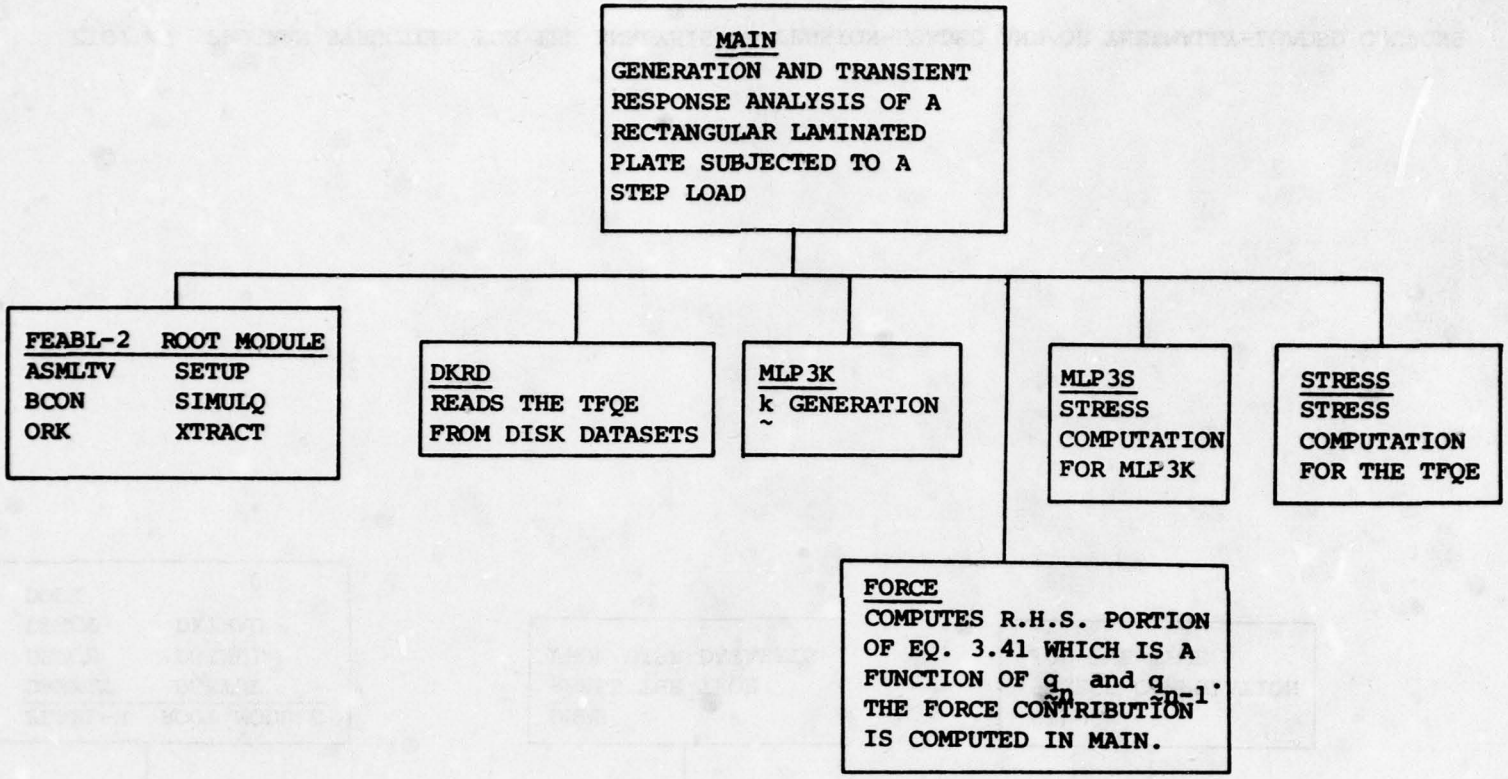

FIG. A8 PROGRAM STRUCTURE FOR TRANSIENT RESPONSE ANALYSIS

DISTRIBUTION LIST

	No. of Copies
Office of Deputy Under Secretary of Defense for Research and Engineering (ET) ATTN: Mr. J. Persh, Staff Specialist for Materials and Structures (Room 3D1089) The Pentagon Washington, DC 20301	1
Office of Deputy Chief of Research Development and Acquisition ATTN: DAMA-CSS-D/Dr. J. I. Bryan (Room 3D424) The Pentagon Washington, DC 20310	1
Commander U.S. Army Materiel Development and Readiness Command ATTN: DRCLDC, Mr. R. J. Zentner 5001 Eisenhower Avenue Alexandria, VA 22333	1
Director Ballistic Missile Defense Systems Command ATTN: BMDSC-TEN, Mr. N. J. Hurst BMDSC-H BMDSC-T BMDSC-AOLIB P. O. Box 1500 Huntsville, AL 35807	1 1 1 1
Ballistic Missile Defense Program Office ATTN: DACS-BMT DARCOM Bldg., Seventh Floor 5001 Eisenhower Avenue Alexandria, VA 22333	1
Director Ballistic Missile Defense Advanced Technology Center ATTN: ATC-M, Mr. M. Whitfield ATC-M, Dr. D. Harmon ATC-M, Mr. J. Papadopoulos P. O. Box 1500 Huntsville, AL 35807	1 1 1

	No. of Copies
Director Defense Nuclear Agency ATTN: SPAS, Mr. J. F. Moulton, Jr. SPAS, Mr. D. Kohler Washington, DC 20305	 1 1
Director Army Ballistic Research Laboratories ATTN: DRDAR-BLT, Dr. N. J. Huffington, Jr. DRDAR-BLT, Dr. T. W. Wright DRDAR-BLT, Dr. G. L. Moss Aberdeen Proving Ground, MD 21005	 1 1 1
Commander Harry Diamond Laboratories ATTN: DRXDO-NP, Dr. F. Wimenitz 2800 Powder Mill Road Adelphi, MD 20783	 1
Commander U.S. Army Combat Development Command Institute of Nuclear Studies ATTN: Technical Library Fort Bliss, Texas 79916	 1
Commander Air Force Materials Laboratory Air Force Systems Command ATTN: LNE/Dr. W. Kessler LNC/Dr. D. Schmidt Wright-Patterson Air Force Base, Ohio 45433	 1 1
Space and Missile Systems Organization ATTN: RSSE/LTC J. McCormack P. O. Box 92960 World Way Postal Center Los Angeles, CA 90009	 2
Commander Naval Ordnance Systems Command ATTN: ORD-03331, Mr. M. Kinna Washington, DC 20360	 1
Commander Naval Surface Weapons Center ATTN: Dr. C. Lyons Dr. W. Messick Silver Springs, MD 20910	 1 1

	No. of Copies
Lawrence Livermore Laboratory	
ATTN: Dr. E. M. Wu	1
P. O. Box 808 (L-342)	
Livermore, CA 94550	
Los Alamos Scientific Laboratory	
ATTN: GMX-6, Dr. J. W. Taylor	1
P. O. Box 1663	
Los Alamos, NM 87544	
Sandia Laboratories	
ATTN: Dr. Frank P. Gerstle, Jr.	1
Dr. L. D. Bertholf	1
Dr. J. Lipkin	1
P. O. Box 5800	
Albuquerque, NM 87115	
Aerospace Corporation	
ATTN: Dr. R. Cooper	1
Dr. W. Barry	1
P. O. Box 92957	
Los Angeles, CA 90009	
AVCO Corporation	
Government Products Group	
ATTN: Dr. W. Reinecke	1
Mr. P. Rolincik	1
201 Lowell Street	
Wilmington, MA 01997	
ETA Corporation	
ATTN: Mr. D. L. Mykkanen	1
P. O. Box 6625	
Orange, CA 92667	
Effects Technology, Inc.	
ATTN: Dr. R. Wengler	1
Dr. R. Parisse	1
Mr. J. Green	1
5383 Hollister Avenue	
Santa Barbara, CA 93111	
Fiber Materials, Inc.	
ATTN: Mr. M. Subilia, Jr.	1
Mr. L. Landers	1
Mr. G. Williams	1
Mr. P. Marchol	1
Biddeford Industrial Park	
Biddeford, ME 04005	

	No. of Copies
General Electric Company Valley Forge Space Technology Center ATTN: Mr. K. Hall Mr. J. Brazel Ms. B. McGuire P. O. Box 8555 Philadelphia, PA 19101	 1 1 1
General Dynamics Corporation Convair Division ATTN: Mr. J. Hertz Mr. H. McCutcheon, Jr. 5001 Kearny Villa Road San Diego, CA 92138	 1 1
General Dynamics Corporation ATTN: Dr. D. J. Wilkins Mail Zone 2884 P. O. Box 748 Fort Worth, Texas 76101	 1
Kaman Sciences Corporation ATTN: Mr. F. Shelton P. O. Box 7463 Colorado Springs, CO 80933	 1
Ktech ATTN: Dr. D. Keller 911 Pennsylvania Avenue, N.E. Albuquerque, NM 87110	 1
Lockheed Missiles and Space Company ATTN: Mr. D. Aspinwall P. O. Box 504 Sunnyvale, CA 94088	 1
Martin Marietta Aerospace ATTN: Dr. M. Hendricks Mr. R. Hewitt Mr. Frank H. Koo P. O. Box 5837 Orlando, Florida 32805	 1 1 1
McDonnell Douglas Corporation ATTN: Dr. L. Cohen Mr. H. Parachanian 5301 Bolsa Avenue Huntington Beach, CA 92647	 1 1

	No. of Copies
Prototype Development Associates, Inc. ATTN: Mr. J. Schultzler Mr. N. Harrington 1740 Garry Avenue, Suite 201 Santa Ana, CA 92705	 1 1
R&D Associates ATTN: Dr. A. Field 4640 Admiralty Way P.O. Box 9695 Marina del Rey, CA 90291	1
Radkowski Associates ATTN: Dr. P. Radkowski P. O. Box 5474 Riverside, CA 92507	1
Southwest Research Institute ATTN: Mr. A. Wenzel 8500 Culebra Road San Antonio, Texas 78206	1
Stanford Research Institute ATTN: Dr. D. Curran Dr. L. Seaman 333 Ravenswood Avenue Menlo Park, CA 90250	 1 1
Terra Tek, Inc. ATTN: Dr. A. H. Jones 420 Wakara Way Salt Lake City, Utah 84108	1
TRW Systems Group ATTN: Mr. D. Gamble One Space Park Redondo Beach, CA 90278	1
Lehigh University Institute of Fracture and Solid Mechanics ATTN: Dr. George C. Sih Bldg. #19, Packard Lab. Bethlehem, PA 18015	 1
Stanford University Department of Applied Mechanics ATTN: Professor E. H. Lee Stanford, CA 94305	 1

	No. of Copies
University of Illinois at Chicago Circle Department of Materials Engineering ATTN: Professor R. L. Spilker Chicago, Illinois 60680	1
Defense Documentation Center Cameron Station, Bldg. 5 5010 Duke Station Alexandria, VA 22314	1
Director Army Materials & Mechanics Research Center	
ATTN: DRXMR-H, Mr. J. F. Dignam	1
DRXMR-H, Mr. L. Aronin	1
DRXMR-H, Dr. S. C. Chou	1
DRXMR-H, Dr. D. Dandekar	1
DRXMR-AP	1
DRXMR-PL	2
DRXMR-PR Watertown, MA 02172	1

Army Materials and Mechanics Research Center
Watertown, Massachusetts 02172

A MULTILAYER, TRACTION-FREE EDGE, QUADRILATERAL WARPING ELEMENT FOR THE STRESS ANALYSIS OF COMPOSITE PLATES AND SHELLS

Alexander Harris, Oscar Orringer, and Emmett A. Witmer, Aeroelastic and Structures Research Laboratory, Department of Aeronautics and Astronautics, Massachusetts Institute of Technology, Cambridge, Massachusetts 02139

Technical Report AMMRC TR 79-26 (MIT-ASRL TR 193-1)
April 1979, pp. illus-tables, Contract DAAG46-78-C-0015
D/A Project 6X363304D215, AMCMS Code: 633304.21500.03
Final Report, March 1, 1978 to April 30, 1979

AD________________________

UNCLASSIFIED
UNLIMITED DISTRIBUTION

Key Words

Finite-Element Method
Elastic Behavior
Composites
Static Response
Transient Response
Stress Analysis
Laminated Plates and Shells
Free-Edge Stress Analysis

Laminated composites develop large interlaminar stresses at traction-free edges; these stresses are significant and often cause ply delaminations. However, these stresses are difficult to analyze and predict accurately because they vary very rapidly over a small region whose extent is of the order of the total laminate thickness at the free edge. Previous solution methods have been able to solve only a very restricted class of free-edge multilayer plate problems.

In the present research, a hybrid stress multilayer warping quadrilateral element with a traction-free edge (TFQE), based on the Principle of Modified Complementary Energy, has been developed for efficient finite element modeling and analysis at and near free edges. The assumed stress distributions in the element were selected so as to satisfy the basic equations of equilibrium; sufficient detail was implemented throughout each layer of each element to model the steep boundary layer stress gradients, including the important interlaminar stresses. The interlayer stress continuity and traction-free conditions at the free-edge are satisfied exactly; the resulting stress distribution was examined for consistency as required by 3-dimensional stress functions. The stress assumption includes no singularity. The traction-free edge is allowed to warp freely.

The interior of the laminate, away from the free edge, is modeled by laminated-plate elements (MLPIE) which are based on lamination theory. These elements include transverse shear deformation and are compatible with the TFQE. Thus, numerical results for general free-edge multilayer plate problems are obtained with efficient lamination-theory element modeling of most of the structure, while TFQE elements provide additional warping degrees of freedom at and near the free edges where the warping effect is important. This method of analysis has been developed for both static (mechanical and thermal loading) and transient response analyses.

Several examples, for which other numerical solutions exist, have been solved by using the TFQE and/or the TFQE in combination with MLPIE elements. The results compare well, but a significant reduction in the number of unknowns of the equations has been achieved in the present TFQE solution.

Finally, some numerical methods for solving static and transient response equations have been reviewed.

Army Materials and Mechanics Research Center
Watertown, Massachusetts 02172

A MULTILAYER, TRACTION-FREE EDGE, QUADRILATERAL WARPING ELEMENT FOR THE STRESS ANALYSIS OF COMPOSITE PLATES AND SHELLS

Alexander Harris, Oscar Orringer, and Emmett A. Witmer, Aeroelastic and Structures Research Laboratory, Department of Aeronautics and Astronautics, Massachusetts Institute of Technology, Cambridge, Massachusetts 02139

Technical Report AMMRC TR 79-26 (MIT-ASRL TR 193-1)
April 1979, pp. illus-tables, Contract DAAG46-78-C-0015
D/A Project 6X363304D215, AMCMS Code: 633304.21500.03
Final Report, March 1, 1978 to April 30, 1979

AD________________________

UNCLASSIFIED
UNLIMITED DISTRIBUTION

Key Words

Finite-Element Method
Elastic Behavior
Composites
Static Response
Transient Response
Stress Analysis
Laminated Plates and Shells
Free-Edge Stress Analysis

Laminated composites develop large interlaminar stresses at traction-free edges; these stresses are significant and often cause ply delaminations. However, these stresses are difficult to analyze and predict accurately because they vary very rapidly over a small region whose extent is of the order of the total laminate thickness at the free edge. Previous solution methods have been able to solve only a very restricted class of free-edge multilayer plate problems.

In the present research, a hybrid stress multilayer warping quadrilateral element with a traction-free edge (TFQE), based on the Principle of Modified Complementary Energy, has been developed for efficient finite element modeling and analysis at and near free edges. The assumed stress distributions in the element were selected so as to satisfy the basic equations of equilibrium; sufficient detail was implemented throughout each layer of each element to model the steep boundary layer stress gradients, including the important interlaminar stresses. The interlayer stress continuity and traction-free conditions at the free-edge are satisfied exactly; the resulting stress distribution was examined for consistency as required by 3-dimensional stress functions. The stress assumption includes no singularity. The traction-free edge is allowed to warp freely.

The interior of the laminate, away from the free edge, is modeled by laminated-plate elements (MLPIE) which are based on lamination theory. These elements include transverse shear deformation and are compatible with the TFQE. Thus, numerical results for general free-edge multilayer plate problems are obtained with efficient lamination-theory element modeling of most of the structure, while TFQE elements provide additional warping degrees of freedom at and near the free edges where the warping effect is important. This method of analysis has been developed for both static (mechanical and thermal loading) and transient response analyses.

Several examples, for which other numerical solutions exist, have been solved by using the TFQE and/or the TFQE in combination with MLPIE elements. The results compare well, but a significant reduction in the number of unknowns of the equations has been achieved in the present TFQE solution.

Finally, some numerical methods for solving static and transient response equations have been reviewed.

Army Materials and Mechanics Research Center
Watertown, Massachusetts 02172

A MULTILAYER, TRACTION-FREE EDGE, QUADRILATERAL WARPING ELEMENT FOR THE STRESS ANALYSIS OF COMPOSITE PLATES AND SHELLS

Alexander Harris, Oscar Orringer, and Emmett A. Witmer, Aeroelastic and Structures Research Laboratory, Department of Aeronautics and Astronautics, Massachusetts Institute of Technology, Cambridge, Massachusetts 02139

Technical Report AMMRC TR 79-26 (MIT-ASRL TR 193-1)
April 1979, pp. illus-tables, Contract DAAG46-78-C-0015
D/A Project 6X363304D215, AMCMS Code: 633304.21500.03
Final Report, March 1, 1978 to April 30, 1979

AD________________________

UNCLASSIFIED
UNLIMITED DISTRIBUTION

Key Words

Finite-Element Method
Elastic Behavior
Composites
Static Response
Transient Response
Stress Analysis
Laminated Plates and Shells
Free-Edge Stress Analysis

Laminated composites develop large interlaminar stresses at traction-free edges; these stresses are significant and often cause ply delaminations. However, these stresses are difficult to analyze and predict accurately because they vary very rapidly over a small region whose extent is of the order of the total laminate thickness at the free edge. Previous solution methods have been able to solve only a very restricted class of free-edge multilayer plate problems.

In the present research, a hybrid stress multilayer warping quadrilateral element with a traction-free edge (TFQE), based on the Principle of Modified Complementary Energy, has been developed for efficient finite element modeling and analysis at and near free edges. The assumed stress distributions in the element were selected so as to satisfy the basic equations of equilibrium; sufficient detail was implemented throughout each layer of each element to model the steep boundary layer stress gradients, including the important interlaminar stresses. The interlayer stress continuity and traction-free conditions at the free-edge are satisfied exactly; the resulting stress distribution was examined for consistency as required by 3-dimensional stress functions. The stress assumption includes no singularity. The traction-free edge is allowed to warp freely.

The interior of the laminate, away from the free edge, is modeled by laminated-plate elements (MLPIE) which are based on lamination theory. These elements include transverse shear deformation and are compatible with the TFQE. Thus, numerical results for general free-edge multilayer plate problems are obtained with efficient lamination-theory element modeling of most of the structure, while TFQE elements provide additional warping degrees of freedom at and near the free edges where the warping effect is important. This method of analysis has been developed for both static (mechanical and thermal loading) and transient response analyses.

Several examples, for which other numerical solutions exist, have been solved by using the TFQE and/or the TFQE in combination with MLPIE elements. The results compare well, but a significant reduction in the number of unknowns of the equations has been achieved in the present TFQE solution.

Finally, some numerical methods for solving static and transient response equations have been reviewed.

Army Materials and Mechanics Research Center
Watertown, Massachusetts 02172

A MULTILAYER, TRACTION-FREE EDGE, QUADRILATERAL WARPING ELEMENT FOR THE STRESS ANALYSIS OF COMPOSITE PLATES AND SHELLS

Alexander Harris, Oscar Orringer, and Emmett A. Witmer, Aeroelastic and Structures Research Laboratory, Department of Aeronautics and Astronautics, Massachusetts Institute of Technology, Cambridge, Massachusetts 02139

Technical Report AMMRC TR 79-26 (MIT-ASRL TR 193-1)
April 1979, pp. illus-tables, Contract DAAG46-78-C-0015
D/A Project 6X363304D215, AMCMS Code: 633304.21500.03
Final Report, March 1, 1978 to April 30, 1979

AD________________________

UNCLASSIFIED
UNLIMITED DISTRIBUTION

Key Words

Finite-Element Method
Elastic Behavior
Composites
Static Response
Transient Response
Stress Analysis
Laminated Plates and Shells
Free-Edge Stress Analysis

Laminated composites develop large interlaminar stresses at traction-free edges; these stresses are significant and often cause ply delaminations. However, these stresses are difficult to analyze and predict accurately because they vary very rapidly over a small region whose extent is of the order of the total laminate thickness at the free edge. Previous solution methods have been able to solve only a very restricted class of free-edge multilayer plate problems.

In the present research, a hybrid stress multilayer warping quadrilateral element with a traction-free edge (TFQE), based on the Principle of Modified Complementary Energy, has been developed for efficient finite element modeling and analysis at and near free edges. The assumed stress distributions in the element were selected so as to satisfy the basic equations of equilibrium; sufficient detail was implemented throughout each layer of each element to model the steep boundary layer stress gradients, including the important interlaminar stresses. The interlayer stress continuity and traction-free conditions at the free-edge are satisfied exactly; the resulting stress distribution was examined for consistency as required by 3-dimensional stress functions. The stress assumption includes no singularity. The traction-free edge is allowed to warp freely.

The interior of the laminate, away from the free edge, is modeled by laminated-plate elements (MLPIE) which are based on lamination theory. These elements include transverse shear deformation and are compatible with the TFQE. Thus, numerical results for general free-edge multilayer plate problems are obtained with efficient lamination-theory element modeling of most of the structure, while TFQE elements provide additional warping degrees of freedom at and near the free edges where the warping effect is important. This method of analysis has been developed for both static (mechanical and thermal loading) and transient response analyses.

Several examples, for which other numerical solutions exist, have been solved by using the TFQE and/or the TFQE in combination with MLPIE elements. The results compare well, but a significant reduction in the number of unknowns of the equations has been achieved in the present TFQE solution.

Finally, some numerical methods for solving static and transient response equations have been reviewed.